Photochimie des molécules d'intérêt exobiologique dans l'UV lointain

Dr. Martin Schwell

Maître de conférences à l'Université Paris 7 Denis Diderot

Notice sur les travaux de recherche pour l'obtention du diplôme d'habilitation à diriger des recherches

Résumé des travaux de recherche

Les travaux et projets de recherche que j'ai menés *depuis* ma thèse de doctorat s'orientent sur 2 axes majeurs. D'une part, une grande partie de mon activité a été consacrée à l'étude des propriétés photophysiques et photochimiques des molécules d'intérêt exobiologique (**axe 1**). D'autre part, je suis en train de développer au LISA (Laboratoire Interuniversitaire des Systèmes Atmosphériques) une nouvelle activité de recherche, qui est l'étude de l'aérosol atmosphérique terrestre par spectrométrie de masse (**axe 2**).

Dans les chapitres 1 à 5 de cette notice intitulée *« Photochimie des molécules d'intérêt exobiologique dans l'ultraviolet lointain (VUV) »*, je résume les résultats principaux que nous avons obtenus sur la photochimie VUV des petites molécules prébiotiques et biologiques (**axe 1**). Nos travaux sont motivés par l'une des grandes questions de l'exobiologie, à savoir quelle est la stabilité de ces molécules dans différents milieux extraterrestres vis-à-vis des champs électromagnétiques qui y règnent. Les techniques utilisées par notre groupe sont la spectrométrie de masse à photoionisation, la spectroscopie de fluorescence induite par rayonnement synchrotron et la spectroscopie photoélectronique. Dans cette notice, je porte une attention particulière aux résultats obtenus par spectrométrie de masse photoionique : Grâce à cette technique, nous avons pu déterminer pour toutes les molécules prébiotiques que nous avons étudiées, les énergies d'ionisation (IE) et les énergies seuil de formation (AE, « *appearance energy* ») des fragments cationiques formés par ionisation dissociative dans le domaine d'énergie de 6 à 23 eV ($\lambda \approx 56$ à 207 nm). Beaucoup de ces valeurs étaient inconnues auparavant. Nous montrons que les monocations des sept bases N-hétérocycliques que nous avons étudiées (dont deux sont des bases de l'ADN et une d'ARN) sont stables même lorsqu'ils sont formés avec une énergie interne (E_{int}) assez élevée, couvrant un domaine de 1.8 eV (pour l'uracile) à 5.35 eV (pour le benzimidazole). La fragmentation de ces molécules par ionisation dissociative a été étudiée : pour les bases N-hétérocycliques, le chemin le plus bas en énergie consiste le plus souvent en la perte de l'acide cyanhydrique (HCN) ou en la perte de l'acide isocyanique (HNCO).

Au contraire, les monocations formés à partir des cinq acides aminés que nous avons étudiés sont moins stables puisqu'ils fragmentent à des énergies beaucoup plus faibles. Leur chemin de fragmentation le plus bas en énergie est la rupture de la liaison C-C entre le carbone-α et le carbone du groupe carboxylique COOH, à l'exception de la molécule de β-alanine où la fragmentation la plus basse implique une rupture de la liaison entre le C-α et le C-β.

La photochimie VUV des espèces prébiotiques comme l'acide formique, l'acide acétique, le méthylformate et l'acétonitrile, toutes observées par radioastronomie dans le milieu interstellaire (MIS), a été étudiée par spectroscopie d'absorption et de fluorescence, et par spectrométrie de masse utilisant le rayonnement synchrotron comme source de lumière excitatrice. Les spectres d'absorption de ces espèces dans le VUV, enregistrés généralement dans le domaine de 6 à 20 eV, sont dominés par des séries de Rydberg qui convergent aux différents seuils d'ionisation. Les fragments neutres, comme par exemple CN et OH, formés par photodissociation sont observés par leur émission dans le domaine spectral de l'UV proche / visible. Les spectres d'excitation que nous avons enregistrés pour les fragments émetteurs importants renseignent, en les comparant avec les spectres d'absorption des molécules mères, sur les états électroniques qui donnent naissance aux fragments observés. Finalement, une autre quantité importante pour l'exobiologie, le rendement quantique de photoionisation, a été déterminée pour quelques espèces. Les implications astrophysiques et exobiologiques de nos résultats seront discutées en chapitre 5. Cinq publications importantes sont également jointes à cet ouvrage.

Récemment, un programme de recherche sur la spectroscopie d'absorption VUV des polyynes et cyanopolyynes à basse température a été commencé. Ce type de molécules linéaires est observé dans l'atmosphère de Titan. Pour modéliser la photochimie atmosphérique de ce satellite de Saturne, il est indispensable de connaître les sections efficaces d'absorption aux températures qui y règnent. Les résultats obtenus sont également importants pour interpréter les mesures de télédétection dans ce domaine spectrale.

Les compétences acquises pendant ma thèse de doctorat (diffusion élastique des particules individuelles à résolution angulaire) ainsi que lors des travaux dans le cadre de l'axe 1 (spectroscopie et photochimie VUV, spectrométrie de masse) m'ont également permis de développer un outil pour l'analyse chimique de l'aérosol organique de l'atmosphère (**axe 2**). La motivation pour ces travaux, qui sont décrits dans le chapitre 6 de cette notice, est née des connaissances lacunaires qui persistent actuellement sur la composition chimique des aérosols atmosphériques terrestres. L'instrument dénommé SPLAM (*Single Particle Laser Ablation Mass Spectrometry*) fait également appel à la spectrométrie de masse à photoionisation, effectuée ici par un laser UV ou VUV. Pour analyser la composition chimique d'un aérosol, un jet de particules est formé via des lentilles aérodynamiques. Ce jet est focalisé dans la source d'un spectromètre de masse à temps de vol où il est analysé, *particule par particule*. Cet instrument, actuellement en développement, sera exploité dans le futur afin d'analyser des

particules formées dans une chambre de simulation atmosphérique ou sur le terrain. Il est prévu d'y étudier la cinétique et les mécanismes impliqués lors de la formation d'un aérosol organique secondaire à partir des précurseurs gazeux, biogéniques et anthropiques.

Pendant mon séjour post-doctoral à l'Observatoire de Paris-Meudon, j'ai également étudié les propriétés photophysiques des nouveaux dérivés de fullerènes ayant des applications possibles dans l'optoélectronique. Néanmoins je n'ai pas poursuivi cette activité après mon entrée à l'Université Paris 7. Je joins une publication à titre d'exemple à cette notice.

Table des matières

1. Introduction

La motivation générale pour les travaux que nous avons entrepris dans les dernières huit années est née d'une question fondamentale de l'exobiologie, à savoir quelles chances de survie auraient de petites molécules biologiques ainsi que des molécules prébiotiques dans différents milieux extraterrestres, comme par exemple le milieu interstellaire (MIS) ou les atmosphères planétaires, vis à vis des champs électromagnétiques qui y règnent. Ainsi, explorer la photochimie dans l'ultraviolet du vide (VUV, $E_{photon} \approx$ 6-20 eV; $\lambda \approx$ 62-200 nm)[1] des molécules biologiques et prébiotiques est d'un intérêt considérable du point de vue d'un exobiologiste, à cause de l'apport possible de ces molécules de l'espace vers la terre jeune, ou bien vers d'autres corps planétaires, et le rôle qu'elles auraient pu jouer pour l'origine et le développement de la vie sur ces corps (Brack, 1998; Maurel et Décout, 1999; Sowerby et Heckel 1998; Sowerby et al., 2001).

Dans le domaine spectral du VUV, la section efficace de photoabsorption des biomolécules simples est souvent beaucoup plus élevée par rapport à l'UV proche ($\lambda \approx$ 400-200 nm, $E < 6$ eV ; voir par exemple la monographie pionnière de Robin, 1974). En particulier, elles absorbent fortement à $E = 10.21$ eV, énergie correspondante à l'émission Lyman-α de l'hydrogène atomique. La plupart des molécules que nous avons étudiées ont des énergies d'ionisation bien en dessous de cette énergie. C'est pourquoi l'ionisation et l'ionisation dissociative représentent des sujets importants à étudier.

Le domaine spectral de l'UV lointain est d'autant plus important pour l'exobiologie que la luminosité VUV du jeune soleil (pendant l'ère de l'Hadéen, lors du bombardement intense de la terre il y a environ 4 milliards d'années) était plus élevée par 2 ordres de grandeurs par rapport à notre ère, malgré que la luminosité totale du soleil (intégrée sur toutes les longueurs d'onde) était quant à elle plus basse que maintenant (Chyba et Sagan, 1992). Nos travaux de photochimie dans l'UV lointain constituent ainsi une base indispensable, parmi d'autres, pour mener des réflexions sur la chimie qui aurait menée à l'origine de la vie telle que nous la connaissons.

J'évoque un autre aspect, plus fondamental, de nos travaux : les mesures en phase gazeuse des petites biomolécules ont de l'importance en biologie parce que leurs propriétés intrinsèques,

[1] Dans cette notice, les termes « ultraviolet du vide (VUV) » et « UV lointain » sont considérés comme synonymes.

c'est à dire sans interaction avec un environnement de solvatation liquide ou de matrice solide, peuvent ainsi être étudiées (par exemple les mécanismes de dynamique interne de relaxation, les forces intramoléculaires, l'interconversion des conformères, la tautomérisation etc…). En plus, les résultats expérimentaux sont plus facilement comparables aux résultats de calculs quanto-chimiques pour lesquels, en général, des molécules isolées sont étudiées. L'étude des biomolécules en phase gazeuse est un domaine de recherche en pleine expansion au niveau international et elle jouera certainement un rôle important au sein des Sciences du Vivant. C'est pourquoi, j'ai co-organisé, avec Jean Demaison, Thérèse Huet (Laboratoire PhLAM, Université de Lille 1) et Isabelle Kleiner (LISA, CNRS, Universités Paris 7 & 12), une école d'été autour de cette thématique afin de structurer les activités de recherche menées en France dans ce domaine.[1]

Le présent document est structuré comme suit :

- ♦ Dans le prochain chapitre, intitulé **contexte scientifique**, je décrirai les éléments de chimie prébiotique telle que nous la concevons aujourd'hui. Dans cette partie je ferai aussi brièvement référence aux expériences de type « simulation spatiale » (paragraphe 2.1). Ensuite, je détaillerai les connaissances que nous possédons actuellement sur l'abondance des molécules biologiques et prébiotiques dans les différents milieux extraterrestres, y inclus les météorites et micrométéorites qui ont été découvertes et étudiées sur terre (paragraphe 2.2). Je donnerai un résumé des importants processus photophysiques et photochimiques dans le domaine du VUV (paragraphe 2.3). Enfin je récapitulerai les travaux de photochimie UV et VUV qui sont menés au niveau international sur les petites molécules biologiques (paragraphe 2.4).

- ♦ Le chapitre 3 décrira en détail les **méthodes expérimentales** que nous avons utilisées pour étudier la photochimie dans l'UV lointain.

- ♦ Le chapitre 4 résumera **les principaux résultats** que nous avons obtenus. Je mettrai un accent particulier sur les résultats obtenus par spectrométrie de masse photoionique.

- ♦ Enfin le chapitre 5 exposera les **conclusions** issues de nos travaux et leurs implications en astrophysique et exobiologie.

[1] *« BIOMIMETIQUE 2005 - Contribution des méthodes spectroscopiques et quanto-chimiques à l'étude des molécules d'intérêt biologique »* était une école d'été d'une semaine financée par le CNRS et l'Université Paris 7.

- ♦ Le chapitre 6 est dédié à la présentation de l'**étude de l'aérosol atmosphérique** terrestre par une nouvelle méthode expérimentale que je suis en train de développer.
- ♦ Enfin, le chapitre 7 présentera les **perspectives** de mon travail, à la fois dans la chimie atmosphérique et dans l'exobiologie.

Le chapitre 9 comprendra mon CV incluant la liste complète de mes publications dont le chapitre 10 donnera une sélection de 6 articles en texte intégral.

2. Contexte scientifique

2.1 Chimie prébiotique

La majorité des théories sur l'origine de la vie est basée sur le concept d'une évolution chimique en amont de la formation d'un organisme vivant (Raulin et al., 2005). Cette évolution, dénommée couramment « chimie prébiotique », s'appuierait sur les lois fondamentales de la chimie physique. Il est généralement admis aujourd'hui qu'aucune molécule ne constitue un élément indispensable dans la chimie prébiotique, à l'exception de l'eau éventuellement (Despois, 2006). Parmi les espèces prébiotiques nous pouvons distinguer 3 familles :

♦ *Famille 1 :* Petites molécules réactives (comme HCN, H_2CO, NH_3, HC_3N, HC_5N, C_4H_2….), dites « prébiotiques », qui sont capable de former des molécules biologiques plus complexes, à savoir celles des familles 2 et 3, au travers des réactions telles que par exemple la synthèse Strecker, la réaction Formose et autres (pour un aperçu synthétique de cette chimie voir Raulin et al., 2005). J'y inclus également les acides carboxyliques HCOOH et CH_3COOH, ainsi que l'acétonitrile (CH_3CN), molécules dont le comportement VUV a été étudié de manière exhaustive par notre groupe.

♦ *Famille 2 :* Ce sont les monomères des biopolymères que nous connaissons sur terre, i.e. les 20 acides aminés qui sont les monomères des protéines, les bases N-hétérocycliques guanine, adénine, thymine cytosine et uracile qui sont les briques constituantes de l'ARN et de l'ADN, les acides gras qui forment les membranes biologiques et les monosaccharides qui édifient les glucides (sucres). Dans cette notice, ces molécules sont également appelées « biologiques » ou « biomolécules » afin de les distinguer de la famille 1 mais également parce que ce sont des molécules que nous trouvons dans les organismes vivants.

♦ *Famille 3 :* Ce sont les bases N-hétérocyliques et acides aminés *non-biologiques* (ou extrêmement rares sur terre), comme par exemple l'acide α-amino-isobutyrique (AIB) ou le benzimidazole. Indépendamment de la classification biologique, les bases N-hétérocycliques peuvent être reparties en *purines, pyrimidines* et *triazines* en référence à leur structure moléculaire.

La chimie prébiotique pourrait avoir lieu en phase liquide, dans un océan primordial par exemple, mais les atmosphères planétaires et cométaires sont aussi considérées comme

systèmes réacteurs. Les atmosphères gazeuses sont relativement faciles à étudier par des moyens de télédétection (sur terre et ailleurs dans le système solaire), tandis que les phases condensées des systèmes extraterrestres sont difficiles d'accès parce que des mesures in-situ s'imposent en général pour mesurer leur composition chimique.

Simulation expérimentale de la chimie prébiotique au laboratoire

Comme les missions spatiales restent des opérations lourdes à mettre en oeuvre et très coûteuses, les expériences de type « simulation spatiale » menées au laboratoire offrent une alternative scientifiquement riche pour étudier la chimie prébiotique « extraterrestre ». L'étude expérimentale de la formation des petites biomolécules dans des conditions astrophysiques simulées est un domaine large et il ne peut pas être décrit en détail dans cette notice. Le lecteur intéressé peut se référer aux divers livres qui sont apparus dans la dernière décade (par exemple Brack, 1998 ; Chela-Flores et al., 2001 ; Gargaud et al., 2005). Un récent numéro spécial de *Advances in Space Research* adressant, en grande partie, ce sujet est également recommandé (volume 33, tome 1, année 2004).

Pour donner un très bref aperçu de ce domaine ici, je note que tout a certainement commencé avec l'expérience « Miller-Urey » (Miller, 1953), sur la formation des acides aminés dans une atmosphère primordiale. Plus tard, les travaux de Basile et al. (1984) ont montré que les purines et pyrimidines pourraient être formées à partir de HCN ou HC_3N, ou même à partir de gaz simples tels que NH_3, N_2, CO_2 et H_2O (Lavrentiev et al., 1984). La pyrolyse-CPG-SM (chromatographie en phase gazeuse couplée à la spectrométrie de masse) a été appliquée afin d'étudier les polymères de HCN dont on pense qu'ils font partie des macromolécules organiques les plus abondants dans le système solaire (Minard et al., 1998), par exemple dans les noyaux cométaires. Ces expériences ont menés à l'identification des bases adénine et xanthine (comme dérivés méthylés) ensemble avec d'autres N-hétérocycles (Minard et al., 1998). D'autres chercheurs (Coll et al., 1999) utilisent un plasma froid afin de simuler la chimie dans les atmosphères planétaires, mais ces expériences n'ont pas mené à l'identification de molécules biologiques à ce jour.

Très récemment Muñoz Caro et collaborateurs (2002) ont démontré que l'extrait à l'acide chlorhydrique (6M) des glaces interstellaires modèles (H_2O:CH_3OH:NH_3:CO:CO_2.= 2:1:1:1:1 composition molaire), irradiées au laboratoire à 12 K et sous vide avec une lampe VUV (E_{photon} = 7.3 à 9.2 eV), contient beaucoup d'acides aminés (ce mélange solide irradié est parfois appelé *« yellow stuff »* à cause de sa couleur caractéristique).

2.2 Recherche des biomolécules et molécules prébiotiques dans différents milieux extraterrestres

2.2.1 Milieu interstellaire (MIS)

Des biomolécules simples, telles qu'acides aminés ou bases nucléiques, n'ont pas encore été identifiés dans le MIS, à part de la molécule glycine qui aurait été observée par Kuan et al. (2003a) par radioastronomie dans les noyaux moléculaires chauds Sgr B2 (N-LMH), Orion KL, et W51 e1/e2. Mais cette découverte est controversée (Snyder et al., 2005). Des limites supérieures d'abondances ont été établies pour les bases pyrimidine (Kuan et al., 2003b) et imidazole (Irvine et al., 1981). Très récemment, l'acétamide (CH_3CONH_2) a pu être identifiée par Hollis et al. (2006). La liste exhaustive des molécules identifiées dans le MIS par radioastronomie a été publiée récemment par Müller et al. (2005). Parmi ces molécules on trouve des espèces importantes pour la chimie prébiotique telle que l'acide formique, l'acide acétique, ou encore l'ammoniac.

Pour la discussion de la stabilité des biomolécules envers des champs électromagnétiques VUV du MIS il est important d'y distinguer 2 régions : les régions dites « HI » ou le degré d'ionisation[1] de l'hydrogène atomique est proche de zéro. Dans ces régions, on peut considérer qu'il n'y a pratiquement pas de photons disponibles avec des énergies supérieures à 13.6 eV (énergie d'ionisation de H). Des molécules complexes y sont donc protégées contre les rayonnements avec $\lambda < 91.1$ nm. Les régions HI se trouvent par exemple dans les domaines froids des grands nuages moléculaires. Dans nos expériences, le domaine d'énergie $E < 13.6$ eV est donc particulièrement intéressant à étudier.

Notons que les régions riches en molécules complexes se trouvent souvent très proches des régions dites « HII » (degré d'ionisation proche de 1) (Bergmann et Schäfer, 1997). Dans un nuage moléculaire, ces régions se trouvent dans l'entourage des jeunes étoiles chaudes et sont facilement identifiées par leur émission dans le domaine de l'UV et du visible (par exemple émission des raies H-Balmer et H-Lyman à cause de la recombinaison des électrons et protons résultant en la formation de H avec $n > 2$). Il est donc également intéressant d'étudier les processus photophysiques des molécules prébiotiques au-delà de 13.6 eV.

[1] Le degré d'ionisation x est définie par $x = N_1 / (N_0 + N_1)$ avec N_0 = nombre d'atomes d'hydrogène dans l'état neutre et N_1 = nombre d'atomes d'hydrogène ionisés.

2.2.2 Atmosphères planétaires et cométaires

Kissel et Krüger (1987) ont rendu compte de l'abondance des pyrimidines et purines, les squelettes moléculaires des bases d'ADN et d'ARN, dans la queue de la comète Halley. Par contre, aucune spéciation moléculaire n'a pu être inférée de ces spectaculaires mesures in-situ effectuées par le spectromètre de masse à impact de poussières PUMA à bord du vaisseau spatial soviétique VEGA1. Néanmoins, un grand nombre de molécules prébiotiques plus simples, de la famille 1, ont été observées par télédétection dans les comas et queues cométaires (Despois et Cottin, 2005).

En ce qui concerne les atmosphères planétaires, celle de Titan est actuellement la cible la plus intéressante pour l'exobiologie dans le système solaire, malgré que d'autres objets tels que Europe, un des satellites de Jupiter, ainsi que la planète Mars méritent une attention particulière à cause de l'abondance probable de l'eau en état liquide, au présent ou dans une ère passée. L'atmosphère dense de Titan est actuellement explorée par la mission spatiale Cassini / Huygens. Parmi les molécules les plus abondantes on trouve dans sa stratosphère des hydrocarbures simples telles que l'acétylène (C_2H_2), le diacétylène (C_4H_2), ou le propyne (C_3H_4). On détecte également le HCN et des cyanopolyynes, telles que HC_3N (proprionitrile) et HC_5N, et l'acétonitrile, CH_3CN. Une liste complète des molécules trouvées dans l'atmosphère de Titan est compilée par Raulin et al. (2005). Les nitriles sont potentiellement intéressants pour la chimie prébiotique parce qu'ils pourraient être à l'origine de la formation de bases d'ADN et d'ARN (Ferris et al., 1968, 1974 ; Raulin et Toupance 1975).

La difficulté d'identifier des molécules plus grandes, telles que les bases d'ADN, par des techniques de télédétection est vraisemblablement liée à leur abondance faible et des limites de détection encore trop élevées des instruments. De plus, l'intensité des transitions micro-ondes et infrarouges des molécules complexes est généralement réduite à cause d'une fonction de partition élevée. Un autre problème est lié à l'état microphysique des biomolécules : du fait de leur faible pression de vapeur saturante elles peuvent en effet se trouver en état condensé (aérosols dans atmosphères planétaires, grains interstellaires etc...). Dans ce contexte, des caractéristiques spectrales seraient encore plus difficiles à détecter à cause des interactions de la molécule avec la matrice.

2.2.3 Météorites et Micrométéorites carbonés

Les météorites carbonés sont des fragments d'anciens astéroïdes ou comètes qui sont restés relativement inchangés depuis la formation du système solaire (Sephton, 2005). Leur

composition chimique est donc représentative pour une chimie prébiotique qui aurait pu se dérouler à cette période. Les météorites carbonés les plus étudiés sont les météorites Murchison, Murray, Orgueil et Allende.

En 1975, Hayatsu et al. rendent compte de l'identification des bases N-hétérocyliques, notamment des purines et triazines, dans l'extrait HCl de la météorite de Murchison. Ce résultat a été confirmé en 1981 par Stoks et Schwartz qui ont trouvé des purines (hypoxanthine, xanthine, adénine et guanine) dans des extraits à l'acide formique des météorites Murchison, Murray et Orgueil, mais pas dans la météorite Allende. En 1985, un autre groupe (Hua et al., 1985) a identifié et quantifié les bases cytosine, uracile, guanine, thymine et adénine dans un extrait HCl / HCOOH des trois météorites susmentionnés. Très récemment, ces résultats ont été confirmés par Glavin et Bada (2004). Ces expériences suggèrent donc une présence extraterrestre de ces biomolécules.

Soixante-quatorze acides aminés ont été identifiés dans la météorite Murchison (Cronin et Pizzarello, 1986 ; Cronin, 1989), dont uniquement 8 sont biologiques. 11 autres sont non-protéiques mais connus sur terre, mais les 55 acides aminés restant sont uniquement trouvés dans les météorites. Leur diversité structurale a été discutée par Cronin et al. (1995). Elle nous suggère fortement que ces acides aminés sont d'origine extraterrestre. Très récemment, des acides monocarboxyliques di-aminés ont été identifiés par Meierhenrich et al. (2004) dans la météorite Murchison (extrait HCl 6M). Notons que les acides (di-) aminés sont probablement enveloppés par une matrice en polymère dans les météorites carbonés. La structure chimique de ce polymère n'est pas connu en détail à ce jour (cf. Cronin, 1976a,b; Cronin et Pizzarello, 1983; Muñoz Caro, 2002).

La chiralité étant considérée comme une trace ultime de la vie, de nombreuses tentatives ont été entreprises afin de démontrer un éventuel excès énantiomérique des acides aminés extraterrestres. Néanmoins, la plupart des études montrent que les mélanges présents dans les météorites sont racémiques, à l'exception d'un récent travail présenté par Cronin et Pizzarello (2000). Dans leurs analyses, ce groupe trouve des excès énantiomériques de forme L (gauche) de 1 à 9.2 % pour six α-méthyle-α-acides aminés des météorites Murchison et Murray. L'origine de cet excès pourrait être la photodissociation préférentielle des énantiomères de forme D (droite) par la lumière UV circulairement polarisée dans le nuage pré-solaire (Sephton, 2005). Cette hypothèse a été fortement appuyée par une récente expérience réalisée par Meierhenrich et al. (2005). Ces chercheurs ont trouvé un excès énantiomérique de 2.6 %

en irradiant un échantillon de leucine racémique solide, avec un rayonnement VUV circulairement polarisé de $\lambda = 182$ nm.

Récemment, il y a eu des tentatives d'identification des acides aminés dans les micrométéorites antarctiques (Brinton et al., 1998 ; Glavin et al., 2004). Il s'agit de particules larges (50 à 500 μm), dénommées « AMMs » dans la littérature (pour *« Antarctic micrometeorites »*). Le flux d'impact sur terre est estimé à 40 000 tonnes par an. Ce flux massique est 100 fois plus grand par rapport aux impacts d'objets plus grands comme les météorites. Il représente donc une source extraterrestre importante de matière organique. Dans les études mentionnées, uniquement quelques échantillons analysés présentent de petites quantités de l'acide aminé AIB (22 à 280 ppm) qui est classée dans la famille 3 (non-biologiques ou très rares sur terre). Tous les autres acides aminés identifiés sont biologiques (famille 2) et sont donc considérés comme étant des contaminations terrestres.

2.3 Processus photophysiques et photochimiques dans le VUV

Photoabsorption

Dans le domaine spectral du VUV on trouve des transitions électroniques de valence et des séries de transitions dites de « Rydberg ». Ces transitions sont en général plus fines spectralement, et sont ainsi distinguables des transitions de valence spectralement plus larges. Un électron dans une orbitale de Rydberg se trouve loin du cœur atomique de la molécule. L'attribution d'une série de Rydberg peut être accomplie utilisant la formule modifiée des séries de Rydberg pour l'hydrogène (Robin, 1974) :

$$E_n = IE - [\, R/ (n-\delta)^2 \,] \qquad (1)$$

Ici, la valeur E_n est l'énergie de la transition de Rydberg et $IE - E_n$ représente l'écart en énergie de cette transition et l'énergie d'ionisation (IE) correspondante. Le nombre quantique n et la constante de Rydberg R ($R = 13.605$ eV) ont le même sens que pour la structure des orbitales de l'hydrogène. Pour l'hydrogène, $\delta = 0$, et le premier membre de la série Rydberg ($n = 2$) se trouve à ¾ de son énergie d'ionisation (≈ 10.2 eV). Cette valeur est en général utilisée afin de trouver le premier membre d'une série Rydberg. Pour les molécules, on introduit le « défaut quantique », δ, qui représente la déviation du point de charge idéal (H^+ !)

de l'ion moléculaire positivement chargé. δ dépend donc de la structure électronique de ce cation.

Les séries de Rydberg peuvent converger à la première énergie d'ionisation ainsi qu'à des énergies d'ionisation supérieures. Au-delà de la 1ère IE, les transitions Rydberg peuvent être identifiées lorsqu'elles sortent de l'absorption « quasi-continue » de la molécule. En effet, la densité des états excités au delà de la limite d'ionisation est très grande ayant pour conséquence que ces états sont quasi-liés et le spectre d'absorption apparaît continu.

La structure vibrationelle des transitions de Rydberg peut souvent être identifiée avec l'aide du spectre photoélectronique de la molécule : comme une orbitale de Rydberg est localisée loin du « noyau » moléculaire chargé, les fréquences de vibrations de ce dernier sont très proches de celles du cation correspondant.

Processus photophysiques et photochimiques dans le VUV

L'absorption des photons VUV peut induire plusieurs processus photophysiques et photochimiques[1] dont les plus importants sont listés dans la suite. Un schéma général simplifié est exposé en figure 1.

- l'ionisation directe,
- l'autoionisation qui consiste en l'excitation résonante d'un état *neutre* au delà de la 1ère énergie d'ionisation suivie d'un couplage avec le continuum d'ionisation libérant l'espèce ionique,
- l'ionisation dissociative (dissociation directe ou prédissociation de l'ion mère),
- la fluorescence de la molécule neutre ou de l'ion mère excité,
- la fluorescence des fragments formés dans un état moléculaire excité lors d'une dissociation,
- la formation des paires d'ions dont chacun porte une charge de signe opposée,

[1] Sont considérés dans cette notice comme (a) processus « *photophysiques* » tous les phénomènes internes de la molécule *sans* fragmentation et comme (b) processus « *photochimiques* » tous les processus qui impliquent la rupture d'une liaison chimique (y inclus la réorganisation et la tautomérisation de la molécule).

- ou encore la conversion interne entre états électroniques (appelée ci-dessous *« IC »* = *Internal conversion*). La redistribution vibrationelle et rotationelle (appelée *« IVR »* = *Internal vibrational rotational redistribution*) peut « aider » à la conversion interne entre états électroniques.

Le lecteur intéressé par plus de détails est invité à se référer à Berry et Leach (1981). Ces auteurs donnent un aperçu général très complet de tous ces processus.

Les processus photophysiques et photochimiques du VUV peuvent être explorés par de nombreuses techniques expérimentales, telle que la spectroscopie photoélectronique « HeI » (énergie du rayonnement excitateur 21.21 eV), la spectrométrie de masse photoionique ou bien la spectroscopie de fluorescence pour n'en nommer que quelques-unes. Dans le chapitre 3, je présenterai plus en détail les techniques que nous avons utilisées pour nos travaux : la spectroscopie d'absorption, la spectrométrie de masse photoionique et la spectroscopie de fluorescence induite par rayonnement synchrotron.

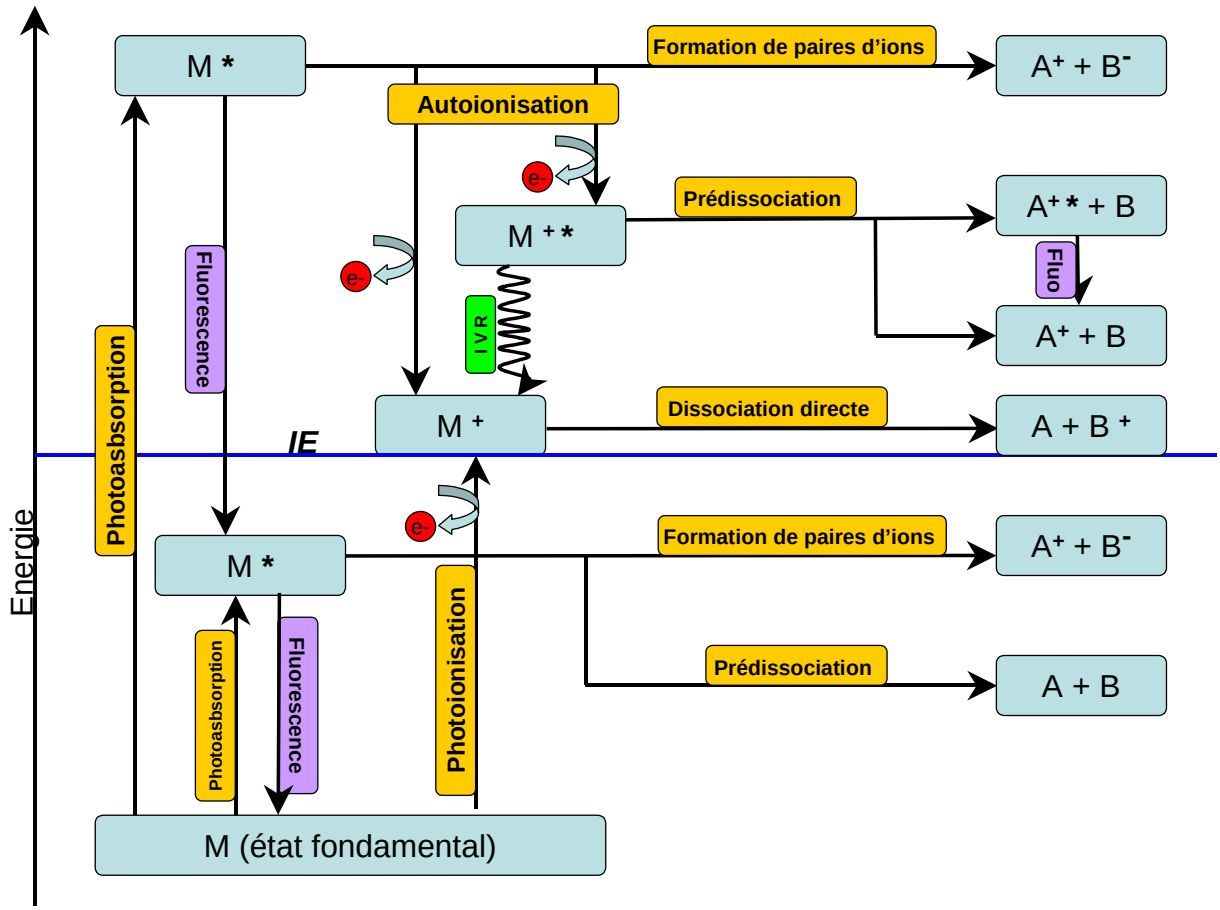

Figure 1 : Schéma général simplifié des processus photophysiques et photochimiques.

2.4 Photochimie des molécules biologiques dans l'UV moyen - résumé des expériences d'autres groupes

Naturellement, il est important de considérer également la photochimie qui suit l'excitation dans l'UV moyen ($\lambda \approx 200$ à 400 nm). Un numéro spécial du *European Physical Journal* a été consacré à ce sujet en 2002 (Weinkauf et al., 2002). Ce domaine d'énergie est davantage accessible que le VUV aux expériences utilisant des lasers pulsés qui permettent l'étude des processus photophysiques et photochimiques rapide et ultrarapides (c'est à dire à l'échelle de temps de la nanoseconde et en dessous).

Par exemple, la photochimie dans l'UV moyen des bases d'ADN a été étudiée récemment par spectroscopie d'ionisation résonante à 2 photons (Nir et al., 2001, 2002 ; Lührs et al., 2001; Plützer et al., 2001 et 2002). Le résultat le plus important de ces études, du point de vue d'un exobiologiste, est que toutes les bases impliquées dans la réplication des gènes présentent des durées de vies très courtes des états excités de l'UV moyen (250-300 nm), de l'ordre de la picoseconde et inférieures (Nir et al., 2002 et références citées dans cet article). Y sont associés des rendements quantiques de fluorescence et de phosphorescence très faibles. En conclusion, la désexcitation (angl. « *quenching* ») de ces états excités procède principalement via conversion interne vers l'état fondamental. Les bases d'ADN et d'ARN sont donc protégées contre la fragmentation induite par les photons de l'UV moyen. De nombreux auteurs ont supposé que ce type de briques élémentaires ont été finalement sélectionnées par l'évolution pour transcrire l'information génétique (Broo, 1998 ; Nir et al., 2002).

Très récemment, la photochimie des acides aminés et des bases d'acides nucléiques a été étudiée en matrice de gaz rare à 12 K, irradiés par une lampe d'hydrogène à basse pression excitée par micro-ondes (Ehrenfreund et al., 2001; Peeters et al., 2003). Ce genre de lampes délivre un spectre d'émission multi-lignes, entre 165 et 135 nm ($7.5 \text{ eV} < E < 9.2 \text{ eV}$). Ces expériences indiquent, par observation des spectres infrarouges de la matrice, que les bases et acides aminés étudiés (adénine, uracile, glycine, alanine, acide α-amino isobutyrique) sont dégradées photochimiquement en matrice d'argon à 12 K, dans le domaine spectral évoqué ci-dessus. Malheureusement, les résultats obtenus ne fournissent pas des données en fonction de la longueur d'onde d'irradiation. Les « sections efficaces de destruction » déterminées dans ces expériences, moyennés sur toutes les longueurs d'ondes émises par la lampe d'hydrogène, peuvent être considérées comme le produit entre section efficace d'absorption σ_{abs} et section efficace de photodissociation σ_{diss} en état solide mélangé avec l'argon. Ces valeurs sont très

probablement dépendantes de (a) l'état de mélange en phase solide et de (b) la nature chimique de cette phase solide. L'utilisation de ces « sections efficaces de destruction » pour déduire la stabilité photochimique des biomolécules condensées sur (ou mélangés avec) d'autres phases solides que l'argon, comme par exemple des grains interstellaires, doit donc être considérée avec beaucoup de précaution. L'application de ces valeurs à des biomolécules gazeuses paraît également difficilement concevable.

3. Photochimie VUV : Méthodes expérimentales utilisées

L'ensemble de nos expériences ont été menées en utilisant le rayonnement synchrotron (RS) comme source de lumière VUV. La figure 2a-d donne les schémas des différentes réalisations expérimentales que nous avons utilisées (Fig. 2a : schéma général ; fig. 2b-d différentes expériences connectées, via des étapes de pompage différentiel, au monochromateur primaire de la ligne de lumière synchrotron utilisée). Dans la suite de ce chapitre je décrirai en détails ces techniques.

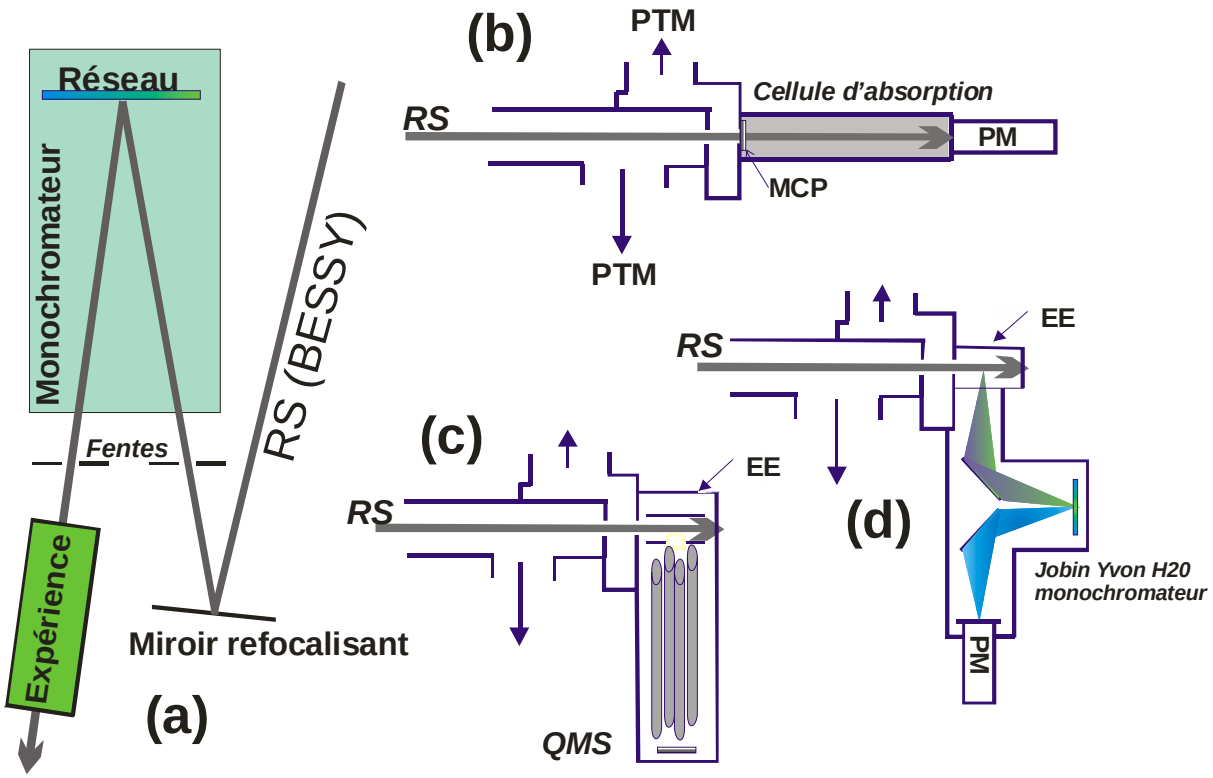

Figure 2 : Schéma des différentes réalisations expérimentales. (a) schéma général, (b-d) différentes expériences connectées au monochromateur primaire : (b) mesures de sections efficaces de photoabsorption, (c) spectrométrie de masse photoionique, (d) spectroscopie de fluorescence induite par rayonnement synchrotron (RS). PTM = Pompe turbomoléculaire. PM = Photomultiplicateur. QMS = spectromètre de masse quadripolaire. MCP = Détecteur à microcanaux (*Microchannelplate)*, EE = entrée effusive d'un échantillon gazeux.

3.1 Le rayonnement synchrotron comme source de lumière VUV

Le rayonnement synchrotron est une source de lumière brillante, spectralement large, polarisée et pulsée. La brillance (angl. « *brilliance* » ou « *brightness* ») caractérise l'intensité du faisceau de lumière synchrotron, sa focalisation ainsi que sa cohérence en longueur d'onde. Elle s'exprime en photons/s/mm^2/mrad^2 (flux de photons par unité d'angle solide et de surface

transverse de la source). C'est une quantité généralement plus importante que le flux seulement (en photons/s), plus particulièrement dans les applications qui utilisent un monochromateur (*« throughput-limited applications »*) (Samson et Ederer, 2000).

Le RS, connecté à un monochromateur, est une source de lumière extrêmement importante pour l'exploration de la photochimie dans le VUV. Son avantage, par rapport aux lasers par exemple, est principalement dû à l'étendue de la gamme spectrale des photons disponibles et la facilité correspondante de faire varier la longueur d'onde des photons. Par exemple, les énergies respectives d'apparition des voies de fragmentation peuvent être facilement étudiées.

Les anneaux de stockage conçus spécialement comme source de RS offrent trois différentes sources de lumière : (1) les aimants dipolaires, (2) les *« wigglers »* qui consistent en une série d'aimants de polarité opposée et (3) les onduleurs qui eux aussi consistent en une séquence d'aimants de polarité alternante mais dans lesquels les déplacements du faisceau sont faibles, par rapports aux wigglers, ce qui produit une interférence cohérente. Le faisceau correspondant est par conséquent très brillant. Dans un anneau de stockage typique les électrons circulent en paquets qui peuvent contenir jusqu`à 10^{12} électrons. Les aimants de focalisation d'un tel anneau sont capables de concentrer les électrons en paquets de section droite très petite et de vitesse transverse minimisée. La combinaison d'une source de lumière de haute intensité et petite dimension résulte en une brillance maximale (S.L. Hulbert et G.P. Williams dans Samson et Ederer (2000)).

Dans nos expériences, le RS a été obtenu aux anneaux de stockage BESSY I (fermeture 2001) et BESSY II (ouverture 2002), à Berlin. BESSY II est un anneau de stockage de 3ème génération dont la circonférence est de 240 m. L'énergie finale atteinte par les électrons est de 1.7 GeV. Le courant dan l'anneau est typiquement de 250 mA (juste après l'injection) est sa durée de vie est 10h environ. Quatorze unités d'insertion (onduleurs, wigglers) sont installées dans les sections droites de l'anneau. Nos manipulations sont toutes de nature continue, c'est à dire elles n'utilisent pas la structure pulsée de la lumière. Dans la plupart des expériences, un monochromateur NIM (monochromateur à incidence normale ; McPherson 1.5 m de focale) a été utilisé. Très récemment, à BESSY II, nous avons employé également des monochromateurs NIM de 3 et 10 m. Sur ce dernier une résolution spectrale de 0.05 Å ou moins peut être atteinte en utilisant un réseau de 1200 traits par mm.

Des mesures de très haute résolution peuvent être nécessaires, par exemple, afin d'explorer la dépendance en température des bandes d'absorption. Une autre raison est la modélisation

photochimique : comme la raie Lyman-α de l'émission de l'hydrogène solaire est spectralement fine (largeur 0.1 Å), les sections efficaces de photoabsorption qu'on souhaite inclure dans un modèle de photochimie planétaire doivent être mesurées avec la même résolution.

3.2 Mesures de sections efficaces de photoabsorption VUV en phase gazeuse

Il est difficile d'étudier la photoabsorption VUV en phase gazeuse des molécules biologiques de volatilité réduite (acides aminés, bases nucléiques). C'est pourquoi, dans le passé, ces mesures ont été effectuées en utilisant des couches minces comme substrat. La fragilité thermique des biomolécules ne permet en effet pas de les étudier à haute température. Lorsque l'on étudie des couches minces, la réflexion optique peut être mesurée et les constantes optiques peuvent être extraites (voir par exemple Arakawa et al., 1986). Une autre possibilité pour acquérir les constantes optiques d'un composé très peu volatil est de mesurer la perte d'énergie des électrons lorsqu'ils traversent le substrat (« *EELS* » = *Electron Energy Loss Spectroscopy*, voir par exemple Isaacson, 1972).

Dans nos programmes de recherche nous avons étudié la photoabsorption absolue des espèces prébiotiques volatiles á température ambiante (HCOOH, CH_3COOH, $HCOOCH_3$, CH_3CN et autres). Un problème inhérent aux mesures en phase gazeuse dans le VUV est le matériel utilisé pour limiter le chemin optique de la cellule utilisée. Les anciennes mesures sont souvent limitées à une énergie maximale d'environ 11 eV, valeur correspondant à la coupure spectrale des fenêtres fabriquées en fluorure de magnésium ou de lithium (voir par exemple Robin, 1974; Suto et al., 1988). Dans nos mesures nous avons utilisé un disque à microcanaux comme délimiteur de chemin optique qui laisse passer une quantité suffisante de lumière et en même temps est une excellente barrière pour les molécules de la phase gazeuse (voir fig. 2b). Ce dispositif nous a permis de déterminer des sections efficaces absolues de photoabsorption en utilisant la Loi Lambert-Beer au-delà de la limite mentionnée ci-dessus. Ceci est intéressant, de manière générale, pour la photochimie du milieu interstellaire (voir contexte scientifique).

En 2005, nous avons en plus commencé un programme de recherche sur la spectroscopie d'absorption VUV à basse température des polyynes et cyanopolyynes (collaboration avec Y.

Bénilan, M.-C. Gazeau, A. Jolly, N. Fray).[1] Pour cela, une nouvelle cellule, refroidissable, a été conçue et construite. Le but est d'étudier la variation du coefficient d'absorption avec la température de ces espèces prébiotiques qui sont observées dans l'atmosphère de Titan. Les molécules sous étude sont HCN, HC_3N, HC_5N, C_4H_2, C_6H_2 (non-observée sur Titan mais prédite par les modèles photochimiques) et C_2N_2. Ces coefficients sont importants à connaître afin de (a) mieux modéliser les processus photochimiques qui se déroulent dans l'atmosphère de Titan, et (b) d'améliorer l'interprétation des mesures qui sont actuellement effectuées avec l'instrument UVIS (*Ultraviolet Imaging Spectrograph*) à bord de la sonde spatiale CASSINI. Nos résultats préliminaires, sur HCN, HC_3N, HC_5N et C_4H_2 montrent que l'effet de la température sur le coefficient d'absorption, entre 115 et 210 nm, de ces molécules est considérable entre 150 à 298 K (cf. chapitre sur les perspectives, discutées au paragraphe 7.2.1)[2]

3.3 Mesure du rendement quantique de photoionisation γ_i

Afin d'estimer l'importance des processus *ioniques* dans la photochimie VUV des petites biomolécules, il est nécessaire de mesurer le rendement quantique de photoionisation γ_i, *en fonction de l'énergie du photon*. La technique que nous avons utilisée est celle décrite par Jochims et al. (1996) : elle utilise une cellule de photoabsorption (comme schématisée en fig. 2b) qui comporte en plus deux électrodes posées en haut et en bas de la cellule pour mesurer le faible courant ionique en phase gazeuse produit par les ions formés lors de la photoionisation. Dans ces mesures, le courant ionique est mesuré par un électromètre et intègre naturellement le nombre de cations mères formés par photoionisation et celui des cations filles issus de la photoionisation dissociative. Le rendement photoionique total est proportionnel au rapport entre le nombre d'ions formés et le nombre de photons absorbés dans la cellule. Lorsque ce rapport devient constant on peut considérer que le rendement quantique de photoionisation γ est égal à 1 (Berry et Leach, 1981) et la courbe entière peut ainsi être

[1] Ce programme est soutenu par le GDR Exobiologie et le programme national de physico-chimie du milieu interstellaire (PCMI). Les expériences sont effectuées à BESSY II (Berlin-Adlershof). Une thèse de doctorat, que je co-encadre, a débuté également en 2005 (T. Ferradaz).

[2] Pour la présente notice, j'ai décidé de ne pas montrer en détail ces nouveaux résultats, non-publiés à ce jour.

calibrée. Pour des molécules de grande taille, on observe généralement que γ_i devient 1 à plusieurs eV au dessus de l'énergie d'ionisation (Berry et Leach, 1981).

La valeur $1-\gamma_i$ désigne, par conséquent, la somme des rapports de branchement des processus photophysiques et photochimiques *neutres*, c'est à dire ceux sans formation des espèces chargées. Il s'agit notamment de la fluorescence, de la conversion interne, de la dissociation en espèces non-chargées, et de la formation des paires d'ions qui est un processus électriquement neutre.

3.4 Spectrométrie de masse photoionique (*« Photoion Mass Spectrometry, PIMS »*)

La photoionisation et la photoionisation dissociative sont des phénomènes très importants dans le VUV. C'est pourquoi la spectrométrie de masse est un outil idéal pour étudier la photochimie dans ce domaine. Dans nos expériences, le RS monochromatisé est focalisé, via des étapes de pompage différentiel, dans la source d'ions d'un spectromètre de masse quadripolaire (Leybold Q200 ; fig. 2c). Ce dispositif expérimental a été décrit en détail dans Schwell et al. (2000). Dans cette source, on introduit un échantillon gazeux au travers d'une entrée effusive. La pression qui y règne est d'environ 10^{-5} mbar. La cellule de la source peut également être chauffée jusqu'à 400°C afin d'y vaporiser des composés liquides ou solides, thermiquement non-fragiles comme par exemple les hydrocarbures aromatiques polycycliques (HAP). Dans ce cas, l'échantillon est posé très près de la zone d'interaction photons / matière de la source d'ions

Dans le cas des composés biologiques, la température doit être maintenue le plus bas possible afin d'éviter toute dégradation thermique. Par exemple, pendant les expériences sur les bases nucléiques une température de 100°C était suffisante pour fournir un flux de molécules permettant d'enregistrer un spectre de rapport signal sur bruit (S/B) satisfaisant. Notons que, dans le cas des acides aminés, une dégradation thermique a pu être constatée facilement en observant un pic de CO_2^+ (m/z = 44) important. Les paramètres expérimentaux ont été ajustés de sorte que la dégradation thermique soit minimale et que le rapport signal sur bruit (S/B) soit maximal sur les ions à étudier.

L'enregistrement de l'intensité d'un ion en fonction de l'énergie incidente donne un spectre de rendement photoionique (appelé « spectre PIMS » ou « courbe de rendement photoionique » ; voir par exemple fig. 4, page 33). L'intervalle de mesure est typiquement autour de 10 meV. Les spectres sont normalisés par rapport au flux lumineux arrivant dans la

source d'ions qui est mesuré en observant, par un photomultiplicateur, la fluorescence visible induite par le RS d'une couche de sodium salicylate placée sur une fenêtre. La variation de ce flux est principalement due à la transmission du réseau du monochromateur en fonction de l'énergie du photon ainsi qu'à la décroissance continue du courant dans l'anneau de stockage. La résolution spectrale d'un spectre PIMS est typiquement 2 Å (25 meV à une longueur d'onde de 1000 Å).

Dans le cas des seuils de formation d'un ion en dessous de 115 nm (~10.8 eV), des spectres PIMS supplémentaires ont pu être enregistrées en utilisant un filtre en fluorure de magnésium (MgF_2, coupure spectrale vers 115 nm), afin de supprimer la lumière diffusée de haute énergie et la lumière issue des ordres supérieurs du réseau du monochromateur, problèmes inhérents des expériences avec le RS. La détermination de l'énergie d'ionisation (IE) ainsi que des énergies seuil de formation des photofragments (appelées ci-dessous « AE », de l'anglais *« appearance energy »*) est effectuée à l'aide des graphes semi-logarithmiques comme montrés, par exemple, dans la figure 4 (page 33).

Exploitation des mesures PIMS

Pour beaucoup de molécules biologiques, les IE adiabatiques ainsi que les divers AE n'étaient pas connues auparavant. En plus, le peu de valeurs disponibles pour ces énergies étaient souvent de précision insatisfaisante car basées sur des mesures utilisant l'impact électronique (EI) comme méthode d'ionisation. De plus, une sensibilité de détection insuffisante des appareils employés dans le passé a souvent mené à des mesures trop élevées des IE et AE (voir plus bas). Ces lacunes ont donc constitué une très forte motivation pour nos travaux : des données plus précises de ces valeurs permettent en effet souvent la distinction, pour des raisons thermochimiques, entre différents chemins de fragmentation. Pour exploiter une nouvelle mesure d'AE, deux effets doivent être pris en compte :

1) Les mesures d'AE des photofragments sont des valeurs thermochimiques *effectives*. Elles peuvent être plus élevées par rapport à la différence entre les enthalpies de formation des réactifs et produits de la réaction de dissociation respective à cause d'une éventuelle barrière d'activation E_0 de la réaction. La différence en énergie entre la barrière d'activation et le seuil thermochimique de la réaction est stockée en tant que énergie interne (cinétique, vibration, rotation) dans le fragment considéré, formé lors de la photoionisation dissociative.

2) Les valeurs d'AE reflètent également un certain décalage cinétique (*« kinetic shift »*). En effet, un processus de fragmentation particulier (équation de réaction (2)) doit posséder une

certaine vitesse, *spécifique au spectromètre de masse utilisé*, pour que le cation formé par dissociation soit détectable.

$$M + h\nu \rightarrow M^+ + e^- \rightarrow m_1^+ + x\, n_i \qquad (2)$$

Généralement, cette vitesse est fonction de l'énergie interne (E_{int}) qu'on dépose dans la molécule. Cette fonction peut être décrit selon la théorie de Rice, Ramsperger et Kassel (théorie « RRK »; Forst, 1973 ; équation 3) :

$$k\,(E_{int}) = \nu\,[(E_{int} - E_0) / (E_{int})]^{s-1} \qquad (3)$$

Ici, s (= 3 N_A-6) est le nombre des oscillateurs vibrationnels de la molécule. s-1 représente donc le nombre de degrés de liberté de la molécule moins celui qui correspond à la coordonnée de la réaction. Le facteur de fréquence ν représente, en partie, l'efficacité de la redistribution vibrationnelle intramoléculaire (IVR). Il est lié à au rapport des fonctions de partition de l'état fondamental électronique et de l'état de transition de la réaction. E_0 est la barrière d'activation de la réaction.

Il a été démontré par Jochims et al. (1994) que *dans notre expérience* le taux de photodissociation est de l'ordre de $k_{diss} \approx 10^4\ s^{-1}$ au seuil de la formation du fragment cationique respectif. Ces auteurs ont utilisé le même spectromètre de masse qui a été utilisé pour les mesures présentées dans cet ouvrage. Leur estimation est basée sur une étude de Neusser (1989) qui a mesuré les taux de dissociation k_{diss} de la perte d'hydrogène du benzène (réaction 4) *en fonction de l'énergie interne* déposée dans l'ion mère.

$$C_6H_6 + h\nu \rightarrow C_6H_5^+ + H + e- \qquad (4)$$

Jochims et al. (1994) ont ensuite effectué des calculs RRK concernant la photodissociation des HAP, en particulier leur réaction de perte d'hydrogène, afin de connaître les énergies internes nécessaires pour les photodissocier avec $k_{diss} = 10^2\ s^{-1}$. Ceci est intéressant parce que les taux d'émission infrarouge des espèces aromatiques neutres et ioniques se trouvent dans le domaine de 1 à $10^3\ s^{-1}$. Ainsi, on peut distinguer à quelle énergie interne (cette valeur est dénommée « E critique », E_{crit}) une molécule fragmente ou subit plutôt une conversion interne liée à l'émission IR. Pour les HAP étudiés par Jochims et al. (1994), E_{crit} se situe uniquement entre 8 à 14 % en dessous de E_{int}.

3) A cause du décalage cinétique, les AE sont donc de fait dépendantes de la sensibilité de détection du spectromètre de masse utilisé parce qu'un certain nombre de cations doit être formé rapidement afin de pouvoir observer un pic de masse. Comme la vitesse de fragmentation augmente avec E_{int}, une sensibilité de détection trop faible mène à une mesure d'AE trop élevée.

En conclusion, les AE mesurées représentent toujours des valeurs limites supérieures. En appliquant l'équation (5) ci-dessous, des enthalpies de formation « *apparentes* », « *app-*$\Delta_f H°$ *(*m_1^+*)* » pour un cation m_1^+ peuvent être calculées. Chaque cation peut être formé via un chemin différent, non-connu à priori. Ainsi, dans l'équation (2) et (5), un ou plusieurs (!) fragments neutres n_i doivent être considérés, incluant leurs isomères.

$$M + h\nu \rightarrow M^+ + e^- \rightarrow m_1^+ + x\, n_i \qquad (2)$$

$$app\text{-}\Delta_f H°_{gas}(m_1^+) = AE + \Delta_f H°_{gas}(M) - \sum_{i=1}^{x} [\Delta_f H°_{gas}(n_i)] \qquad (5)$$

La valeur (apparente) $\Delta_f H°_{gas}$ (m_1^+) mesurée est ensuite comparée à l'enthalpie de formation de ce cation de la littérature, si elle est connue. Dans le cas d'un accord, le chemin de fragmentation particulier peut être approuvé. Par exemple, le schéma de fragmentation montré en figure 5 (page 33) a été dérivé ainsi (détails voir discussions dans Jochims et al., 2005, publication ci-jointe). Si une valeur $\Delta_f H°_{gas}$ (m_1^+) n'est pas disponible dans la littérature, l'enthalpie $\Delta_f H°_{gas}$ (m_1^+) mesurée représente une *nouvelle valeur* à employer désormais pour m_1^+.

Nous souhaitons donc susciter des travaux de chimie théorique grâce à nos expériences PIMS, concernant la thermochimie et la structure des fragments formés (cationiques et neutres), mais également concernant les constantes de vitesse de fragmentation, afin de clarifier encore plus les chemins de fragmentation dans le VUV.

3.5 Observation des fragments neutres : spectroscopie de fluorescence induite par rayonnement synchrotron (*FIRS)*

Pour des mesures de fluorescence, le RS est focalisé dans une cellule qui contient la vapeur du composé à étudier sous une pression de typiquement 10^{-3} mbar (fig. 2d) A cette cellule est attachée, via une fenêtre en quartz, un monochromateur secondaire (Jobin-Yvon H20, dispersion linéaire 4 nm/mm) suivi d'un photomultiplicateur. La fluorescence induite,

généralement produite par des fragments photoexcités, est observée dans un domaine spectral de 250 à 550 nm. La résolution spectrale dépend du choix de la fente de sortie (0.5, 1, 2 mm ou sans fente résultant à une largeur de fente effective de 8 mm), la « fente d'entrée » étant définie par l'extension spatiale du faisceau du RS. La fonction de transmission spectrale de ce système a été déterminée par l'enregistrement du spectre d'émission d'une lampe tungsten (2500 K). Les spectres observés ont été déconvolués en utilisant la loi de Planck.

Pour enregistrer un spectre d'excitation (*« fluorescence excitation spectrum, FEX »*), le monochromateur secondaire est fixé à une longueur d'onde choisie (par exemple à λ = 310 nm correspondant à la transition $X^2\Pi \leftarrow A^2\Sigma^+$ du fragment OH), avec fente de sortie large. Le monochromateur primaire est ensuite balayé avec des pas de typiquement 30 meV. Le spectre FEX ainsi observé est divisé par la fonction de transmission spectrale du monochromateur primaire. La calibration absolue de l'intensité observée de fluorescence est effectuée en la normalisant par rapport à la fluorescence du N_2^+ ($X\ ^2\Sigma_g^+ \leftarrow B\ ^2\Sigma_u^+$) dont le rendement quantique = 1, suite à une photoexcitation à E = 18 eV, est connu. Le spectre FEX révèle, en conjonction avec le spectre de photoabsorption, les états électroniques de la molécule mère (neutre) produisant le photofragment émetteur. Les rendements quantiques de fluorescence, *spécifiés par état électronique*, peuvent ainsi être déterminés.

Contrairement à la spectrométrie de masse, la spectroscopie de fluorescence nous permet l'étude des processus de fragmentation en dessous de la première énergie d'ionisation de l'espèce.

4. Résumé et discussion des résultats principaux

La figure 3 montre toutes les molécules prébiotiques étudiées par notre groupe à ce jour. Par contre, pour cette notice j'ai décidé de ne présenter que des résultats sélectionnés qui ont été obtenus depuis ma thèse de doctorat. Ainsi, dans ce chapitre 4, sont décrits nos résultats principaux sur les bases N-hétérocycliques, les acides aminés et les espèces HCOOH, CH_3COOH et $HCOOCH_3$. Des discussions plus détaillées peuvent être trouvées dans mes publications dont cinq sont ci-jointes en texte intégral. Aussi, nos résultats très récents sur les coefficients d'absorption à basse température des polyynes et cyanopolyynes, non-publiés à ce jour, ne font pas partie de cette notice.

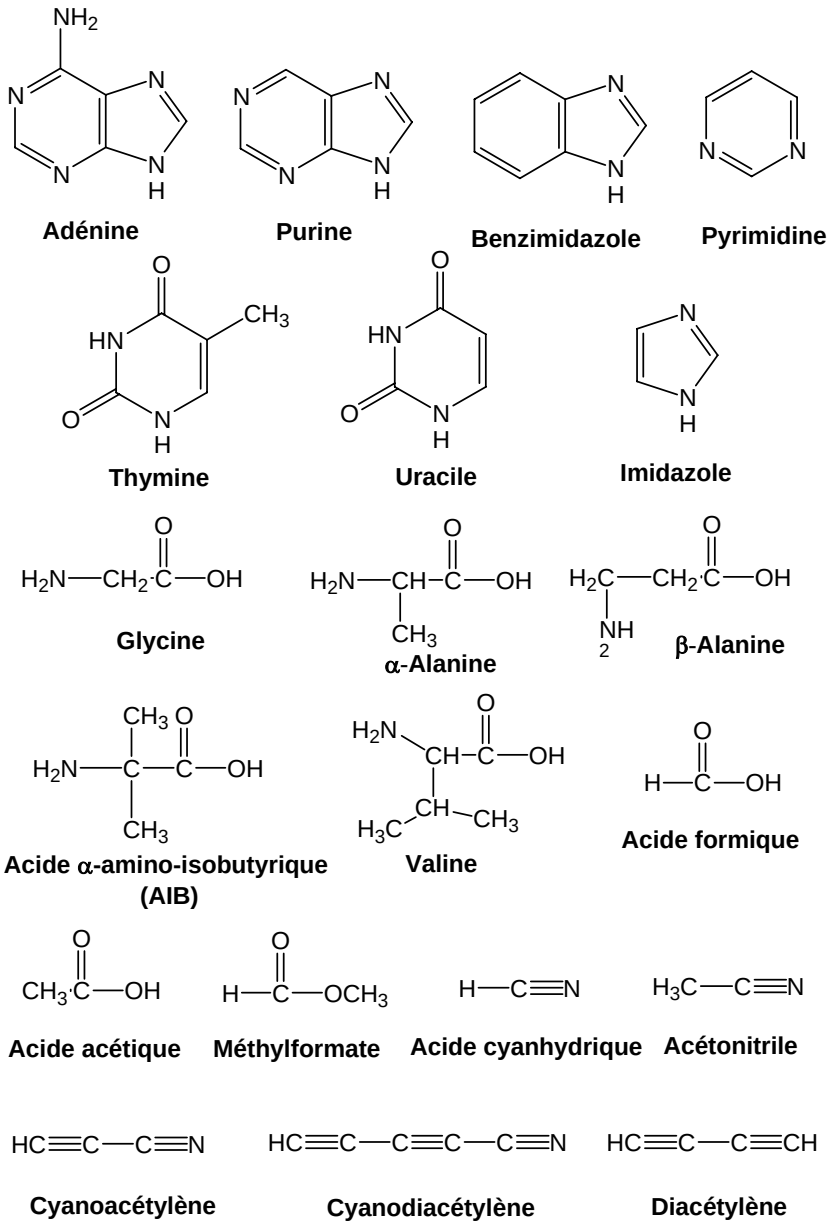

Figure 3 : Molécules prébiotiques dont la photochimie VUV a été étudiée par notre groupe.

4.1. Ionisation et ionisation dissociative des bases N-hétérocyliques

Les bases N-hétérocycliques ont été étudiées par spectrométrie de masse photoionique (PIMS) (Jochims et al., 2005; Schwell et al., 2006). La partie supérieure du tableau 1 résume ces résultats. Nos résultats sur les acides aminés, qui sont discutés au paragraphe 4.2, sont également intégrés dans la partie inférieure de ce tableau. Nous montrons les mesures de la première énergie d'ionisation ($1^{ère}$ IE) ainsi que l'énergie seuil de formation du fragment formé par le chemin d'ionisation dissociative *le plus bas en énergie* (appelée $1^{ère}$ AE). La troisième colonne de ce tableau donne la différence entre ces 2 valeurs, dénommé E_{int}. E_{int} indique l'énergie nécessaire pour photodissocier la molécule avec un taux de dissociation $k_{diss} = 10^4\ s^{-1}$ (cf. paragraphe 3.4).

Tableau 1 : Mesures des premières énergies d'ionisation (valeurs adiabatiques), énergies seuil du chemin de fragmentation le plus bas en énergie ($1^{ère}$ AE), énergie interne au seuil de le fragmentation (E_{int} = $1^{ère}$ IE – $1^{ère}$ AE), et chemin de fragmentation correspondant.

	$1^{ère}$ IE_{ad} [eV]	$1^{ère}$ AE [eV]	E_{int} [eV]	Chemin de Fragmentation
Adénine	8.20 ± 0.03	11.56 ± 0.05	3.36 ± 0.08	Perte de HCN
Purine	9.35 ± 0.05	12.6 ± 0.05	3.25 ± 0.1	Perte de HCN
Benzimidazole	8.22 ± 0.05	13.57 ± 0.1	5.35 ± 0.15	Perte de HCN
Thymine	8.82 ± 0.03	10.70 ± 0.05	1.88 ± 0.08	Perte de HNCO
Uracile	9.15 ± 0.03	10.95 ± 0.05	1.80 ± 0.08	Perte de HNCO
Pyrimidine	9.05 ± 0.05	12.27 ± 0.05	3.22 ± 0.1	Perte de HCN
Imidazole	8.66 ± 0.03	11.41 ± 0.05	2.75 ± 0.08	Perte de HCN [(a)]
Glycine	9.02 ± 0.02	9.38 ± 0.05	0.36 ± 0.07	$NH_2CH_2^+$ + COOH
α-Alanine	8.75 ± 0.05	9.05 ± 0.1	0.3 ± 0.15	$NH_2CH_3CH^+$ + COOH
β-Alanine	8.8 ± 0.1	9.3 ± 0.1	0.5 ± 0.2	$NH_2CH_2^+$ +CH_2COOH
Acide α-amino-isobutyrique	9.6 ± 0.2	9.1 ± 0.1 [(b)]	(0)	$NH_2C(CH_3)_2^+$ + $COOH^-$
Valine	8.9	-	-	$NH_2(CH_3)_2(CH)_2^+$ [(c)]+ COOH

[(a)] Deux autres chemins de fragmentation (perte de H ; perte de HCNCH) ont des énergies seuil de formation similaires (Schwell et al., 2006).
[(b)] Formation des paires d'ions en dessous du seuil du premier seuil d'ionisation.
[(c)] Ion le plus intense à E = 20 eV.

Les bases d'ADN/ARN étudiées ont des valeurs d'E_{int} qui vont de 1.80 eV (uracile) à 3.36 eV (adénine). Pour la base non-biologique benzimidazole E_{int} est égale à 5.35 eV. Ces valeurs sont assez élevées indiquant ainsi la stabilité du cation mono-chargé de ces molécules. Par contre elles sont plus basses que pour les hydrocarbures polycycliques aromatiques (HAP),

pour lesquels les valeurs d'E_{int} situées entre 4.62 eV (benzène) et 12.05 eV (coronène) ont été trouvées (Jochims et al., 1994, 1999). Une autre différence caractéristique entre HAP et bases d'ADN est que le chemin d'ionisation dissociative le plus bas en énergie n'est pas la perte d'hydrogène dans les bases d'ADN, comme cela a été observé dans les études sur les HAP, mais la perte de l'acide cyanhydrique (HCN) ou de l'acide isocyanique (HNCO). Notons que la perte de HCN (ou de HNCO) implique la rupture de deux liaisons. La raison pour ce comportement est très certainement la grande stabilité thermodynamique de la molécule HCN ($\Delta_f H° = 1.401$ eV (Chase, 1998)). Pour toutes les bases étudiées on peut observer que, en dessous de 20 eV, ou bien la perte d'hydrogène n'est pas observée, ou bien l'ion $(M-H)^+$ est d'intensité très faible, à l'exception de l'imidazole (masse moléculaire 68.08 u.m.a.) dont le seuil de formation du fragment m/z = 67 est égale à 12.05 ± 0.03 (Schwell et al., 2006).

La figure 4 donne un exemple de nos mesures PIMS : nous montrons des courbes de rendement photoionique de l'adénine (masse moléculaire = 135.13 u.m.a.) et de ses ions fragments les plus importants. L'énergie d'ionisation adiabatique est 8.20 ± 0.03 eV. La figure 5 montre les chemins de fragmentation déduits de nos mesures avec également l'aide des mesures antérieures utilisant l'impact électronique comme méthode d'ionisation (voir aussi notre discussion détaillée et références citées dans Jochims et al., 2005). Sont inclus dans la figure 5 les énergies seuil de formation des fragments ainsi que des hypothèses sur la structure chimique de certains fragments. Ces propositions de structure doivent être étayées dans le futur (par exemple par des calculs ab-initio).

Le chemin de fragmentation principal de l'adénine concerne la perte successive de 4 molécules de HCN (cf. fig. 5). La perte initiale inclut les atomes 1 et 2 (numérotation fig. 5) de cette molécule (Barrio et al., 1981, Sethi et al., 1982 : ces travaux sont discutés dans Jochims et al., 2005) et requiert, comme cela a été déjà mentionné, la rupture de deux liaisons. Cette perte consomme plus d'énergie par rapport aux pertes de HCN suivantes, probablement parce que ces dernières ne requièrent que la rupture d'*une* liaison de l'ion précurseur respectif et/ou parce que l'énergie totale de réorganisation structurale du système devient de plus en plus petite. Les mécanismes de pertes successives de HCN peuvent être très complexes et ne sont pas connus en détail à ce jour. Ils peuvent impliquer la perte de l'isomère HNC également.

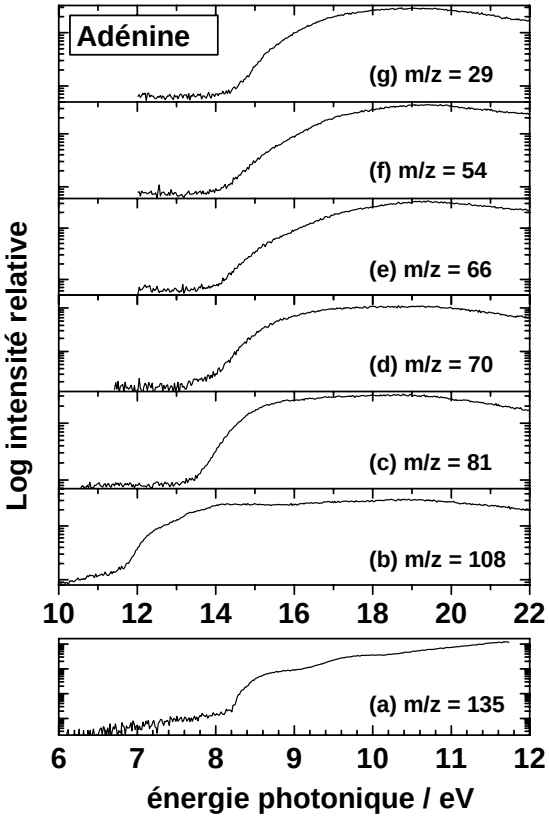

Figure 4 : Spectres PIMS des différents fragments cationiques d'adénine. L'énergie seuil de formation (AE) de chaque cation est déterminée graphiquement, par le point d'intersection entre la tangente de la courbe dans la région du seuil et une droite qui passe par la moyenne du bruit avant le seuil.

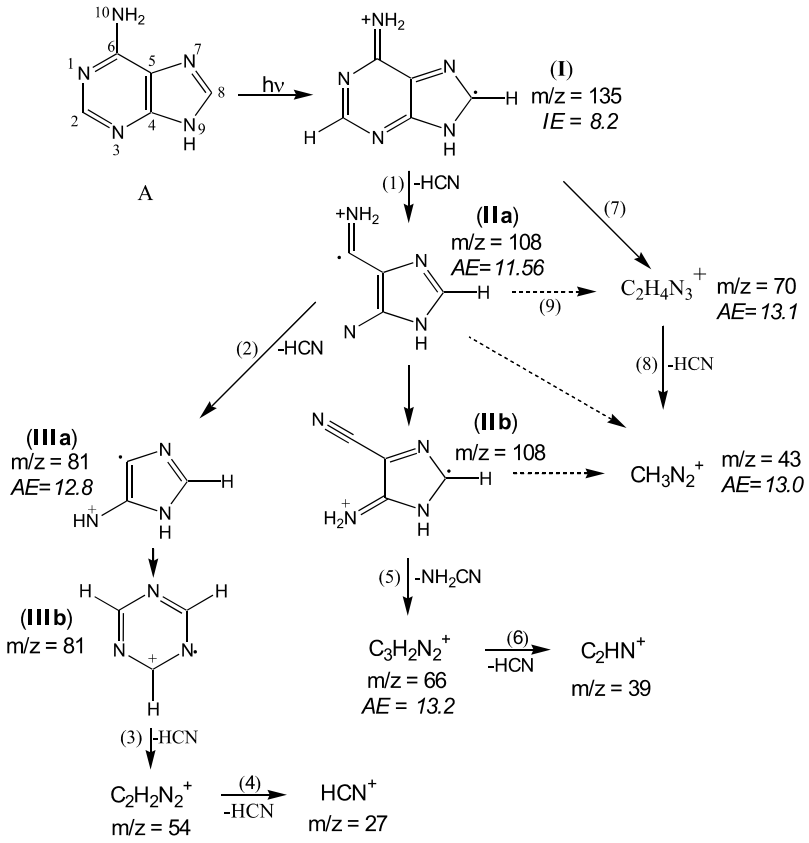

Figure 5 : Schéma de fragmentation de l'adénine ($C_5H_5N_5$) dans le VUV. Les énergies seuil de formation de chaque ion (AE), telles que mesurées lors de nos expériences, sont données également.

Le destin du fragment primaire IIa (m/z = 108 u.m.a.) peut être la perte de l'espèce C_2N pour donner naissance à l'ion m/z = 70 (réaction 9 dans la fig. 5) ou bien son isomérisation pour donner l'espèce IIb qui est probablement thermodynamiquement plus stable que IIa. L'espèce IIb fragmente en générant l'ion important[1] m/z = 66 via la perte de NH_2CN. L'ion m/z = 66 peut perdre une molécule de HCN par la suite pour former l'ion m/z = 39. L'ion intense m/z = 43 ($CH_3N_2^+$) peut être formé par plusieurs chemins comme cela est indiqué en figure 5.

Nous avons constaté un comportement similaire lors d'une étude très récente sur le bases purine et benzimidazole (Schwell et al., 2006). Concernant la purine (masse moléculaire = 120.11 u.m.a.), la perte successive de 2 molécules de HCN prédomine aux basses énergies photoniques (E < 13.6 eV). Les énergies seuils correspondantes sont 12.6 ± 0.05 eV et 13.24 ± 0.1 eV. L'ion parent de la base benzimidazole (masse moléculaire = 118.14 u.m.a.) dévoile un domaine de stabilité remarquable, de 8.22 ± 0.05 eV jusqu'à 13.57 ± 0.1 eV (E_{int} = 5.35 ± 0.15 eV, voir tableau 2).

Concernant la base thymine, la fragmentation dominante est la perte d'acide isocyanique (HNCO) via réaction Rétro-Diels-Alder du cation parent (Jochims et al., 2005). Ceci donne naissance au fragment m/z = 83 u.m.a. (AE = 10.7 eV). L'ion m/z = 83, qui pourrait posséder une structure cyclique, est assez stable puisqu'il faut ajouter 1 eV supplémentaire afin d'induire une fragmentation supplémentaire (perte de CO). Dans l'uracile également (masse moléculaire 112.09 u.m.a.), la perte de HNCO est le chemin de fragmentation le plus bas en énergie (AE = 13.75 eV). La fragmentation supplémentaire donne naissance à l'ion intense $HCNH^+$ (m/z = 28, AE = 13.75 eV) qui a de l'importance en astrophysique (cf. discussion en chapitre 5). Dans la fragmentation des bases non-biologiques de pyrimidine et d'imidazole, la perte de HCN domine comme c'est le cas pour l'adénine, la purine et le benzimidazole.

Notons enfin que des calculs quanto-chimiques, comme ceux effectués par Improta et al. (2000) sur la structure et la thermodynamique des cations radicalaires issus de la fragmentation de la thymine, sont extrêmement utiles dans l'analyse des chemins de dégradation. Nos expériences de spectrométrie de masse pourraient ainsi inciter des travaux théoriques sur la stabilité des fragments (neutres et cationiques).

[1] Un ion « important » veut dire de forte intensité dans cette notice.

4.2. Ionisation et ionisation dissociative des acides aminés

Une discussion détaillée de nos résultats sur les acides aminés est donnée par Jochims et al. (2004). Les 5 acides aminés que nous avons étudiés sont tous trouvés dans la matière météoritique (Cronin, 1995). Les résultats principaux sont résumés dans le tableau 1. Je signale que dans les milieux biologiques en phase condensée, les acides aminés existent en tant que *« zwitterions »* dans un domaine large de valeurs pH, mais qu'en phase gazeuse cette forme particulière n'a jamais été observée auparavant. C'est pourquoi nous supposons que, dans nos études, seuls les monomères neutres d'acides aminés existent en phase gazeuse.

La photoabsorption des acides aminés a été étudiée par calculs quanto-chimiques auparavant (Serrano-Andrés et Fülscher, 1996 et références qui y sont citées). Les acides aminés absorbent fortement à la fréquence de la raie de Lyman-α (10.2 eV). A notre connaissance, aucune mesure de photoabsorption en phase gazeuse n'est disponible dans la littérature.

Fragmentation VUV de la glycine (NH_2CH_2COOH)

Le spectre de masse de la glycine (masse moléculaire = 75.07) à 10 eV présente 3 pics de masse correspondant aux ions m/z = 75, 30, 28. L'énergie d'ionisation de la glycine a été déterminée à IE = 9.02 ± 0.02 eV. C'est la première valeur d'IE mesurée par photoionisation pour cette molécule. Elle est 0.2 eV plus basse par rapport aux mesures effectuées utilisant l'impact électronique comme méthode d'ionisation.

Avec l'aide du spectre de masse glycine-D5 nous avons pu attribuer la masse m/z = 30 au cation radicalaire aminométhyle, $NH_2CH_2^+$, formé par rupture simple de la liaison C-C de la molécule (perte de COOH) :

$$NH_2\text{-}CH_2\text{-}COOH \rightarrow NH_2CH_2^+ (m/z = 30) + COOH \qquad (6)$$

La formation de H_2CO^+ peut ainsi être exclue parce que l'ion D_2CO^+ (m/z = 32) est absent dans le spectre de masse de glycine-D5. La formation de l'isomère CH_3NH^+ est très invraisemblable parce que cette espèce est thermodynamiquement moins stable par 88 kJ/mol et sa formation impliquerait en plus le réarrangement de l'ion parent ou de l'ion fragment initialement formé. La formation de $NH_2CH_2^+$ est donc le chemin de fragmentation le plus plausible. L'énergie seuil de formation de cette espèce a été déterminée comme étant AE = 9.38 ± 0.05 eV.

Pendant la rédaction de ce document, un article de Wilson et al. (2006a) a paru : ce groupe utilise la technique de spectrométrie de masse à nanoparticules afin de mesurer des courbes de rendement photoioniques, avec le RS comme rayonnement VUV ionisant. Cette technique est pratiquement la même que celle que je suis en train de développer pour l'étude l'aérosol atmosphérique (cf. chapitre 6.2 : description de SPLAM, et chapitre 7.2.2). Il est à noter que Wilson et al. (2006a) ne trouvent pas le même résultat que nous : en particulier l'ion m/z = 30 est absent de leur spectre de masse de glycine enregistré à E = 10.5 eV. D'un autre coté, la courbe photoionique de l'ion mère mesurée par Wilson et al. (2006a) est quasiment identique à la nôtre, dans la région du seuil d'ionisation. Dans nos mesures, un filtre LiF a été utilisé : il est donc exclu que notre ion m/z = 30 ait été formé par la lumière diffusée de haute énergie, problème inhérent des expériences avec le RS.

Wilson et al. (2006a) sont par ailleurs en contradiction avec les mesures antérieures de Svec et Junk (1967) utilisant l'impact électronique comme méthode d'ionisation. Svec et Junk (1967) donnent une valeur de AE = 10.23 ± 0.09 eV pour l'ion $(M\text{-}COOH)^+$ de la glycine. Une autre mesure est fournie par Zaretskii et al. (1971) qui trouve AE (m/z = 30) = 10.27 ± 0.05 eV. Ces valeurs sont bien plus élevées que la notre (AE = 9.38 ± 0.09 eV) mais cette différence n'est néanmoins pas étonnante pour des raisons de sensibilité réduite des détecteurs utilisés antérieurement. Aussi, la section efficace d'ionisation par impact électronique est généralement plus faible par rapport à la photoionisation, ce qui réduit encore plus la sensibilité des appareils utilisés auparavant (voir la discussion dans le paragraphe 3.4).

Nous concluons que l'absence de l'ion m/z = 30 dans le spectre de masse de Wilson et al. (2006a) à 10.5 eV est probablement liée à une vitesse de fragmentation faible de la réaction (6) : l'ion mère de la glycine serait donc « métastable » par rapport à sa dissociation en $NH_2CH_2^+$ et COOH dans leurs conditions d'extraction de la source d'ions. En effet, Wilson et al. (2006a) utilisent un spectromètre de masse à temps de vol. Le temps de vol des petits ions étant de quelques microsecondes, les réactions plus lentes ne peuvent donc pas être observées. Le spectromètre de masse quadripolaire employé par notre groupe est par contre capable de « voir » des réactions plus lentes, de l'ordre de 100 μs environ (voir paragraphe 3.4).

L'ion mère de la glycine perd donc très facilement le groupe COOH, c'est-à-dire à une énergie E_{int} = 0.36 ± 0.07 eV au-dessus de la première énergie d'ionisation. L'ion m/z = 28 est également présent dans les spectres de masse de la glycine. Il est attribué au cation $HCNH^+$ parce que les isomères H_2CN^+ et CNH_2^+ sont moins stables thermodynamiquement (De Frees et McLean, 1985). Notons que le seuil de formation de cet ion a été difficile à déterminer

(autour de 9 eV) parce que la courbe de rendement photoionique est assez aplatie aux faibles énergies. Différents chemins peuvent mener à la formation de $HCNH^+$ comme cela a été discuté dans Jochims et al. (2004).

Notons également que $HCNH^+$ a été observé dans plusieurs sources galactiques dans le MIS (Schilke et al., 1991), incluant la région où la glycine aurait été observée (SgrB2). La capture d'électron par $HCNH^+$ est considérée comme étant une source importante de HCN (+H) et HNC (+H), molécules importantes dans la chimie prébiotique, dans les nuages moléculaires sombres (Schilke et al, 1991 ; Semianak, 2001). Nos résultats suggèrent donc que l'ion $HCNH^+$ puisse être formé à partir de la glycine dans les régions HI du MIS où la limite énergétique supérieure des photons disponibles est 13.6 eV. Il est donc raisonnable de proposer que les recherches futures de la glycine devraient se concentrer plutôt dans les régions où simultanément l'ion $HCNH^+$ est observé et où en plus la glycine pourrait être protégée du rayonnement VUV, par exemple par la présence des grains interstellaires. Notons finalement que $HCNH^+$ est aussi un ion important dans l'ionosphère de Titan (Molina-Cuberos et al., 1999).

Fragmentation VUV d'autres acides aminés

En dessous de 13.6 eV, les chemins de fragmentation principaux de l'α-alanine (masse moléculaire = 89.09 u.m.a.) concernent la formation des ions m/z = 44, 42, 28, 18. Les mesures de leurs énergies seuil de formation sont présentées dans Jochims et al. (2004). Des travaux antérieurs (Junk et Svec, 1963) utilisant l'impact électronique comme méthode d'ionisation ont aidé à l'attribution des structures chimiques des ions observés. Comme c'est le cas pour la glycine, le chemin de fragmentation ionique le plus bas en énergie correspond à la rupture de la liaison C(α)-C(OOH) de l'ion parent pour donner naissance à l'ion $NH_2CH_3CH^+$ (m/z = 44, AE = 9.05 ± 0.1 eV) :

$$CH_3\text{-}CH(NH_2)\text{-}COOH \rightarrow NH_2CH_3CH^+ (m/z = 44) + COOH \qquad (7)$$

$HCNH^+$ (m/z = 28) est aussi un ion très intense dans la fragmentation du α-alanine (AE = 12.35 eV). L'ion m/z = 74, formé par la perte du groupe méthyle attaché au carbone-α, est de faible intensité ce qui signifie que ce chemin de fragmentation est mineur.

Dans l'ionisation dissociative du β-alanine, la formation de l'ion le plus important (m/z = 30, attribué au $NH_2CH_2^+$, AE = 9.3 ± 0.1 eV) correspond à une rupture entre carbone-α et carbone-β. Avec l'aide de la thermochimie nous avons pu conclure que l'espèce *neutre*

formée dans ce chemin de fragmentation est le radical CH_2COOH et non pas le CH_3COO (Jochims et al, 2004) :

$$H_2N\text{-}CH_2\text{-}CH_2\text{-}COOH \rightarrow NH_2CH_2^+ (m/z = 30) + CH_2COOH \quad (8)$$

La formation de $HCNH^+$ est moins important dans l'ionisation dissociative de la β-alanine (AE = 14.2 ± 0.1 eV) que dans celle de l'α-alanine.

Un autre cas intéressant est l'acide α-amino isobutyrique (« AIB », masse moléculaire 103.12 u.m.a.), le seul acide aminé rare sur terre qui a été étudié par notre groupe. L'énergie seuil de formation de son fragment le plus intense (m/z = 58, AE = 9.1 ± 0.1 eV) est plus basse que son énergie d'ionisation (IE = 9.6 ± 0.2 eV) ce qui signifie que la formation de la paire d'ions $NH_2C(CH_3)_2^+$ et $COOH^-$ contribue largement au pic de masse m/z = 58. Un autre ion très intense est observé à m/z = 42 (AE = 9.3 eV). Cet ion est formé très probablement par la perte de NH_2 à partir de $NH_2C(CH_3)_2^+$, issue de la formation de la paire d'ions mentionnée ci-dessus (Jochims et al., 2004).

4.3. Autres molécules prébiotiques : Acide formique, acide acétique et formate de méthyle

L'acide formique, l'acide acétique et le formate de méthyle ont toutes été observées dans le milieu interstellaire (Müller et al., 2005). C'est pourquoi nous avons mené une campagne intensive afin d'explorer plus les propriétés photophysiques VUV de ces importantes molécules (Schwell et al., 2002; Leach et al., 2002, 2003, 2006a et b).

Acide formique (HCOOH)

Notons d'abord que nos spectres photoélectroniques HeI (E_{exc} = 21.21 eV) à haute résolution (15 meV) des 4 isotopologues de l'acide formique (HCOOH, DCOOH, HCOOD, DCOOD) ont été utilisés par Rudberg et Brinck (2004) pour améliorer le calcul des facteurs Franck-Condon des transitions de l'état fondamental vers les états électroniques les plus bas du cation moléculaire de l'acide formique. Pour cette notice, j'ai choisi de montrer les spectres de fluorescence induite par photoexcitation VUV de cette molécule (figures 6 et 7).

La figure 6 montre le spectre de fluorescence *dispersée* à une énergie d'excitation de E_{exc} =12 eV (Schwell et al., 2002). Le spectre exposé est non-lissé et corrigé pour la réponse spectrale du système de détection (monochromateur secondaire et photomultiplicateur). A cette énergie nous observons 2 systèmes de bandes de fluorescence : le premier système peut

être attribué à l'émission du radical OH ($X^2\Pi \leftarrow A^2\Sigma^+$), à 308 nm (0-0) et 282 nm (1-0). Le second système consiste en une progression vibrationnelle entre 330 et 480 nm, dont le maximum d'intensité se trouve à 375 nm. L'espacement des bandes, de 600 ± 40 cm^{-1}, est très régulier et leur largeur est probablement limitée par la résolution spectrale de notre monochromateur secondaire (5 nm ici). Il s'agit très probablement du mode de pliement dans le groupement OCO de la molécule émettrice qui a été attribuée comme étant le radical HCOO avec l'aide des travaux antérieures à plus basse énergie (10 eV : Suto et al., 1988 ; cf. discussion dans Schwell et al., 2002). A 10 eV une progression très similaire a été observée. HCOO est un isomère de COOH (COOH est souvent appelé « HOCO » dans la littérature). L'identification tentative de l'état émetteur et de l'état final de l'émission du radical HCOO ($^2A_2 \leftarrow {}^2B_1$) a été discutée dans Schwell et al. (2002, publication ci-jointe). Elle a pu être réalisée à l'aide de calculs ab-initio antérieurs (Rauk et al., 1995).

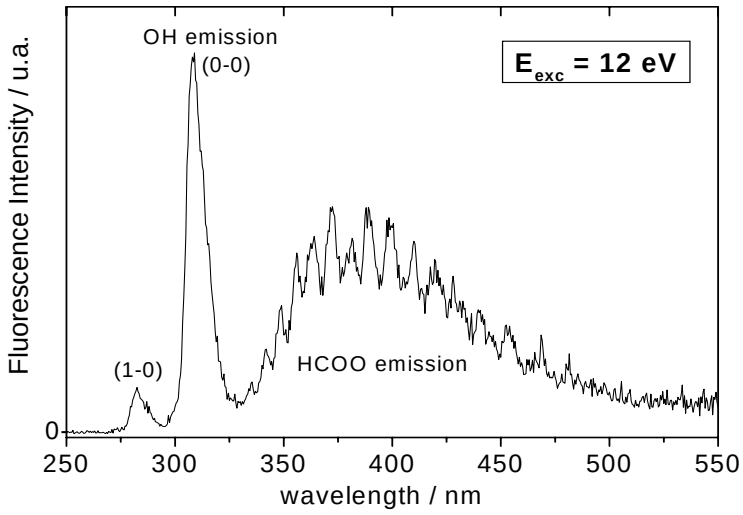

Figure 6 : Spectre de fluorescence *dispersée* suivant photoexcitation de l'acide formique à E = 12 eV. Résolution spectrale : 5 nm.

En figure 7 nous montrons les spectres d'*excitation* de fluorescence (FEX), entre 9 et 13 eV, de l'émission OH ($X^2\Pi \leftarrow A^2\Sigma^+$) et de l'émission HCOO ($^2A_2 \leftarrow {}^2B_1$) (fig. 7b), en comparaison avec le spectre de photoabsorption de l'acide formique (fig. 7a). Le spectre d'absorption de HCOOH a été discuté en détail par Leach et al. (2002). L'émission du radical OH est observée à $\lambda_{obs} = 310$ nm et celle de HCOO est observée à $\lambda_{obs} = 375$ nm. Généralement, on constate que les spectres FEX évoluent parallèlement avec le spectre

d'absorption. Les positions des bandes FEX coïncident pratiquement toutes avec les bandes d'absorption, mais leurs rapports d'intensités sont différents indiquant différents rapports de branchement des réactions (9) et (10) ci-dessous :

$HCOOH \rightarrow HCO + OH\ (A^2\Sigma^+)$ $\quad E > 8.85$ eV (calc.) (9)

$HCOOH \rightarrow HCOO\ (^2B_1) + H$ $\quad E > 9.075 \pm 0.1$ eV (exptl.) (10)

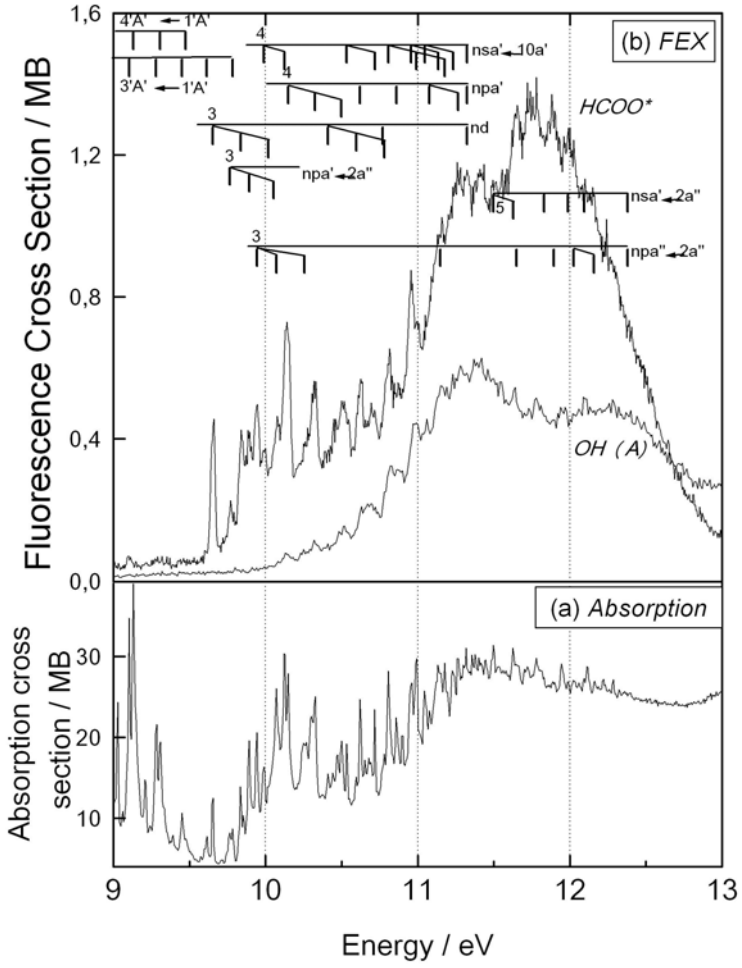

Figure 7 : (a) Spectre d'absorption de l'acide formique et (b) Spectres *d'excitation* de fluorescence (FEX) de l'acide formique entre 9 et 13 eV. Emetteurs : (1) OH ($A^2\Sigma^+$), λ_{obs} = 310 nm ; (2) HCOO ($^2B_1$), λ_{obs} = 375 nm).

Dans le spectre FEX de l'espèce OH nous pouvons identifier le seuil de l'émission à 9.15 ± 0.03 eV (136.6 nm ; voir aussi la région du seuil agrandie dans la publication originale Schwell et al. (2002), ci-jointe). L'énergie du terme électronique T_e de l'état OH ($A^2\Sigma^+$) étant de 32684.1 cm^{-1} (Huber et Herzberg, 2005), le seuil thermochimique de la réaction (9) est

calculé à 8.85 eV. Ce seuil calculé est environ 400 meV plus bas que notre seuil observé, ce qui pourrait signifier qu'il existe une barrière de potentiel entre l'état excité du HCOOH et la surface de potentiel qui mène à la dissociation pour former le fragment OH dans son état excité $A^2\Sigma^+$. La croissance douce de l'émission, en fonction de l'énergie, est de plus typique d'une dissociation photochimique avec une barrière de potentiel. Néanmoins, la sensibilité de détection de l'appareil est certainement limitée ce qui signifie que notre valeur de 9.15 ± 0.03 eV représente en effet une limite supérieure. La barrière de potentiel serait donc en réalité plus basse que 400 meV. Au-delà de l'énergie d'ionisation de HCOOH (IE = 11.33 eV), l'intensité de fluorescence OH ($X^2\Pi \leftarrow A^2\Sigma^+$) baisse avec l'énergie, sans doute à cause de l'ouverture des chemins de fragmentation ioniques.

L'intensité de fluorescence de HCOO formé par la réaction (10) croit également en fonction de l'énergie (en dessous de 11.8 eV). La plupart des bandes FEX de HCOO ($^2A_2 \leftarrow {}^2B_1$) sont également observées dans le spectre FEX du OH ($X^2\Pi \leftarrow A^2\Sigma^+$), mais avec des intensités différentes. Ceci est particulièrement évident entre 10 et 11 eV (voir fig. 7b) indiquant que les états excités correspondants du HCOOH peuvent conduire à au moins 2 chemins de fragmentations mais dont les rapports de branchement varient de manière considérable.

Acide acétique (CH_3COOH)

Le spectre de photoabsorption de l'acide acétique, entre 6 et 20 eV, a été mesuré et analysé récemment par Leach et al. (2006a) (voir fig. 8a, résolution spectrale 0.9 Å). En première vue, nous pouvons observer des transitions de valence, par exemple entre 6 et 9 eV, et des transitions de Rydberg qui convergent à la première énergie d'ionisation. D'autres bandes, plus larges, apparaissent entre 12 et 18 eV.

Afin de mieux comprendre le spectre d'absorption observé, et plus particulièrement de distinguer les transitions de valence des transitions de Rydberg, nous avons effectué des calculs ab-initio sur l'acide acétique (Leach et al., 2006a). D'abord, les énergies d'ionisation des hautes orbitales moléculaires ont été calculées (par notre collaborateur S. Un) et comparées aux valeurs expérimentales issues des spectres photoélectroniques plus anciens (Carnovale et al., 1980 : ces valeurs sont indiqués avec des flèches en figure 8a). L'accord entre les IE_v mesurées et nos calculs est très satisfaisant (cf. Tableau 2 dans Leach et al. (2006a), publication ci-jointe en texte intégral). Ensuite, d'autres calculs ont été effectués sur les transitions de valence. Dix transitions de valence ont été identifiées entre 5.825 et 9.0417 eV par les calculs, avec des forces oscillateurs très différentes (cf. Tableau 3 dans

Leach et al., 2006a). Dans ce domaine d'énergie, la comparaison avec les forces oscillateurs observées permet d'estimer quelles transitions de valence contiennent des contributions de transitions de Rydberg (Leach et al., 2006a). Les bandes larges à plus hautes énergies (E > 12 eV) ont été attribuées à des transitions Rydberg superposées qui convergent à des limites d'ionisation supérieures (bandes à 12.92 eV, 13.33 eV, 15.13 eV et 15.77 eV) mais également à des transitions de valence de caractère σ–σ* (C-H) (bandes à 14.5 eV et 16.83 eV).

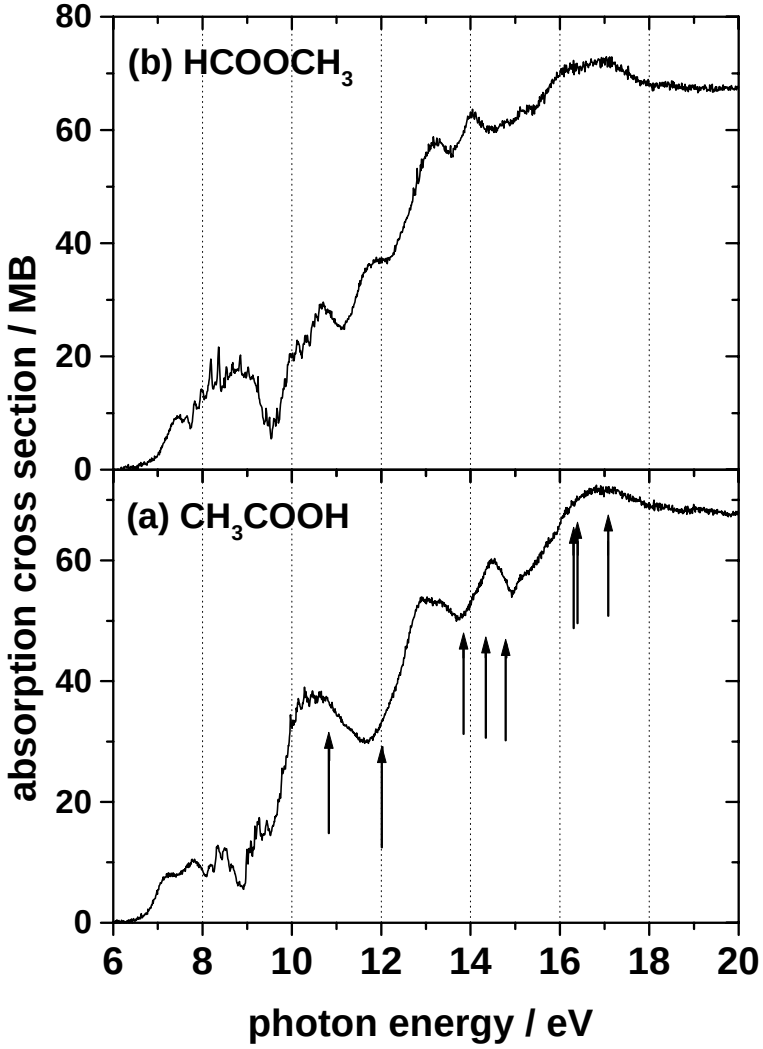

Figure 8 : Spectres d'absorption de (a) l'acide acétique et de (b) son isomère formate de méthyle. Les flèches dans figure 8a indiquent les différentes énergies d'ionisation de l'acide acétique (valeurs expérimentales de Carnovale et al., 1980).

Nous avons aussi effectué des expériences PIMS et FIRS sur l'acide acétique (Leach et al., 2006b, publication ci-jointe). L'énergie d'ionisation de CH_3COOH a été déterminée à IE = 10.58 ± 0.02 eV, légèrement plus basse que la valeur utilisée précédemment dans la littérature (base de données du NIST). Les fragments principaux formés par l'ionisation dissociative en dessous de 13.6 eV sont m/z = 45 ($COOH^+$, AE = 11.7 ± 0.05 eV) et m/z = 43

(CH_3CO^+, AE = 11.45 ± 0.05 eV). Les mesures de fluorescence ont dévoilé la formation des fragments neutres excités OH (X←A) et CH (X←A,B), mais principalement au delà de la première IE, contrairement à HCOOH. Les bandes FEX des ces émissions coïncidant parfaitement avec des bandes de photoabsorption. L'émission H-Balmer (β,γ,δ) est également observée à haute énergie (E > 15 eV), cependant les spectres FEX n'ont pas été mesurés pour ces émissions. Les processus de fragmentation qui mènent à la formation de ces émetteurs ont été discutés par Leach et al. (2006b).

Formate de méthyle ($HCOOCH_3$)

Figure 8b montre le spectre de photoabsorption du formate de méthyle (résolution spectrale 0.9 Å), un isomère de l'acide acétique. Le spectre de cette molécule présente également des transitions Rydberg qui convergent vers la première énergie d'ionisation à 10.835 eV (Waterstradt et al., 1994). Des bandes larges, entre 11 et 18 eV sont également observées ici, comme c'est le cas dans l'acide acétique. Une analyse détaillée est en cours.

A notre connaissance, les spectres de photoabsorption ainsi que de fluorescence de ces deux espèces n'étaient pas connus auparavant dans ce domaine d'énergie. Les mesures antérieures de Suto et al. (1988) étaient limitées à E < 11.2 eV. Les deux spectres d'absorption sont qualitativement similaires, dans la mesure où la section efficace de photoabsorption augmente, de 6 à 17 eV pour y atteindre un plateau à 70 MB. Notons qu'autour de 6 eV la section efficace n'est pas exactement zéro comme cela semble être le cas dans la figure 8. Une bande très faible (maximum de l'absorption $\sigma_{abs} \approx 0.3$ MB) s'étend de 200 nm (6.2 eV) à 240 nm (5.2 eV) (Suto et al., 1988). Cette bande correspond à la transition électronique $\pi^* \leftarrow n_O$. Dans nos expériences, la transmission du réseau du monochromateur primaire n'était pas suffisante pour l'observer.

Dans le milieu interstellaire, l'abondance du formate de méthyle est supérieure à celle de son isomère l'acide acétique, et ce dans plusieurs sites d'observations (Sagittarius B2-LMH ; OMC-1 ; W51 Main) (Mehringer et al., 1997 ; Hollis et al., 2001) et malgré la stabilité thermochimique supérieure de CH_3COOH. Notons qu'un troisième isomère de $C_2H_4O_2$, le glycolaldéhyde, d'abondance encore inférieure aux deux autres, peut être observé dans le MIS. Thermodynamiquement, le glycolaldéhyde est l'isomère est le moins stable. Dans SgrB2-LMH, le rapport de mélange (acide acétique) : (formate de méthyle) est estimé à 1 : 26 (Hollis et at., 2001). Pour expliquer cette différence, Mehringer et al. (1997) mettent en avant une plus grande facilité de formation d'une structure moléculaire contenant un squelette C-O-

C (formate de méthyle) par rapport à un squelette C-C-O (acide acétique), dans les conditions du MIS. Nous pensons que des différences dans le comportement photochimique dans le domaine du VUV pourraient également expliquer ces différences d'abondance déduites des observations radioastronomiques : l'acide acétique serait donc plus facilement dégradable que le formate de méthyle. Néanmoins, les spectres d'absorption de ces deux espèces ne se distinguent guère, en ce qui concerne les intensités de bandes. Ainsi, nous ne pouvons pas conclure sur ce point sans avoir étudié en détail la fragmentation photochimique VUV du formate de méthyle.

5. Conclusions et implications astrophysiques et exobiologiques

J'ai résumé dans cette notice les résultats récemment obtenus sur la photochimie des petites molécules prébiotiques et biologiques dans le domaine spectral du VUV (6-23 eV). Généralement, ces résultats sont importants dans le contexte exobiologique

- parce qu'ils pourraient permettre d'observer des espèces par télédétection dans le domaine spectral du VUV.
- et parce qu'ils aident à prédire la photostabilité des ces molécules dans les champs électromagnétiques VUV qui règnent dans les différents milieux extraterrestres (MIS, atmosphères planétaires et cométaires),
- Les photofragments principaux des molécules étudiées ont été identifiés, en fonction de la longueur d'onde d'excitation dans le VUV. Ceci est important pour comprendre la chimie prébiotique qui s'aurait déroulée ailleurs dans l'espace.
- La connaissance de l'identité de photofragments permet de contraindre les recherches spatiales futures des molécules mères.

Les molécules que nous avons étudiées sont 7 bases N-hétérocyliques, dont 2 sont des bases d'ADN (adénine, thymine) et une d'ARN (uracile), 5 acides aminés, dont 1 extrêmement rare sur terre (AIB), et des molécules considérées comme prébiotiques (HCOOH, CH_3COOH, $HCOOCH_3$, et CH_3CN). Nos résultats sur la molécule CH_3CN n'ont pas été discutés dans cette notice parce qu'ils sont en cours d'analyse.

Plus récemment j'ai commencé également d'étudier la photoabsorption à basse température des polyynes (C_4H_2, C_6H_2) et des cyanopolyynes (HCN, HC_3N, HC_5N, C_2N_2). Ces molécules sont aussi considérées en tant que petites espèces réactives avec le potentiel de participer à la chimie prébiotique qui aurait mené à l'origine des la vie. Nos résultats préliminaires, sur HCN, HC_3N, HC_5N et C_4H_2 montrent que l'effet de la température sur le coefficient d'absorption de ce s molécules est considérable entre 150 à 298 K (entre 115 et 210 nm).

Les techniques expérimentales que nous avons utilisées sont la **spectroscopie d'absorption classique** (utilisation de la loi Beer-Lambert), la **spectroscopie de fluorescence** et la **spectrométrie de masse**, toutes en connexion avec le rayonnement synchrotron comme source de lumière excitatrice. La photoabsorption a été étudiée pour HCOOH, CH_3COOH, $HCOOCH_3$, CH_3CN, CD_3CN, HCN, HC_3N, HC_5N et C_4H_2. L'observation des spectres de fluorescence, permettant l'observation des fragments neutres excités, a été réalisée pour

HCOOH, CH_3COOH, $HCOOCH_3$, et CH_3CN. Des mesures par spectrométrie de masse photoioniques (PIMS) ont été réalisées sur pratiquement toutes les molécules que nous avons étudiées, y comprises les bases N-hétérocycliques et les acides aminés. Les résultats obtenus par PIMS ont permis la détermination de beaucoup de valeurs thermochimiques inconnues auparavant, pour les cations parents et les fragments.

Bases N-hétérocycliques

Les chemins de fragmentation ont été discutés en détail dans Jochims et al. (2005) et Schwell et al. (2006). Dans cette notice, j'ai discuté les chemins de dégradation les plus importants. Concernant ces molécules, nous trouvons que leurs ions moléculaires, formés par photoionisation dans le VUV, sont stables dans des domaines d'énergie assez grands. Par exemple, le cation parent de l'adénine est stable entre 8.2 et 11.56 eV (140-107 nm, E_{int} = 3.36 eV). Puisque nous savons que le taux d'ionisation dissociative au seuil énergétique de formation du fragment respectif est $k_{diss} = 10^4\ s^{-1}$ (Jochims et al., 1994) dans notre expérience, nous pouvons conclure que dans le domaine d'énergie de la 1ère IE à la 1ère AE, les cations des bases d'ADN/ARN se désexcitent de préférence via conversion interne dans des conditions sans collisions du milieu interstellaire. Cette conversion interne serait liée à une émission dans l'infrarouge. Il serait donc utile de confirmer cette hypothèse par des mesures de taux d'émission IR de ces molécules et par des calculs de k_{diss} en fonction de l'énergie interne dans le domaine $k_{diss} < 10^4\ s^{-1}$. La stabilité relative des bases d'ADN/ARN est probablement liée à leur système aromatique qui est capable de stabiliser une charge positive.

La réaction de fragmentation principale des bases N-hétérocyliques dans le domaine d'énergie E < 13.6 eV est la perte de HCN qui est observée pour les monocations d'adénine, de purine, de benzimidazole, de pyrimidine et d'imidazole. La fragmentation la plus basse en énergie de la thymine et de l'uracile est la perte d'HNCO par réaction Rétro-Diels-Alder. Notons que HCN et HNCO sont observées dans les atmosphères cométaires (Cottin et al., 1999). HCN (mais pas HNCO) est également observé dans l'atmosphère de Titan et son profil vertical a récemment été mesuré par le spectromètre UVIS à bord de la sonde spatiale Cassini (Shemansky et al., 2005). Nous émettons l'hypothèse que ces molécules pourraient, en partie, être formées à partir des bases d'ADN ou d'autres hétérocycles d'azote, photodégradées par le rayonnement VUV. Nous suggérons donc que les recherches des bases d'ADN/ARN dans le système solaire puissent se focaliser aux régions où leurs fragments HCN et HNCO sont observés.

Le radical CN est une autre espèce importante observée dans les atmosphères cométaires (cf. Fray et al., 2005 et références qui y sont citées) et dans le milieu interstellaire (Müller et al., 2005). Ce radical n'est apparemment pas formé dans l'ionisation dissociative des bases N-hétérocycliques gazeuses dans le domaine $E < 20$ eV parce que l'ion $(M\text{-}CN)^+$ n'est pas observé et aucun des chemins de fragmentation postulés incluent la perte de CN (Jochims et al., 2005). Dans les atmosphères cométaires, l'origine de CN est surtout la photodissociation de HCN, mais d'autres sources, comme des polymères organiques solides de HCN, ont été également considérées (Fray et al., 2005).

Acides aminés

Les cations d'acides aminés fragmentent déjà à des énergies internes très faibles en dessus de l'énergie d'ionisation (Jochims et al., 2004). Leur stabilité en présence des champs électromagnétiques VUV est donc réduite par rapport aux bases d'ADN. Pour les α-acides aminés que nous avons étudiés le chemin de fragmentation le plus bas en énergie consiste en la perte du groupe carboxylique neutre COOH (rupture de la liaison αC-COOH).

Ce résultat est qualitativement consistant avec les expériences effectuées par Ehrenfreund et al. (2001). Ce groupe de scientifiques observe les bandes d'absorption infrarouges du CO_2 à la suite d'une irradiation des acides aminés (glycine, α-L-alanine, β-alanine, AIB) en matrice, avec des photons d'énergies quantiques comprises entre 7.5 eV et 9.2 eV. Si nous supposons qu'*à ces énergies* COOH est également formé comme fragment primaire des α-acide aminés, la perte additionnelle d'un atome d'hydrogène de COOH est nécessaire pour former le CO_2. Cette perte pourrait être induite par la matrice parce qu'en phase gazeuse, la perte d'un atome d'hydrogène de COOH (parfois appelé « HOCO » dans la littérature) parait improbable étant donné que cette réaction est endothermique (En revanche la réaction de l'isomère HCOO → CO_2 + H est exothermique !). Notons que $COOH^+$ (= $HOCO^+$) est un cation observé dans le milieu interstellaire (Müller et al., 2005). Cela corrobore notre hypothèse qu'en phase gazeuse la perte spontanée d'hydrogène de la molécule COOH est improbable ce qui permet la formation du cation $COOH^+$. Néanmoins nous ne pouvons pas exclure que d'autres états électroniques peuplés suivant photoexcitation entre 7.5 eV et 9.2 eV pourraient donner naissance à la formation directe du CO_2 à partir des α-acides aminés.

L'ionisation dissociative des acides aminés étudiés par notre groupe donne également naissance au cation $HCNH^+$ qui est un ion important en astrophysique (seuil de formation pour la glycine : AE = 13.0 ± 0.1 eV , pour l'α-alanine : 12.35 eV et pour le β-alanine : AE =

14.2 ± 0.1 eV ; la détermination du seuil de formation de $HCNH^+$ issu de l'acide α-amino isobutyrique et de α-valine n'était elle pas possible à réaliser). Les recherches spatiales dans le MIS, ainsi que dans les atmosphères planétaires et cométaires, pour ces acides aminés devraient donc se focaliser sur les régions où $HCNH^+$ est observé et en même temps une protection par la matière solide des acides aminés contre le rayonnement VUV peut être attendue.

Autres espèces prébiotiques

Nos études sur les espèces prébiotiques HCOOH, CH_3COOH, $HCOOCH_3$, et CH_3CN, molécules observées dans les MIS, ont révélé les principaux chemins de fragmentation de ces molécules dans le VUV. De plus, leurs spectres d'absorption ont été mesurés entre 6 et 22 eV (résolution spectrale 0.9 Å). Les spectres d'absorption au-delà de 11.2 eV n'étaient pas connus auparavant.

La photoexciation de l'acide formique dans le domaine d'énergie correspondant aux régions interstellaires HI (E < 13.6 eV) résulte en la formation des fragments OH et HCOO (à ne pas confondre avec son isomère COOH !). Nous avons observé les émissions de ces fragments dans l'UV/visible (OH : émission $X^2\Pi \leftarrow A^2\Sigma^+$; HCOO : émission $^2A_2 \leftarrow {}^2B_1$). Elles sont liées aux photoréactions HCOOH → OH ($A^2\Sigma^+$) + HCO et HCOOH → H + HCOO ($^2B_1$), avec des rapports de branchement de quelque % entre 10 et 13 eV. Dans nos expériences de spectroscopie de fluorescence induite par rayonnement synchrotron (FIRS), nous ne pouvons pas observer des fragments dans leurs états électroniques fondamentaux. Cependant, il est raisonnable de supposer que pour une photoréaction observée menant à un fragment excité, la réaction correspondante qui forme le même fragment dans son état fondamental, est également importante. Les rendements de branchement de ces processus restent néanmoins à quantifier. Néanmoins, nous pensons que les processus de photodissociation HCOOH → OH + HCO et HCOOH → H + HCOO constituent les chemins de fragmentation les plus importants en dessous de 13.6 eV.

Les fragments ioniques principaux de l'acide acétique sont $COOH^+$ (AE = 11.7 ± 0.05 eV) et CH_3CO^+ (AE = 11.45 ± 0.05 eV) en dessous de 13.6 eV. Dans ce domaine d'énergie nous avons aussi détecté l'émission OH ($X^2\Pi \leftarrow A^2\Sigma^+$). Le seuil de cette émission est 9.2 ± 0.1 eV et le rendement quantique maximal est de 0.9 % à 13.3 eV. Cette observation montre que le processus neutre $CH_3COOH \rightarrow CH_3CO + OH$ (X,A) est également important à E <13.6 eV. Nos résultats indiquent ainsi que l'acide acétique serait facilement dégradable dans les régions

HI du MIS. Malgré cela cette molécule a été observée dans les nuages moléculaires (par exemple SgrB2). Les chemins de *formation* doivent donc être particulièrement efficaces ou bien la densité des poussières dans ces régions est telle qu'une protection de CH_3COOH contre le rayonnement VUV est effective. D'autres implications astrophysiques, notamment en ce qui concerne les atmosphères cométaires, ont été discutées par Leach et al. (2006b, publication ci-jointe).

A plus hautes énergies (E > 13.6 eV), les émissions CH ($X^2\Pi \leftarrow A^2\Delta$), CH ($X^2\Pi \leftarrow B^2\Sigma^-$) ainsi que des transitions H-Balmer après photoexcitation de CH_3COOH ont été observées dans le domaine de l'UV/Visible. Les processus de fragmentation liés à ces émissions ont été analysés en détail (Leach et al., 2006b). L'émission du radical HCOO ($^2A_2 \leftarrow {}^2B_1$) n'a pas été observée lors de l'excitation VUV de cette molécule. Cela corrobore, pour des raisons de structure chimique de HCOOH et CH_3COOH, notre attribution de HCOO (en non pas le COOH) comme étant le photofragment primaire dans la photodissociation VUV de l'acide formique.

Le spectre d'absorption du formate de méthyle est qualitativement similaire à celui de l'acide acétique, en ce qui concerne les intensités de bandes. De nouvelles mesures, sur la photofragmentation de $HCOOCH_3$, sont donc nécessaires pour savoir si la photochimie VUV est responsable de la différence notable en abondance de ces 2 isomères dans le MIS.

Rendement quantique de photoionisation

Etant donné l'importance des chemins de fragmentations ioniques dans les régions HI du MIS (E < 13.6 eV), nous avons mesuré le rendement quantique de photoionisation, γ_i, en fonction de la longueur d'onde d'excitation pour l'acide formique (Schwell et al., 2002). Cette courbe croît de manière continue, partant de l'IE de la molécule à 11.33 eV pour atteindre le plateau γ_i = unité à 18 ± 0.1 eV. Le domaine de processus compétitifs *non-ioniques* de l'acide formique est donc compris dans IE + 6.67 ± 0.1 eV. Ce domaine est donc plus petit que celui des HAP pour lesquelles $\gamma_i \approx 1$ pour $E \geq IE + 9.2$ eV a été observé (Jochims et al., 1996). La courbe de rendement quantique de photoionisation de HCOOH présente des plateaux chaque fois qu'un état ionique est accessible énergétiquement.

Les mesures de rendement quantique de photoionisation γ_i sont envisagées dans le futur, également pour les autres molécules biologiques présentées dans cet ouvrage. Il est cependant utile, de reconsidérer les mesures antérieures effectuées sur les HAP (Jochims et al., 1996).

Elles montrent que γ_i peut atteindre 50 % à une énergie interne E_{int} de 3 eV en dessus de l'énergie d'ionisation (pour les HAP étudiées). Nous émettons l'hypothèse que pour les bases d'ADN et d'ARN dont la structure chimique est semblable aux HAP, γ_i pourrait être de même ordre de grandeur. L'ionisation serait ainsi un moyen de stabiliser ces bases contre les champs de rayonnement électromagnétiques VUV parce que, comme nous avons conclu plus haut, elles fragmentent peu via l'ionisation dissociative. Dans un contexte astrophysique, les cations formés pourraient recombiner ultérieurement avec des électrons lents afin de reconstituer la forme neutre de la base.

Références des chapitres 1 à 5

Arakawa, E.T., Emerson, L.C., Juan, S.I., Ashley, J.C., Williams, M.W., 1986. *The optical properties of Adenine from 1.8 to 80 eV.* Photochemistry and Photobiology, 44, p. 349-353.

Basile, B., Lazcano, Oro, J., 1984. *Prebiotic syntheses of purines and pyrimidines.* Advances in Space Research, 4, p. 125-131.

Barrio, M.G., Scopes, D.I.C., Holtwick, J.B., Leonard, N.J., 1981. *Syntheses of all singly labelled [^{15}N]adenines : Mass spectral fragmentation of adenine.* Proceedings of the National Academy of Sciences of the USA, 78, p. 3986-3988.

Bergmann et Schäfer, 1997. *Lehrbuch der Experimentalphysik. Tome 8 : Sterne und Weltraum.* Wilhelm Raith (ed.). Walter de Gryuter, Berlin et NewYork.

Berry, R.S., Leach, S. 1981. *Elementary Attachment and Detachment Processes II.* Advances in Electronics and Electron Physics, 57, p. 1.

Brack, A. (ed.), 1998. *The Molecular Origins of Life.* Oxford University Press.

Brinton, K.L.F., Engrand, C., Glavin, D.P., Bada, J.L., Maurette, M., 1998. *A search for extraterrestrial amino acids in carbonaceous Antarctic micrometeorites.* Origins of Life and Evolution of the Biosphere, 28, p. 413-424.

Broo, A., 1998. *A Theoretical Investigation of the Physical Reason for very different Luminescence Properties of the Two Isomers Adenine and 2-Aminopurine.* Journal of Physical Chemistry, 102, p. 526.

Callis, P.R., 1983. *Electronic states and luminescence of nucleic acid systems.* Annual Review of Physical Chemistry, 34, p. 329.

Carnovale, F., Gan, T.H., Peel, J.B., 1980. *Photoelectron spectroscopic studies of the monomers and dimers of acetic and trifluoracetic acids.* Journal of Electron Spectroscopy and Related Phenomena, 20, p. 53-67.

Chase, M.W., Jr., 1998. *NIST-JANAF Themochemical Tables, Fourth Edition.* Journal of Physical Chemistry References Data Monograph 9, 1-1951, accessible through http://webbook.nist.gov.

Chela-Flores, J., Owen, T., Raulin, F. (eds.), 2001. *First Steps in the Origin of Life in the Universe.* Kluwer Academic Publishers.

Chyba, C., Sagan, C., 1992. *Endogenous production, exogenous delivery and impact-shock synthesis of organic molecules: an inventory for the origins of life.* Nature, 355, p. 125.

Coll, P., Coscia, D., Smith, N., Gazeau, M.-C., Ramirez, S.I., Cernogora, G. Israël,G., F. Raulin, F., 1999. *Experimental laboratory simulation of Titan's atmosphere (aerosols & gas phase).* Planetary and Space Science, 47,p. 1331-1340.

Cottin, H., Gazeau, M.C., Raulin, F., 1999. *Cometary organic chemistry: a review from observations, numerical and experimental simulations.* Planetary and Space Science, 47, p. 1141-1162.

Cronin, J.R, 1976a. *Acid-labile amino acid precursors in the Murchison meteorite 1: Chromatographic Fractionation.* Origins of Life, 7, p. 337-342.

Cronin, J.R, 1976b. *Acid-labile amino acid precursors in the Murchison meteorite 2: A Search for peptides and Amino Acyl Amides.* Origins of Life, 7, p. 343-348.

Cronin, J.R., Pizzarello, S., 1983. *Amino Acids in Meteorites.* Advances in Space Research 3, p. 5-18.

Cronin, J.R., Pizzarello, S., 1986. *Amino acids of the Murchison meteorite. III. Seven carbon acyclic primary α-amino alkanoic acids.* Geochimica et Cosmochimica Acta, 50, p. 2419.

Cronin, J.R., 1989. *Origin of Organic Compounds in carbonaceous chondrites.* Advances in Space Research 9, (2)59-(2)64.

Cronin, J.R., Cooper, G.W., Pizzarello, S., 1995. *Characteristics and formation of Amino acids and hydroxyl acids of the Murchison meteorites.* Advances in Space Research, 15, (3)91-(3)97.

DeFrees, D.J., McLean, A.D., 1985. Does carbon-protonated Hydrogen cyanide, H_2CN^+, exist ? Journal of the American Chemical Society 107, 4350-4351.

Despois, D., 2006. *Biological Molecules.* Chapitre dans : F. Combes, F. Casoli, E. Falgarone, L. Palgani (eds.). Hunt for Molecules. Paris Observatory publications.

Despois, D., Cottin, H., 2005. *Comets: Potential Sources of Prebiotic Molecules for the Early Earth.* Dans Gargaud et al., 2005

Ehrenfreund, P., Bernstein, M.P., Dworkin, J.P., Sandford, S.A., Allamandola, L.J., 2001. *The photostability of amino acids in space.* Astrophysical Journal, 550, L95-L99.

Ferris, J.P, Sanchez, R.A., Orgel., L.E., 1968. *Studies in prebiotic synthesis III Synthesis of pyrimidine from cyanoacetylene.* Journal of Molecular Evolution, 3, p. 301-309.

Ferris, J.P., Zameck, O.S., Altbuch, A.M., Freiman, H., 1974. *Chemical Evolution XVIII Synthesis of pyrimidines from guanidine, cyanoacetylene and cyanate.* Journal of Molecular Biology, 33, p. 693-704.

Forst, W., 1973. *Theory of Unimolecular Reactions.* Academic Press, New York.

Fray, N., Benilan, Y., Cottin, H., Gazeau, M.-C., Crovisier, J., 2005. *The origin of the CN radical in comets: A review from observations and models.* Planetary and Space Science, 53, p. 1243-1262.

Gargaud, M., Barbier, B., Martin, H., Reisse, J. (eds.), 2005. *Lectures in Astrobiology, Volume 1.* Springer Verlag, Berlin Heidelberg.

Glavin, D.P., Matrajt, G., Bada, J.L., 2004. *Re-examination of amino acids in Antarctic micrometeorites.* Advances in Space Research, 33, p. 106-113.

Glavin, D.P., Bada, J.L., 2004. *Isolation of purines and pyrimidines from the Murchison meteorite using sublimation.* 35th Lunar and Planetary Science Congress, Houston. Extended abstract no. 1022. http://www.lpi.usra.edu/meetings/lpsc2004/1022.pdf

Hayatsu, R., Studier, M.H., Moore, L.P., Anders, E., 1975. *Purines and Triazines in the Murchison Meteorite.* Geochimica and Comsmochimica Acta, 39, p. 471-488.

Hollis, J.M., Vogel, S.N., Snyder, L.E., Jewell, P.R., Lovas, F.J., 2001. *The spatial scale of glycolaldhyde in the Galactic Center.* Astrophysical Journal, 554, L81-L85.

Hollis, J.M., Lovas, F.J., Remijan, A.J., Jewell, P.R., Ilyushyn, V.V., Kleiner, I., 2006. *Detection of Acetamide (CH_3CONH_2) : The largest Interstellar Molecule with a peptide bond.* Astrophysical Journal, 643, L25-L28.

Hua, L.-L., Kobayashi, K., Ochiai, E.-I., Gerke, C.W., Gerhardt, K.O., Ponnamperuma, C., 1986. *Identification and Quantification of Nucleic acid cases in carbonaceous chondrites.* Origins of Life, 16, p. 226-227.

Huber, K.P., Herzberg, G., 2005. *Constants of Diatomic Molecules* (data prepared by J.W. Gallagher and R.D. Johnson, III) dans le WebBook de Chimie NIST, Base de Données Standard de Référence NIST Numéro 69, Eds. P.J. Linstrom and W.G. Mallard, June 2005, National Institute of Standards and Technology, Gaithersburg MD, 20899 (http://webbook.nist.gov).

Improta, R., Scalmani, G., Barone, V., 2000. *Radical cations of DNA bases: some insights on structure and fragmentation patterns by density functional methods.* International Journal of Mass Spectrometry, 201, p. 321-336.

Irvine, W.M., Elldér, J., Hjalmarson, A., Kollberg, E., Rydbeck, O.E.H., Sorensen, G.O., Bak, B., Svanholt, H., 1981. *Searches for interstellar imidazole and cyanoform.* Astronomy & Astrophysics, 97, p. 192-194.

Isaacson, M., 1972. *Interaction of 25 keV Electrons with the Nucleic Acid Bases Adenine, Thymine, and Uracil. I. Outer shell excitation.* Journal of Chemical Physics, 56, p. 1803-1812.

Jochims, H.-W., Rühl, E., Baumgärtel, H., Tobita, S., Leach, S., 1994. *Size effects on dissociation rates of polycylic aromatic hydrocarbons: laboratory studies and astrophysical implications.* Astrophysical Journal, 420, p. 307-317.

Jochims, H.-W., Baumgärtel, H., Leach, S., 1996. *Photoionization quantum yields of polycyclic aromatic hydrocarbons.* Astronomy and Astrophysics, 314, p. 1003-1009.

Jochims, H.-W., Baumgärtel, Leach, S., 1999. *Structure-dependent Photostability of Polycyclic Aromatic Hydrocarbon Cations: Laboratory Studies and Astrophysical Implications.* Astrophysical Journal, 512, p. 500-510.

Jochims, H.-W., Schwell, M., Chotin, J.-L., Clémino, M., Dulieu, F., Baumgärtel, H., Leach, S., 2004. *Photoion Mass Spectrometry of Five amino acids in the 6-22 eV photon energy range.* Chemical Physics, 298, p. 279-297.

Jochims, H.-W., Schwell, M., Baumgärtel, H., Leach, S., 2005. *Photoion Mass Spectrometry of Adenine, Thymine and Uracil in the 6-22 eV energy range.* Chemical Physics, 314, p. 263-282.

Junk, G., Svec, H., 1963. *The Mass spectra of the α-amino acids.* Journal of the American Chemical Society, 85, p. 839-845.

Kissel, J., Krueger, F.R., 1987. *The Organic component in dust from comet Halley as measured by the PUMA mass spectrometer on board Vega 1.* Nature, 326, p. 755.

Kuan, Y-J., Yan, C-H., Charnley, S.B., Huang, H.C., Tseng, W.-L., Kisiel, Z., 2003a. *Interstellar glycine.* Astrophysical Journal, 593, p. 848-867.

Kuan, Y-J., Yan, C-H., Charnley, S.B., Kisiel, Z., Ehrenfreund, P., Huang, H-C., 2003b. *A search for interstellar pyrimidine.* Monthly Notices of the Royal Astronomic Society, 345, p. 650.

Lavrentiev, G.A., Strigunkova, T.F., Egorov, I.A. 1984. *A Biological Synthesis of Amino Acids, Purines and Pyrimidines Under Conditions Simulating the Volcanic Ash-Gas Cloud.* Origins of Life, 14, p. 205-212.

Leach, S., Schwell, M., Dulieu, F., Chotin, J.-L., Jochims, H.W., Baumgärtel, H., 2002. *Photophysical studies of formic acid in the VUV. Absorption spectrum in the 6–22 eV region.* Physical Chemistry Chemical Physics, 4, p. 5025-5039.

Leach, S., Schwell, M., Talbi, D., Berthier, G., Hottmann, K., Jochims, H.W., Baumgärtel, H., 2003. *He I photoelectron spectroscopy of four isotopologues of formic acid: HCOOH, HCOOD, DCOOH and DCOOD.* Chemical Physics, 286, p. 15-43.

Leach, S., Schwell, M., Un, S., Jochims, H.-W., Baumgärtel, H., 2006a. *VUV Absorption spectrum of Acetic Acid between 6 and 20 eV.* Chemical Physics, 321, p. 159-170.

Leach, S., Schwell, M., Jochims, H.-W., Baumgärtel, H., 2006b. *VUV Photophysics of Acetic Acid: Fragmentation, Fluorescence and Ionisation in the 6-23 eV region.* Chemical Physics, 321, p. 171-182.

Lührs, D.C., Viallon, J., Fischer, I. 2001. *Excited state spectroscopy of isolated adenine and 9-methyl adenine.* Physical Chemistry Chemical Physics, 3, p. 1827-1831.

Maurel, M.C., Décout, 1999. *Origins of Life: Molecular Foundations and New Approaches.* Tetrahedron, 55, p. 3141-3182.

Mehringer, D.M., Snyder, L.E., Miao, Y., 1997. *Detection and confirmation of Interstellar Acetic Acid.* Astrophysical Journal, 480, L71-L74.

Meierhenrich, U.J., Muñoz Caro, G.M., Brederhöft, J.K., Jessberger, E.K., Thiemann, W.H.P., 2004. *Identification of diamino acids in the Murchison meteorite.* Proceedings of the National Academy of Sciences, 101 (25), p. 9182-9186.

Meierhenrich, U.J., Nahon, L., Alcaraz, C., Bredehöft, J.H., Hoffmann, S.V., Barbier, B., Brack, A., 2005. *Asymmetric Vacuum UV photolysis of Amino Acid Leucine in the Solid State.* Angewandte Chemie International Edition, 44, p. 5630-5634.

Miller, S.L., 1953. *A production of amino-acids under possible primitive earth conditions.* Science, 117, p. 528-529.

Minard, R.D., Hatcher, P.G., Gourley, R.C., Matthews, C.N., 1998. *Structural investigation of hydrogen cyanide polymers: new insights using TMAH thermochemolysis/GC-MS.* Origins of Life and Evolution of the Biosphere, 28, p. 461-473.

Molina-Cuberos, G.J., Lopez-Moreno, J.J., Rodrigo, R., Lara, L.M., O'Brien, K., 1999. *Ionisation by cosmic rays of the atmosphere of Titan.* Planetary and Space Science, 47, p. 1347-1354.

Müller, H.S.P., Schlöder, F., Stutzki, J., Winnewisser, G., 2005. *The Cologne Database for Molecular Spectroscopy, CDMS: a useful tool for astronomers and spectroscopists.* Journal of Molecular Structure, 742, p. 215-227.

Muñoz Caro, G.M., Meierhenrich, U.J., Schutte, W.A., Barbier, B., Arcones Segovia, A., Rosenbauer, H., Thiemann, W., Brack, A., Greenberg, J.M., 2002. *Amino acids from ultraviolet irradiation of interstellar ice analogues.* Nature, 416, p. 403.

Neusser, H.J., 1989. *Lifetimes of energy and angular momentum selected ions.* Journal of Physical Chemistry, 93, p. 3897.

Nir, E., Kleinermanns, K., Grace, L., de Vries, M.S., 2001. *On the photochemistry of Purine Nucleobases.* Journal of Physical Chemistry A, 105, p. 5106-5110.

Nir, E., Plützer, C., Kleinermanns, K., de Vries, M., 2002. *Properties of isolated DNA bases, base pairs and nucleosides examined by laser spectroscopy.* European Physical Journal D 20(3), p. 317-329.

Peeters, Z., Botta, O., Charnley, S.B., Ruiterkamp, R., Ehrenfreund, P., 2003. *The astrobiology of nucleobases.* Astrophysical Journal, 593, L129-L132.

Plützer, C., Nir, E., de Vries, M.S., Kleinermanns, K., 2001. *IR-UV double resonance spectroscopy of the nucleobase adenine.* Physical Chemistry Chemical Physics, 3, p. 5466-5469

Plützer, C., Kleinermanns, K., 2002. *Tautomers and electronic states of jet-cooled adenine investigated by double resonance spectroscopy.* Physical Chemistry Chemical Physics, 4, p. 4877-4882.

Rauk, A., Yu, D., Borowski, P., Roos, B., 1995. *CASSCF, CASPT2, and MRCI investigations of the formyloxyl radical (HCOO).* Chemical Physics, 197(1), p. 73-80.

Raulin, F., Toupance, G., 1975. *Etude cinétique du cyanoacétaldéhyde en solution aqueuse.* Bulletin de la société de chimie 1975, pages 188-195.

Raulin, F., Coll, P., Navarro-Gonzáles, R., 2005. *Prebiotic Chemistry : Laboratory Experiments and Planetary Observations.* Dans Gargaud et al., 2005.

Robin, M.B., 1974. *Higher Excited States of Polyatomic Molecules.* Academic Press, New York.

Rudberg, E., Brinck, T., 2004. *Computation of Franck-Condon factors for many-atom systems: simulated photoelectron spectra of formic acid isotopologues.* Chemical Physics, 302, p 217-226.

Samson, J.A.R., Ederer, D.L. (eds.), 2000. *Vacuum ultraviolet spectroscopy.* Academic Press, London.

Schilke, P., Walmsley, C.M., Millar, T.J., Henkel, C., 1991. *Protonated HCN in molecular clouds.* Astronomy and Astrophysics, 247, p. 487-496.

Schwell M., Dulieu, F., Gée, G., Jochims, H.-W., Chotin, J.-L., Baumgärtel, H., Leach, S., 2000. *Photionisation mass spectrometry of six isomers of C_7H_8 in the 7-22 photon energy range.* Chemical Physics, 260, p. 261.

Schwell, M., Dulieu, F., Jochims, H.-W., Fillion, J.-H., Lemaire, J.-L., Baumgärtel, H., Leach, S., 2002. *Photophysical Studies of Formic Acid in the vacuum-UV: Fragmentation, Fluorescence and Ionisation.* Journal of Physical Chemistry A, 106, p. 10908-10918.

Schwell, M., Jochims, H.-W., Baumgärtel, H., Leach, S., 2006. *Photoion mass spectrometry of purine, pyrimidine, benzimidazole and imidazole in the 7-15 eV energy range.* Manuscrit en préparation.

Semaniak, J., Minaev, B.F., Derkatch, A.M., Hellberg, F., Neau, A., Rosén, S., Thomas, R.; Larsson, M., Danared, H., Paál, A., Af Ugglas, M., 2001. *Dissociative Recombination of $HCNH^+$: Absolute Cross-Sections and Branching Ratios.* Astrophysical Journal Supplement Series, 135, p. 275-283.

Sephton, M.A., 2005. *Organic matter in carbonaceous meteorites: past, present and future*

research. Philosophical Transactions of the Royal Society A, 363, p. 2729-2742.

Serrano-Andrès, L., Fülscher, M.P., 1996. *Theoretical Study of the Electronic Spectroscopy of Peptides. 2. Glycine and N-Acetylglycine.* Journal of the American Chemical Society, 118, p. 12200-12206.

Sethi, S.K., Gupta, S.P., Jenkins, E.E., Whitehead, C.W., Townsend, L.B., McCloskey, J.A., 1982. *Mass Spectrometry of Nucleic Acid Constituents. Electron Ionization of Spectra of Selectively Labelled Adenines.* Journal of the American Chemical Society, 104, p. 3349-3353.

Shemansky, D.E., Stewart, A.I.F., West, R.A., Esposito, L.W., Hallett, J.T., Liu, X., 2005. *The Cassini UVIS Stellar Probe of the Titan Atmosphere.* Science, 308, p. 978-982.

Snyder, L.E., Lovas, F.J., Hollis, J.M., Friedel, D.N., Jewell, P.R. Remijan, A., Ilyushin, V.V., Alekseev, E.A., Dyubko, S.F., 2005. *A Rigorous Attempt to Verify Interstellar Glycine.* Astrophysical Journal, 619, p. 914-930.

Sowerby, S.J., Heckel, W.M., 1998. *The Role of Self-Assembled Monolayers of the Purine and Pyrimidine Bases in the Emergence of Life.* Origins of Life and Evolution of the Biosphere, 28, p. 283-310.

Sowerby, S.J., Petersen, G.B., Holm, N.G. 2001. *Primordial Coding of Amino Acids by Adsorbed Purine Bases.* Origins of Life and Evolution of the Biosphere, 32, p. 35-46.

Stoks, P.G., Schwartz, A.W., 1981. *Nitrogen-heterocyclic compounds in meteorites : significance and mechanisms of formation.* Geochimica and Cosmochimica Acta, 45, p. 563-569.

Suto, M., Wang, X., Lee, L.C., 1988. *Fluorescence yields form photodissociative excitation of HCOOH, $HCOOCH_3$, CH_3COOH in the vacuum-ultraviolet region.* Journal of Physical Chemistry, 92, p. 3764-3768.

Svec, H.J., Junk, G.A., 1967. *Electron-Impact Studies of Substituted Alkanes.* Journal of the American Chemical Society, 89(4), p. 790-796.

Waterstradt, E., Jung, R., Belling, T., Muller-Dethlefs, K., 1994. *Zero kinetic energy (ZEKE) photoelectron spectrum and coincident mass spectra of methylformate.* Berichte der Bunsengesellschaft für Physikalische Chemie, 98, p. 176.

Weinkauf, R., Schermann, J.-P., De Vries, M.S., Kleinermanns, K., 2002. *Molecular physics of building blocks of life under isolated or defined conditions.* Editorial du numéro spécial portant le même nom. The European Physical Journal D, 20(3), p. 309-316.

Wilson, K.R., Jimenez-Cruz, M., Nicolas, C., Belau, L., Leone, S.R., Ahmed, M., 2006a. *Thermal Vaporization of Biological Nanoparticles: Fragment-Free Vacuum Ultraviolet Photoionization Mass Spectra of Tryptophane, Phenylalanine-Glycine-Glycine, and β-carotene.* Journal of Physcial Chemisty A, 110(6), p. 2106-2113.

Zaretskii, V.I., Sadovskaya, V.L., Wulfson, N.S., Sizoy, V.F., Merimson, V.G., 1971. *Mass Spectrometry of Steroid Systems – XXI. Appearance and Ionization Potentials for the Stereo-isomers of the D-Homostrane Series.* Organic Mass Spectrometry, 5, p. 1179-1182.

6. L'étude de l'aérosol atmosphérique par spectrométrie de masse

SPLAM – *« Single Particle Laser Ablation Mass Spectrometry »*

Les compétences acquises précédemment sur la spectrométrie de masse à photoionisation ainsi que sur les expériences « particules individuelles » (travaux pendant ma thèse de doctorat) m'ont permis de proposer, en 2003, le développement d'un nouvel instrument dédié à l'analyse chimique des particules individuelles de l'aérosol atmosphérique. Ce projet, dénommé SPLAM, a été soutenu par un ACI du Ministère de Recherche (MRT), par le Programme de Recherche Interorganisme pour une Meilleure Qualité de l'Air (PRIMEQUAL, Ministère de l'Environnement et du Développement Durable et ADEME) et par le programme national de chimie atmosphérique (PNCA). L'instrument est en cours de développement et 3 étudiants ont déjà travaillé sur ce développement (Stage DEA Aikaterina Bougiatioti 2004 ; doctorat François Gaie-Levrel, début 2005 ; *Diplomarbeit* et semestre pratique de Christoph Stoll 2005 et 2006).

Dans la suite je présenterai brièvement le contexte scientifique de ce développement instrumental (paragraphe 6.1) et je continuerai avec une description des spécificités techniques et la présentation de quelques résultats préliminaires (paragraphe 6.2). Dans le chapitre 7 (intitulé « perspectives ») je détaillerai les domaines scientifiques que nous envisageons aborder dans le futur en utilisant cette technique.

6.1 Contexte scientifique

Un des enjeux essentiels dans la compréhension du cycle de vie de l'aérosol atmosphérique (formation, vieillissement, dépôt) est d'améliorer les technologies et les instruments de mesure de particules. Ceci est évident si on souhaite comprendre, au niveau moléculaire, le rôle important que joue l'aérosol et ses composés adsorbés pour la santé humaine et le développement futur du climat. Il est indispensable de se doter des nouveaux moyens analytiques capables de fournir des mesures de façon très rapide, c'est à dire en temps quasi-réel, tant que pour la surveillance de la qualité de l'air que pour les études plus fondamentales menées dans les chambres de simulation de la communauté scientifique française et européenne. Ces nouveaux instruments devraient permettre l'identification des espèces chimiques, en fonction de la granulométrie de l'aérosol.

Les spectromètres de masse type temps de vol, à vaporisation / ionisation laser, possèdent la capacité d'avancer d'une manière considérable et innovante dans cette optique. Ces

instruments intègrent l'échantillonnage, la détection et l'identification des espèces chimiques présentes sur l'aérosol. Ils évitent ainsi les artéfacts et la complexité du processus classique de l'analyse chimique des particules et préservent ainsi leurs propriétés physico-chimiques lors de la mesure. Il s'agit d'une méthode qui analyse, après détection optique, *particule par particule*. Elle fournit donc une spéciation chimique en fonction de la granulométrie *en nombre* de l'aérosol.

L'amélioration des techniques lasers et d'acquisition rapide des données permettra dans l'avenir une cadence d'analyse de plus en plus rapide (100 particules par seconde ne parait pas irréaliste à moyen terme). Notons que l'utilisation de la spectrométrie de masse en combinaison avec la photoionisation laser permet une spéciation moléculaire, via l'ion mère, tout en gardant une sensibilité très élevée (de l'ordre du femtogramme de l'espèce considérée). La variété des sources lasers disponibles aujourd'hui permet d'analyser des molécules organiques (aromatiques, aliphatiques, alcènes, aldéhydes, cétones) mais aussi et des espèces minérales de l'aérosol. Ceci permettra de répondre à un éventail très large de questionnements scientifiques en chimie atmosphérique (cf. chapitre 7).

La transportabilité d'un tel l'appareil permet son emploi par la communauté scientifique entière. Il existe aujourd'hui des lasers puissants peu encombrants permettant leur embarquement sur plate-formes routières ou aéroportées. Par ailleurs, l'utilisation de la spectrométrie de masse à photoionisation laser, appliquée pour l'analyse en temps réel des composés organiques traces *en phase gazeuse* a été établie dans le groupe d'Ulrich Boesl à l'Université de Munich, tant en recherche fondamentale qu'au milieu industriel (Zimmermann et al., 1997 et 1999 ; Heger et al., 1999 ; Boesl, 2000). Les instruments de ce groupe sont parfaitement transportables dans une camionnette. Récemment, la grande utilité d'une expérience telle que SPLAM a été démontrée sur le terrain (Trimborn et al., 2000 ; Gross et al., 2001 ; Vogt et al., 2003).

6.2 SPLAM - Spectrométrie de masse à photoionisation laser, appliquée pour particules nanométriques individuelles

La figure 9 donne un schéma de SPLAM. L'aérosol est aspiré au travers d'une entrée à lentilles aérodynamiques qui crée un jet de particules peu divergent. Ce jet rentre, au travers d'un système à pompage différentiel, dans la chambre à détection optique et puis dans la source d'ions d'un spectromètre de masse à temps de vol. Nous avons développé un spectromètre qui repose sur un châssis transportable. *Une* particule, détectée optiquement,

sera ensuite vaporisée à l'aide d'un laser pulsé infrarouge. Les espèces dans le nuage moléculaire formé seront ionisées par un laser UV (photoionisation directe ou ionisation multiphotonique renforcée à résonance). Le grand challenge est de pousser la cadence d'analyse (aujourd'hui entre 1 et 5 particules par seconde) vers des cadences plus élevées (50 à 100 particules par seconde à moyen terme).

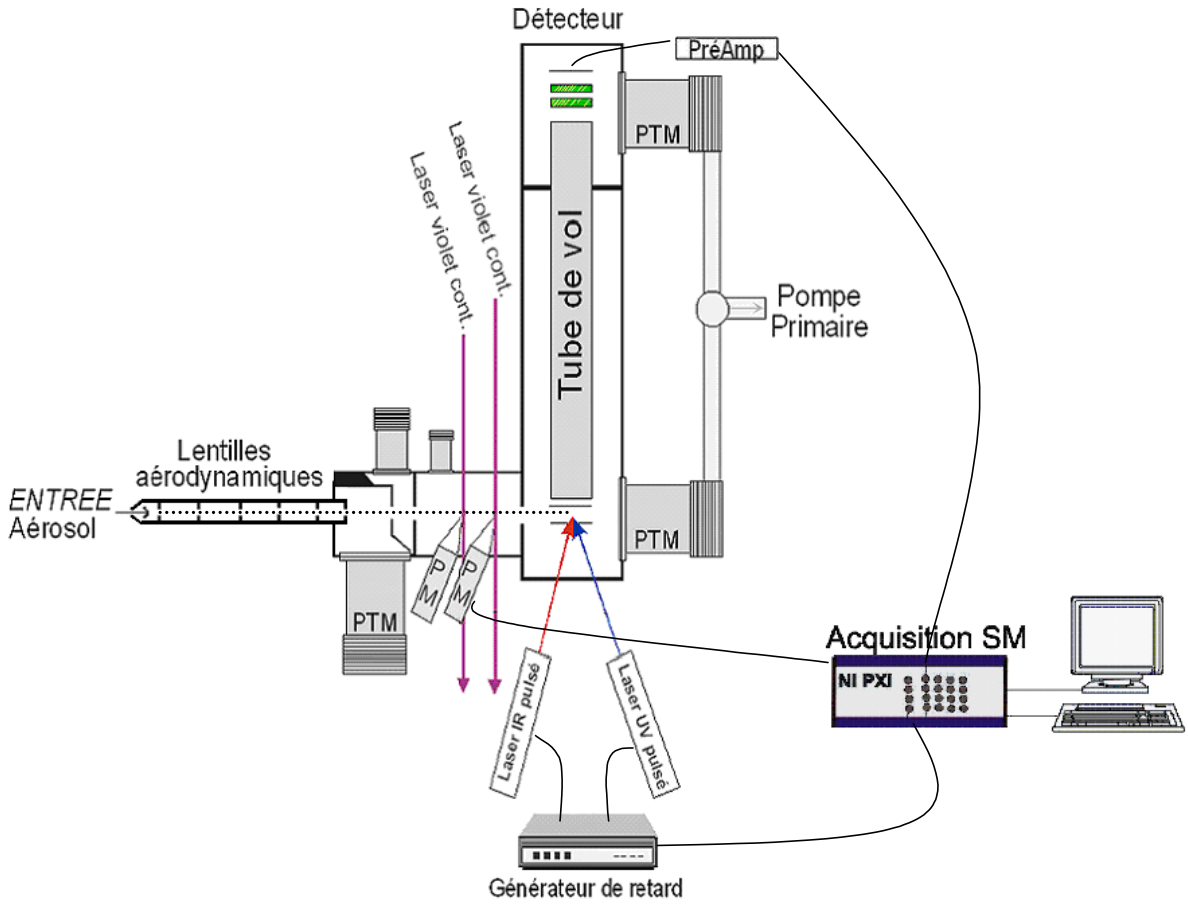

Figure 9 : Schéma du dispositif expérimental de SPLAM (PM : Photomultiplicateur, PréAmp : Préamplificateur, PTM : Pompe turbomoléculaire)

Nous utilisons un système d'acquisition PXI (National Instruments : ordinateur, carte oscilloscope, carte d'acquisition 64 MS/s sur 14 bit de dynamique verticale, le tout sur un châssis très compact) et nous développons nous-mêmes les logiciels de traitement et de représentation des nombreuses données attendues en utilisant le langage LabVIEW. Etant donné la variabilité des données (analyse en haute ou basse cadence, de différents types d'aérosols, avec ou sans détermination du diamètre aérodynamique, etc…), cette option offre davantage de liberté et plus de flexibilité par rapport à un logiciel tout fait.

Dans la suite de ce paragraphe je détaillerai brièvement les différents éléments de l'instrument et les avances qui ont été réalisées à ce jour.

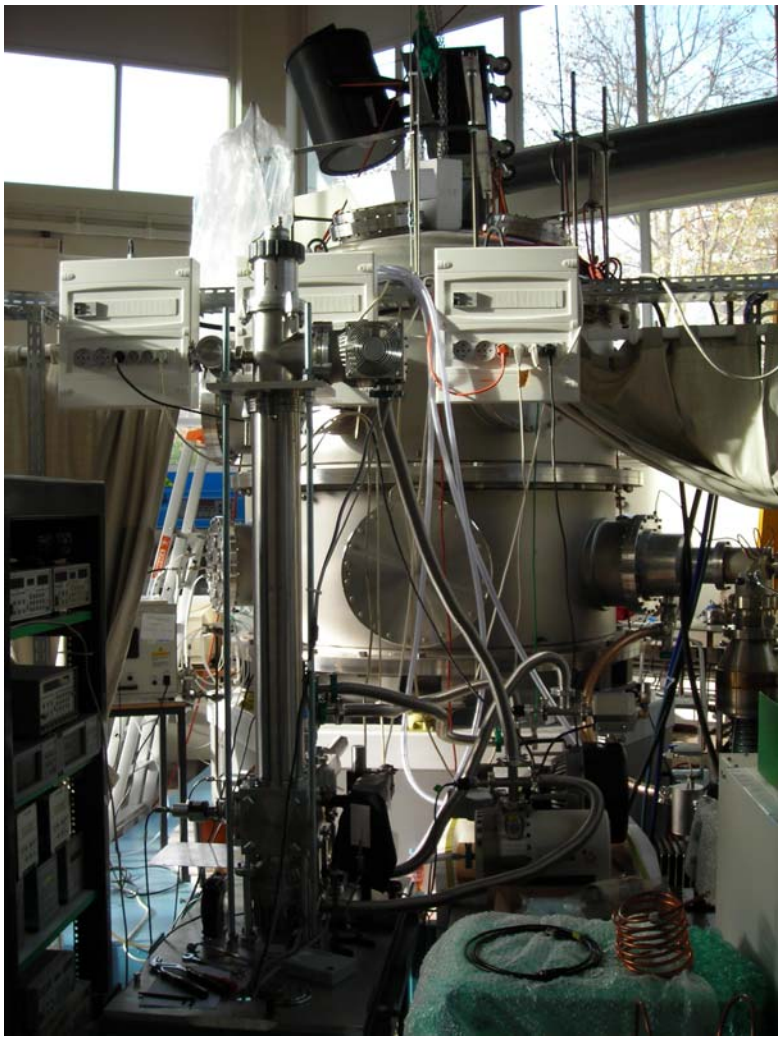

Figure 10 : Photo du montage actuel de SPLAM. Dans le fond de l'image on voit la chambre de simulation CESAM.

6.2.1 Entrée de l'aérosol dans SPLAM

L'entrée à aérosol de SPLAM consiste en 3 pièces : des lentilles aérodynamiques (selon Liu et al., 1995a,b ; Jayne et al., 2000), 2 chambres d'expansion et une chambre à détection optique (cf. fig. 9). Ces 3 pièces ont été conçues et usinées récemment. La géométrie des lentilles aérodynamiques a été conçue en collaboration avec l'Université de Minnesota (simulation des trajectoires de particules : Xiaoliang Wang, Peter McMurry). Une grande partie du travail (dessins techniques) a été réalisée par un stagiaire ingénieur de l'Université de Bielefeld qui a effectué son semestre pratique et sa *Diplomarbeit* au LISA (C. Stoll). Le couplage de cette entrée à aérosols avec le spectromètre de masse à temps de vol est en train d'être réalisée actuellement.

Les lentilles aérodynamiques choisies dans un premier temps transmettent des particules de 40 à 1100 nm de diamètre aérodynamique avec une efficacité de pratiquement 100 %. L'atout

de notre système d'entrée d'aérosol est que les disques qui forment les lentilles sont facilement échangeables. Ainsi, d'autres domaines de taille deviendront aisément accessibles (par exemple les nanoparticules de diamètre inférieur à 40 nm).

(a)

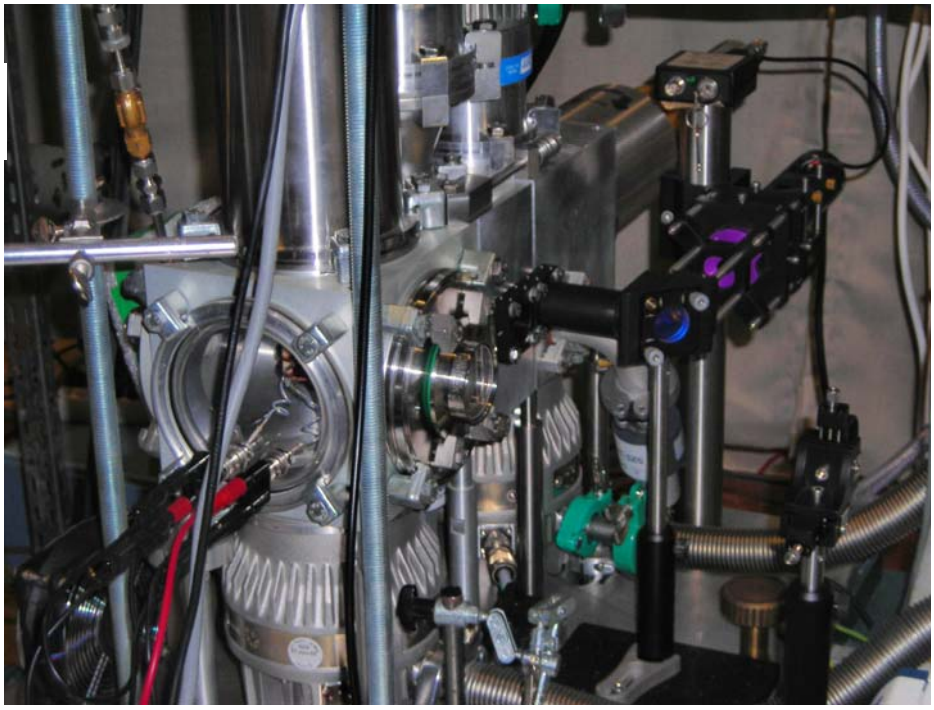

(b)

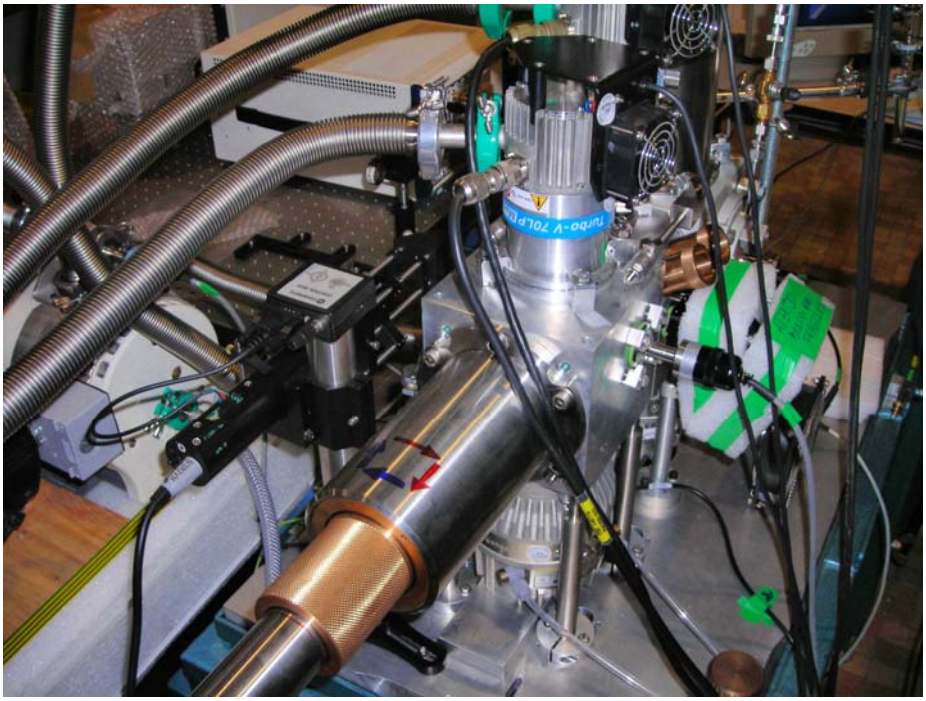

Figure 11 : Détails du montage actuel de SPLAM. (a) A droite de l'image on remarque le laser diode, qui est focalisé dans la chambre à détection optique (uniquement une de 2 entrées est utilisée au moment). A gauche on reconnaît, au travers d'une bride transparente, la source d'ions avec ses plaques d'extraction en cuivre. (b) Au premier plan, on voit les lentilles aérodynamiques, amovibles en direction z via une roue (en laiton). A droite de l'image on aperçoit 2 inserts (en laiton) qui accueilleront les 2 photomultiplicateurs prévus pour détecter la lumière diffusée des particules.

6.2.2 Détection optique et vaporisation des particules

Cette partie de l'instrument SPLAM n'est pas encore opérationnelle à ce jour. Le faisceau des particules croise, dans une chambre la plus noire possible, 2 faisceaux lasers continus ($\lambda = 403$ nm, Coherent « Radius »). La détection optique de la particule par deux photomultiplicateurs est cruciale pour le fonctionnement de l'appareil. On espère pouvoir détecter des particules d'un diamètre aérodynamique d'au moins 150 nm. Le signal des 2 PM, enregistré par la carte d'acquisition, permet de calculer la vitesse de la particule et par la suite son diamètre aérodynamique. Il permet en plus de déclencher les deux lasers pulsés (IR + UV) avec un délai adapté vis à vis la vitesse de la particule. Ce délai sera calculé en temps réel avec un module de LabVIEW « temps réel ».

Afin de vaporiser les particules individuelles, le faisceau d'un laser IR rentrera dans la source d'ions de notre spectromètre de masse à temps de vol. On utilisera de préférence un laser CO_2 pulsé ($\lambda = 10.6$ μm), focalisé par une lentille en ZnSe permettant de régler l'extension spatiale du foyer du laser. La vaporisation d'une particule organique se fait à une densité de puissance de 10^9 W/cm^2/impulsion (Durée d'impulsion du laser CO_2 : environ 100 ns). Cette densité de puissance est suffisante pour vaporiser une particule entière comme le montrent les travaux du groupe de R. Zenobi à Zürich (Haefliger et al., 1998, 1999, 2000a,b) et également pour désorber des couches de surface en diminuant la densité d'énergie du faisceau incidente (Woods et al., 2001, 2002). Le laser IR, d'énergie ajustable, permettra d'analyser des couches de surface d'une particule. A ce jour, la vaporisation (complète ou partielle) des nanoparticules individuelles *volantes* par laser IR suivie de l'ionisation douce proche su seuil d'ionisation est maîtrisée par un seul groupe dans le monde (celui de T. Baer à l'Université de la Caroline du Nord en Etats Unis). C'est un domaine encore à explorer expérimentalement dans le futur.

6.2.3 Photoionisation des molécules vaporisées

Le nuage moléculaire est directement formé dans la source d'ions du spectromètre de masse, c'est à dire entre les plaques d'extraction. Les molécules sont ensuite ionisées par un laser UV pulsé, dont l'impulsion suit celle du laser IR de quelques microsecondes. Pour ioniser des molécules organiques nous avons envisagé plusieurs possibilités détaillées dans la suite de ce paragraphe.

α) Photoionisation des molécules organiques aromatiques – résumé des études préliminaires

Nous utilisons actuellement un laser excimère KrF (λ = 248 nm, E_{photon} = 5 eV) qui nous permet d'effectuer une ionisation exaltée à résonance (angl. *« REMPI » = Resonance-Enhanced-Multiphoton-Ionisation ;* cf. schéma fig. 12).

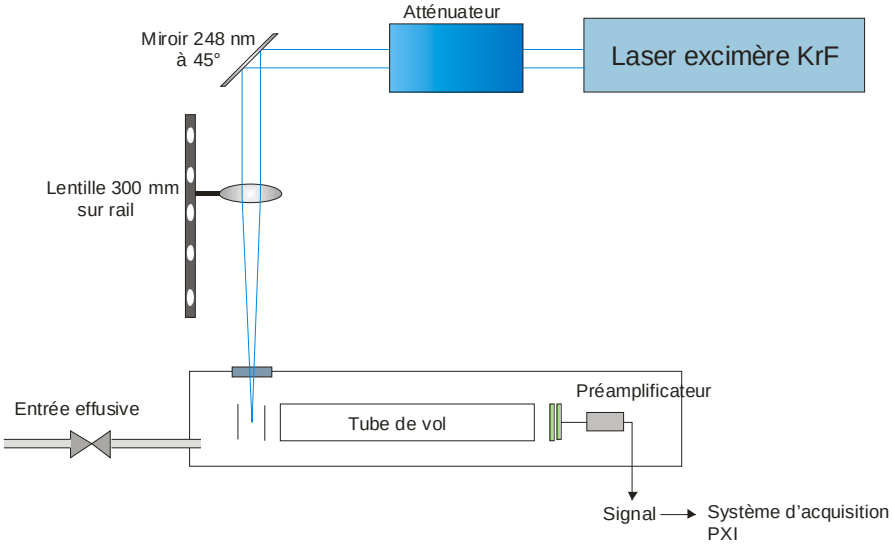

Figure 12 : Dispositif utilisé pour les études préliminaires.

La sensibilité de SPLAM est particulièrement élevée pour les espèces absorbant fortement à 248 nm ce qui concerne surtout les molécules aromatiques dont la section efficace d'absorption y est très élevée à cause de leurs transitions intenses $S_0 \rightarrow S_n$. Ces bandes d'absorption sont larges dans nos conditions (molécules à température ambiante, pas de conditions de jet moléculaire). La plupart des molécules aromatiques peuvent être ionisées près du seuil d'ionisation avec uniquement 2 photons de 248 nm. Le grand avantage de la photoionisation proche du seuil d'ionisation réside le fait quelle implique peu d'ionisation dissociative parce que les seuils énergétiques de fragmentation ne sont pas atteints en général. Lors des études préliminaires que nous avons menées avec le dispositif expérimental montré en Figure 10, nous observons un maximum de sensibilité pour les molécules aromatiques (cf. Tableau 2). A part leur forte section efficace d'absorption à 248 nm, une autre raison pour la grande sensibilité de SPLAM est qu'à cette longueur d'onde la photoionisation d'autres molécules présentes dans la source, telles que l'oxygène, l'azote, le dioxyde de carbone, les alcanes, les alcènes et aldéhydes non-aromatiques, est quasiment supprimée. Ceci diminue le bruit de fond dans les spectres de masse d'une manière significative (Zimmermann et al., 1997) et permet donc l'identification des espèces de très faible concentration.

Notons que les molécules d'impact sanitaire sont souvent des molécules aromatiques et leurs divers dérivés (Hydrocarbures polycycliques aromatiques, nombreux pesticides, dioxines / furanes, polychloro-biphényles, chlorobenzènes, molécules dites « BTX » : benzène, toluène, xylène etc…). Beaucoup de ces molécules (sauf BTX) ont de faible tension de vapeur saturante. C'est pourquoi on les trouve condensées sur les particules de l'aérosol troposphérique.

Tableau 2: Limites de détection obtenues dans des conditions REMPI à 248 nm pour quelques composés aromatiques semi-volatils.

	Pression de vapeur saturante à 298 K	Limite de détection [concentration phase gazeuse]	Limite de détection [# molécules dans volume d'ionisation]
Naphthalène	110 μbar	67 ppb	145
2-Méthyl-naphthalène	73 μbar	46 ppb	104
Biphényle	11.8 μbar	227 ppb	662

β) Photoionisation des molécules <u>non</u>-aromatiques – résumé des études préliminaires

Certains composés organiques volatils biogéniques (COV-B ; par exemple terpènes et autres) sont responsables de la formation d'une grande quantité d'aérosol organique secondaire (AOS) dans l'atmosphère terrestre. Pour cette raison, nous avons très récemment effectué une étude sur ces composés et certains de leurs produits de dégradation atmosphérique afin de tester si l'ionisation exaltée à résonance à $\lambda = 248$ nm serait une méthode d'ionisation utilisable pour ces composés *non-aromatiques*. Notons que certains terpènes (par exemple le α-pinène) ont des sections efficaces d'absorption non-zéro à 248 nm (Ces travaux on fait l'objet de la Diplomarbeit de Christophe Stoll). Cette étude s'est fait aussi dans la perspective du couplage de SPLAM à la nouvelle chambre de simulation CESAM du LISA (CESAM = <u>C</u>hambre <u>E</u>xpérimentale de <u>S</u>imulation <u>A</u>tmosphérique <u>M</u>ultiphasique). Il est prévu d'étudier, dans cette chambre, la formation et le vieillissement des aérosols organiques secondaires à partir des composés organiques volatiles biogéniques (COV-B) et anthropiques (COV-A : par exemple alkylbenzènes, indène, autres HAP) en interactions avec l'ozone ou le radical OH (voir aussi chapitre 7).

Le comportement de fragmentation des composés suivants a été étudié en phase gazeuse : α-pinène, β-pinène, acide pinique, acide trans-norpinonique, acide cis-pinonique, sabinène, sabinacétone, limonène, et méthylbuténol. Nous avons enregistré les spectres de masse de tous ces composés en fonction de l'énergie du faisceau laser. La figure 13 illustre le type de

résultats obtenus lors de cette étude. Nous y comparons les courbes de rendement de fragments formés par photoionisation dissociative du HAP biphényle (cation moléculaire m = 154.21 u.m.a.) et du terpène α-pinène (cation moléculaire m = 136.23 u.m.a.). La conclusion principale de cette étude est que les cations mères des terpènes fragmentent beaucoup dans des conditions d'ionisation renforcée à résonance à 248 nm parce qu'ils n'absorbent que très peu à cette longueur d'onde (par exemple α-pinène : log ε ≈ 1.3). Ainsi, pour détecter les ions mères des terpènes, l'énergie du laser doit être assez élevée et par conséquent le nombre de photons absorbés ne peut pas être contrôlé : la fragmentation devient inévitable dans les conditions d'absorption multiphotonique. Ceci est illustré dans la figure 13 : aux faibles énergies laser (E < 2 mJ), l'ion mère du α-pinène est à peine détectable mais son fragment m/z = 93 est déjà très intense. D'autres fragments (m/z = 39, 65) ont pratiquement la même intensité que l'ion mère (fig. 13a). Au contraire, l'ion mère du HAP biphényle, dont la molécule neutre absorbe fortement à λ = 248 nm (log ε ≈ 4.2), est très intense déjà à 1 mJ tandis que ses fragments sont pratiquement invisibles à cette énergie (fig 13b).

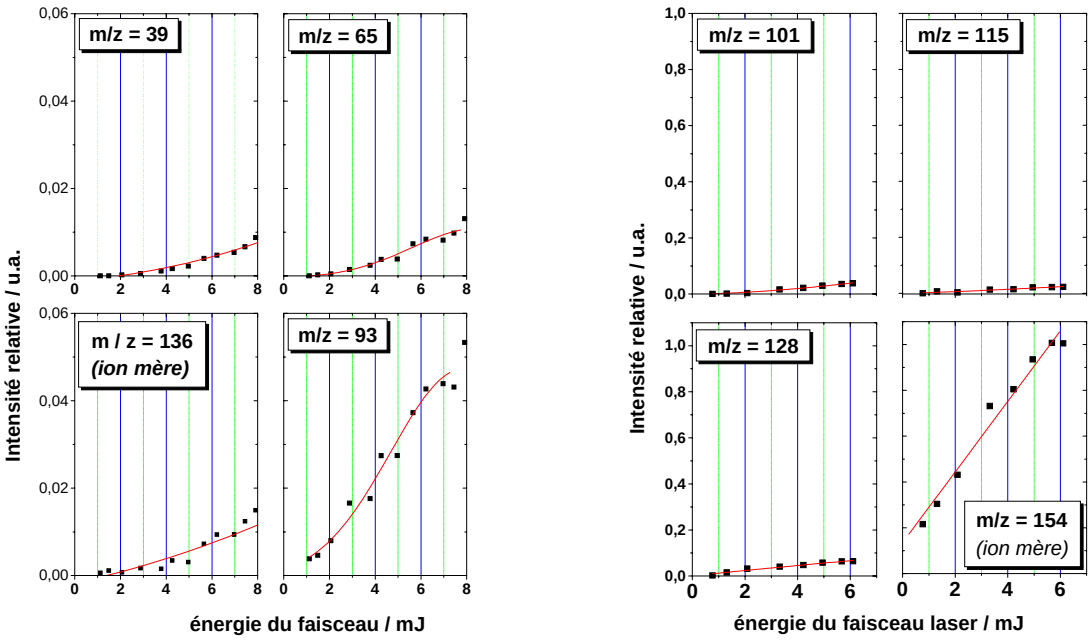

(a) α-pinène **(b) Biphényle**

Figure 13 : Intensité des fragments en fonction des l'énergie du faisceau laser excimère KrF (λ = 248 nm). (a) α-Pinène et (b) Biphényle.

Nous concluons de ces études préliminaires avec le laser excimère KrF, que le REMPI à 248 nm est très probablement la méthode d'ionisation idéale pour détecter des molécules aromatiques sur les particules individuelles d'un aérosol. La formation d'un aérosol organique secondaire (AOS) à partir des précurseurs *aromatiques* (par exemple les alkyle-benzènes ; indène) pourra donc être étudiée parfaitement avec SPLAM intégrant la méthode d'ionisation REMPI à 248 nm. Une autre perspective intéressante de SPLAM / REMPI est certainement la détection, en phase particulaire, des composés semi-volatils de première importance environnementale telles que les dioxines, les furannes, ou encore les polychlorobiphényles (voir perspectives, paragraphe 7.1.2/2.) qui sont toutes des molécules aromatiques.

Par contre, l'identification par SPLAM / REMPI à 248 nm des produits de dégradation issus de l'ozonolyse des terpènes via la masse de leurs ions mères sera très difficile, voire impossible dans des mélanges complexes que sont les particules réelles. Néanmoins nous voulons étudier les AOS formés par des COV-B tels que les terpènes. Une alternative est la photoionisation directe (ou *Single Photon Ionisation, « SPI »*) proche du seuil d'ionisation. Pour cela, deux possibilités sont envisageables : soit l'utilisation d'un laser Nd:YAG (SPI à λ = 118 nm après triplage de la troisième harmonique à λ = 355 nm), soit l'utilisation des nouvelles lampes excimères opérant dans le VUV.[1] Notons que ces lampes, très compactes et de faible poids et consommation électrique, sont très intéressantes pour les futures applications de SPLAM sur le terrain.

[1] Un développement très récent de la société TUI-Laser s'avère très prometteur : Il s'agit des lampes excimères opérant à des longueurs d'onde d'émission entre 60 et 120 nm. La qualité de la lumière VUV émise (focalisation, intensité) permettrait leur utilisation en spectrométrie de masse à temps de vol. Cette lampe sera commercialisée en 2007.

Références du chapitre 6

Boesl, U., 2000. *Laser mass spectrometry for environmental and industrial chemical trace analysis.* Journal of Mass Spectrometry, 35, p. 289.

Gross, D.S., Gälli, M.E., Silva, P.J., Wood, S.H., Liu, D.-Y., Prather, K.A., 2001. *Single Particle Characterization of automobile and Diesel Truck Emissions in the Caldecott Tunnel.* Aerosol Science and Technology, 32, p. 152.

Haefliger, O.P., Zenobi, R., 1998. *New Sample Preparation for quantitative laser desorption mass spectrometry and optical spectroscopy*. Review of Scientific Instruments, 69, p. 1828.

Haefliger, O.P., Bucheli, T.D., Zenobi, R., 1999. *Evolution de la teneur en composés aromatiques des aérosols urbains au cours d'une journée. Etude par spectrométrie de masse à deux lasers*. Analusis, 27, p. 337.

Haefliger, O.P., Bucheli, T.D., Zenobi, R., 2000a. *Laser Mass Spectrometric Analysis of Organic Atmospheric Aerosols. 1. Characterization of Emission Sources.* Environmental Science and Technology, 34, p. 2178.

Haefliger, O.P., Bucheli, T.D., Zenobi, R., 2000b. *Laser Mass Spectrometric Analysis of Organic Atmospheric Aerosols. 2. Elucidation of Urban Air Pollution Processes.* Environmental Science and Technology, 34, p. 2184.

Heger, H.J., Zimmermann, R., Dorfner, R., Beckmann, M., Griebel, H., Kettrup, A., Boesl, U., 1999. *On-line emission analysis of Polycyclic Aromatic Hydrocarbons down to pptv Concentration Levels in the Flue Gas of an Incineration Pilot Plant with Mobile Resonance-Enhanced Multiphoton Ionization Time-of-Flight Mass Spectrometer.* Analytical Chemistry, 71, p. 46.

Jayne, J.T., Leard, D.C. Zhang, X., Davidovits, P., Smith, K.A., Kolb, C.E., Worsnop, D.R., 2000. *Development of an Aerosol Mass Spectrometer for Size and Composition Analysis of Submicron Particles.* Aerosol Science and Technology, 33, p. 49.

Liu, P., Ziemann, P.J., Kittelson, D.B., McMurry, P.H., 1995a. *Generating Particle Beams of Controlled Dimensions and Divergence I. Theory and Particle Motion in Aerodynamic Lenses and Nozzle Expansions.* Aerosol Science and Technology, 22, p. 293.

Liu, P., Ziemann, P.J., Kittelson, D.B., McMurry, P.H., 1995b. *Generating Particle Beams of Controlled Dimensions and Divergence : II. Experimental Evaluation of Paticle Motion in Aerodynamic Lenses and Nozzle Expansions.* Aerosol Science and Technology, 22, p. 314.

Palm, W.-U., Elend, L.-E., Krüger, U., Zetzsch, C., 1999. *Atmospheric degradation of a semivolatile aerosol-borne pesticide: reaction of OH with pyrifenox (an oxime-ether) adsorbed on SiO_2.* Chemosphere, 38, p. 1241.

Trimborn, A., Hinz, K.P., Spengler B., 2000. *On-line analysis of Atmospheric Particles with a transportable Laser Mass Spectrometer. Aerosol* Science and Technology, 33, p. 191.

Vogt, R., Kirchner, U., Scheer, V., Hinz, K.P., Trimborn, A., Spengler, B., 2003. *Identification of diesel exhaust particles at an Autobahn, urban and rural location using single-particle mass spectrometry.* Journal of Aerosol Science, 34, p. 319.

Woods, E., Smith, G.D., Dessiaterik, Y., Baer, T., Miller, R.E., 2001. *Quantitative Detection of Aromatic Compounds In Single Aerosol Particle Masse Spectrometry.* Analytical Chemistry, 73, p. 2317.

Woods, E., Smith, G.D., Miller, R.E:, Baer, T., 2002. *Depth Profiling of Heterogeneously Mixed Aerosol Particles Using Single Particle Mass Spectrometry.* Analytical Chemistry, 73, p. 2317.

Zimmermann, R., Heger, H.J., Kettrup, A., Boesl, U., 1997. *A Mobile Resonance Laser Ionization Time-of-flight Mass Mass Spectrometry – Device for On-line Analysis of Aromatic Pollutants in Waste Incinerator Flue Gases.* Rapid Communication in Mass Spectrometry, 11, p. 1095.

Zimmermann, R., Heger, H.J., Blumenstock, M., Dorfner, R., Schramm, K.W., Boesl, U., Kettrup, A., 1999. *On-line Measurement of Chlorobenzene in Waste Incineration Flue Gas as a Surrogate for the Emission of Polychlorinated Dibenzo-p-dioxines /furanes (I-TEQ) Using Mobile Resonance Laser Ionization Time-of-flight Mass Spectrometry.* Rapid Communication in Mass Spectrometry, 13, p. 307.

7. Perspectives

J'envisage de poursuivre, dans le futur, les deux axes de recherches qui m'ont guidé à ce jour, notamment la chimie atmosphérique et l'exobiologie. Cette double activité a été toujours très fructueuse et captivante pour moi, surtout en vue des nombreux liens entre ces deux domaines. Ces liens se trouvent non seulement dans les techniques expérimentales employées, qui se distinguent à peine, mais également dans les questionnements scientifiques actuels :

Par exemple, les aérosols, comme dans l'atmosphère terrestre, jouent aussi un rôle très important dans les atmosphères planétaires (par exemple sur Titan). Un autre exemple est la chimie prébiotique qui aurait menée à l'origine de la vie : Il est très probable que cette chimie est de caractère *hétérogène*, à la frontière entre deux phases microphysiques (Maurel et Ricard, 2006). Dans l'atmosphère terrestre, la chimie hétérogène, entre la phase solide et gazeuse, est également un sujet très actuel où de nombreuses lacunes persistent toujours.

En ce qui concerne les techniques expérimentales utilisées, la spectrométrie de masse à photoionisation et la spectroscopie de fluorescence (induite par laser ou rayonnement synchrotron), techniques sur lesquelles j'ai été formé abondamment pendant mon chemin, sont utilisées pleinement dans le deux domaines scientifiques auxquels je me suis dédié. A noter enfin que le LISA, laboratoire auquel je suis rattaché, est pour moi un endroit idéal pour évoluer dans les deux directions.

7. 1 Etude de la chimie de l'aérosol par SPLAM

En terme de recherches sur les aérosols terrestres, on peut distinguer deux grandes thématiques dans lesquels l'instrument SPLAM s'intégrera dans le futur :

- *Thématique I :* L'étude du cycle de vie de l'aérosol atmosphérique et ses impacts en climatologie.
- *Thématique II :* Impacts environnementaux des particules atmosphériques en tant que polluants atmosphériques.

Je détaillerai, aux paragraphes 7.1.1 et 7.1.2 les questionnements importants liés à ces deux thématiques auxquels l'expérience SPLAM pourra fournir des éléments de réponse. Dans la suite je discuterai brièvement d'autres perspectives liées à l'expérience SPLAM (paragraphes 7.1.3 et 7.1.4)

7.1.1 L'étude du cycle de vie de l'aérosol et ses impacts en climatologie

α) Caractérisation en temps réel de l'aérosol organique secondaire (AOS)

La meilleure caractérisation des aérosols atmosphériques reste certainement l'identification des espèces chimiques qui le constituent. Une modélisation complète du cycle de vie de l'aérosol (formation / vieillissement) devra prendre en compte toutes les espèces chimiques intervenantes, le plus complètement possible. Un instrument analytique capable de mesurer ces espèces de manière quantitative est donc indispensable afin de comparer les résultats de ces modèles avec des mesures sur le terrain ou au laboratoire. L'étude de la formation et du vieillissement de l'AOS est notre principal objectif scientifique dans l'avenir proche et sera menée dans la nouvelle chambre de simulation CESAM au LISA. J'envisage d'y étudier, en collaboration avec J.F Doussin, E. Perraudin et S. Perrier du LISA, la formation des AOS à partir des précurseurs biogéniques (terpènes et autres) et anthropiques (alkyle-benzènes, indène) qui seront mis en interaction avec l'ozone ou le radical OH.

β) Différences entre la composition surfacique et la composition de la particule entière

Au cœur de SPLAM se trouve un laser infrarouge pulsé dédié à la vaporisation de la particule. L'énergie de ce laser sera variable : on peut ainsi vaporiser soit la particule entière soit uniquement des couches de surfaces de différentes épaisseurs. Il y a donc la possibilité de différencier entre la spéciation chimique de la surface (l'épaisseur de la couche étant bien définie par l'énergie du faisceau laser IR) et la spéciation en volume. Notre appareil SPLAM sera pratiquement unique en Europe à cet égard. Notons que les espèces d'une couche de surface seront vraiment identifiées par SPLAM, contrairement à d'autres techniques qui spécifient uniquement les groupements fonctionnels *sur* la surface (comme c'est fait par exemple par Demirdjian et Rossi, 2002). Des expériences de ce genre ont été déjà effectuées par le groupe de Tomas Baer à l'Université de la Caroline du Nord (Woods et al., 2002) et s'avèrent particulièrement prometteuses pour l'étude du vieillissement *surfacique* des particules. Ces investigations sont importantes parce qu'un lien avec l'hygroscopicité des particules peut être établie. L'hygroscopicité, notamment le facteur de grossissement d'un type de particules, est un paramètre très important à connaître en climatologie.

γ) Réactivité des particules envers d'autres gaz atmosphériques

Les particules influencent de fait les propriétés physico-chimiques de l'atmosphère : on peut considérer que les mécanismes réactionnels en phase gazeuse sont perturbés par la chimie

hétérogène entre phase gazeuse et phase condensée (« *Chimie multiphasique* »). Ceci affecte les taux de formation et de destruction de polluants primaires (NO_x, NO_y, COV) et secondaires (ozone, PAN etc…). Ainsi les particules peuvent avoir des effets indirects sur la qualité de l'air. L'importance de ce rôle de l'aérosol atmosphérique est loin d'être compris aujourd'hui.

La réactivité rapide des particules, et de leurs composés adsorbés, envers l'ensemble des gaz réactifs présents dans l'atmosphère (« chimie hétérogène ») reste difficile à étudier expérimentalement au laboratoire si on souhaite connaître simultanément l'évolution des espèces en phase gazeuse *et* particulaire (différenciée par surface et volume si possible…). Ceci n'est pas réalisable avec les moyens expérimentaux classiques, tels que les cellules de Knudsen et tubes à écoulement (avec particules déposées), etc... Par contre, les techniques en « temps réel » de spectrométrie de masse pour aérosols, couplées à un réacteur à écoulement ou une chambre de simulation, pourront fournir, dans l'avenir, des données expérimentales de cinétique rapide en deux phases simultanément (Schwell et al., 2000 ; Smith et al., 2002).

7.1.2 Impacts environnementaux des aérosols en tant que polluants atmosphériques

Les effets des particules sur la santé ont été mis en évidence par de nombreuses études épidémiologiques (voir par exemple Dab et al., 2001). Cependant, les éléments déterminant la toxicité des particules (taille, masse, métaux lourds, matière organique, polluants adsorbés ?) ne sont pas encore bien identifiés (Lambrozo, 2000). Les particules atmosphériques constituent de véritables micro-réacteurs, de morphologie et de composition extrêmement complexe et variable. Il parait nécessaire, pour comprendre leur impact sur un organisme vivant, d'être capable d'identifier la composition chimique de l'aérosol atmosphérique, en volume et en surface.

α) Origine de particules fines et ultrafines dans les zones d'exposition des populations

Un spectromètre de masse pour aérosols qui est capable de déterminer les espèces au niveau moléculaire permettra une classification chimique plus détaillée des *particules réelles de terrain*, par rapport à ce qui est possible aujourd'hui. A partir de cette classification, des études de « *source apportionment* » (suivi et quantification des traceurs de pollution) d'une nouvelle qualité seront ainsi possibles. On se libérerait ainsi des classifications EC (*« elemental carbon »*), OC (*« organic carbon »*), BC (*« black carbon »*), WSOC et WISOC (*« water-soluble »* et *« water-insoluble organic carbon »*) etc…, classifications souvent trop grossières pour identifier précisément une source de pollution. La spéciation chimique, en

fonction de la granulométrie en nombre, permettra l'identification et par la suite l'analyse du cycle de vie des traceurs moléculaires de pollution. Le système SPASS (Single Particle Analysis and Sizing System) du JRC[1], qui est très similaire à notre instrument SPLAM, a été déjà employé sur le terrain avec succès (Erdmann et al., 2005).

β) Responsabilités des particules atmosphériques dans la dissémination des pesticides et d'autres polluants organiques persistants (POP)

La dégradation de la qualité de l'air par des polluants difficilement dégradables tels que HAP, polychlorobiphényles (PCB), pesticides, dioxines etc… crée des problèmes importants en matière de santé publique et de qualité de l'environnement (Xhillari, 2000 ; Lamiot, 2001). Une grande partie de ces polluants ont de faibles tensions de vapeur saturante : on les retrouve donc pour partie ou complètement condensés sur les particules de l'aérosol atmosphérique (voir par exemple Brunciak et al., 2001a,b ; Venkataraman et al., 1999). L'étude de la répartition entre phases de ces espèces (par exemple en chambre de simulation) est donc nécessaire afin de déterminer le rôle des particules dans la dissémination de ces composés dans l'environnement. De plus, les taux de dégradation de ces composés en phase condensée (ou adsorbée) peuvent être plus bas par rapport à la dégradation en phase gazeuse homogène (voir par exemple Palm et al., 1999). En effet, depuis la découverte inattendue de certains POP dans des milieux lointains (Arctique, lacs de montagne etc…), l'hypothèse a été émise que leurs taux de dégradation seraient réduits en phase particulaire.

En conclusion, les durées de vie de ces polluants semi-volatils dans la troposphère sont donc difficilement prévisibles aujourd'hui. Une modélisation réaliste de leur dissémination dans l'environnement troposphérique exige la connaissance des coefficients de répartition entre phases, et de la cinétique de dégradation des ces composés. C'est un domaine de recherche émergent auquel l'expérience SPLAM pourra participer dans le futur grâce à sa capacité d'analyser les composés aromatiques avec des limites de détections très basses.

[1] JRC = Joint Research Center : Centre Européen de Recherche à Ispra (Italie). Le SPASS est actuellement développé dans l'IES (*Institue for Environment and Sustainability*) par plusieurs chercheurs (C. Grüning, J. Hjorth, D. Mira-Salama,).

7.1.3 Propriétés photochimiques des COV biogéniques et anthropiques et leurs produits de dégradation dans l'ultraviolet lointain

La plupart des énergies d'ionisation et des énergies seuil de fragmentation sont inconnues pour les COV-B et aussi pour certains COV-A. Ces données de base en spectrométrie de masse sont encore moins connues pour leurs produits de dégradation dans l'atmosphère. Or, pour l'interprétation des spectres de masse à photoionisation utilisant un rayonnement monochromatique (laser ou lampe eximère), ces données sont pratiquement indispensables. Nous avons donc décidé de mener une campagne au synchrotron BESSY utilisant la méthode PIMS (cf. paragraphe 3.4), afin de mesurer les IEs et AEs de certains COV-B et COV-A qui nous intéressent dans le cadre de l'étude de l'AOS avec l'expérience couplée SPLAM / CESAM (thématique 7.1.1). Les premières expériences au synchrotron BESSYII, dédiées à ce projet, ont été réalisées en octobre 2006. La deuxième période de mesure est programmée en Mars 2007. Il s'agit d'un projet en collaboration avec l'Université libre de Berlin (Prof. Eckart Rühl).

7.1.4 Perspectives de développement technique de SPLAM

Ils existent de nombreuses perspectives concernant le développement technique de SPLAM :

α) La première priorité est un développement technique qui a été entamé cette année (2006) par Sébastien Perrier, ingénieur de recherche au LISA. Il s'agit du développement d'un mode de thermodésorption de particules du spectromètre de masse. Pour cela, un petit manipulateur est intégré dans la source d'ions. La pointe de ce manipulateur est chauffable jusqu'à 400°C et il se trouvera dans l'axe du jet de particules. Les particules y seront vaporisées, de manière continue, lors de leur impact. Ce mode nous permet

- de travailler à très haute concentration de particules (10^5 à 10^6 cm^{-3}) ce qui n'est pas possible dans le mode « *single particle* » à cause des fausses coïncidences dans la détection optique. Nous serons ainsi plus sensible chimiquement, mais au prix de la perte d'information sur la taille des particules.
- d'analyser également, *en temps réel*, les molécules organiques sur particules *ultrafines* (<150 nm) (toutes tailles confondues). Notons que, dans le mode « *single particle* », nous ne verrons pas ces particules parce qu'elles ne diffusent pas assez de lumière pour être détectées dans la chambre optique.

Dans ces expériences, le spectromètre de mass à temps de vol fonctionnerait à une cadence *régulière*, c'est-à-dire non-déclenché par l'arrivée d'une particule. Ce mode de fonctionnement est adapté à l'étude de la formation de l'AOS en chambre de simulation où nous avons accès à de très hautes concentrations de particules (y inclues des particules ultrafines en début d'une expérience typique).

β) Une deuxième perspective de développement technique concerne l'utilisation d'une lampe VUV compacte au lieu d'un laser pour l'ionisation directe des molécules proche de leur seuil d'ionisation. L'utilité d'une telle lampe a été déjà discutée au paragraphe 6.2.3. Une telle capacité parait très avantageuse en vue des applications de SPLAM sur le terrain (cf. paragraphes 7.1.2 α,β).

γ) Une autre méthode afin de produire des photons VUV pour la photoionisation proche du seuil d'ionisation consiste en le développement d'une source de lumière VUV à plasma laser (Flesch et al., 2000 ; Richardson, 2000). L'avantage serait la production des photons VUV *de longueur d'onde accordable* ce qui donnerait la possibilité d'analyser les molécules sélectionnées en triant sur leurs énergies d'ionisation. Par contre, une telle source sera certainement limitée aux expériences de simulation menée au laboratoire. Cette perspective est envisagée à long terme.

7. 2 Etude de la photochimie VUV des molécules prébiotiques et biologiques

Dans la continuation de mes travaux sur la photochimie VUV des molécules d'intérêt exobiologique, deux champs d'investigation se dessinent dans le futur.

7.2.1 Etude de la photoabsorption VUV des molécules d'intérêt exobiologique et astrophysique à basse température

Ceci est un projet qui a été commencé très récemment au LISA en collaboration avec le groupe de physico-chimie organique spatiale, sur les molécules HCN C_4H_2, HC_3N, HC_5N et CH_3CN (cf. paragraphe 3.2) qui sont toutes détectées dans la haute atmosphère de Titan.

L'instrument UVIS à bord de la sonde Cassini est un spectrographe chargé de mesurer des spectres de l'atmosphère de Titan dans l'UV lointain (110-190 nm) et l'UV « extrême » (56-118 nm) avec une résolution de 2.75 Å au mieux. Les mesures d'UVIS sont effectuées durant les occultations stellaires et les profils verticaux des composés présents dans la haute atmosphère (1600 km à 400 km d'altitude) peuvent ainsi être obtenus (Shemansky et al., 2005). Néanmoins, pour ces analyses les coefficients d'absorption des différentes espèces

présentes doivent être connus. Or, ces données n'existent pas *à basse température*. Dans l'atmosphère de Titan, on peut distinguer une mésophère, de 615 à 300 km d'altitude avec des températures de 114 à 180 K (Shemansky et al., 2005 ; Flasar et al., 2005) et une stratosphère, de 300 à 50 km d'altitude environ, avec des températures entre 180 et 70 K (Flasar et al., 2005).

Nous avons donc développé une cellule d'absorption réfrigérante dans le but d'obtenir les coefficients d'absorption dans le domaine de l'UV lointain (> 115 nm) et dans des domaines de température de la mésosphère et de la stratosphère de Titan. Le but de cette expérience est donc de (a) pouvoir mieux interpréter les données UVIS et de (b) améliorer les modèles photochimiques de Titan en apportant des sections efficaces de photoabsorption aux basses températures. Les spectres d'absorption peuvent être mesurés à une résolution de 0.05 Å ou mieux utilisant le monochromateur 10 m sur la ligne onduleur U125/2 du synchrotron BESSY.

Les premiers résultats obtenus lors de 3 campagnes au synchrotron BESSY en 2005/2006 montrent clairement que l'effet de la température sur les coefficients d'absorption dans le VUV est loin d'être négligeable pour HCN, HC_3N, HC_5N, et C_4H_2. Généralement, les bandes d'absorption sont moins larges et le maximum de l'absorption est plus élevé lorsque la température baisse. Ce résultat est important et nous envisageons de continuer et approfondir ce programme de recherche.

7.2.2 Etude de la photochimie VUV des molécules biologiques plus grandes en phase gazeuse

Dans la continuation de nos expériences de spectrométrie de masse photoionique sur les petites biomolécules j'envisage, à moyen terme, d'utiliser spectrométrie de masse à thermodésorption d'aérosols (cf. paragraphe 7.1.4α, fig. 14) pour étudier l'ionisation et l'ionisation dissociative des biomolécules *plus grandes* en phase gazeuse.

Il a été démontré très récemment que la production des nanoparticules biologiques, en utilisant un atomiseur, suivie de leur entrée dans le vide d'un spectromètre de masse et leur thermodésorption (à température relativement basse !), est un moyen très efficace pour mettre des biomolécules plus grandes en phase gazeuse (Wilson et al., 2006a et b). Notons que, avec l'expérience PIMS utilisée actuellement au synchrotron BESSY, il n'est pas possible d'étudier des molécules moins volatiles que l'uracile ou l'acide α-amino isobutyrique (AIB). La *spectrométrie de masse à thermodésorption des nanoparticules* permet ainsi de propulser de grandes molécules en phase gazeuse ce qui est d'un grand intérêt pour les études

fondamentale menées dans l'exobiologie mais aussi, plus généralement, dans les Sciences du Vivant.

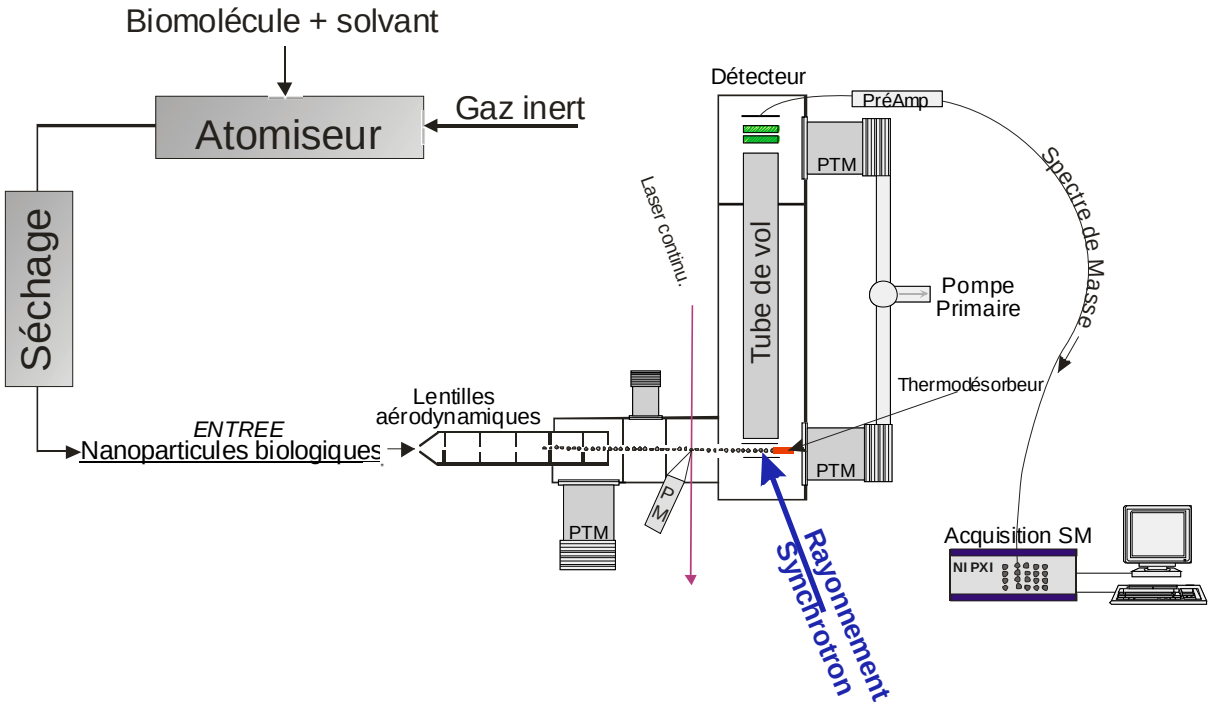

Figure 14 : Spectrométrie de masse photoionique des nanoparticules biologiques.

Ainsi, j'envisage d'étudier dans un premier temps les base d'ADN cytosine et guanine pour savoir si les cations de ces bases sont également stable dans le VUV (<13.6 eV), mais aussi d'entamer des études de photochimie VUV sur des Di- et Tripeptides, et des sucres. L'utilisation d'un spectromètre de masse à temps de vol permettra en plus de connaître les « vrais » rapports de branchement des photoréactions, a cause de sa transmission ionique proche de 100 % sur toute l'échelle de masse. Les spectres de masse enregistrés précédemment avec notre spectromètre quadripolaire possèdent le désavantage que les rapports des fragments observés ne représentent pas correctement les rapports de branchement des photoréactions, parce que sa transmission n'est pas constant sur l'échelle de masse.

Références du chapitre 7

Brunciak, P.A., Dachs, J., Gigiliotti, C.L., Nelson, E.D., Eisenreich, J., 2001a. *Atmospheric polychlorinated biphenyl concentration and apparent degradation in coastal New Jersey.* Atmospheric Environment, 35, p. 3325.

Brunciak, P.A., Dachs, J., Franz, T.P., Gigiliotti, C.L., Nelson, E.D., Turpin, J., Eisenreich, J., 2001b. *Polychlorinated Biphenyls and particulate organic/elemental carbon in the atmosphere of Chesapeake Bay, USA.* Atmospheric Environment, 35, p. 5663.

Dab, W., Ségala, C., Dor, F., Festy, B., Lamelouse, P., Le Moullec, Y., Le Tertre, A., Médina., S., Quénel, P., Wallaert, B., Zmirou, D., 2001. *Pollution atmosphérique et santé : corrélation ou causalité ? Le cas entre exposition aux particules et la mortalité cardio-pulmonaire.* Pollution Atmosphérique No. 170, 219.

Demirdjian, B., Rossi, M.J., 2002. *The Characterization of Surface Functional Groups of Secondary Organic Aerosols (SOA) generated under Laboratory Conditions.* Proceedings of the EC/EUROTRAC-2 Joint CMD-Workshop, Paris 2002.

Erdmann, N., Dell'Acqua, A., Cavalli, P., Grüning, C., Omenetto, N., Putaud, J.-P., Raes, F., Van Dingenen, R., 2005. *Instrument characterization and first application of the single particle analysis and sizing system (SPASS) for atmospheric aerosols.* Aerosol Science and Technology, 39, p. 377-393.

Flasar, F.M., Achterberg, R.K., Conrath, B.J., Gierasch, P.J., Kunde, V.G., Nixon, C.A., Bjoraker, G.L., Jennings, D.E., Romani, P.M., Simon-Miller, A.A., Bézard, B., Coustenis, A., Irwin, P.G., Teanby, N.A., Brasunas, J., Pearl, J.C., Segura, M.E., Carlson, R.C., Mamoutkine, A., Schinder, P.J., Barucci, A., Courtin, R., Fouchet, T., Gautier, D., Lellouch, E., Marten, A., Prangé, R., Vinatier, S., Strobel, D.F., Calcutt, S.B., Read, P.L., Taylor, F.W., Bowles, N., Samuelson, R.E., Orton, G.S., Spilker, L.J., Owen, T.C., Spencer, J.R., Showalter, M.R., Ferrari, C., Abbas, M.M., Raulin, F., Edgington, S., Ade, P., Wishnow, E.H., 2005. *Titan's Atmospheric Temperatures, Winds, and Composition.* Science, 308, p. 975.

Flesch, R., Schürmann, M.-C., Hunnekuhl, M.. Meiss, H., Plenge, J., Rühl, E., 2000. *A Pump-Probe Photoionization Mass Spectrometer Utilizing Tunable Extreme Ultraviolet Laser-Produced-Plasma Radiation.* Review of Scientific Instruments, 71, p. 1319-1324.

Lambrozo, J., 2000. *Remarques sur le Congrès "PM2000 – Particulate Matter and Health " (24-28 January 2000, Charleston, US).* Pollution Atmosphérique, No. 166, 191.

Lamiot, F., 2001. *Les pesticides dans l'air : quels enjeux ?* Pollution Atmosphérique No. 170, 237.

Palm, W.-U., Elend, L.-E., Krüger, U., Zetzsch, C., 1999. *Atmospheric degradation of a semivolatile aerosol-borne pesticide: reaction of OH with pyrifenox (an oxime-ether) adsorbed on SiO_2.* Chemosphere, 38, p. 1241.

Maurel, M.-C., Ricard, J., 2006. *The evolution of catalytic function.* Physics of Life Reviews, 3, p. 56-64.

Richardson, M., 2000. *Laser Produced Plasmas.* Chapitre 5 dans Samson et Ederer, 2000 (voir références des chapitres 1 à 5).

Schwell, M., Baumgärtel, H., Weidinger, I., Krämer, B., Vortisch, H., Rühl, E., Wöste L., Leisner, T., 2000. *Uptake Dynamics and Diffusion of HCl in Sulfuric Acid Solution Measured in Single Levitated Microdroplets.* Journal of Physical Chemistry A, 104, p. 6726-6732.

Shemansky, D.E., Stewart, A.I.F., West, R.A., Esposito, L.W., Hallett, J.T., Liu, X., 2005. *The Cassini UVIS Stellar Probe of the Titan Atmosphere.* Science, 308, p. 978-982.

Smith, G.D., Woods, E., DeForest, C.L., Baer, T., Miller, R.E., 2002. *Reactive Uptake of Ozone by Oleic Acid Aerosol Particles : Application of Single Particle Mass Spectrometry to Heterogeneous Reaction Kinetics.* Analytical Chemistry, 74, p. 2048.

Venkataraman, C., Thomas, S., Kulkarni, P., 1999. *Size Distribution of PAHs - gas/particle partitioning to urban aerosols.* Journal of Aerosol Science, 30, p. 759.

Wilson, K.R., Jimenez-Cruz, M., Nicolas, C., Belau, L., Leone, S.R., Ahmed, M., 2006a. *Thermal Vaporization of Biological Nanoparticles: Fragment-Free Vacuum Ultraviolet Photoionization Mass Spectra of Tryptophane, Phenylalanine-Glycine-Glycine, and β-carotene.* Journal of Physcial Chemisty A, 110(6), p. 2106-2113.

Wilson, K.R., Belau, L. Nicolas, C., Jimenez-Cruz, M., Leone, S.R., Ahmed, M., 2006b. *Direct determination of the ionization energy of histidine with VUV synchrotron radiation.* International Journal of Mass Spectrometry, 249-250, p. 155-161.

Woods, E., Smith, G.D., Miller, R.E:, Baer, T., 2002. *Depth Profiling of Heterogeneously Mixed Aerosol Particles Using Single Particle Mass Spectrometry.* Analytical Chemistry, 73, p. 2317.

Xhillari, D., 2000. Health impact assessment of air Pollution in the WHO european region – A standardized approach. Pollution Atmosphérique No. 166, 561 et références y citées.

8. Remerciements

Je remercie tout d'abord Sydney Leach (*Observatoire de Paris-Meudon*) qui m'a accompagné dans ces huit dernières années. Sans lui je n'aurais sans doute pas abouti à la réalisation des travaux qui ont permis la rédaction de cet ouvrage. Son aide et ses conseils, toujours de valeur très précieuse, m'ont constamment poussé d'aller plus loin.

Je remercie beaucoup Jean-Louis Colin (*Université Paris 7*) pour m'avoir accueilli dans son équipe au LISA, et le soutien qu'il m'apporte au quotidien. Un grand merci aussi à Jean-Paul Quisefit (*Université Paris 7*) pour son soutien pour le projet SPLAM.

Merci au Professeur Helmut Baumgärtel (*Freie Universität Berlin*) pour son grand soutien dans la dernière décade. Son enthousiasme m'a toujours beaucoup encouragé.

Un grand merci également à Hans-Werner Jochims (*Freie Universität Berlin*) qui m'a beaucoup appris dans la photochimie expérimentale utilisant le rayonnement synchrotron. Je remercie Jean-Louis Chotin (*Observatoire de Paris-Meudon*) et François Dulieu (*Université de Cergy-Pontoise*) pour leur aide compétente pendant les « runs » à BESSY.

Je remercie Antoine Jolly, Nicolas Fray, Marie-Claire Gazeau et Yves Bénilan (*Université Paris 12*) pour notre belle collaboration sur les polyynes et les cyanopolyynes. C'est génial que nous continuions ensemble à explorer la photochimie VUV des espèces qui auraient pu mener à l'origine de la vie.

Finalement je remercie mes sponsors : le programme national de chimie atmosphérique, le ministère de recherche, le ministère de l'environnement pour leur soutien dans le projet SPLAM. Je remercie le GDR Exobiologie, le synchrotron BESSY, le programme national de physico-chimie interstellaire pour leur soutien des projets que je mène dans l'exobiologie.

Un grand merci à Isabelle Kleiner pour ces fermes encouragements pendant la rédaction de cette notice, et pour avoir lu et corrigé le manuscrit.

9. Curriculum Vitae et liste de publications

Dr. Martin SCHWELL
Maître de conférences Université Paris 7 Denis Diderot
Laboratoire Interuniversitaire des Systèmes Atmosphériques (LISA), UMR 7583 du CNRS

né le 9.7.1967 à Bonn (Allemagne), vie maritale, 1 enfant

Domicile : 35, Bd Auguste Blanqui, F-75013 PARIS
Tél.: 01 4588 2875 et 06 2028 2003

e-mail: schwell@lisa.univ-paris12.fr

FORMATION:

1986-1988	Formation Officier de l'armée.
1988-1994	**Etudes de chimie** et de *Romanistik* à la *Rheinische Friedrich-Wilhelms-Universität Bonn* et à la *Freie Universität Berlin*, diplôme de chimie de la *Freie Universität Berlin* (Mention "très bien").
1998	**Thèse de doctorat** de la *Freie Universität Berlin:* Titre: *"Observation de l'absorption de gaz chlorhydrique par des gouttelettes isolées d'acide sulfurique dans des conditions stratosphériques"* (Soutenue le 18 Juin 1998, mention "avec les félicitations").

DOMAINES DE CONNAISSANCES APPROFONDIES

Physico-chimie de l'atmosphère terrestre, physico-chimie des aérosols.

Physico-chimie des systèmes extraterrestres et exobiologie.

Spectroscopie d'absorption et d'émission dans l'UV/Vis et l'UV lointain.

Spectrométrie de masse, pièges ioniques, techniques lasers pulsés.

Utilisation du rayonnement synchrotron.

LANGUES ETRANGERES

Français, anglais : niveau bilingue ; Espagnol : connaissances élémentaires

ACTIVITES DE RECHERCHE

Janv 1997	**Cours Européen de Recherche sur les Atmosphères (ERCA) à Grenoble (France)**
Mars 94 - Octobre 94:	**Chercheur à la *Freie Universität Berlin* dans le cadre du *Programme national allemand de la recherche sur l'ozone:*** Travaux sur la spectroscopie et la photochimie des oxydes de chlore OClO et Cl_2O_2 en phase gazeuse, expériences laser pompe/sonde : détermination des rapports de branchements des réactions élémentaires, utilisation de lumière synchrotron.
Novembre 94 - Septembre 98:	**Chercheur à la *Freie Universität Berlin* dans le projet universitaire :** ***« Propriétés des aérosols atmosphériques importants en climatologie »*** Montage d'un nouvel appareil conçu pour l'étude des propriétés optiques et du comportement physico-chimique des particules micrométriques individuelles dans un piège ionique et dans des conditions de la stratosphère terrestre (basses température et basses pressions). Développement des nouvelles méthodes pour l'étude de l'interaction phase gaz/phase condensée. Etude de l'absorption de HCl (g) par des gouttelettes d'acide sulfurique sous-refroidies. Détermination des taux de nucléation de congélation des divers liquides abondants dans la stratosphère. Préparation de la thèse de doctorat à la *Freie Universität Berlin.*
Octobre 98 – septembre 2001	**Chercheur postdoctoral à l'Observatoire de Paris-Meudon et à l'Université de Cergy-Pontoise dans le cadre du réseau européen USEFULL: *« Usable Fullerene Derivatives: Synthesis, Stabilisation, Spectroscopy and Systematics »*** Travaux sur la spectroscopie et la photochimie des molécules d'intérêt astrophysique et exobiologie, utilisation du rayonnement synchrotron (LURE/Orsay et BESSY/Berlin), utilisation de spectroscopie de masse (temps de vol et quadripolaire), utilisation de la spectroscopie de fluorescence et d'absorption. Travaux sur la spectroscopie et les propriétés photophysiques des nouveaux dérivés des fullerènes ayants des applications potentielles en optoélectronique et en médecine : Etude par spectroscopie stationnaire et par spectroscopie résolue en temps (CEA/Saclay), par photolyse laser et radiolyse pulsée (*Paterson Institute for Cancer Research*, Manchester).
Depuis Septembre 2001	**Enseignant-chercheur à l'Université Paris 7, rattaché au LISA.** Développement de spectrométrie de masse appliquée à l'étude de l'aérosol atmosphérique, soutenu par le programme national de chimie atmosphérique (PNCA). Responsable scientifique d'une ACI du MRT : *« Nouvelles Méthodes pour l'analyse chimique de l'aérosol atmosphérique »,* en partenariat avec l'université d'Aix Marseille 1. Responsable scientifique du projet « *SPLAM - Single Particle Laser Ablation Mass spectrometry »* du programme PRIMEQUAL « Particules » du Ministère de l'environnement et du développement durable (MEDD) et de l'ADEME. Spectroscopie et photochimie VUV des molécules d'intérêt exobiologique, utilisation du rayonnement synchrotron (BESSY/Berlin). Nombreux projets soutenus par le GDR Exobiologie, le programme national de physico-chimie interstellaire (PCMI), et le synchrotron BESSY à Berlin.

ACTIVITES D'ENSEIGNEMENT A L'UNIVERSITE PARIS 7 DENIS DIDEROT :

- Licence :
  - Projet expérimental de chimie (L2S3, UE obligatoire de 6 ECTS)
- Master Sciences et Génie de l'environnement (SGE)
  - M1 :
    - UE « Métrologie » (UE obligatoire de 6 ECTS). Cours de métrologies des aérosols.
    - UE « Chimie analytique » (UE optionnel de 3 ECTS). Cours et travaux pratiques de chromatographie en phase gazeuse couplée à la spectrométrie de masse.
  - M2 spécialités « Atmosphères et Qualité de l'Air (AQA) » et « Aérocontamination, aérosols et bioaérosols (AERO)»
    - Responsable pédagogique UE « Chimie des aérosols » (UE obligatoire AQA et AERO, de 3 ECTS)
    - UE « Projet pratique de terrain » (UE obligatoire AQA, de 6 ECTS)
    - Responsable pédagogique UE « Polluants non-réglementés » (UE optionnel AQA, de 3 ECTS).
    - UE « Métrologie de l'atmosphère » (3 ECTS, UE obligatoire AQA). Cours avancé de métrologie de particules atmosphériques.

ACTIVITES ACADEMIQUES A L'UNIVERSITE PARIS 7 DENIS DIDEROT :

- Membre élu du Conseil Scientifique de l'Université Paris 7 (depuis 2006).
- Membre élu du Conseil Scientifique de l'UFR de Chimie de l'Université Paris 7 (depuis 2004).
- Membre élu de la Commission des Spécialistes 32e section CNU (depuis 2003).
- Délégué de l'UFR de Chimie pour le développement des cursus intégrés avec les universités allemandes.
- Responsable de programme « Licence Franco-Allemande de chimie » en partenariat avec l'Université de Bielefeld (Rhénanie-du-Nord-Westphalie).
- Responsable des Relations Internationales du Master « Sciences et Génie de l'Environnement (SGE) »

MEMBRE DES SOCIETES SAVANTES :

- Deutsche Bunsengesellschaft für Physikalische Chemie (DBG)
- Association Française d'Etudes et de Recherches sur les Aérosols (ASFERA)
- European Exo/Astrobiology Network Association (EANA)
- Société Française de Chimie

ACTIVITES D'ENCADREMENT DEPUIS 2001 :

Stages de maîtrise
1) Stage de maîtrise chimie Université Paris 7, **2003.** Maître de stage de M Michael REYNAUD : Titre du mémoire de stage de maîtrise : *Etude des produits phytosanitaires dans l'atmosphère urbaine par chromatographie en phase gazeuse couplée à la spectrométrie de masse.*
Stages DEA
1) DEA « Chimie de la Pollution atmosphérique et physique de l'environnement » **2002.** Maître de stage de M Mathieu GORIAUX Titre du mémoire de DEA : *Les particules automobiles à l'émission : granulométrie et partition gaz particule des Hydrocarbures aromatiques polycycliques (HAP).*
2) DEA « Chimie de la Pollution atmosphérique et physique de l'environnement » **2004.** Maître de stage de Mlle Aikaterini BOUGIATIOTI Titre du mémoire de stage DEA : *Mise au point d'un spectromètre de masse à ionisation laser pour l'analyse en temps réel des polluants organiques semi-volatils*
Thèses de doctorat
1) Codirecteur de thèse et encadrant principal de M François GAIE-LEVREL (Bourse MRT, ED129 - Sciences de l'environnement Ile-de-France), **depuis Octobre 2005**. Sujet de thèse : *Mise au point d'un spectromètre de masse à ionisation laser pour l'analyse des particules individuelles de l'aérosol organiques secondaire (SPLAM – Single Particle Laser Ablation Mass Spectrometry)*
2) Co-encadrant de thèse M Thomas FERRADAZ et membre de comité de suivi de thèse (Bourse MRT, ED129 - Sciences de l'environnement Ile-de-France), **depuis Octobre 2005**. Sujet de thèse : *Spectroscopie VUV à basses températures de molécules d'intérêt planétologiques - Application à l'atmosphère de TITAN*
Encadrement des stages dans le cadre de la convention de l'Université Paris 7 avec l'Université de Bielefeld (Allemagne)
1) Semestre pratique M Christoph STOLL, Université de Bielefeld, **2005.** Thème : *Dessin et construction d'un système d'entrée à aérosols pour un spectromètre de masse à temps de vol*
2) Diplomarbeit M Christoph STOLL, Université de Bielefeld, **2006**. Titre de la Diplomarbeit : *Charakterisierung eins Flugzeitmassenspektrometers mit Laserionisation im Hinblick auf seine Anwendung zur Analyse sekundärer organischer Aerosole*
3) Bachelorarbeit Mme Lisa BUBLITZ, Université de Bielefeld, **2007.** Titre (préliminaire): *Untersuchng der Aerosolbildung durch Ozonolyse von Inden.*

Publications dans Revues à Comité de Lecture

1. B. Krämer, **M. Schwell**, O. Hübner, H. Vortisch, T. Leisner, E. Rühl, H. Baumgärtel, L. Wöste :
   « **Homogeneous Ice Nucleation observed in Single Levitated Microdroplets** »
   Berichte der Bunsengesesllschaft für Physikalische Chemie **100** (1996), 1911-1915.
2. **M. Schwell**, H.-W. Jochims, B. Wassermann, U. Rockland, R. Flesch and E. Rühl :
   « **Ionization Energies of ClO and Cl_2O_2** »
   Journal of Physical Chemistry **100** (1996), 10070-10075.
3. B. Krämer, **M. Schwell**, O. Hübner, H. Vortisch, E. Rühl, H. Baumgärtel, L. Wöste, T. Leisner :
   « Homogeneous Nucleation Rates of Supercooled Water Measured in Single Levitated Microdroplets »
   Journal of Chemical Physics **111** (1999), 6521-6527.
4. H. Vortisch, B. Krämer, I. Weidinger, L. Wöste, T. Leisner, **M. Schwell**, H. Baumgärtel, E. Rühl :
   « **Homogeneous freezing nucleation rates and crystallization dynamics of single levitated sulfuric acid solution droplets** »
   Physical Chemistry Chemical Physics (PCCP) **2** (2000), 1407-1413.
5. **M. Schwell** and H. Baumgärtel, I. Weidinger, B. Krämer, H. Vortisch, E. Rühl, L. Wöste, T. Leisner :
   « **Uptake Dynamics and Diffusion of HCl in Sulfuric Acid Solution Measured in Single Levitated Microdroplets** »
   Journal of Physical Chemistry A **104** (2000), 6726-6732.
6. **M. Schwell,** F. Dulieu, C. Gée, H.-W. Jochims, J.-L. Chotin, H. Baumgärtel and S. Leach :
   « Photoionization Mass Spectrometry of Six Isomers of C_7H_8 in the 7-22 eV Photon Energy Range »
   Chemical Physics **260** (2000), 261-279.

7. **M. Schwell,** T. Gustavsson, S. Marguet, B. de La Vassière, N. Wachter, P. Birkett, J.-C. Mialocq, S. Leach :
   « The fluorescence of the phenylated fullerenes $C_{70}Ph_4$, $C_{70}Ph_6$, $C_{70}Ph_8$, and $C_{70}Ph_{10}$ in room temperature solution »

   Chemical Physics Letters **350** (2001)**,** 33-38**.**

8. **M. Schwell**, N. Wachter, J. Rice, J.P. Galaup, S. Leach, R. Taylor, E. Land, R.V. Bensasson:
   « **Coupling a dendrimer and a fullerene chromophore: A study of excited state properties of C_{61}(poly(aryl)acetylene)$_2$** »

   Chemical Physics Letters **339** (2001), 29-35.

9. **M. Schwell**, S. Leach, K. Hottmann, H.-W. Jochims, H. Baumgärtel :
   « **He I photoelectron spectroscopy of formic acid isoptopomers HCOOH and DCOOD** »

   Chemical Physics **272** (2001), 77-90.

10. R.V. Bensasson, **M. Schwell**, M. Fanti, N. Wachter, J. Lopez, J.-M. Janot, P. Birkett, E.J. Land, S. Leach, P. Seta, R; Taylor and F. Zerbetto:
    « **Photophysical properties of the ground and triplet state of four multi-phenylated [70] Fullerene compounds** »

    ChemPhysChem. **2** (2001), 109-114.

11. **M. Schwell,** F. Dulieu, H.-W. Jochims, J.-H. Fillion, J.-L. Lemaire, H. Baumgärtel and S. Leach :
    « Photophysical Studies od Formic Acid in the 6-23 eV Photon Energy Range : II Fragmentation, Fluorescence and Ionisation »

    Journal of Physical Chemistry A 106 (2002), 10908-10918

12. S. Leach, **M. Schwell,** F. Dulieu, H.-W. Jochims, H. Baumgärtel :
    « Photophysical Studies od Formic Acid in the 6-23 eV Photon Energy Range : I Photoabsorption »

    Physical Chemistry Chemical Physics (PCCP) **4** (2002), 5025-5039.

13. S. Leach, **M. Schwell**, D. Talbi, G. Berthier, K. Hottmann, H.-W. Jochims, H. Baumgärtel :

    « He I photoelectron spectroscopy of four isotopologues of formic acid: HCOOH, HCOOD, DCOOH and DCOOD »

    Chemical Physics **286** (2003), 15-43.

14. H.-W. Jochims, **M. Schwell**, J.-L. Chotin, M. Clemino, F. Dulieu, H. Baumgärtel, S. Leach :

    « Photoion mass spectrometry of five amino acids in the 6–22 eV photon energy range »

    Chemical Physics **298** (2004), 279-297.

15. H.W. Jochims, **M. Schwell**, H. Baumgärtel, S. Leach:

    « Photoion mass spectrometry of adenine, thymine and uracil in the 6–22 eV photon energy range »

    Chemical Physics **314** (2005), 263-282.

16. H.-W. Jochims, **M. Schwell**, S. Un, H. Baumgärtel, S. Leach :

    « VUV Absorption spectrum of Acetic Acid between 6 and 22 eV »

    Chemical Physics **321** (2006), nos. 1-2, 159-170.

17. H.-W. Jochims, **M. Schwell**, S. Un, H. Baumgärtel, S. Leach :

    « VUV Photophysics of Acetic Acid: Fragmentation, Fluorescence and Ionization in the 6-23 eV region »

    Chemical Physics **321** (2006), nos. 1-2, 171-182.

18. **M. Schwell**, H.-W. Jochims, H. Baumgärtel, S. Leach :

    « VUV photochemistry of small biomolecules »

    Planetary and Space Science **54** (2006), 1073-1085.

Chapitres dans des Livres

1. C. George, B. Aumont, B. Bessagnet, M. Rossi, **M. Schwell**, C. Seigneur, E. Villenave: **« Physicochimie et Transport des Particules »**

   Dans: *« Pollution par les particules atmosphériques: état des connaissances et perspectives de recherche »* Editeurs : P. Ebner, Y. Le Moullec, A. Weill. La Documentation française, Paris 2005.

Autres Publications

1. **Martin Schwell** et Jean-Paul Quisefit: **« L'analyse chimique des particules en atmosphère contrôlée – par spectrométrie de masse laser »**

   Salle Propres et maîtrise de la contamination, Octobre 2002.

2. M.C. Gazeau, **M. Schwell**, A. Jolly, Y. Bénilan, I. Kleiner : **« Photochimie dans les atmosphères planétaires »**

   Actualité chimique de la SFC (2006), Numéro Spécial (2006) « Photochimie », sous presse.

Manuscrits en préparation

1. S. Leach, **M. Schwell**, N. Fray, H.-W. Jochims, H. Baumgärtel: **« VUV Photophysics of CH_3CN and CD_3CN : Absorption, Fluorescence and Ionization in the 6-23 eV region »**
2. **M. Schwell**, S. Leach, H.-W. Jochims, H. Baumgärtel: **« Photoionsiation mass spectrometry study of purine, pyrimidine, benzimidazole and imidazole, in the 6-20 eV region »**
3. T. Ferradaz, N. Fray, A. Jolly, Y. Bénialn, A. Jolly, **M. Schwell**: **« Low temperature VUV absorption spectrum of HCN, C_4H_2, HC_3N and HC_5N between 110 and 150 nm »**
4. F. Gaie-Levrel, H.-W. Jochims**,** E. Rühl, **M. Schwell** : **« Photoionsiation mass spectrometry study of anthropogenic aerosol precursors, in the 6-15 eV region »**

Conférences Invitées

1. M. Schwell : **« Gas/Particle partitionig of PAHs in the case of a road tunnel near Paris (La Défense, A14) »**

   Conférence Invitée CERC3 (Chairpersons and Directors of European Research Councils' Chemistry Committees) - Young Chemist's Workshop on *« Atmospheric Chemistry and Particulate Matter »*, Birkerød (Denmark), June 2002.

2. M. Schwell **: « Photochimie VUV des petites biomolécules »**

   Conférence Invitée à l'école thématique BIOMIMETIQUE 2005 du CNRS : *« Contributions spectroscopiques et quanto-chimiques appliqués à l'étude des molécules biologiques »*, Aussois (Savoie), 28 août- 2 septembre 2005.

3. M. Schwell : **« Ou nous sommes dans la réalisation du LMD, en France et en Allemagne ? »**

   Invitation à une table ronde publique lors de la réunion des Responsables de programmes de l'Université Franco-Allemande, Rennes 17 mai 2006.

4. M. Schwell : **« Spectroscopie et photochimie VUV des molécules prébiotiques et biologiques »**

   Conférence Invitée au Colloque Utilisateur Soleil (Table Ronde « Milieux Dilués »), Ecole Polytechnique, Palaiseau 17./18. Janvier 2007.

Communications et Actes de Congrès

1997

1. M. Schwell : **« Homogene Nukleation in levitierten Mikrotröpfchen »**

   Bunsentagung Darmstadt (Germany), May 1997 (oral).

2. M. Schwell : **« Chemical behavior of single, trapped micro-droplets under atmospheric conditions »**

   European Research Course on Atmospheres (ERCA), Grenoble (France), January 1997 (oral et poster).

3. B. Krämer, M. Schwell, H. Vortisch, T.Leisner, L. Wöste, E. Rühl, H. Baumgärtel : **« Freezing of Sulfuric Acid Solution Measured in Single Levitated Microdroplets »**

   European Aerosol Conference (EAC), Hamburg (Germany), September 1997 (poster).

4. M. Schwell, I. Weidinger, B. Krämer, T.Leisner, L. Wöste, E. Rühl, H. Baumgärtel : **« Direct Determination of the Henry's Law Constants of HCl in Sulfuric Acid Solution droplets »**

   European Aerosol Conference, Hamburg (Germany), September 1997 (poster).

5. B. Krämer, M. Schwell, H. Vortisch, T.Leisner, L. Wöste, E. Rühl, H. Baumgärtel : **« Freezing of Sulfuric Acid Solution Measured in Single Levitated Microdroplets »**

   Proceedings of the fourth European Symposium on Polar stratospheric ozone at Schliersee (Germany), September 1997, pages 577-580, Luxembourg: EC publications EUR 18032 EN (+poster).

6. M. Schwell, I. Weidinger, B. Krämer, T.Leisner, L. Wöste, E. Rühl, H. Baumgärtel : **« Direct Determination of the Henry's Law Constants of HCl in Sulfuric Acid Solution droplets »**

   Proceedings of the fourth European Symposium on Polar stratospheric ozone at Schliersee (Germany), September 1997, pages 577-580, Luxembourg: EC publications EUR 18032 EN (+poster).

1998

7. M. Schwell, I. Weidinger, B. Krämer, T.Leisner, L. Wöste, E. Rühl, H. Baumgärtel : **« The Dynamices of the HCl Uptake by Single, Sulfuric Acid Solution Droplets »**

   DPG Früjahrstagung: Symposium Physik für die Umwelt, Regensburg (Germany), March 1998 (poster).

8. M. Schwell : **« Dynamik der HCl-Gasaufnahme einzelner Mikrotröpfchen unter stratosphärischen Bedingungen »**

   Bunsentagung Münster (Germany), May 1998 (oral).

1999

9. M. Schwell, F. Dulieu, H.-W. Jochims, J.-L. Chotin, H. Baumgärtel, S. Leach: **« VUV photophysics of molecules relevant to Astrochemistry »**

   Colloque Ultilisateur LURE, Orsay (France), 9./10 December 1999 (poster).

10. M. Schwell : **« Fluorescence Studies on a Series of Phenylated [70] fullerenes compounds »**

    European workshop on Usable Fullerene Derivatives, Reykjavik (Iceland), June 1999 (oral).

11. B. Krämer, M. Schwell, H. Vortisch, I. Weidinger, J. Klein, O. Hübner, P. Stöckel, F. Weritz, T. Leisner, H. Baumgärtel : **« The Rate of Homogeneous Nucleation of Supercooled Water measured in levitated Microdroplets »**

    International Bunsen Discussion Meeting *« Metastable Water »*, Schloss Nordkirchen (Germany), September 1999 (poster).

2000

12. M. Schwell : **« Photoionization Mass Spectrometry of Six Isomers of C_7H_8 in the 7-35 eV Photon Energy Range »**

    ERIG 99 (Energétique et Réactivité des ions en phase gazeuse: Expérience et Théorie), Gif-sur-Yvette (France), 15.-17. November 1999 (oral).

13. M. Schwell : **« Determination of photophysical properties of fullerenes derivatives and astrophysical fullerene precursors »**

    European workshop on Usable Fullerene Derivatives, Exeter (United Kingdom), July 2000 (oral).

14. M. Schwell, F. Dulieu, H.-W. Jochims, J.-L. Chotin, H. Baumgärtel, S. Leach : **« VUV Photophysics of prebiotic molecules »**

    XIIème Rencontres de Blois : *« Frontiers of Life »*, Blois (France), 25. Juin - 1. Juillet 2000 (poster).

2001

15. F. Dulieu, J.L Chotin, J. H Fillion, H. W. Jochims, S. Leach, J.L. Lemaire, and M. Schwell : **« Photophysics of Acetic Acid and other Molecules of Astrophysical Interest in the 10-100 eV energy range »**

    Colloque Ultilisateur LURE, Orsay (France), 18./19 January 2001 (poster).

16. M. Schwell : **« VUV Response of Prebiotic and Biotic Molecules »**

    Proceedings of the First European Workshop on Exo-/Astrobiology, Frascati (Italy), 21 - 23 May 2001, ESA SP-496 (August 2001), abstract published in Astrobiology **1** (2001), 210. (oral).

17. M. Schwell : **« Determination of photophysical properties of 6 deca-substituated [70] fullerenes »**

    European workshop on Usable Fullerene Derivatives, Heraklion (Greece), May 2001 (oral).

2002

18. Schwell, M., Quisefit, J.P., Gariviat, S., Goriaux, M., Steiner : **« Automobile emissions measured at its source : Latest Results »**

    EC / EUROTRAC-2 Joint Workshop "Shaping the Future of Atmospheric Chemistry Research in Europe", 9-11 September 2002, Paris (France) (poster).

19. Quisefit, J.P., Gariviat, S., M. Schwell, M., Goriaux, M., Steiner, E. : **« Size Ditribution and Gas/Particle partitionig of PAHs and elements in the case of a road tunnel near Paris »**

    General Assembly of the European Geophysical Society (EGS), Nice (France), April 2002, session OA17 : Urban air pollution (oral).

2003

20. M. Schwell, N.K. Wachter, P.B. Birkett, R. Taylor, E.J. Land, S. Leach, and R.V. Bensasson :
« Photophysical Properties of the Triplet State of Deca-Functionalized [70]Fullerenes »

    203rd Meeting of the Electrochemical Society, Paris, April 27-May 2 2003 (oral).

21. M. Schwell, J.P. Quisefit : **« SPLAM – Single Particle Laser Ablation Mass Spectrometry »**

    CNRS-INSU, Atelier Expérimentation et Instrumentation, Brest (France), January 2003 (oral).

2004

22. Martin Schwell: **« SPLAM – Single Particle Laser Ablation Mass Spectrometry »**

    Séminaire Particules du programme PRIMEQUAL 2, Ministère de Recherche, 5 octobre 2004.

2005

23. Nicolas Fray, Thomas Ferradaz, Antoine Jolly, **Martin Schwell**, Yves Bénilan, Sydney Leach, Hans-Werner Jochims, Helmut Baumgärtel :
« VUV absorption spectroscopy of planetary molecules at low temperature »

    New trends in gas phase VUV/soft X-ray high resolution spectroscopies at SOLEIL, 21st & 22nd March 2005, Université Paris-Sud (Orsay, France).

24. Martin Schwell**,** François Dulieu, Hans-Werner Jochims, Helmut Baumgärtel, Sydney Leach : **« VUV photochemistry of small biomolecules »**

    General Assembly of the European Geosciences Union (EGU) 2005, Avril 24-29, Vienne (Autriche), (orale).

25. Antoine Jolly, Yves Benilan, Thomas Ferradaz, Nicolas Fray, et Martin Schwell:
« VUV Absorption Spectroscopy of Planetary Molecules at Low Temperature »

    37th Annual Meeting of the Division for Planetary Sciences (DPS) of the American Astronomical Society, Cambridge (UK), 4-8 Septembre 2005 (orale).

26. François Gaie-Levrel, David Clainquart, Christoph Stoll, Jean-Paul Quisefit et Martin Schwell :
    « Time-of-Flight Aerosol Mass Spectrometry with VUV laser ionisation »

    Workshop on European On-line Particle Mass Spectrometry (ACCENT), Joint Research Centre, Institute for Envinronment and Sustainability, Ispra (Italie), (orale).

27. Martin Schwell:
    « Nouvelles Méthodes pour l'Analyse Chimique de l'Aérosol Atmosphérique : Single Particle Laser Ablation Mass Spectrometry – SPLAM et Thermal Desorption Chemical Ionisation Mass Spectrometry - TDCIMS »

    Journées de Bilan des ACI « Nouvelles Méthodologies Analytiques et Capteurs (NMAC) » et « Non-Pollution- dépollution (NPD) », 19 - 20 décembre 2005 au Ministère délégué à l'Enseignement Supérieur et à la Recherche, Paris (poster).

2006

28. M. Schwell : « **SPLAM Single Particle Laser Ablation Mass Spectrometry, avances récentes »**

    Séminaire d'avancement « PARTICULES » du Programme de Recherche Interorganisme pour une Meilleure Qualité de l'Air à l'Echelle Locale (Primequal), Avignon, 30 et 31 Mars 2006 (oral).

29. T. Ferradaz, Y. Bénilan, N. Fray, A. Jolly, M. Schwell :
    « Spectroscopie VUV à basses températures de molécules d'intérêt planétologique, Application à l'atmosphère de TITAN »

    Colloque national d'exobiologie, Orléans 22-24 Mai 2006 (poster).

30. Y. Benilan, T. Ferradaz, N. Fray, A. Jolly, M. Schwell, J.C. Guillemin:
    « Photoabsorption cross sections of organic molecules in the VUV at low temperatures : application to Titan's atmosphere observations »

    36th COSPAR Scientific Assembly (Committee on Space Research), Pékin, Chine, 16 – 23 Juillet 2006.

31. Y. Benilan, T. Ferradaz, N. Fray, A. Jolly, M. Schwell, J.C. Guillemin :
    « HC_3N and C_4H_2 low temperature VUV photoabsorption cross sections: application to their observation in Titan's atmosphere by UVIS »

European Planetary Science Congress 2000, *« Europlanet #1 »,* Berlin (Germany), 18 – 22 September 2006.

32. T. Ferradaz, Y. Benilan, N. Fray, A. Jolly, M. Schwell, J.C. Guillemin :
« Sections efficaces d'absorption dans le VUV à basses températures de HCN, HC_3N et C_4H_2 »

Colloque général du Programme National de Physique et Chimie du Milieu Interstellaire (PCMI), Grenoble, 23-26 octobre 2006.

2007

33. M.C Gazeau, Y. Bénilan, A. Jolly, T. Ferradaz, J.C. Guillemin, F. Raulin, M. Schwell :
« **Laboratory studies in support of the Cassini-Huygens Mission »**

General Assembly of the European Geosciences Union (EGU) 2007, Avril 15-20, Vienne (Autriche), (orale). Session PS2.5 « Spectroscopy and Radiative Transfer in Planetary Atmospheres ».

10. Textes intégraux des publications sélectionnées

1. **M. Schwell,** T. Gustavsson, S. Marguet, B. de La Vassière, N. Wachter, P. Birkett, J.-C. Mialocq, S. Leach :
   « The fluorescence of the phenylated fullerenes $C_{70}Ph_4$, $C_{70}Ph_6$, $C_{70}Ph_8$, and $C_{70}Ph_{10}$ in room temperature solution »

   Chemical Physics Letters 350 (**2001**)**,** 33-38**.**

2. **M. Schwell,** F. Dulieu, H.-W. Jochims, J.-H. Fillion, J.-L. Lemaire, H. Baumgärtel and S. Leach :
   « Photophysical Studies od Formic Acid in the 6-23 eV Photon Energy Range : II Fragmentation, Fluorescence and Ionisation »

   Journal of Physical Chemistry A 106 (**2002**), 10908-10918

3. H.W. Jochims, **M. Schwell**, H. Baumgärtel, S. Leach :
   « Photoion mass spectrometry of adenine, thymine and uracil in the 6–22 eV photon energy range »

   Chemical Physics 314 (**2005**), 263-282.

4. H.-W. Jochims, **M. Schwell**, S. Un, H. Baumgärtel, S. Leach :
   « VUV Absorption spectrum of Acetic Acid between 6 and 22 eV »

   Chemical Physics 321 (**2006**), nos. 1-2, 159-170.

5. S. Leach, **M. Schwell**, H.-W. Jochims, H. Baumgärtel :
   « VUV photophysics of Acetic Acid : Fragmentation, Fluorescence and Ionization in the 6-23 eV region »

   Chemical Physics 321 (**2006**), nos. 1-2, 171-182.

6. **M. Schwell**, H.-W. Jochims, H. Baumgärtel, S. Leach :
   « VUV photochemistry of small biomolecules »

   Planetary and Space Science 54 (**2006**), 1073-1085.

14 December 2001

ELSEVIER

Chemical Physics Letters 350 (2001) 33–38

CHEMICAL PHYSICS LETTERS

www.elsevier.com/locate/cplett

The fluorescence properties of the phenylated fullerenes $C_{70}Ph_4$, $C_{70}Ph_6$, $C_{70}Ph_8$, and $C_{70}Ph_{10}$ in room temperature solutions

Martin Schwell [a,*], Thomas Gustavsson [b,1], Sylvie Marguet [b,1], Benoît de La Vaissière [b], Norbert K. Wachter [c], Paul R. Birkett [c], Jean-Claude Mialocq [b], Sydney Leach [a]

[a] *DAMAp, Observatoire de Paris-Meudon, UMR 8588 du CNRS, F-92195 Meudon Cedex, France*
[b] *CEA/Saclay, DRECAM/SCM, URA 331 CNRS, F-91191 Gif-sur-Yvette, France*
[c] *School of Chemistry and Molecular Sciences, University of Sussex, Brighton BN1 9QJ, Sussex, UK*

Received 10 August 2001; in final form 10 October 2001

Abstract

The emission and excitation spectra of four phenylated [70] fullerenes, $C_{70}Ph_4$, $C_{70}Ph_6$, $C_{70}Ph_8$, and $C_{70}Ph_{10}$ in cyclohexane and toluene solutions have been measured. The fluorescence spectra and related excited state properties are found to depend strongly on the number of attached phenyl groups, but with no systematic trends. Quantum yields and fluorescence lifetimes were measured for $C_{70}Ph_6$, $C_{70}Ph_8$, and $C_{70}Ph_{10}$, allowing the determination of $S_1 \rightarrow S_0$ radiative transition rates k_R. It is found that k_R for $C_{70}Ph_{10}$ is about six times larger than for the other compounds. This is consistent with measured absorbtivities for these compounds. The particular character of $C_{70}Ph_{10}$ is also manifested by its higher intersystem crossing rate k_{ISC}.

1. Introduction

The recently reported synthesis of phenylated [70] fullerenes [1] has created speculation about their potential for optoelectronics applications [2,3]. We therefore carried out spectroscopic and photophysical studies on this class of compounds and reported the ground and triplet state absorption spectra as well as the quantum yields of singlet to triplet intersystem crossing (Φ_T) of $C_{70}Ph_4$, $C_{70}Ph_6$, $C_{70}Ph_8$, and $C_{70}Ph_{10}$ [2]. The Φ_T values of these species have been shown to be generally high, similar to the case of C_{60} ($\Phi_T = 0.88$ [4]) and C_{70} ($\Phi_T = 0.76$ [5]). Our study also showed that Φ_T decreases with the number of phenyl rings attached to the C_{70} cage, with the exception of $C_{70}Ph_{10}$ whose triplet yield is close to unity. Its

* Corresponding author. Present address: Laboratoire Interuniversitaire des Systèmes Atmosphériques (LISA), 61, avenue du Géneral de Gaulle, Université Paris 12, F-94010 Creteil Cedex, France; Fax: +33-1-45-17-15-64.

E-mail address: schwell@lisa.univ-paris12.fr (M. Schwell).

[1] Present address: CEA/Saclay, DRECAM/SPAM, Laboratoire Francis Perrin (FRE 2298 CNRS), F-91191 Gif-sur-Yvette, France.

0009-2614/01/$ - see front matter
PII: S0009-2614(01)01217-9

behaviour was attributed to the fact that addition of 10 phenyls saturates the same number of carbons and separates the π-electron system of the C_{70} cage into two patches which interact only via σ-bonds. This electron pattern effectively makes this molecule akin to non-planar aromatics rather than to fullerenes. In order to further characterise the pathways subsequent to photoexcitation, we decided to undertake an emission study, the results of which confirm some aspects of the recently reported work of Coheur et al. [3] and provide complementary information due to the following: (1) The dispersed fluorescence spectra have been corrected for the spectral response of the detection system, (2) fluorescence excitation spectra have been recorded and (3) fluorescence lifetimes and quantum yields have been obtained.

2. Experimental

The synthesis of $C_{70}Ph_{10}$ and $C_{70}Ph_8$ is described in detail in [1]. $C_{70}Ph_6$ and $C_{70}Ph_4$ are obtained as by-products during the synthesis [6]. For each compound, the purity was controlled by carefully comparing absorption and fluorescence excitation spectra, described in detail below. Some $C_{70}Ph_8$ samples displayed non-negligible traces of $C_{70}Ph_{10}$. All results presented here are however based on pure samples.

We used an SPEX Fluorolog-2 F111 A1 spectrofluorometer entirely corrected for the spectral response function of both the emission and the excitation. The excitation source is a 150 W Xenon lamp, the excitation grating is blazed at 250 nm, the emission grating at 500 nm and the photomultiplier is a red-sensitive Hamamatsu R928. The entrance and exit slits were 0.5 mm wide giving a ~2 nm spectral bandwidth. The fluorescence quantum yields were measured using two fluorescence standards, quinine bisulphate in perchloric acid (0.1 M) solution and rhodamine 6G in ethanol solution [7].

The fluorescence lifetimes were recorded by using the time-correlated single photon counting (TCSPC) method. The laser source used was a cavity-dumped rhodamine 6G dye laser synchronously pumped by a mode-locked Nd:YAG laser. The fundamental output was frequency doubled in a KDP crystal, providing the 295 nm excitation pulses of a few picoseconds width at a repetition rate of 3.8 MHz. Fluorescence was detected by a Hamamatsu R1564 U microchannel plate, characterised by a 120 ps FWHM response function.

3. Results and discussion

3.1. General description of fluorescence spectra

Fig. 1 shows the fluorescence spectra of $C_{70}Ph_4$, $C_{70}Ph_6$, $C_{70}Ph_8$, and $C_{70}Ph_{10}$ in cyclohexane solution upon photoexcitation at $\lambda = 360$ nm ($C_{70}Ph_8$ and $C_{70}Ph_{10}$) or $\lambda = 355$ nm ($C_{70}Ph_4$ and $C_{70}Ph_6$). The spectra are recorded at room temperature. As can be seen, the positions and shapes of the fluorescence bands depend strongly on the number of phenyl groups. Red-shifts of the fluorescence band, as compared to C_{70} [8], are observed for $C_{70}Ph_4$ and $C_{70}Ph_6$, while they are blue-shifted for $C_{70}Ph_8$ and $C_{70}Ph_{10}$, as already reported elsewhere [2]. This is, as will be discussed more in detail below, due to the modification of the π-system by the presence of saturated carbon atoms. For $C_{70}Ph_6$, $C_{70}Ph_8$, and $C_{70}Ph_{10}$, the emission bands are

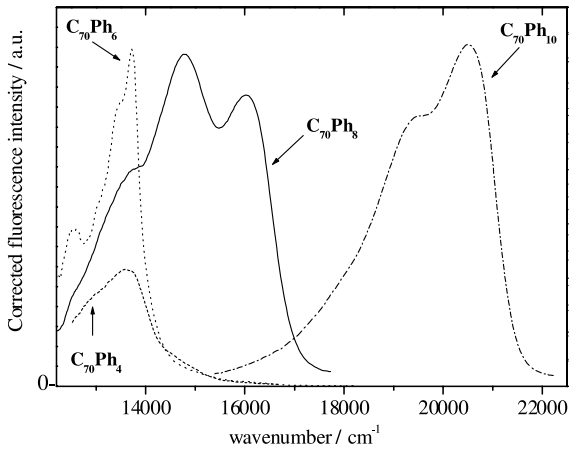

Fig. 1. Fluorescence spectra of phenylated [70] fullerenes in cyclohexane solution at room temperature. The excitation wavelengths used were: $C_{70}Ph_{10}$, $C_{70}Ph_8$: 360 nm; $C_{70}Ph_6$, $C_{70}Ph_4$: 355 nm. The spectra are entirely corrected for the spectral response of the detection system but each spectrum has a different scaling.

structured due to vibrational features as in the case of C_{70} [9,10]. We also examined the band shape and the fluorescence quantum yield for $C_{70}Ph_6$ and $C_{70}Ph_{10}$ in toluene and found that they are unchanged, within experimental precision, with respect to cyclohexane solutions.

For every compound under investigation, the emission is assumed to take place from the first singlet excited state S_1, as inferred from a comparison with absorption spectra [2]. Indeed, for each compound the first fluorescence band is always situated close to the first absorption band, only slightly shifted to the red. This is shown more in detail in Fig. 2, where the fluorescence band is shown together with the red wing of the absorption. For clarity, the first fluorescence and absorption peaks are given equal height. The Stokes shifts $\Delta\nu$, taken as the difference between the first peaks of the fluorescence and absorption bands, are rather small (see Table 1). The Stokes shift is estimated to be 100 cm^{-1} for $C_{70}Ph_6$ and 750 cm^{-1} for $C_{70}Ph_{10}$. The case of $C_{70}Ph_8$ is somewhat special, due to the presence of a first very weak absorption band around 15000 cm^{-1}, and the very broad fluorescence band. Using the first weak absorption band and the second fluorescence peak gives a Stokes shift of 350 cm^{-1}. While using the shoulder of the absorption band at 17050 cm^{-1} and the first fluorescence band gives a value of $\sim$1000 cm^{-1}.

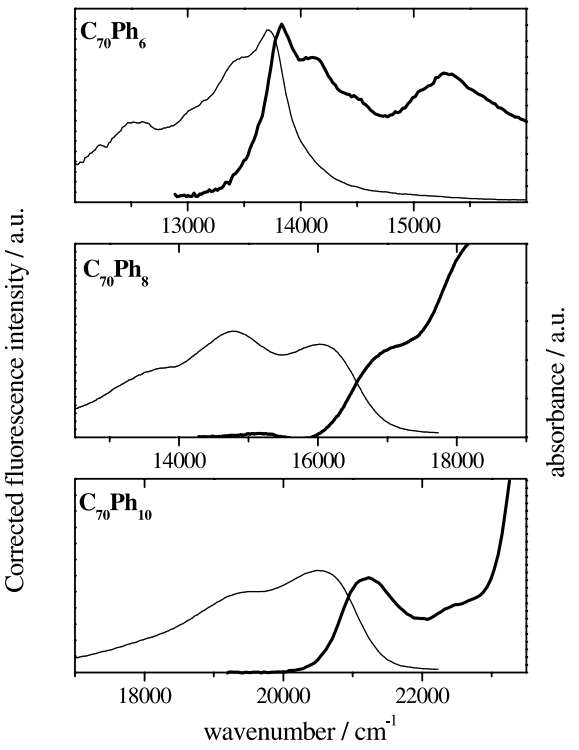

Fig. 2. Fluorescence (thin lines) and absorption spectra (thick lines) of $C_{70}Ph_6$, $C_{70}Ph_8$ and $C_{70}Ph_{10}$. For the absorption spectra only the red edge is shown in a blown-up scale in order to allow a comparison with the fluorescence band.

For $C_{70}Ph_4$, $C_{70}Ph_8$ and $C_{70}Ph_{10}$, the fluorescence spectrum cannot be judged to be a mirror image of the absorption spectrum. This is similar to what is found for C_{70} [11], for which the S_1–S_0 transition is only weakly allowed. The molar extinction coefficients are not known for all compounds treated here, but it is known that the absorptivity of the lowest lying electronic states of $C_{70}Ph_{10}$ is about 10 times stronger as compared to C_{70} [2]. In spite of this, the mirror relation is far from respected (Fig. 2). It should be noted, though, that the fluorescence and the absorption spectrum of $C_{70}Ph_6$ are closer to a mirror image, but it is difficult to draw any further conclusions lacking the absolute value of its absorptivity. The existence of close-lying electronic states in these compounds can also contribute to the absence of mirror image relation between fluorescence and absorption features and can play a role in determining the value of the observed Stokes-shift.

3.2. Fluorescence quantum yields (Φ_F)

Fluorescence quantum yields were calculated by a comparative method following [12]:

$$\Phi_{\mathrm{ref}} = \Phi_{\mathrm{s}}\left(\frac{A_{\mathrm{ref}}^{\lambda_{\mathrm{abs}}}\cdot F_{\mathrm{s}}\cdot n_{\mathrm{s}}^2}{A_{\mathrm{s}}^{\lambda_{\mathrm{abs}}}\cdot F_{\mathrm{ref}}\cdot n_{\mathrm{ref}}^2}\right). \tag{1}$$

In Eq. (1), Φ_{ref} and Φ_{s} are the fluorescence quantum yields, $A_{\mathrm{ref}}^{\lambda_{\mathrm{abs}}}$ and $A_{\mathrm{s}}^{\lambda_{\mathrm{abs}}}$ the number of photons absorbed in the sample ($A^{\lambda_{\mathrm{abs}}} = A_0^{\lambda_{\mathrm{abs}}}(1-10^{-\mathrm{OD}(\lambda_{\mathrm{abs}})})$, where A_0^{λ} is the number of incoming photons and $\mathrm{OD}(\lambda)$ is the optical density at wavelength λ), F_{ref} and F_{s} the total areas of the fluorescence spectra and n_{ref} and n_{s} the refraction indices of the reference and the fullerene samples, respectively.

Table 1
Fluorescence properties of the fullerene derivatives $C_{70}Ph_{2n}$ ($n = 3$–5) in cyclohexane (chx)

	$C_{70}Ph_6$	$C_{70}Ph_8$	$C_{70}Ph_{10}$
$\Delta\nu$ (cm^{-1})	100 ± 50	1000 ± 50	750 ± 50
Φ_F (in tol)	$(2.1 \pm 0.5)\%$ (355 nm)		$(2.0 \pm 0.5)\%$ (360 nm)
(λ_{exc})			$(2.5 \pm 0.5)\%$ (469 nm)
Φ_F (in chx)	$(2.2 \pm 0.5)\%$ (355 nm)	$(1.3 \pm 0.5)\%$ (520 nm)	$(2.3 \pm 0.5)\%$ (355 nm)
(λ_{exc})			$(1.8 \pm 0.5)\%$ (469 nm)
τ_F (in chx)	(6.62 ± 0.05) ns	(4.83 ± 0.05) ns	(1.12 ± 0.05) ns
$\lambda_{exc} = 295$ nm	($\lambda_{obs} = 720$ nm)	($\lambda_{obs} = 620$ nm)	($\lambda_{obs} = 520$ nm)
k_R (in chx)	$(3.3 \pm 0.8) \times 10^6$ s^{-1}	$(2.7 \pm 1.1) \times 10^6$ s^{-1}	$(1.8 \pm 0.5) \times 10^7$ s^{-1}
k_{NR} (in chx)	$(1.5 \pm 0.4) \times 10^8$ s^{-1}	$(2.0 \pm 0.8) \times 10^8$ s^{-1}	$(8.7 \pm 2.4) \times 10^8$ s^{-1}
Φ_T (in chx)	0.5 ± 0.1	0.18 ± 0.04	1.0 ± 0.2
k_{ISC} (in chx)	$(7.6 \pm 1.5) \times 10^7$ s^{-1}	$(3.7 \pm 0.8) \times 10^7$ s^{-1}	$(8.7 \pm 1.9) \times 10^8$ s^{-1}
k_{IC} (#in chx)	$(7.4 \pm 2.3) \times 10^7$ s^{-1}	$(1.6 \pm 0.7) \times 10^8$ s^{-1}	($<10^8$ s^{-1})[a]

Stokes shifts $\Delta\nu$, quantum yields Φ_F (also in toluene (tol)), singlet state life times τ_F, radiative transition rates k_R. Also given are non-radiative transition rates k_{NR}, intersystem crossing rates k_{ISC} and internal conversion rates k_{IC} determined from the experimental data. The triplet quantum yields Φ_T were taken from [2].

[a] Undetermined.

The quantum yields of fluorescence, Φ_F (Table 1), are fairly low for $C_{70}Ph_6$, $C_{70}Ph_8$, and $C_{70}Ph_{10}$, ranging mainly between 1% and 2.5%. The small variation of the Φ_F values between these three compounds should be taken with some care, though, since the experimental uncertainties of the Φ_F values are about 25%. For $C_{70}Ph_{10}$, Φ_F has been measured at two different excitation wavelengths, giving equal values within the experimental error limits. $C_{70}Ph_4$ is somewhat exceptional because of its significantly lower quantum yield (0.13%).

The generally low Φ_F values are in accordance with the high singlet to triplet intersystem crossing efficiencies that were measured for these molecules [2]. However, the Φ_F values are much higher than those of unsubstituted fullerenes such as C_{60} ($\Phi_F = 2.6 \times 10^{-4}$) and C_{70} ($\Phi_F = 5.4 \times 10^{-4}$) [11]. This indicates that internal conversion towards the S_0 ground state is relatively less important in the series of phenylated C_{70} molecules than in C_{70}. In other words, it points towards a more allowed nature of the $S_1 \rightarrow S_0$ transition than in the pristine molecule. No consistent trend concerning Φ_F was observed within the $C_{70}Ph_{2n}$ series (see Table 1).

3.3. Fluorescence excitation (FEX) spectra

FEX spectra have been recorded for each compound and found to be very similar to the

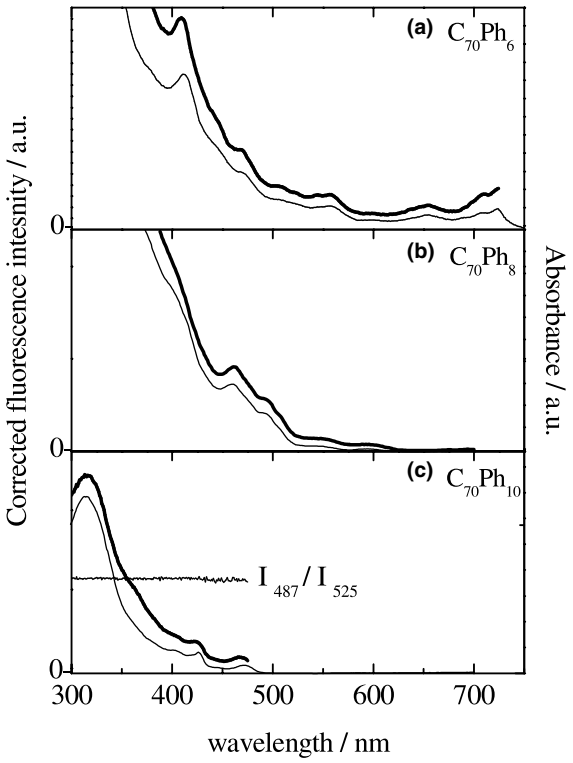

Fig. 3. Absorption (thin line) and fluorescence excitation (thick line) spectra for $C_{70}Ph_6$ ($\lambda_{obs} = 728$ nm), $C_{70}Ph_8$ ($\lambda_{obs} = 619$ nm) and $C_{70}Ph_{10}$ ($\lambda_{obs} = 525$ nm). For $C_{70}Ph_{10}$ is also shown the ratio of the fluorescence excitation spectra with $\lambda_{obs} = 487$ and $\lambda_{obs} = 525$ nm.

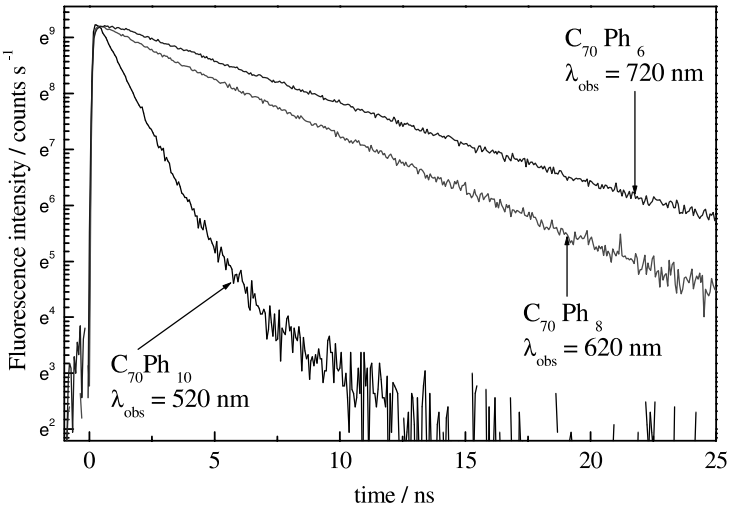

Fig. 4. Fluorescence decay for $C_{70}Ph_6$, $C_{70}Ph_8$ and $C_{70}Ph_{10}$ after photoexcitation at $\lambda = 295$ nm.

absorption spectra. Fig. 3 shows the FEX spectra of $C_{70}Ph_6$ ($\lambda_{obs} = 728$ nm), $C_{70}Ph_8$ ($\lambda_{obs} = 619$ nm) and $C_{70}Ph_{10}$ ($\lambda_{obs} = 525$ nm) together with their ground state absorption spectra (taken from [2]), both of them being recorded in cyclohexane. The excitation spectrum follows the absorption spectrum, reproducing every feature of the latter. This behaviour indicates that on increasing the energy of excitation no new channels for internal conversion are opened. Similarly, for $C_{70}Ph_{10}$, the FEX detected at 487 and 525 nm, near the maxima of the two fluorescence bands, do not show any differences between 300 and 500 nm as illustrated by the intensity ratio I_{487}/I_{525} in Fig. 3c. This fact further supports the assumption that the two fluorescence bands at $\lambda = 487$ and $\lambda = 525$ nm are vibronic bands emitted with the same probability when exciting to the S_1 state or to higher S_n states. In other words, the intersystem crossing and the internal conversion occur from the S_1 state. Similar conclusions were drawn regarding C_{70} [8].

3.4. Fluorescence lifetimes and radiative rate constants

Fig. 4 shows the observed time-resolved fluorescence decay of $C_{70}Ph_6$, $C_{70}Ph_8$ and $C_{70}Ph_{10}$. On the nanosecond time-scale, we observe almost purely exponential decays over three orders of magnitude for each compound studied. The observed fluorescence lifetimes, τ_F, are given in Table 1. Radiative decay rates (k_R) can be obtained by using Eq. (2):

$$k_R = \Phi_F/\tau_F. \quad (2)$$

These values are also shown in Table 1. The ratio of the radiative rates for $C_{70}Ph_{10}$ and $C_{70}Ph_8$, about seven, compare well with the ratio of the molar extinction coefficients of their respective lowest absorption bands [2]. A ratio of this order of magnitude is obtained on introducing the integrated S_1–S_0 absorption and fluorescence spectra of these compounds into the Strickler–Berg equation [13]. The high radiative rate k_R of $C_{70}Ph_{10}$ is noteworthy since this compound also has the highest triplet yield Φ_T, close to unity [2], thus suggesting a very efficient singlet to triplet intersystem crossing pathway. This behaviour further underlines the peculiar chromophore character of $C_{70}Ph_{10}$ as compared to the other phenylated compounds. The radiative rate k_R of $C_{70}Ph_6$ is 20% larger than that of $C_{70}Ph_8$. In general, the greater radiative rates of phenylated C_{70} as compared to C_{70} ($k_R = 8.8 \times 10^5$ s^{-1} [11]) are readily rationalised by the stronger absorption to their lowest-lying singlet states.

3.5. Non-radiative rate constants k_{IC} and k_{ISC}

From the radiative rates k_R together with measured quantum yields for triplet state formation Φ_T [2], the rate constants for $S_1 \rightarrow T_1$ intersystem crossing, k_{ISC}, and $S_1 \rightarrow S_0$ internal conversion, k_{IC}, can be calculated according to the following Eqs. (3)–(5):

$$k_{ISC} = \frac{\Phi_T}{\tau_F}, \tag{3}$$

$$k_{NR} = \frac{1}{\tau_F} - k_R, \tag{4}$$

$$k_{IC} = k_{NR} - k_{ISC}. \tag{5}$$

The resulting values are given in Table 1. Since the Φ_T values were given with 20% relative uncertainties, and our Φ_F values have relative uncertainties on the order of 25%, it is evident that these values of k_{ISC} and k_{IC} are only crude estimates. One may, however, once again note the particularly high k_{ISC} and k_R values for $C_{70}Ph_{10}$ in line with the much shorter fluorescence lifetime observed.

4. Conclusion

We have performed a systematic study of the fluorescence properties of four phenylated [70] fullerenes, $C_{70}Ph_4$, $C_{70}Ph_6$, $C_{70}Ph_8$, and $C_{70}Ph_{10}$ in non-polar (cyclohexane) and weakly polar (toluene) solvents. These fluorescence data are compatible with the singlet–triplet yields, already known from an earlier study. However, we observe no systematic trends of the fluorescence properties as a function of the number of attached phenyl groups. In fact, the data imply that the excited state electronic properties are very specific for each compound.

Acknowledgements

This work was carried out with partial support from the European Union, TMR Network 'USEFULL', contract FRMX-CT97-0126. The authors express their thanks to Francesco Zerbetto for many helpful discussions. PRB acknowledges the EPSRC for the award of an Advanced Fellowship.

References

[1] A.G. Avent, P.R. Birkett, A.D. Darwish, H.W. Kroto, R. Taylor, D.R.M. Walton, Tetrahedron 52 (14) (1996) 5235, $C_{70}Ph_4$ and $C_{70}Ph_6$ can be isolated as minor by-products in this synthesis.
[2] R.V. Bensasson, M. Schwell, M. Fanti, N.K. Wachter, J.O. Lopez, J.-M. Janot, P.R. Birkett, E.J. Land, S. Leach, P. Seta, R. Taylor, F. Zerbetto, Chem. Phys. Chem. 2 (2001) 109.
[3] P.F. Coheur, J. Cornil, D.A. dos Santos, P.R. Birkett, J. Liévin, J.L. Brédas, D.R.M. Walton, R. Taylor, H.W. Kroto, R. Colin, J. Chem. Phys. 112 (2000) 6371.
[4] R.V. Bensasson, T. Hill, E.J. Land, S. Leach, T.G. Truscott, Chem. Phys. Lett. 201 (1993) 326.
[5] R.V. Bensasson, T. Hill, C. Lambert, E.J. Land, S. Leach, T.G. Truscott, Chem. Phys. Lett. 206 (1993) 197.
[6] A.G. Avent, P.R. Birkett, M. Carano, A.D. Darwish, H.W. Kroto, J.O. Lopez, F. Paolucci, S. Roffia, R. Taylor, N. Wachter, D.R.M. Walton, F. Zerbetto, J. Chem. Soc. Perkin Trans. 2 (2) (2001) 140.
[7] R.A. Velapoldi, in: C. Burgess, K.D. Mielenz (Eds.), Advances in Standards and Methodology in Spectrophotometry, Elsevier, Amsterdam, 1987, p. 175.
[8] R.M. Williams, J.W. Verhoeven, Chem. Phys. Lett. 194 (1992) 446.
[9] Y.-P. Sun, B. Ma, C.E. Bunker, J. Chem. Soc., Chem. Commun. (1994) 2099.
[10] A. Sassara, G. Zerza, M. Chergui, J. Phys. Chem. A 102 (1998) 3072.
[11] B.M. Ma, Y.P. Sun, J. Chem. Soc. Perkin Trans. 2 (1996) 2157.
[12] D.F. Eaton, J. Photochem. Photobiol. B: Biol. 2 (1988) 523.
[13] S.J. Strickler, R.A. Berg, J. Chem. Phys. 37 (1962) 814.

Photophysical Studies of Formic Acid in the Vacuum UV: Fragmentation, Fluorescence, and Ionization in the 6−23 eV Photon Energy Range†

Martin Schwell,[⊥,‡,§] François Dulieu,[⊥,‡] Hans-Werner Jochims,[#] Jean-Hugues Fillion,[⊥,‡] Jean-Louis Lemaire,[⊥,‡] Helmut Baumgärtel,[#] and Sydney Leach*,[⊥,‡]

DAMAp - UMR 8588, Observatoire de Paris-Meudon, 5 place Jules Janssen, 92195 Meudon, France, LAMAp - UMR 8588, Département de Physique, Université de Cergy-Pontoise, 95031 Cergy Pontoise Cedex, France, and Institut für Physikalische und Theoretische Chemie der Freien Universität Berlin, Takustrasse 3, 14195 Berlin, Germany

Received: March 27, 2002; In Final Form: September 3, 2002

Vacuum-UV (VUV) photodissociation of gaseous formic acid (HCOOH) has been studied in the 6−23 eV range using photofragment fluorescence spectroscopy and synchrotron radiation excitation. Previous studies were limited to the region below 11.4 eV. Emission of OH (A), CH (A, B), HCOO, and H Balmer radiation is observed at various excitation energies in the VUV. Bands in the corresponding fluorescence excitation spectra can be associated with specific absorption bands of HCOOH. The HCOO fluorescence between 330 and 480 nm is assigned to the $^2B_1 \rightarrow {}^2A''$ transition. The quantum yield of photoionization, γ, measured from 10 to 23 eV, reaches unity at 18 ± 0.1 eV. The energy domain, ΔE, of competitive nonionic decay processes of superexcited molecular states above the ionization threshold is thus found to be $\Delta E(\mathrm{HCOOH}) = 6.68 \pm 0.1$ eV. Between 15.7 and 17 eV, Rydberg absorption bands converging to the $3^2A'$ state of $HCOOH^+$ are mirrored in the $\gamma(E_{exc})$ spectrum, from which an autoionization rate $k_{ai} \approx 7.5 \times 10^{13}\ s^{-1}$ was determined for the Rydberg levels. Below the astrophysical HI limit (13.6 eV), the neutral processes HCOOH → OH + HCO and HCOOH → CO_2 + 2H dominate the fragmentation of formic acid. The quantum yield of ionic dissociation processes $HCOOH^+ \rightarrow COOH^+ + H$ and $HCOOH^+ \rightarrow HCO^+ + OH$ is determined to be less than 25% in this energy region. Although the ionic processes become more important between 13.6 and 18 eV, neutral dissociation processes with large quantum yields still occur. The astrophysical relevance of the photophysical properties of formic acid is briefly discussed.

1. Introduction

Absorption of vacuum-UV (VUV) photons by a molecule opens up many photophysical processes, including a variety of relaxation processes.[1] Previous studies of the VUV spectroscopy and photophysics of the astrophysically interesting species formic acid (HCOOH) have been mainly limited to absorption and fluorescence measurements below 11.4 eV,[2−4] apart from a photoionization mass spectrometric study up to 19 eV.[5] This 11.4 eV limit, essentially due to experimental restrictions on window transparency in the VUV, also exists for studies on many other small molecules important in prebiotic chemistry and which are also observed in the interstellar medium (ISM). This can be seen, for example, in the photoabsorption spectra of molecules related to formic acid, such as acetic acid (CH_3-COOH) and its isomer methyl formate ($HCOOCH_3$).[2] We remark that the VUV photoabsorption of these molecules is often much stronger than the UV photoabsorption[2] and that at E = 10.2 eV, at which the intense Lyman-α emission of stars is located, they are found to absorb strongly. We further note that the VUV photon flux from the early sun was probably 10−100 times greater than is the case today, although the total spectral luminosity was less.[6] This gives additional interest to exploration of the VUV photophysics of prebiotic species such as formic acid.

Photodissociation and dissociative photoionization processes[1] can give rise to reactive species such as radicals and ions, which can be formed not only in the ground but also in electronically or vibrationally excited states or both, as will be seen to be the case in formic acid. This species, as well as many other small molecules, is observed in the ISM, so improvement of molecular cloud astrochemical models[7] requires photophysical data both below and above the experimental 11.4 eV limit, in particular because important processes, such as neutral photodissociation, photoionization, and dissociative photoionization, can be very efficient in the VUV. Furthermore, ion−molecule reactions are thought to play an important role in the formation of interstellar molecules in dense clouds.[7]

We have carried out extensive studies on the spectroscopy and photophysics of formic acid in the 6−23 eV energy region. A detailed analysis of the 6−23 eV photoabsorption spectrum has been made,[8] and the He(I) photoelectron spectra of HCOOH and its isotopologues HCOOD, DCOOH, and DCOOD have been recorded and analyzed.[9] In the present work, we have used photofragment fluorescence spectroscopy as an analytical tool to provide insight into the photoprocesses of formic acid (for a recent review of this method, see ref 10 and references therein). We have also measured the quantum yield of ionization of

† Part of the special issue "R. Stephen Berry Festschrift".

* To whom correspondence should be addressed. E-mail: sydney.leach@obspm.fr. Fax: +33-1 4507 7100.

⊥ Observatoire de Paris-Meudon.

‡ Université de Cergy-Pontoise.

§ Present address: Laboratoire Interuniversitaire des Systèmes Atmosphériques (LISA), Université Paris 7 et 12, 61 Avenue du Général de Gaulle, 94010 Creteil Cedex, France.

Institut für Physikalische und Theoretische Chemie der Freien Universität Berlin.

10.1021/jp020809t CCC: $22.00
Published on Web 10/16/2002

HCOOH as a function of photon excitation energy. This is an important parameter in the modeling of astrophysical processes involving formic acid.

Identification of the emission features observed in the dispersed fluorescence spectra of HCOOH is followed by a fluorescence excitation (FEX) spectral study of the excitation energy dependence of these features. Particular attention is paid to the identification and assignment of emission from the HCOO radical. Analysis of the FEX spectra and the ionization quantum yield measurements is made with the aid of data from the VUV absorption spectra and the He(I) photoelectron spectrum. This information is also used to suggest new interpretations of the photoionization breakdown curves of formic acid,[5] as well as to discuss some astrophysical observations involving this species.

2. Experimental Section

Monochromatized synchrotron radiation was obtained from the Berlin electron storage ring BESSY I (multibunch mode) in association with a 1.5 m McPherson monochromator (normal incidence (NIM), dispersion 5.6 Å/mm). Complementary experiments, with the same equipment, were performed at LURE/Orsay (SA63 beamline, 3 m NIM monochromator).

The grating transmission function of the monochromator is recorded by detecting the visible fluorescence emitted by the sodium salicylate layer placed on a quartz window. For fluorescence measurements, the synchrotron light beam is focused into an open brass cell, differentially pumped, containing formic acid vapor at a pressure typically around 10^{-3} mbar. Fluorescence induced in the irradiated target molecules passes through a quartz window and is dispersed using a 20 cm focal length secondary monochromator (Jobin-Yvon H 20 UV, grating blazed at 300 nm). This monochromator has a fixed, exchangeable exit slit but has no entrance slit. The width of the effective "entrance slit" is given by the spatial extension of the exciting light beam (approximately 1 mm). The emitted fluorescence light, measured in the 250−550 nm wavelength range, is detected by a photon-counting Hamamatsu R6060 photomultiplier, cooled to 250 K by a Peltier element. The spectral response function of this arrangement has been determined by recording the spectrum emitted by a tungsten halogen lamp, which is then deconvoluted according to Planck's law. A dispersed fluorescence spectrum typically contains 1 point per 2 nm. The resolution of these spectra is between 5 and 8 nm depending on the choice of the effective exit slit width.

In recording the fluorescence excitation (FEX) spectra, the secondary monochromator is fixed at a desired wavelength with a large exit slit and the primary monochromator is tuned in steps of typically 50−100 meV (400−800 cm^{-1}). The FEX spectra are corrected for the grating transmission function of the primary monochromator and for the VUV photon flux, respectively. Their spectral resolution is about 30 meV. We show unsmoothed fluorescence spectra in all figures (except Figure 5c), but appropriate smoothed spectra (not shown) were used sometimes to measure the peak locations. A high-resolution VUV absorption spectrum of acetone was used for calibration of the observed FEX spectral wavelengths.

The optimum energy resolution of our photoabsorption spectra[8] (photoelectron spectra[9]) is 3 meV (16 meV), while the absolute precision of the their energy scales is 10 meV (2−3 meV). We note that our measured photoabsorption cross sections are about 15% smaller than those measured by Tabayashi et al.,[4] but this is not surprising in view of the error limit, which is of the same order of magnitude in their work and in our own work.[8] At BESSY I, we measured the quantum yield of ionization, $\gamma(E_{exc})$, between 10 and 19 eV at a resolution of 25−50 meV using a technique previously described.[11] A low-resolution spectrum of γ was measured up to 23 eV at LURE.

Commercial formic acid of highest available purity was used without further purification. We note that eventual contamination with water can easily be revealed during the experiments by observing the well-known fluorescence excitation spectrum of OH ($A^2\Sigma^+ \rightarrow X^2\Pi$) emission, which is known to follow VUV photoexcitation of H_2O between 140 and 100 nm.[12]

3. Results and Discussion

3.1. Energetics of UV and VUV HCOOH Fragmentation Reactions. The existing photophysical data of HCOOH in the energy region under study is summarized in Table 1. This survey of HCOOH electronic states and dissociation channels, the latter shown together with their respective thermochemical threshold energies, will be used in the analysis of the dispersed fluorescence, the FEX spectra, and the total photoion yield (γ) curve.

The lowest-lying excited electronic state $1^1A''$, the photoabsorption cross section to which is very small, has been attributed to the $\pi^* \leftarrow n_o$ transition. The photodissociation dynamics of this state have been studied in detail using laser-induced fluorescence spectroscopy.[13−15] Its origin is experimentally found at 4.64 eV (0_0^0, 37 431 cm^{-1}, 267.2 nm).[13] Nonradiative decay to the ground state with subsequent decomposition into H_2O and CO occurs following excitation close to the origin, whereas at higher excitation energies (>4.94 eV), this state predissociates predominantly into OH and HCO.[14,15]

In the VUV regime, below the first ionization energy (IE, 11.3246 eV), additional valence transitions, as well as many Rydberg series, converging to the first IE, have been identified in the absorption spectrum of HCOOH (see Figure 3).[2,8,16−18] Their absorption cross sections are large as compared to the UV absorption populating the $1^1A''$ state. Above the first ionization energy, we observe increasing photoabsorption until a plateau of about 45 MB is reached at about 18 eV (see Figure 5a). Additional series of Rydberg bands are observed in the 11.3−22 eV absorption region. They are superimposed on a continuous absorption background. These bands, which have been analyzed recently,[8] converge to higher ionization limits the energies of which correspond to the six electronic states of the $HCOOH^+$ ion identified in the He(I) photoelectron spectrum of formic acid.[9,19] The VUV photofragmentation behavior will be discussed in sections 3.2−3.5.

3.2. Dispersed Fluorescence Spectra at Excitation Energy E_{exc} = 12 eV. Figure 1 shows dispersed fluorescence spectra of formic acid at an excitation energy of $E_{exc} = 12$ eV (spectral resolution ≈ 5 nm). The intensity is scaled linearly. We show the unsmoothed original spectrum (Figure 1b), as well as the same unsmoothed spectrum corrected for the response function of the detection system (Figure 1a). The amplitude of the OH ($A^2\Sigma^+ \rightarrow X^2\Pi$) (0−0) band at $\lambda = 308$ nm was used to normalize the intensities of the two spectra with respect to each other. At this excitation energy, we observe two band systems, the first being the OH ($A^2\Sigma^+ \rightarrow X^2\Pi$) emissions at 308 (0−0) and 282 nm (1−0) and the second consisting of a long vibrational progression between 330 and 480 nm (Table 2), the intensity maximum of which is at 375 nm, superimposed on a broad continuous background. These two systems have been observed previously upon VUV excitation of HCOOH at lower excitation energies (6.2−10 eV).[3,20]

3.2.1. OH ($A^2\Sigma^+ \rightarrow X^2\Pi$) Emission. The profiles of the (0,0) and (1,0) bands of OH have been theoretically simulated by

TABLE 1: Energetics of Electronic Transitions and Dissociation Channels of HCOOH and $HCOOH^+$

state/MO transition	band or state energy [eV]	dissociation channels	thermochemical threshold energy [eV]
neutral ground state $1^1A'$	0	neutral dissociation channels	
$1^1A'' \pi^* \leftarrow n_o$ [a]	4.641[b] (origin)	HCO + OH	4.795[c]
		HCOO (X) + H	4.83[d]; 4.85[e]
		HCOO (A) + H	5.366[d]
		COOH + H	4.17[f]
$2^1A'' \pi^* \leftarrow \sigma_{co}$ [a]	broad, E_{max} 7.53 [a]		
$2^1A' \pi^* \leftarrow \pi_{c=o}$ [a]	8−8.8[a]		
Rydberg and valence transitions[a]	8.75−11.5[a]	HCO + OH (A)	8.847[c,g]
		HCOO* + H	9.075[h]
cation ground state $1^2A'$	11.3246[h]	ionic dissociation channels	
		$HCOO^+$ + H	not known[i]
cation excited states		$COOH^+$ + H	12.36[f]
$1\ ^2A''$	12.3783[h]		
		HCO^+ + OH	12.79[j]
		COH^+ + OH	14.21[c]
$2\ ^2A'$	14.81 (IE_v)[h]		
$2\ ^2A''$	15.75 (IE_v)[h]		
$3\ ^2A'$	16.971[h]	HCO^+ + OH (A)	16.84[j,g]
		COH^+ + OH (A)	18.26[c]
		HCO + OH^+(X)	17.97[j]
superexcited molecular states[a]		higher-energy neutral dissociation channels	
		CH (X) + O + OH (X)	13.07[k]
		CH (A) + O + OH (X)	15.95[g,k]
		CH (B) + O + OH (X)	16.3[g,k]
		COOH + H ($n = 4$)	16.92[f]
		COOH + H ($n = 5$)	17.23[f]
		CH (X) + O + OH (A)	17.122[g,k]
		HCOO (X) + H ($n = 4$)	17.58[d]; 17.6[e]
		HCOO (X) + H ($n = 5$)	17.88[d]; 17.9[e]
		HCOO ($^2A_2$) + H ($n = 4$)	18.11[d]
		HCOO ($^2A_2$) + H ($n = 5$)	18.42[d]
		CH (A) + O + OH (A)	20.00[g,k]

[a] See assignments and discussion in ref 8. [b] Reference 13. [c] Reference 31. [d] Reference 24. [e] Reference 21. [f] Reference 45. [g] Reference 32. [h] From the He(I) PE spectrum[9] (see also Figure 5a). [i] The $HCOO^+$ ion is not stable and has so far not been observed experimentally. [j] Reference 46. [k] Reference 47.

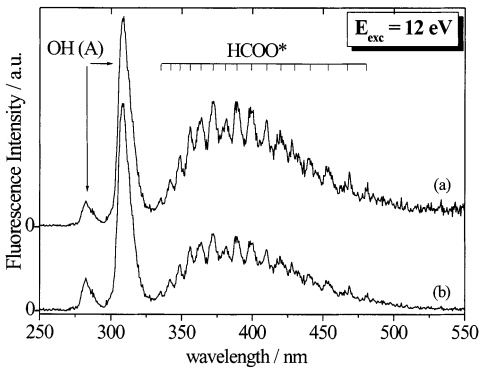

Figure 1. Dispersed fluorescence spectrum observed upon photoexcitation of formic acid at $E_{exc} = 12$ eV (103.3 nm): (a) spectrum corrected for the response function of the fluorescence detection system; (b) uncorrected spectrum. Spectral resolution is ~5 nm. Vertical bars indicate bands listed in Table 2.

TABLE 2: Bands Observed in the Dispersed Fluorescence Spectrum with Formic Acid Excitation Energy $E_{exc} = 12$ eV

wavelength (nm)	energy (cm^{-1})	band spacing (cm^{-1})	corrected intensity (au)
OH ($A^2\Sigma^+ \rightarrow X^2\Pi$) Emission			
308.5 (0−0)	32 415		2500
282.5 (1−0)	35 398		340
HCOO* Emission			
335.3	29 820		330
342	29 240	584	548
348.6	28 690	554	823
355.8	28 110	581	1154
363.4	27 520	588	1255
372	26 880	636	1471
380.7	26 270	614	1243
388.9	25 710	554	1442
399.2	25 050	664	1388
410.1	24 380	666	1215
419.9	23 820	569	1071
429.8	23 270	549	914
440.7	22 690	576	801
453.4	22 060	636	686
467	21 410	642	537
480.4	20 820	597	443

Tabayashi et al.,[4] assuming a thermal Boltzmann population of the $A^2\Sigma^+$ state rovibronic levels, for comparison with the OH fluorescence produced by two-photon (KrF) laser excitation of HCOOH at 9.98 eV (2 × 248.5 nm) and by one-photon (synchrotron radiation) excitation at 9.96 eV and at 11.27 eV. These authors derived OH rotational and vibrational temperatures of the $A^2\Sigma^+$ state as a function of the available excess energy. In our case, we were unable to fit a simulated thermal Boltzmann population of OH $A^2\Sigma^+$ levels to our two observed bands at $E_{exc} = 12$ eV. This is not surprising because there can build up a non-Boltzmann distribution in the $A^2\Sigma^+$ state upon photodissociation of HCOOH at high excess energies (3.153 eV in our case). We also note that the excitation energies in the work of Tabayashi et al.[4] correspond, according to our analysis of the absorption spectrum,[8] to Rydberg excitation of a 10a′ electron, which is mainly nonbonding n_o on the oxygen

atom lone pair of the carbonyl group in HCOOH, whereas in our case, at $E_{exc} = 12$ eV, it is a $\pi_{C=O}$ 2a″ electron that is promoted. The bonding properties are therefore different in these two cases, so the photodissociation dynamics could differ and lead to different energy level population distributions in the OH products.

3.2.2. HCOO Emission and Its Assignment. The work of Dyne, Style, and Ward,[20] using deuterium isotope diagnostics, showed that the emitter of the fluorescence bands between 350 and 450 nm, which they observed upon VUV photon or high-frequency discharge excitation of HCOOH, is most probably the formyloxyl radical, HCOO, in which the hydrogen atom is connected to the carbon atom, and not its isomer, the hydrocarboxy radical COOH (also referred to as HOCO in the literature), which is thermodynamically more stable.[21]

The emitting state of HCOO formed in the VUV dissociation of HCOOH has not been identified hitherto, and one of the objectives of our present work is to assign it. In earlier matrix work on the reaction between fluorine atoms and formic acid, Jacox was able to trap the *t*-HOCO radical in an Ar matrix and assign its infrared absorption spectrum.[22] The isomer HCOO, however, was apparently not stable enough to be trapped and characterized, although there was indirect evidence for its formation.[22]

Lee and Pimentel,[23] upon warming up matrix-isolated CH_2N_2/O_2/Ar mixtures that had been photolyzed at 8 K, observed two chemiluminescence progressions of bands in the same spectral region as our HCOO emission in the gas phase. A set of four bands between 310 and 360 nm were tentatively assigned to the $\tilde{a}^3A'' \rightarrow \tilde{X}^1A'$ transition of formic acid, the latter being formed by reaction of CH_2 ($^3B_1$) with O_2 ($^3\Sigma_g^-$) in the cryogenic matrix, and another set of bands, between 390 and 490 nm, were attributed to the HCOOH $\tilde{A}'^1A' \rightarrow \tilde{A}^1A''$ transition. These two transitions are, respectively, $1^3A'' \rightarrow 1^1A'$ and $2^1A' \rightarrow 1^1A''$ in our nomenclature.[8] The results of Lee and Pimentel might therefore imply that HCOOH, and not HCOO, is the emitter of the VUV excited fluorescence that we observed between 330 and 480 nm in our experiments. We therefore decided to investigate this in more detail, first of all by reconsideration of the experimental findings of Lee and Pimentel.

These authors observed vibrational spacings of about 1390 and 1124 cm^{-1} in the respective assigned $1^3A'' \rightarrow 1^1A'$ and $2^1A' \rightarrow 1^1A''$ transitions of HCOOH. We remark that the 1390 cm^{-1} frequency is greater than, but compatible with, the $\nu_4 =$ 1356 cm^{-1} value calculated for the $1^3A''$ state of HCOOH,[13] of which the $1^3A'' \rightarrow 1^1A'$ O^o_o transition is calculated to be at 3.093 eV, that is, at ∼401 nm, close to the observed 360−390 nm progression, but there are no independent measurements of the energy of the lowest triplet state of formic acid. Observed vibrational frequencies in the $2^1A'$ state are in the 1300−1500 cm^{-1} region,[8] but the $1^1A''$ state has a frequency of 1115 cm^{-1},[13] compatible with the observed 1124 cm^{-1} vibrational spacing. The experimentally determined energy difference between the $2^1A'$ and $1^1A''$ states[8] would give a value 3.467 eV (∼358 nm) for the O^o_o transition which, being greater than that of the observed 390−490 nm progression, is compatible with the displaced oscillators corresponding to the two electronic states involved in the extensive progression.

Because there remained ambiguities concerning the assignment to HCOOH of the two progressions observed by Lee and Pimentel, we decided to directly compare our gas-phase HCOO emission spectra with the chemiluminescence spectra of Lee and Pimentel,[23] taking into account matrix effects. Our study showed that the set of four bands in the 310−360 nm region of Lee and Pimentel can be fitted with four bands in our HCOO spectrum, but this would necessitate an improbable gas to matrix blue shift on the order of 2000 ± 500 cm^{-1}. Furthermore, no correspondence was observed between the 390−490 nm matrix spectrum and our gas-phase spectrum. We add that the $2^1A'$ state of formic acid can be populated already at $E_{exc} = 8.107$ eV,[8] but we observed an onset excitation energy for the gas phase 330−480 nm emission bands (monitored at 375 nm) greater than 9 eV (see later). We thus conclude that HCOOH is not the emitter of the 330−480 nm band progression in the gas phase.

The vibrational spacing is 600 ± 40 cm^{-1} throughout almost the whole HCOO progression at $E_{exc} = 12$ eV. The observed band energies are listed in Table 2 and are shown as bars in Figure 1. The observed bandwidths (fwhm ≈ 150−200 cm^{-1}) are of the same order of magnitude of, and are presumably limited by, the spectral resolution of our detection system (5 nm). The fairly regular spacing of about 600 cm^{-1} corresponds most probably to excitation of the bending mode of the OCO group in the emitter molecule (the corresponding vibrational mode frequency in HCOOH is $\nu_7 = 625$ cm^{-1}),[8,9] and the long progression is indicative of a substantial change in OCO angle in going from the upper to the lower electronic state. The maximum of the HCOO emission is found at about 375 nm in our spectrum. This is at a significantly shorter wavelength than in the observation of Suto et al.[3] at $E_{exc} = 10$ eV, at which the maximum emission wavelength is at about 400 nm. The difference indicates that a significant fraction of the excess energy upon excitation at $E_{exc} = 12$ eV is stored as vibrational energy in the OCO bending mode of excited HCOO.

We remark that Suto et al.[3] did not classify the HCOO emission vibronic bands as a single progression as we have done but into two progressions displaced from each other by 690 cm^{-1}, each of which has an average frequency spacing of 1195 cm^{-1}, unassigned to any specific mode. According to ab initio calculations of Kim et al.,[24] a frequency on the order of 1195 cm^{-1} could correspond to the symmetric CO stretch vibration of HCOO. However, Kim et al. also recorded photoelectron spectra (PES) upon photodetachment of the formate ion, $HCOO^-$. They were thus able to experimentally characterize the three lowest-lying electronic states of HCOO, assuming C_{2v} symmetry, as two quasi-degenerate states, (1^2A_1 as ground state and 1^2B_2, 0.027 eV above) and a third state, 1^2A_2, lying 0.536 eV above the ground state. The $HCOO^-$ PE spectra show partially resolved vibrational features in each state, primarily involving progressions in the OCO bending mode ($\nu = 600-700$ cm^{-1}). Because we see a similar band spacing frequency in our fluorescence spectrum (Table 2), this further confirms the identity of HCOO as the emitting fragment molecule in the VUV excited fluorescence of HCOOH. Additional experiments with higher spectral resolution are required for an accurate assignment of the observed vibronic progression. We turn now to identification of the electronic states involved in the HCOO emission.

We first determine the energies of the upper and lower electronic states in the HCOO emission, using the following data. The fluorescence excitation spectrum of this emission, monitored at 375 nm, presented in section 3.4, shows an onset at $E = 9.075 \pm 0.01$ eV. From the dispersed fluorescence spectrum (Figure 1), the highest energy HCOO emission band is observed to be at $\lambda = 335$ nm (3.7 eV), and we assume that this corresponds to a 0−0 Franck−Condon transition. Assuming further that our observed fluorescence onset energy in the FEX spectrum (9.075 eV) corresponds to a potential barrier of the

corresponding dissociation reaction of no greater than some tenths of 1 eV, we can calculate that the energy of the HCOO state populated by the emission is about 5.375 eV (9.075−3.7 eV) above the ground-state energy of HCOOH. Because the thermochemical threshold for HCOO formation in its ground state from HCOOH dissociation is $E = 4.83$ eV (see Table 1), we can further deduce that the final state of the HCOO fluorescence must lie 0.545 eV above the ground state of this radical. This final (excited) state could be the 1^2A_2 state of HCOO (π-character, C_{2v}), which has been experimentally characterized[24] to be situated 0.536 eV above the HCOO ground state, as mentioned above.

Further information on the HCOO emitting and final states can be obtained from the ab initio calculations of Rauk et al.[25] of the energies of HCOO electronic states in both C_{2v} (two equal carbon−oxygen bond lengths) and C_s (unequal carbon−oxygen bond lengths) symmetries. In C_{2v} symmetry, these authors find twin ground states (σ-states, $^2A_1$ and $^2B_2$) almost degenerate in energy and a π-state ($^2A_2$ symmetry, C_{2v}) lying roughly 0.5 eV above the ground state, agreeing well with the experimental findings of Kim et al.[24] In C_s symmetry, they calculate a $^2A''$ π-state to be energetically close to the $^2A_2$ (C_{2v}) excited state of HCOO. These authors also find a $^2B_1$ π-state (C_{2v}), lying approximately 4 eV above the ground state of HCOO. Because their calculations are successful in reproducing the energies of the three states experimentally characterized by Kim et al.,[24] we go one step further and suggest that the $^2B_1$ state could be the emitting state of HCOO in our experiments. If the final state was the C_s symmetry $^2A''$ π-state, one would expect that the symmetry change from C_{2v} ($^2B_1$) to C_s ($^2A''$) would give rise to excitation of the CO asymmetric stretch mode, calculated to have a frequency on the order of 750 cm^{-1} in the $^2A''$ state.[25] Taking into acount experimental and theoretical uncertainties, this value is not inconsistent with the observed strong vibronic excitation of a mode the frequency of which is on the order of 600 cm^{-1}. However, as assumed and discussed above, an apparently more reasonable mode assignment is the OCO bending mode. This implies that there is a notable change in the OCO bond angle in going from the upper to the lower state. However, in a $^2B_1$ (C_{2v}) to $^2A''$ (C_s) transition, this angle is calculated (CASSCF level)[25] to change from 123.3° to 121.3°, which is a relatively small modification. If the radical remained C_{2v} in both states, so that the lower state was $^2A_2$, the calculated OCO angle change would be 123.3° to 121.1°, an equally small modification. We note that earlier MO calculations in C_{2v} symmetry by Peacock et al.[26] predicted that a $^2B_1 \rightarrow {}^2A_2$ transition would give rise to a band at 386 nm with an oscillator strength of 0.174.

This discussion leads us to suggest that the best assignment of the HCOO fluorescence observed following VUV photodissociation of HCOOH is a $^2B_1$ (C_{2v}) to $^2A''$ (C_s) transition involving excitation of the asymmetric CO mode, possibly coupled to the OCO bending mode. Final assignment requires analysis of a high-resolution emission spectrum of HCOO.

3.3. Dispersed Fluorescence Spectra at Excitation Energy $E_{exc} = 20.66$ eV. *3.3.1. CH and H Balmer Emission at Higher Excitation Energies.* The dispersed fluorescence spectrum obtained on excitation of formic acid at $E_{exc} = 20.66$ eV is shown in Figure 2. Spectral resolution is on the order of 8 nm. OH emission is observed, but HCOO emission is not observed. There are also observed some bands in the 330−500 nm region that were not present at $E_{exc} = 12$ eV. These new bands were assigned by considering their respective excitation spectra, which

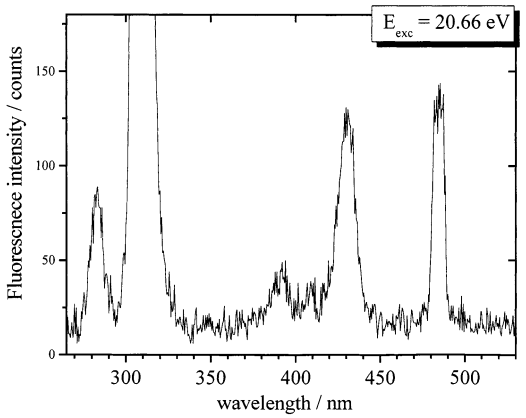

Figure 2. Dispersed fluorescence spectrum observed upon photoexcitation of formic acid at $E_{exc} = 20.66$ eV (60 nm). Spectral resolution is ~8 nm.

are presented in section 3.4, together with the thermochemistry of the related fragmentation processes (Table 1).

The emission band at $\lambda = 431$ nm is broad, so it is necessary to investigate whether it has more than one component. A possible component would be H Balmer-γ ($n = 5 \rightarrow 2$) emission at $\lambda = 434$ nm; another could be the 431.4 nm (0,0) band of the $A^2\Delta \rightarrow X^2\Pi$ transition of the CH radical. H Balmer-γ could result from the dissociation processes HCOOH → COOH + H ($n = 5$) or HCOOH → HCOO + H ($n = 5$), which have thermodynamic onset energies of 17.23 and 17.88 eV, respectively (Table 1). However, these thermodynamic values are higher than the observed onset energy for $\lambda = 431$ nm, which is $E = 16.25 \pm 0.1$ eV, as discussed in section 3.4.3. The value $E = 16.25 \pm 0.1$ eV is consistent with the 15.95 eV thermodynamic threshold of the reaction HCOOH → CH (A) + O + OH (X) (Table 1). We therefore assign the $\lambda = 431$ nm band to CH (A) emission but do not exclude a contribution of H Balmer-γ (5−2) at excitation energies above 17.2 eV (Table 1), especially because the H Balmer-α (3−2) and H Balmer-δ (6−2) emissions were observed at $E_{exc} = 20$ eV (see below).

We next discuss the fluorescence band at $\lambda = 484$ nm, the small bandwidth of which suggests that it is due to an atomic emitter. The wavelength of H Balmer-β emission is 486.1 nm, so at our spectral resolution, this could be the assignment. However, the lowest thermodynamic threshold energy for the appearance of the H Balmer-β emission is 16.92 eV (Table 1), whereas the observed onset energy of $\lambda = 484$ nm is 16.25 ± 0.1 eV (section 3.4.3, Figure 5c), so this atomic emission cannot be present at 16.25 eV. Another possible assignment is to the (0,1) band of the $A^2\Delta \rightarrow X^2\Pi$ transition of the CH radical the Q head of which should occur at 489 nm.

We therefore propose that the 484 nm band is, at least in part, due to the CH $A^2\Delta \rightarrow X^2\Pi$ (0,1) transition. In the fluorescence excitation spectrum of the 484 nm emission, there is a sudden increase in its intensity above 17.6 eV (section 3.4.3, Figure 5c). This is consistent with a H Balmer-β component occurring above 17.6 eV because the opening of the dissociation channel HCOOH → HCOO + H ($n = 4$) has a thermodynamic onset energy that is precisely 17.6 eV (Table 1). Remarkably, as is the case for excitation in the 9−13 eV energy regime, it seems that it is the less-stable isomer HCOO that is preferably formed also at higher excitation energies.

We turn now to a weak emission feature at $\lambda = 410$ nm (Figure 2). This is undoubtedly the H Balmer-δ ($n = 6 \rightarrow 2$) emission line, of which the known wavelength is 410.1 nm. Interestingly, Ma et al.[28] also observe, but do not mention, this

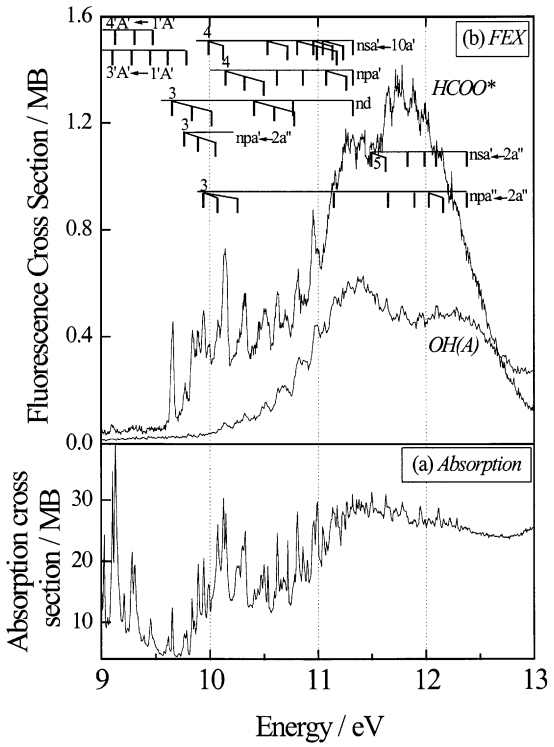

Figure 3. (a) Photoabsorption spectrum of formic acid in the 9−13 eV region[8] and (b) fluorescence excitation (FEX) spectra of formic acid in the 9−13 eV photon excitation region: OH (A) (λ_{obs} = 310 nm) and HCOO* (λ_{obs} = 375 nm) emissions. Vertical bars indicate absorption band assignments.

band upon photoexcitation of CH_3OH at E_{exc} = 27.13 eV (45.7 nm), as well as that of CH_4 at E_{exc} = 22.5 eV (55.1 nm). In additional dispersed fluorescence experiments at LURE, at E_{exc} = 20 eV and with appropriate wavelength detection range, we also observed the H Balmer-α ($n = 3 \rightarrow 2$) emission line at 656.2 nm.

The dispersed fluorescence spectrum also contains a weaker band at λ = 390 nm, which we assign to CH ($B^2\Sigma^- \rightarrow X^2\Pi$) (0,0) band emission. The CH (A−X) and (B−X) bands, which are usually observed in the heads of comets,[27] are also observed, with very similar B/A emission intensity ratios, in the dispersed fluorescence spectrum recorded upon VUV photoexcitation of CH_4 at E_{exc} = 14.87, 16.21, and 22.5 eV and of CH_3OH at E_{exc} = 13.43, 14.87, 16.21, and 27.13 eV.[28] The striking similarity of the B/A emission intensity ratios in all of these spectra suggests that the CH (B) state is populated first and subsequently decays to the A state. In this respect, it is noteworthy that we observe 16.25 ± 0.1 eV as threshold energy for both the (0,0) and (0,1) bands of the $A^2\Delta \rightarrow X^2\Pi$ transition of the CH radical, which is close to the 16.3 eV thermodynamic onset energy for formation of CH ($B^2\Sigma^-$) (Table 1).

It is not at all clear how excited CH is formed in the case of formic acid. The dissociation reaction HCOOH → CH (A,B) + O + OH (X) might be thought to involve as a first step the reaction HCOOH → HCO* + OH (X) in which the formyl radical is formed in a predissociative state. However, it is known that HCO* predissociates into H + CO, not CH and O.[29] Another possible intermediate is HCOH*, because the equivalent ionic reaction $HCOOH^+ \rightarrow HCOH^+ + O$ is known.[5] However, HCOH*, as formaldehyde H_2CO*, predissociates to HCO + H[16,30] and not to CH and OH. Processes such as HCOOH → CH (A,B) + HO_2 or the triple product reaction HCOOH → CH (A,B) + O + OH (X) are unlikely at first glance but must be further explored. Another avenue to explore is excited HCOO as intermediate, in which a large amplitude OCO bending mode vibration could lead to ejection of the CH radical by the process HCOO → CH + O_2.

3.4. Fluorescence Excitation Spectra. In Figure 3, we show the fluorescence excitation (FEX) spectra of the OH $A^2\Sigma^+ \rightarrow X^2\Pi$ (0,0) emission (λ_{obs} = 310 nm) and of the HCOO emission at 375 nm from 9 to 13 eV excitation energy (Figure 3b). For comparison, we also show the photoabsorption spectrum of formic acid (Figure 3a) taken from Leach et al.[8] In this energy region, our measured relative intensity of the OH and HCOO FEX bands is normalized using the absolute fluorescence cross sections given by Tabayashi et al.[4] for photon excitation energies below 11.4 eV. We calculate that at E_{exc} = 12 eV the quantum yield of fluorescence is 1.8% for the OH (A) emission and 4.6% for the HCOO emission. Although our experiments do not allow us to observe neutral fragments in their electronic ground states, on energy grounds (Table 1) it is reasonable to assume that the direct dissociations HCOOH → HCOO (X) + H and HCOOH → HCO + OH (X) are also efficient relaxation pathways of excited states of HCOOH between 6 and 13 eV. This remains to be verified.

We list the observed FEX bands in Table 3, together with the corresponding absorption bands and their transition assignments. We did not attempt to measure the FEX spectra of the 410 and 390 nm emission bands because of their weak intensity. Our analysis of the observed FEX bands is divided into three energy regions: (1) below the first IE (11.3246 eV) (section 3.4.1), (2) from the first IE up to 13 eV (section 3.4.2), and (3) between 13 and 23 eV (section 3.4.3).

3.4.1. Fluorescence Excitation Spectra from 9 eV up to the First IE at 11.33 eV. In this energy region, Rydberg series, converging to the first IE of HCOOH, as well as valence transitions, are found in the absorption spectrum. In Table 3 and Figure 3, we show band assignments according to our recent detailed analysis of the absorption spectrum in the range 6−22 eV.[8]

In the FEX spectra, the weak onset of OH ($A^2\Sigma^+ \rightarrow X^2\Pi$) emission is observed at E_{exc} = 9.15 ± 0.03 eV (136.6 nm), as shown in the threshold region of the OH (A) FEX spectrum in Figure 4. Our measured onset energy value is slightly higher than that reported by Tabayashi et al.[4] (E = 9.05 ± 0.03 eV). From enthalpy of formation (ΔH_f) data[31] and the OH ($A^2\Sigma^+$) T_0 value,[32] we calculate the thermochemical onset for the reaction HCOOH → HCO + OH ($A^2\Sigma^+$) to be 8.85 ± 0.02 eV (Table 1). This is about 300 meV below our measured onset energy of the OH (A) emission. Tabayashi et al.[4] suggest that the difference between the thermochemical and the measured onset energy could indicate the existence of a potential barrier between the HCOOH excited state and the dissociation surface leading to the OH (A) fragment. This is consistent with the slow rise of the OH emission yield in the first electronvolt beyond the onset (Figure 3b), which is typical for photochemical dissociations involving potential barriers. However, we also note that the detection sensitivity for fluorescence photons is limited, so our measured onset energy is, in a sense, an upper limit. This implies that the potential energy barrier for this reaction is probably smaller than the 0.4 eV difference between our measured and the thermochemical onset.

Our observed onset for emission of HCOO is at E_{exc} = 9.075 ± 0.01 eV (136.6 nm) (Figure 3b). Tabayashi et al. report a much lower onset energy (8.16 eV), but this is not evident from their published spectrum.[4] The energetics involved in the formation and relaxation of the HCOO emitting state were discussed in section 3.2.2. In the threshold region, the HCOO

TABLE 3: HCOO* and OH (A) Fluorescence Excitation (FEX) Bands and Corresponding Absorption Bands of HCOOH

HCOO* FEX band position (eV)	HCOO* FEX band position (nm)	OH (A) FEX band position (eV)	OH (A) FEX band position (nm)	nearest HCOOH absorption band (eV)	assignment of the nearest absorption band[8]
9.10	136.25			9.103	$3^1A' \leftarrow 1^1A' (3^1_0)$
9.30	133.3			9.306	$4^1A' \leftarrow 1^1A' (3^2_0)$
9.654	128.43			9.651	$3da' \leftarrow 10a' (0^0_0)$
9.771	126.89			9.763	$3pa' \leftarrow 2a'' (0^0_0)$
				9.782	$3^1A' \leftarrow 1^1A' (3^5_0)$
9.842	125.98			9.835	$3da' \leftarrow 10a' (3^1_0)$
9.891	125.35			9.891	$3pa' \leftarrow 2a'' (6^1_0)$
9.941	124.72			9.942	$3pa'' \leftarrow 2a'' (0^0_0)$
9.992	124.08			9.987	$4sa' \leftarrow 10a' (0^0_0)$
10.08	123.0			10.071	$3pa'' \leftarrow 2a'' (6^1_0)$
10.14	122.27	10.14	122.27	10.125	$4sa' \leftarrow 10a' (6^1_0)$
				10.147	$4pa' \leftarrow 10a' (0^0_0)$
10.271	120.71	10.25	120.96	10.256	$3pa'' \leftarrow 2a'' (3^1_0)$
10.319	120.15	10.325	120.08	10.299	$4pa' \leftarrow 10a' (6^1_0)$
				10.324	$4pa' \leftarrow 10a' (3^1_0)$
10.455	118.59	10.48	118.31	10.442	$4pa' \leftarrow 10a' (6^2_0)$
				10.47	$4pa' \leftarrow 10a' (3^1_0\, 6^1_0)$
10.509	117.98	10.52	117.86	10.498	$4pa' \leftarrow 10a' (3^2_0)$
10.536	117.67			10.533	$5sa' \leftarrow 10a' (0^0_0)$
10.624	116.7	10.64	116.53	10.621	$5pa' \leftarrow 10a' (0^0_0)$
10.706	115.81	10.70	115.87	10.717	$5sa' \leftarrow 10a' (3^1_0)$; $3da'' \leftarrow 2a'' (0^0_0)$
10.792	114.89			10.78	$4da' \leftarrow 10a' (3^2_0)$
10.812	114.67	10.825	114.54	10.806	$6sa' \leftarrow 10a' (0^0_0)$; $5pa' \leftarrow 10a' (3^1_0)$
		10.88	113.96	10.86	$6pa' \leftarrow 10a' (0^0_0)$; $4sa' \leftarrow 2a'' (0^0_0)$
10.958	113.15	10.985	112.87	10.956	$7sa' \leftarrow 10a' (0^0_0)$; $5da' \leftarrow 10a' (3^1_0)$; $5pa' \leftarrow 10a' (3^1_0\, 6^1_0)$
10.998	112.73			10.989	$6sa' \leftarrow 10a' (3^1_0)$; $7pa' \leftarrow 10a' (0^0_0)$; $4sa' \leftarrow 2a'' (6^1_0)$
		11.06	112.1	11.045	$8sa' \leftarrow 10a' (0^0_0)$; $6pa' \leftarrow 10a' (3^1_0)$
11.158	111.12	11.16	111.08	11.148	$4pa'' \leftarrow 2a'' (0^0_0)$; $4sa' \leftarrow 2a'' (3^1_0)$
11.269	110.02	11.285	109.87	11.264	$8pa' \leftarrow 10a' (3^1_0)$
11.324	109.49			11.317	$9pa' \leftarrow 10a' (3^1_0)$
11.412	108.64	11.395	108.81	11.417	
11.503	107.78			11.497	$5sa' \leftarrow 2a'' (0^0_0)$
11.649	106.43	11.635	106.56	11.628	$5sa' \leftarrow 2a'' (6^1_0)$
				11.65	$5pa'' \leftarrow 2a'' (0^0_0)$
11.75	105.52				*a*
		11.78	105.25	11.781	$5pa'' \leftarrow 2a'' (6^1_0)$; $5sa' \leftarrow 2a'' (3^1_0)$
11.884	104.33			11.893	$6pa'' \leftarrow 2a'' (0^0_0)$
		11.95	103.75	11.946	$5pa'' \leftarrow 2a'' (3^1_0)$
11.989	103.42			11.988	$7sa' \leftarrow 2a'' (0^0_0)$
		12.1	102.47	12.116	$7sa' \leftarrow 2a'' (6^1_0)$; $6sa' \leftarrow 2a'' (3^1_0)$
12.14	102.13			12.159	$7pa'' \leftarrow 2a'' (6^1_0)$
12.27	101.05	12.275	101	12.221	$8sa' \leftarrow 2a'' (6^1_0)$
				12.286	$7sa' \leftarrow 2a'' (3^1_0)$
12.49	99.27			*b*	
		13.3	93.2	13.48[c]	$x \leftarrow 9a'$ [c]
		14.2	87.3	14.3	strong continuum
		18.4	67.4	17.9[d]	$x \leftarrow 6a'$ [d]

[a] There is no corresponding absorption feature. [b] Not resolved. [c] Region of broad overlapping Rydberg bands converging to the $2^2A'$ ion state. x = ns, np, and nd Rydberg states. [d] Region of broad overlapping Rydberg bands converging to the $5^2A'$ ion state. x = ns, np, and nd Rydberg states.

FEX spectrum shows a weak band at 9.1 eV, which corresponds to the absorption band that is the first member of a CO stretch vibrational progression of the $\pi^* \leftarrow \pi_1$ ($3^1A' \leftarrow 1^1A'$) transition (Table 3).[8] The first intense band of the HCOO FEX spectrum appears at $E_{exc} = 9.654$ eV, corresponding to the origin band of the $3da' \leftarrow 10a'$ Rydberg transition, and it marks the beginning of a series of sharp bands, which can all be easily associated with features observed in the photoabsorption spectrum (see Table 3 for details). This is also the case for the OH (A) FEX spectrum, which is somewhat less well resolved than the HCOO FEX spectrum because of the weaker intensity of the OH emission. Common to both spectra is that the fluorescence cross section of each of these two emitters increases with increasing photon energy below the first IE. Furthermore, within the limits of their spectral resolutions, it appears that most of the features observed in the OH (A) FEX spectrum are also observed in the HCOO FEX spectrum but with different relative intensities. This is particularly evident, for example, in the energy region between 10 and 11 eV (Figure 3b). It indicates that the corresponding HCOOH excited states can fragment into each of the two dissociation channels. However, as indicated by the different relative intensities of the OH and HCOO FEX bands, the branching ratio of the two dissociation reactions HCOOH → HCO + OH (A) and HCOOH → HCOO ($^2B_1$) + H varies considerably as a function of excitation energy.

3.4.2. Fluorescence Excitation Spectra from the First IE at 11.33 eV up to 13 eV. At energies higher than the first IE, the two FEX spectra in Figure 3b exhibit more marked differences in their evolution. The OH (A) emission intensity decreases with increasing photon energy above the first IE, after reaching a

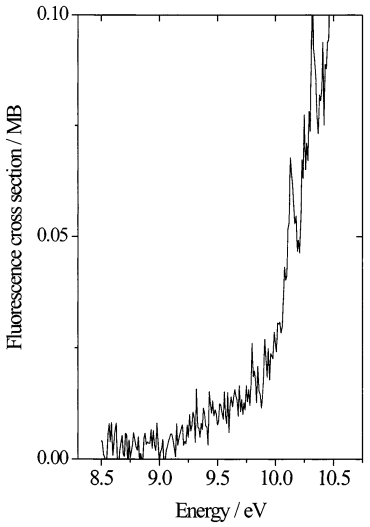

Figure 4. OH (A → X) fluorescence excitation spectrum in the threshold region.

maximum at $E_{exc} = 11.395$ eV, whereas the HCOO emission intensity continues to increase until a maximum is reached at an excitation energy of about $E_{exc} = 11.75$ eV. The OH emission maximum also corresponds to a maximum observed in the photoabsorption curve of HCOOH (Figure 3a).

We note that in this energy region not every OH (A) FEX band can be found in the FEX spectrum of HCOO. The OH (A) FEX bands at $E_{exc} = 11.78$, 11.95, and 12.1 eV are clearly found in the absorption spectrum, corresponding to Rydberg transitions involving promotion of a 2a″ electron (Table 3), but it is difficult to disentangle these bands in the FEX spectrum of HCOO (see Figure 3 and Table 3). Beyond 12 eV, the two FEX spectra differ more markedly. The two signals decrease with increasing photon energy with the HCOO signal falling off rapidly to the background level while the OH (A) fluorescence signal decreases more slowly.

3.4.3. Fluorescence Excitation Spectra between 13 and 23 eV. In Figure 5, we show the FEX spectra of OH (A) emission at higher excitation energies (Figure 5b), as well as the FEX spectra of the emission bands located at $\lambda = 431$ and $\lambda = 484$ nm in the dispersed fluorescence spectrum (Figure 5c). The onsets of the latter have been discussed in section 3.3.1. No HCOO emission was observed at photon energies higher than 13.3 eV. In Figure 5a, we plot the formic acid absorption spectrum, its He(I) photoelectron spectrum, and the quantum yield of ionization, $\gamma(E_{exc})$ as a function of excitation energy.

In the absorption spectrum, we observe three broad bands consisting, respectively, of a shoulder at 13.48 eV and maxima at 14.3 and 17.9 eV. The two bands at 13.48 and 14.3 eV have been attributed to broad overlapping Rydberg transitions, together with their vibrational companions,[8] which probably converge to the second excited state $2^2A'$ ($IE_{vert} = 14.81$ eV) of the ion (see Figure 5a). These two absorption bands correspond to broad bands observed in the FEX spectrum of OH (A). This indicates that neutral dissociation is still an important fragmentation process because OH cannot be formed in its lowest excited $A^2\Sigma^+$ state by any ionic dissociation channel in this energy region (Table 1).

On the other hand, the broad OH (A) FEX band with a shoulder at 17.9 eV and its origin at about 16.8 eV probably corresponds to the dissociative photoionization $HCOOH^+ \rightarrow HCO^+ + OH$ (A), the thermodynamical threshold energy of which is at $E = 16.84$ eV (Table 1). Nishimura et al.[5] recorded threshold photoelectron photoion coincidence (TPEPICO) mass

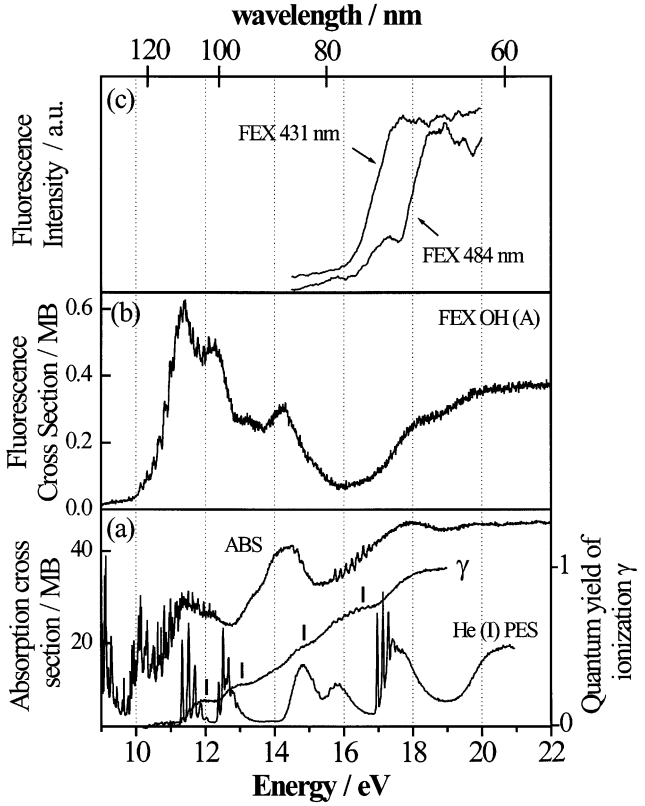

Figure 5. (a) Photoabsorption spectrum,[8] HeI photoelectron spectrum[9] and quantum yield of ionization (γ) of formic acid betwen 9 and 22 eV, (b) fluorescence excitation spectra of OH (A → X) emission, and (c) fluorescence excitation spectra of emission at 431 and 484 nm.

spectra of HCOOH, measuring the ionic fragments as a function of the incident photon energy. They observed a high-energy onset of the formation of the HCO^+ ion at $E \approx 17$ eV, the yield of which reaches its maximum at about 18 eV. This is in excellent agreement with our OH (A) FEX band behavior and thus confirms our suggestion as to its origin. We note that the $HCOOH^+ \rightarrow COH^+ + OH$ (A) dissociation channel, involving formation of the $m/z = 29$ COH^+ isomer in which the hydrogen atom is connected to the O atom, should have a higher appearance energy, which we calculate to be 18.26 eV (Table 1) using the estimated value of its enthalpy of formation given by Lias et al.[31] This may represent an additional channel for formation of OH (A), because Figure 5b shows an increase in the OH (A) emission intensity starting at about 18.3 eV that is mirrored in an increase in the $m/z = 29$ signal at this energy in the breakdown curves given in Figure 2 of Nishimura et al.[5]

In this energy region, we also observe broad bands in the FEX spectrum of the 431 and 484 nm emissions, exhibiting peaks at $E_{exc} = 17.7$ and $E_{exc} = 17.3$ eV, respectively. These emissions have been analyzed in section 3.3.1 and must, on energy grounds, correspond to neutral dissociation. Because the FEX and absorption bands are broad in this energy region, we cannot say whether OH (A) and CH (A) stem from different or common HCOOH superexcited states.

3.5. Photoionization Quantum Yield, γ, and Absorption Spectra in the 9−23 eV Region. *3.5.1. Reaching $\gamma(E_{exc}) = 1$: Autoionization Aspects.* The $\gamma(E_{exc})$ curve grows smoothly with steps occurring whenever an ion state becomes accessible, as discussed in more detail in section 3.5.2. This can be seen when comparing $\gamma(E_{exc})$ with the HeI PE spectrum (Figure 5a, steps are indicated as bars). A similar behavior was found for benzene.[11] This implies that direct ionization of HCOOH is

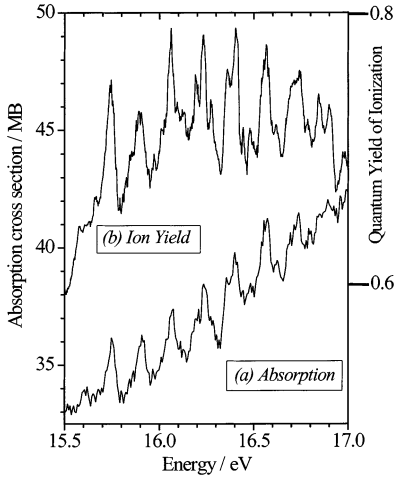

Figure 6. (a) Formic acid absorption spectrum in the 15.5−17 eV region and (b) formic acid ionization quantum yield in the 15.5−17 eV region.

much more important than autoionization of superexcited states. However, HCOOH absorption bands in the 15.7−16.8 eV energy regime, corresponding to Rydberg transitions arising from the 8a′ HCOOH molecular orbital,[8] are clearly seen in the $\gamma(E_{exc})$ curve, indicating autoionization of these states, as discussed below.

Figure 5a shows that the plateau $\gamma(E_{exc}) = 1$ is reached at $E_{exc} = 18 \pm 0.1$ eV. That this plateau extends to at least 23 eV was determined in further ionization quantum yield measurements, carried out at LURE, at a low resolution of ∼200 meV. Defining E_I as the excitation energy value where $\gamma = 1$, we thus determine the energy domain, $\Delta E = E_I - \text{IE}$, of competitive nonionic decay processes of the superexcited molecular states to be 6.68 ± 0.1 eV. This value is similar to that of other astrophysically important small molecules such as CO_2, NH_3, H_2O, and C_2H_4, for which ΔE was found to vary between 6 and 8 eV,[1,33] while for small polycyclic aromatic hydrocarbons (PAHs), $\Delta E \approx 9.2$ eV.[11] Related aspects of the relation between direct ionization and autoionization have been discussed recently by Berkowitz.[34]

It is remarkable that the absorption bands in the 15.7−16.8 eV region appear as features in the ion quantum yield, $\gamma(E_{exc})$, curve, as seen in Figure 5a and in more detail in Figure 6, whereas most of rest of the $\gamma(E_{exc})$ curve is continuous. This behavior indicates that these Rydberg bands, which converge to the $3^2A'$ ion state,[8] undergo autoionization to an ionization continuum on a relatively long time scale. To calculate the autoionization rate, we need to measure the fwhm of the $\gamma(E_{exc})$ and the absorption curve peaks and to compare them, respectively, with the energy resolution of the ion quantum yield and absorption measurements. The $\gamma(E_{exc})$ peaks above the underlying continuum have a fwhm ≈ 50 meV ≈ 400 cm^{-1}. This corresponds to an autoionization rate $k_{ai} \approx 7.5 \times 10^{13}$ s^{-1}, but because the spectral resolution in the $\gamma(E_{exc})$ measurements in the 15.7−16.8 eV region was 50 meV, this k_{ai} value is an upper limit for the autoionization rate. However, the fwhm of the absorption peaks above the underlying continuum in the 15.7−16.8 eV region was also found to have a value of about 50 meV.[8] From this, we infer that the autoionization rate $k_{ai} \approx 7.5 \times 10^{13}$ s^{-1} is a reliable value because the absorption peak fwhm is much greater than the absorption spectral resolution, which is about 10 meV in the 16 eV energy region.[8]

3.5.2. Aspects of Dissociative Ionization. In the following discussion of dissociative ionization in formic acid, we correlate our data on the absorption spectrum, photoelectron spectrum, and ionization quantum yield spectrum with the breakdown curve observations of Nishimura et al.[5] The first step of our γ curve in the region of the first PES band (Figure 5a) corresponds to population of the ion ground state $1^2A'$ (IE = 11.33 eV). This state is stable because no charged fragment is observed below 12 eV.[5] The second step of the γ curve corresponds to the additional population of the first excited state of the HCOOH ion, $1^2A''$ (IE = 12.37 eV).[8,9] This state is not stable because $HCOOH^+$ is no longer observed in the breakdown curves above 12.21 eV and $COOH^+$ appears as the main fragment ion. Steps 3 and 4 of the γ curve can be related to the opening up of population of the ion excited states $2^2A'$ and $2^2A''$, the adiabatic ionization energies of which are ∼14.15 and ∼15.4 eV, respectively.[8,9] Interestingly, the fragmentation behavior of these two ion states is quite similar, as can be deduced from the breakdown diagrams.[5] Both states mainly undergo dissociative photoionization according to $HCOOH^+ \rightarrow COOH^+ + H$ and $HCOOH^+ \rightarrow HCO^+ + OH$, the latter being more important than the former, and it increases considerably in relative yield when the $2^2A''$ state is reached.

The ion state $3^2A'$ ($IE_{ad} = 16.971$ eV),[9] which exhibits a pronounced vibrational structure in the PE spectrum of HCOOH (Figure 5a), also correlates with dissociation into $HCO^+ + OH$ (A) and $COOH^+ + H$. As can be seen from the breakdown curves,[5] the branching ratio of these two reactions varies considerably depending on the exact excitation energy in the 17−18 eV energy region. Measurements of the kinetic energy released in the HCO^+ fragment ion showed that there is a bimodal distribution with a large and a small kinetic energy release (KER) component. The existence of the small KER component led Nishimura et al. to suggest that even at high excitation energies this cation can always be formed in its ground state ($^1\Sigma^+$). Nishimura et al. have therefore questioned whether the dissociation in the 17−18 eV region giving rise to the small KER is a direct process. From the vibrational structure observed in the HeI PES, it is conceivable that the $3^2A'$ state has a relatively long lifetime, so there could exist a fluorescence transition of this ion state to the first excited ion state of $HCOOH^+$ ($1^2A''$), which in turn fragments to produce HCO^+ in its ground state. From the PES spectrum,[9] we estimate that the Franck−Condon maximum of a $3^2A' \rightarrow 1^2A''$ transition would give rise to a fluorescence band at ∼282 nm, which is in the exact spectral region in which we observe the (1,0) band of the OH (A−X) transition. Furthermore, this optical transition should have a small radiative rate because of symmetry selection rules, and a predissociative lower state would create a broad fluorescent band, thus making it even more difficult for us to confirm this suggested pathway for formation of ground-state HCO^+. It is striking, however, that the HCO^+ signal in the PEPICO curves has its onset at 12.6 eV, corresponding to the $HCOOH \rightarrow HCO^+ + OH$ ($X^2\Pi$) channel, which is the energy we estimate to be that of the final state in the Franck−Condon maximum of a $3^2A' \rightarrow 1^2A''$ transition, so there is at present no evidence to negate the proposed fluorescence pathway.

We propose an explanation for another aspect of the observed breakdown curve behavior. In Figure 2b (corrected graph) of Nishimura et al.,[5] the increase in the $COOH^+$ signal begins at about 15.8 eV rising to about 17.3 eV and then drops sharply at higher energies. A similar behavior was also observed by Nishimura et al. for DCOOH in their Figure 3. We propose that the increasing $COOH^+$ signal is produced by dissociative autoionization from the Rydberg levels leading to $3^2A'$ (Figure 6) and decreases when excitation reaches the $4^2A'$ state Franck−

Condon maximum at about 17.3 eV. There is a mirror image behavior for the energy dependence of the formation of HCO^+ (DCO^+), showing that the two channels are competitive if they are formed, as suggested here, by dissociation via autoionization of the Rydberg states. The breakdown curves indicate that the ratio between the $H + COOH^+$ and the $OH + HCO^+$ dissociative autoionization channels increases with increasing energy in the 15.8−17.3 eV region. A study of the breakdown curves of formic acid at an adequately high spectral resolution is necessary to confirm our proposed dissociative autoionization interpretation.

4. Conclusions and Astrophysical Implications

Photofragment fluorescence spectroscopy was used to study the VUV photofragmentation of formic acid in the 6−23 eV energy regime. We also recorded the quantum yield of photoionization (γ) as a function of the incident photon energy. Recent studies of the photoabsorption[8] and the photoelectron spectrum[9] of HCOOH in the same energy region were used to analyze the observations.

When HCOOH is excited with photon energies that correspond to astrophysical HI regions ($E_{photon} < 13.6$ eV), we detect OH ($A^2\Sigma^+ \rightarrow X^2\Pi$) and HCOO emissions in the UV/visible spectral region. Because the ionization energy of HCOOH is 11.33 eV, this indicates that the neutral photoreactions $HCOOH \rightarrow OH\ (A^2\Sigma^+) + HCO$ and $HCOOH \rightarrow HCOO^* + H$ are important photodissociation pathways that must be considered in the gas-phase astrochemistry of this molecule. From the FEX spectra of the two fluorescence signals, we conclude that the branching ratio of the two photoreactions depends on the nature of the initially populated state and its interaction with dissociative neutral states. All features seen in the FEX spectra of OH (A) and HCOO can be associated with absorption bands of HCOOH. Because absolute absorption and fluorescence cross sections are available, it is in principle possible to estimate state-selective quantum yields for the two dissociation channels in the energy range investigated here, but this has not been attempted in the present study. We further conclude from our study that the emitting state of HCOO is most likely 1^2B_1 (C_{2v}) and the lower state $1^2A''$ (C_s), states that were characterized in the ab initio calculations of Rauk et al.[25]

Although, in our experiments, we cannot observe nonfluorescing neutral fragments, it is reasonable to assume that also the photodissociations $HCOOH \rightarrow OH + HCO$ and $HCOOH \rightarrow HCOO + H$, leading to the fragments in their respective electronic ground states, are important. The yields of these two processes, however, remain to be quantified. HCOO is thermodynamically unstable with respect to CO_2 and H by 0.58 eV. It is possible that HCOO, after formation in the excited 1^2B_1 state and radiative relaxation to the $1^2A''$ state, undergoes fragmentation into these neutral products. The photodissociation processes $HCOOH \rightarrow CO_2 + 2H$ (via excited-state relaxation of HCOO) and $HCOOH \rightarrow OH + HCO$ would thus constitute the most efficient fragmentation pathways of formic acid below the astrophysical HI limit.

The dissociative photoionizations $HCOOH^+ \rightarrow COOH^+ + H$ and $HCOOH^+ \rightarrow HCO^+ + OH$ are energetically possible above 12.22 and 12.79 eV, respectively. We can conclude from our measurement of the quantum yield of ionization that the sum of the respective quantum yields of these two ionic channels at energies below the astrophysical HI limit is less than the value at 13.6 eV, at which we measure $\gamma = 0.25$ (Figure 5a). On the other hand, $COOH^+$ is observed in the ISM,[7] where it could be produced, at least in part, from formic acid.

At higher excitation energies ($E_{exc} > 13.6$ eV), OH (A) fluorescence is also detected. Its FEX spectrum shows broad bands that coincide with broad photoabsorption features that have been attributed by Leach et al.[8] to Rydberg series converging to higher ionization limits. Between 13.6 and 16.8 eV, OH (A) is formed by neutral processes, whereas above 16.8 eV, it is most likely formed also by the dissociative photoionization $HCOOH^+ \rightarrow HCO^+ + OH$ (A). Above 16 eV, we detect CH ($A^2\Delta \rightarrow X^2\Pi$) (0,0; 0,1) fluorescence indicating that neutral photodissociation of HCOOH to form CH (A) takes place at these energies through a formation process that remains to be clarified. Above 17.7 eV, there is a rapid increase in the 484 nm signal intensity, which we attribute to a contribution from hydrogen Balmer-β emission indicating that the photodissociation $HCOOH \rightarrow HCOO + H$ ($n = 4$) takes place in this energy region.

The quantum yield of photoionization (γ) of HCOOH exhibits a steplike behavior as a function of the incident photon energy. These steps occur whenever an ion state of HCOOH is accessible, and they also coincide with maxima in the TPEPICO breakdown curves of charged photofragments of HCOOH.[5] Every step in the γ curve can be associated with the opening of a new ionic fragmentation channel. The energy domain ΔE of competitive nonionic decay processes of superexcited molecular states is found to be $\Delta E = 6.68 \pm 0.1$ eV for formic acid. This is similar to the case of small molecules such as CO_2, H_2O, NH_3, and C_2H_4.[1,11,33] One particularly interesting observation in the case of formic acid is that Rydberg absorption bands converging to the $3^2A'$ state of $HCOOH^+$ are mirrored in the $\gamma(E_{exc})$ spectrum between 15.7 and 17 eV. An autoionization rate of $k_{ai} \approx 7.5 \times 10^{13}\ s^{-1}$ was determined for the Rydberg levels. Furthermore, we propose that competitive dissociative autoionization processes from these Rydberg levels are responsible for the increasing $COOH^+$ signal and decreasing HCO^+ signal observed in the breakdown curves of Nishimura et al.[5] above 15.8 eV. The relative signal strengths are modified when excitation reaches the $4^2A'$ state Franck−Condon maximum at about 17.3 eV.

Our results were used to pay particular attention to another aspect of the formic acid ion breakdown curves of Nishimura et al.[5] We discussed the observational implications of their suggestion that there could exist a fluorescence transition of the $3^2A'$ ion state to the first excited ion state of $HCOOH^+$ ($1^2A''$), which in turn fragments to produce HCO^+ in its ground state, and showed the difficulty of its experimental verification.

Our results demonstrate that the spectroscopy and photophysics of formic acid have potential applications in astrophysics and exobiology, in particular, for understanding the formation and dissociation of this species, as well as its dissociation products. Formic acid is one of the potential building blocks of biomolecules[35] and has been observed by radioastronomy in several sites in the interstellar medium (ISM), for example, in the cold dark cloud L134N and in W51, a region of massive star formation.[36] Furthermore, this molecule is found in comets,[37] which are thought to be one of the possible sources of extraterrestrial supply of organic material to the early Earth.[6] HCOOH and the formate ion ($HCOO^-$) have been proposed, among other species, to be the carriers of weak infrared absorption features at 7.24 and 7.41 mm observed in the young stellar object W33A by the short wavelength spectrometer (SWS) on board of ISO Infrared Space Observatory.[38] HCOOH is also observed in high yield in Miller/Urey experiments, which simulate the evolution of early Earth atmospheres.[39] $HOCO^+$, which is protonated CO_2, is also one of the ionic fragments

produced by dissociative ionization of formic acid.[5] It has been observed in the galactic center region and in Sgr B2.[40,41] The photophysical properties of HCOOH are thus of direct interest for radioastronomy searches, as well as for an understanding of observations on comets and interstellar ices containing HCOOH and its dissociation products. Present models of the formation and destruction of these species are inconclusive,[6,38,41−43] and new approaches[44] are worth considering.

Acknowledgment. We thank Jean-Louis Chotin, Christian Alcaraz, Saoud Baouch, and Daniel Tepfer for their valuable assistance during the synchrotron radiation beam time periods, as well as Klaus Hottmann for carefully recording the He(I) photoelectron spectrum of formic acid. M.S. acknowledges the TMR program of the European Union under Contract FMRX-CT97-0126 on "Usable Fullerene Derivatives" (USEFULL) for financial support. H.W.J. is grateful for support from the European Commission program "Access to Research Infrastructures". Welcome support from the CNRS Groupe de Recherche "GDR Exobiologie" and from INSU is gracefully acknowledged.

References and Notes

(1) Berry, R. S.; Leach, S. *Adv. Electron. Electron Phys.* **1981**, *57*, 1.
(2) Robin, M. B. *Higher Excited States of Polyatomic Molecules*; Academic Press: New York, 1974; Vol. 1.
(3) Suto, M.; Wang, X.; Lee, L. C. *J. Phys. Chem.* **1988**, *92*, 3764.
(4) Tabayashi, K.; Ayoama, J.; Matsui, M.; Hino, T.; Saito, K. *J. Chem. Phys.* **1999**, *110*, 9547 and references therein.
(5) Nishimura, T.; Meisels, G. G.; Niwa, Y. *J. Chem. Phys.* **1989**, *91*, 4009.
(6) Chyba, C.; Sagan, C. *Nature* **1992**, *355*, 125.
(7) (a) Herbst, E.; Klemperer, W. *Astrophys. J.* **1973**, *185*, 505. (b) Watson, W. D. *Annu. Rev. Astron. Astrophys.* **1978**, *16*, 585. (c) Herbst, E. *Annu. Rev. Phys. Chem.* **1995**, *46*, 27.
(8) Leach, S.; Schwell, M.; Dulieu, F.; Chotin, J.-L.; Jochims, H.-W.; Baumgärtel, H. *Phys. Chem. Chem. Phys.* **2002**, *4*, 5025.
(9) (a) Schwell, M.; Leach, S.; Hottmann, K.; Jochims, H.-W.; Baumgärtel, H. *Chem. Phys.* **2001**, *272*, 77. (b) Leach, S.; Schwell, M.; Talbi, D.; Berthier, G.; Hottmann, K.; Jochims, H.-W.; Baumgärtel, H. *Chem. Phys.*, in press.
(10) Whitehead, C. *Annu. Rep. R. Soc. Chem., Sect. C* **1999**, *94*, 293.
(11) Jochims, H.-W.; Baumgärtel, H.; Leach, S. *Astron. Astrophys.* **1996**, *314*, 1003.
(12) Lee, L. C.; Suto, M. *Chem. Phys.* **1986**, *110*, 161.
(13) Ioannoni, F.; Moule, D. C.; Clouthier, D. J. *J. Phys. Chem.* **1990**, *94*, 2290.
(14) Brouard, M.; Wang, J.-X. *J. Chem. Soc., Faraday Trans.* **1992**, *88*, 3511.
(15) Brouard, M.; Simons, J. P.; Wang, J.-X. *Faraday Discuss. Chem. Soc.* **1991**, *91*, 63.
(16) Herzberg, G. *Molecular Spectra and Molecular Structure − Vol. III, Electronic Spectra and Electronic Structure of Polyatomic Molecules*; Van Nostrand Reinhold: New York, 1966.
(17) Bell, S.; Ng, T. L.; Walsh, A. D. *J. Chem. Soc., Faraday Trans.* **1974**, *71*, 393.
(18) Fridh, C. *J. Chem. Soc., Faraday Trans.* **1977**, *74*, 190.
(19) Kimura, K.; Katsumata, S.; Yamazaki, T.; Wakabayashi, W. *J. Electron Spectrosc. Relat. Phenom.* **1975**, *6*, 41.
(20) (a) Dyne, P. J.; Style, D. W. G. *J. Chem. Soc.* **1952**, 2122. (b) Style, D. W. G.; Ward, J. C. *J. Chem. Soc.* **1952**, 2125.
(21) Langford, S. R.; Batten, A. D.; Kono, M.; Ashfold, M. N. R. *J. Chem. Soc., Faraday Trans.* **1997**, *93*, 3757.
(22) Jacox, M. *J. Chem. Phys.* **1988**, *88*, 4598.
(23) Lee, Y.-P.; Pimentel, G. C. *J. Chem. Phys.* **1981**, *74*, 4851.
(24) Kim, E. H.; Bradford, S. E.; Arnold, D. W.; Metz, R. B.; Neumark, D. M. *J. Chem. Phys.* **1995**, *103*, 7801.
(25) Rauk, A.; Dak, Y.; Borowzski, P.; Roos, B. *Chem. Phys.* **1995**, *197*, 73.
(26) Peacock, T. E.; Rahman, R.-U.; Sleeman, D. H.; Tuckley, E. S. G. *J. Chem. Soc.* **1963**, 144.
(27) Festou, M. C.; Rickman, H.; West, R. M. *Astron. Astrophys. Rev.* **1993**, *4*, 363; *5*, 37.
(28) Ma, G.; Suto, M.; Lee, L. C. *J. Quant. Spectrosc. Radiat. Transfer* **1990**, *44*, 379.
(29) Loettgers, A.; Untch, A.; Stumpf, M.; Schinke, R.; Werner, H.-J.; Bauer, C.; Rosmus, P. *Chem. Phys. Lett.* **1994**, *230*, 290.
(30) Okabe, H. *Photochemistry of small molecules*; John Wiley: New York, 1978.
(31) Lias, S. G.; Bartmess, J. E.; Liebmann, J. F.; Holmes, J. L.; Levin, R. D.; Mallard, W. G. *J. Phys Chem. Ref. Data* **1988**, *17* (Suppl. 1).
(32) Huber, K. P.; Herzberg, G. Constants of Diatomic Molecules (data prepared by Gallagher, J. W. and Johnson, R. D., III). In *NIST Chemistry WebBook*, Mallard, W. G., Linstrom, P. J., Eds.; NIST Standard Reference Database Number 69; National Institute of Standards and Technology: Gaithersburg, MD, 2000; http://webbook.nist.gov.
(33) Leach, S. In *Polycyclic Aromatic Hydrocarbons and Astrophysics*; Léger, A, d'Hendecourt, L., Boccara, N., Eds.; Reidel: Dordrecht, Netherlands, 1987; p 99 ff.
(34) Berkowitz, J. *Phys. Essays* **2000**, *13*, 248.
(35) Brack, A. *The Molecular Origins of Life*; Cambridge University Press: Cambridge, U.K., 1998.
(36) Irvine, W. M.; Friberg, P.; Kaifu, N.; Matthews, H. E.; Minh, Y. C.; Ohishi, M.; Ishikawa, S. *Astron. Astrophys.* **1990**, *229*, L9.
(37) Cottin, H.; Gazeau, M.-C.; Raulin, F. *Planet. Space Sci.* **1998**, *47*, 1141.
(38) Schutte, W. A.; Boogert, A. C. A.; Tielens, A. G. G. M.; Whittet, D. C. B.; Gerakines, P. A.; Chiar, J. E.; Ehrenfreund, P.; Greenberg, J. M.; de Graauw, Th. *Astron. Astrophys.* **1999**, *343*, 966.
(39) Miller, S. L. In *The Molecular Origins of Life*; Brack, A., Ed.; Cambridge University Press: Cambridge, U.K., 1998; p59.
(40) Thaddeus, P.; Guélin, M.; Linke, R. A. *Astrophys. J.* **1981**, *246*, L41.
(41) Minh, Y. C.; Brewer, M. K.; Irvine, W. M.; Friberg, P.; Johansson, L. E. B. *Astron. Astrophys.* **1991**, *244*, 470.
(42) Bockelée-Morvan, D.; Lis, D. C.; Wink, J. E.; Despois, D.; Crovisier, J.; Bachiller, R.; Benford, D. J.; Biver, N.; Colom, P.; Davies, J. K.; Gérard, E.; Germain, B.; Houde, M.; Mehringer, D.; Moreno, R.; Paubert, G.; Philipps, T. G.; Rauer, H. *Astron. Astrophys.* **2000**, *353*, 1101.
(43) Rodgers, S. D.; Charnley, S. B. *Mon. Not. R. Astron. Soc.* **2001**, *320*, L61.
(44) Chevreau, H.; Boullant, E.; Dézarnaud-Dandine, C.; Sevin, A. *Chem. Phys.* **2000**, *254*, 99.
(45) Rusic, B.; Litorja, M. *Chem. Phys. Lett.* **2000**, *316*, 45.
(46) Warneck, P. *Z. Naturforsch., A* **1974**, *29*, 350.
(47) Chase, M. W., Jr. NIST-JANAF Themochemical Tables, Fourth Edition. *J. Phys. Chem. Ref. Data* **1998**, *Monograph 9*, 1.

Available online at www.sciencedirect.com
SCIENCE DIRECT®
Chemical Physics 314 (2005) 263–282
Chemical Physics
www.elsevier.com/locate/chemphys

Photoion mass spectrometry of adenine, thymine and uracil in the 6–22 eV photon energy range

Hans-Werner Jochims [a], Martin Schwell [b], Helmut Baumgärtel [a], Sydney Leach [c,*]

[a] Institut für Physikalische und Theoretische Chemie der Freien Universität Berlin, Takustr. 3, 14195 Berlin, Germany
[b] Laboratoire Interuniversitaire des Systèmes Atmosphériques (LISA), CNRS-UMR 7583, Universités Paris 7 et 12, 61 Avenue du Général de Gaulle, 94010 Créteil, France
[c] Laboratoire d'Etude du Rayonnement et de la Matière en Astrophysique (LERMA), CNRS-UMR 8112, Observatoire de Paris-Meudon, 5 place Jules-Janssen, 92195 Meudon, France

Received 8 February 2005; accepted 16 March 2005
Available online 12 April 2005

Abstract

Using synchrotron radiation as excitation source in the 6–22 eV photon energy region, a photoionization mass spectrometry study of three nucleic acid bases, adenine, thymine and uracil, revealed VUV-induced degradation pathways of these important biological molecules. The fragmentation patterns, ionization energies and ion appearance energies (AE) are reported, many for the first time, and are compared with results of electron impact and other studies. AE values enabled heats of formation of parent and some fragment ions to be revised or determined for the first time. Thermochemical data, coupled with the observed AEs, were also useful in clarifying dissociative photoionization pathways. The main neutral loss species are HCN for adenine, HNCO and CO for thymine and uracil, but many subsequent and other fragmentation pathways, including some not suggested previously, are observed and discussed. The hyperconjugation properties of the methyl group make CO loss easier in thymine than in uracil. The astrophysically important fragment ion $HCNH^+$ is shown to be formed by several fragmentation pathways in all three nucleobases. The relative importance of competitive fragmentation processes was determined in some cases. Some astrophysical implications concerning the prospects for observation and survival of these nucleic acid bases in the interstellar medium and in meteorites are briefly discussed.

1. Introduction

The vacuum ultraviolet (VUV) photophysics and photochemistry of the pyrimidine and purine nucleic acid base constituents of DNA is of considerable interest in view of the possible delivery of these molecules from space to the early Earth, and the role that they could have played in the origin and development of life on our planet [1]. Some nucleobases have been found in meteorites [2–5], speculation has been made concerning their possible formation in the interstellar medium (ISM) [6,7], and pyrimidines and purines have been reported in the data obtained with the PUMA impact mass spectrometer during the flyby of comet Halley by the Soviet spacecraft VEGA 1 [8]. Gas phase studies of nucleic acid bases are also of significance in biology for understanding and determining properties of these basic units when free from interactions.

Concerning their possible existence in an astrophysical context, the observation of the important nucleobases by radioastronomy requires initial laboratory studies on their gas phase microwave spectra, which have indeed been carried out for the major tautomers

* Corresponding author. Tel.: +33 1 4507 7561; fax: +33 1 4507 7100.
E-mail address: sydney.leach@obspm.fr (S. Leach).

0301-0104/$ - see front matter © 2005 Elsevier B.V. All rights reserved.
doi:10.1016/j.chemphys.2005.03.008

of the three nucleic acid bases studied here, adenine [9], thymine [10] and uracil [11]. Other possibilities of astrophysical observation include their infra-red spectra, which have been measured in the laboratory in the gas phase [12] and in low temperature matrices [13–16], both phases being relevant to possible astrophysical measurements. Gas phase electronic spectra are also known, but the observed UV absorption [17–19] or fluorescence [20,21] bands would be difficult to measure and identify in astrophysical contexts. However, all of these spectroscopic studies have enriched our knowledge of the structure of these nucleobases in their tautomeric variants. Mass spectrometric measurements of cometary grains, already attempted on comet Halley in 1986 [8], will be improved in future space missions to comets, with some specific attempts to detect purine nucleobases [22].

Although the nucleobases studied possess several tautomeric forms, the spectroscopic studies cited above show that at the gas phase temperatures used in our study, 150–200 °C, only one tautomer is present, at more than 99%, with no evidence of tautomerization of uracil or thymine to the enol form, or of adenine to the imino form [12].

Apart from several photoelectron spectral studies [23–31] there has been relatively little previous study of ionization phenomena of adenine, thymine and uracil. Their adiabatic ionization energies are uncertain and there are only a small number of mass spectral studies on unmodified nucleobases, carried out by 20 and 70 eV electron impact, principally by the group of Dudek [32,33], followed by others [34–41]. No dissociative photoionization studies have been reported on these nucleobases. We mention that there has been recent work on the dissociative electron attachment of nucleobases and on their stable anions in the gas phase [42,43]. We also note that energetic fragments resulting from dissociation of nucleobases can cause subsequent damage in biological systems. DeVries et al. [44] have studied the fragmentation of uracil and thymine induced by collision with slow multiply charged Xe(q+, q = 5–25) ions. Complete breakdown into atomic and diatomic fragments occurs via Coulomb dissociation under these conditions.

In this paper, we report results of a photoionization mass spectrometry (PIMS) study of three nucleic acid bases, adenine, thymine and uracil. All three have been found in meteoritic materials [2–5]. The photoion yield curves of the nucleic acid base parent and fragment ions were measured as a function of incident photon energy in the 6–22 eV range. We report ionization energy (IE) and previously unknown fragment appearance energies (AE). Knowledge of the ionization energies of the nucleobases is of importance in understanding the processes of oxidative damage [45,46], as well as in interpreting hole (radical cation) charge transfer and trapping [47–49], in DNA. The photoion fragmentation patterns at an incident energy of 20 eV are compared with the ion fragmentation patterns obtained by 20 and 70 eV electron impact ionization processes. Our proposed fragmentation pathways build on the pioneer studies of Rice et al. [32,33] on the electron impact mass spectra of these nucleobases. These pathways were established in part by making use of metastable peaks and isotope labeling [34–37]. Our measurements of the appearance energies of fragment ions enable us to further investigate the validity of the proposed fragmentation pathways and to consider new aspects and extensions of the dissociative ionization processes. The fragmentation information is not only pertinent to understanding radiation damage in DNA [50] but, as mentioned above, it is also potentially of use for interpretation of data to be obtained by mass spectrometric measurements of species in cometary grains which will be collected during the ROSETTA space mission to the comet 46p/Wirtanen [22].

The photoabsorption cross-section of nucleic acid bases is much higher in the VUV as compared with the UV, as has been observed in absorption and EELS studies on films of nucleobases, usually prepared by vacuum sublimation [51–55]. Low energy EELS measurements have been carried out on gas phase thymine [56], and high energy EELS on solid films of the three nucleobases studied here, which provided data up to 35 eV [57]. We later compare this data, as well as photoelectron spectra, with our nucleobase parent photoion yield curves. MPI spectra of gas phase adenine have also been measured [18]. Optical properties of adenine in the 1.8–80 eV region have been determined by optical reflectance on solid films [58]. Photoacoustic spectra of films of thymine and adenine have also been obtained and compared with absorption measurements in the 4.13–9.54 eV range [59]. In these different studies the bands observed have been assigned to π–π*, n–π*, etc. transitions and to chromophoric groups. We also note the existence of a broad intense ''absorption'' peak of the nucleobases in the 20 eV region. This results mainly from collective excitation of electrons and is commonly observed in organic compounds, as discussed elsewhere [60].

We mention that all of these molecules absorb strongly at 10.2 eV, where the Lyman-α stellar emission is intense. Furthermore, in connection with the possible earthbound delivery of biotic molecules from space, we remark that the VUV luminosity of the early sun, during the Hadean period of considerable bombardment of the Earth from space, was about two orders of magnitude higher than it is today, although the total luminosity was less [61].

Initial accounts of this work, which have been reported elsewhere in an exobiology context [62,63], include preliminary values of the ionization energies and

some fragmentation appearance energies of the three nucleobases [62].

2. Experimental

The experiments were carried out at two separate synchrotron facilities, BESSY I and BESSY II, in Berlin. Synchrotron radiation from the electron storage ring BESSY I was monochromatized by a 1.5 m Au grating monochromator (modified McPherson) and then focused into a differentially pumped gas cell which can be heated up to 400 °C but was here restricted to lower temperatures. The experimental set-up is described in more detail elsewhere [64]. The nucleic acid base vapors were introduced into the ionization chamber by direct evaporation of solid samples in open containers placed 1–2 cm below the position of the incident VUV radiation within the ion extraction zone. The whole chamber was heated to temperatures, typically 120–140 °C, which provided an adequate supply of target molecules but were sufficiently low to ensure that the thermally fragile low volatile nucleic acid bases remained essentially undissociated in the gas phase. When some thermally induced dissociation did occur this was easily identified by the observed mass spectra, thus enabling us to modify experimental parameters so as to achieve satisfactory experimental conditions of minimal thermal dissociation. In cases where water impurity was observed in the mass spectra this generally resulted from residues of cleaning procedures of the apparatus which were carried out between experimental runs.

Parent and fragment ions formed by photoionization of the nucleic acid bases adenine, thymine and uracil were measured using a quadrupole mass spectrometer (Leybold Q200), and ion yield curves were obtained through photon energy scans with measuring intervals of 25 meV. The yield curves of the principal ions observed are presented in the appropriate figures. Transmitted photons were detected by the fluorescence of a sodium salicylate coated window. Spectral bandwidth of the incident monochromatic radiation was typically 2 Å. Some experiments were carried out with an MgF_2 filter (cut-off effective at 11.0 eV) in order to suppress stray light and second-order radiation. Ion appearance energies were determined mainly with the aid of semi-log plots of the ion yield curves. A second set of measurements on uracil was carried out more recently using synchrotron radiation from the BESSY II electron storage ring. Measuring equipment and experimental conditions were similar to those at BESSY I, except that at BESSY II we employed a 3 m normal incidence monochromator. The nucleic acid base samples were commercial products (Sigma–Aldrich) of best available purity. The formulae of the three nucleobases studied are given in Fig. 1.

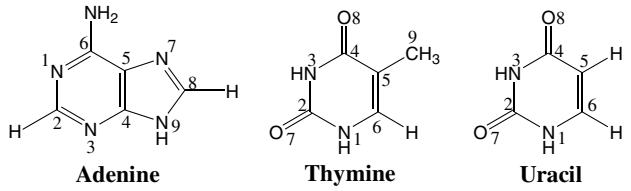

Fig. 1. Molecular structure of adenine, thymine and uracil, including common atom numbering.

3. Results and discussion

3.1. Adenine: mass spectra and ion yield curves

Table 1 gives a comparison between the relative intensities of the m/z peaks in our mass spectrum obtained at 20 eV photon excitation energy and that of Rice and Dudek [33] measured with 70 eV electron impact. It also includes selected proposed loss of neutral species corresponding to the observed molecular ions formed by dissociative ionization. The appearance energies of the major m/z ions are listed, as measured from the onsets in the ion yield curves (Fig. 2).

The 20 eV photon impact and 70 eV electron impact mass spectra have essentially the same m/z features but with differences in their relative intensities. Different relative intensities are also observed between reported electron impact mass spectra of adenine [22,33,38,65]. These differences between the electron impact spectra, and also between electron and photon impact mass spectra, are most probably mainly due to different ion optics, residence times, and detection efficiency. These factors will affect the mass spectral manifestations, especially of metastable ions. We remark also that with 70 eV electron impact, but not with 20 eV photons, doubly charged molecular ions can be formed, with low yields, giving rise to charge separation reactions producing fragment monocations [66]. Differences between reported electron impact mass spectral intensities were also observed for thymine and uracil, as discussed later.

3.1.1. The adenine parent ion

For the parent ion, $m/z = 135$, we measured an ionization energy of 8.20 ± 0.03 eV. The corresponding $m/z = 135$ ion yield curve shown in Fig. 2(a) was measured using the MgF_2 filter. In Table 2 this value is compared with those determined by various techniques. The only other measurement by photoionization is that reported Orlov et al. [67], who did not publish their ion yield curve. Agreement between these two PIMS measurement is good. An early measurement by electron impact [68] gives a much too high value, but later measurements [69,70] are not inconsistent with our IE value. A recent measurement by the R2PI technique gives an upper limiting value 400 meV above the PIMS values [71]. The ionization energies reported from photoelectron

Table 1
Electron impact [33] and photon impact mass spectra and photoion appearance energies: Adenine $m = 135$ ($C_5H_5N_5$)

m/z	Electron impact 70 eV relative intensity	Photon impact 20 eV relative intensity	Photon impact appearance energy (AE, eV)	Ion elemental formula	Neutral loss
135	100	100	8.20 ± 0.03	$C_5H_5N_5^+$	
134	3	10		$C_5H_4N_5^+$	H
120	3	1		$C_5H_4N_4^+$	NH
119	(a)	3		$C_5H_3N_4^+$	NH_2
108	34	57	11.56 ± 0.05	$C_4H_4N_4^+$	HCN
107	3	10		$C_4H_3N_4^+$	H_2CN
92	(a)	9		$C_4H_2N_3^+$	$HCN + NH_2$
81	19	50	12.8 ± 0.1	$C_3H_3N_3^+$	2HCN
80	7	10		$C_3H_2N_3^+$	$H_2CN + HCN$
70	5	17	13.1 ± 0.1	$C_2H_4N_3^+$	C_3NH_2
67	7	10		$C_3H_3N_2^+$	HCN + NHCN
66	15	41	13.2 ± 0.1	$C_3H_2N_2^+$	$HCN + NH_2CN$
65	6	0		$C_3HN_2^+$	$2HCN + NH_2$
54	31	55	13.7 ± 0.1	$C_2H_2N_2^+$	3HCN
53	24	28		$C_2HN_2^+$	$H_2CN + 2HCN$
43	12	34	13.0 ± 0.1	NH_2CNH^+	HCN + HCNCCN
42	3	16		NH_2CN^+	
41	2	7		$NHCN^+$	
40	5	1		NCN^+	2HCN + NHCN
39	8	1		$HCCN^+$	$2HCN + NH_2CN$
38	10	0		C_2N^+	$3HCN + NH_2$
29	12	60	14.0 ± 0.1	NH_2CH^+	
28	78	110	13.1 ± 0.1	$HCNH^+$	$C_4H_3N_4$
27	12	10		HCN^+	4HCN

(a) Reported in [65] and in [38] but not in [33].

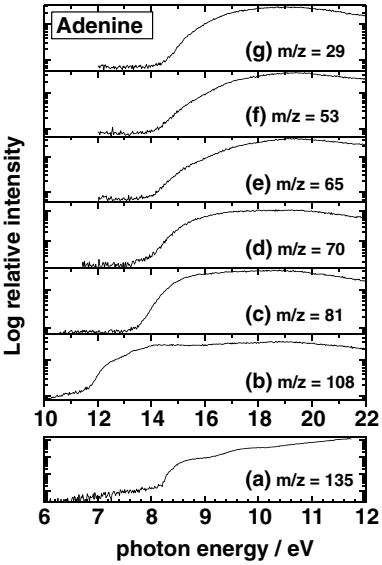

Fig. 2. Selected ion yield curves of adenine. The $m/z = 135$ ion yield curve has been measured using an MgF_2 cut-off filter.

spectroscopy peak measurements [23,31] provide vertical IEs which are 220–280 meV above the adiabatic values determined by our PIMS measurements. However, bracketing experiments measuring the adiabatic recombination energy [72] gave an adiabatic IE = 8.55 ± 0.10 eV, about 350 meV above the PIMS value, and which is close to the vertical IE measured by photoelectron spectroscopy. This points to unrecognized difficulties in the recombination energy measurement technique.

The difference of the order of 250 meV between the adiabatic and vertical IEs of adenine is similar to that calculated theoretically with various degrees of sophistication [73–76]. There is no loss of planarity on ionization of adenine [74]. The difference between the adiabatic and vertical IEs therefore reflects bond length and angle changes (which have been calculated by Improta et al. [75]), between the ground states of neutral and cationic adenine, and which result in Franck–Condon transition shifts. It may appear surprising that electron impact measurements are capable of providing adiabatic values of the ionization energy in cases where there are significant changes in the geometry of neutral species on electron loss, but this has been well demonstrated for many molecular species [77].

Using our measured adiabatic IE of adenine, and the known value of the heat of formation ΔH_f^{298} (adenine) $= 207 \pm 8$ kJ/mol [78], we obtain a value of the heat of formation of the cation ΔH_f^{298} (adenine cation) $= 998 \pm 11$ kJ/mol, which is considerably greater than the value ΔH_f^{298} (adenine cation) $= 960$ kJ/mol given by Lias et al. [78], based on a quoted PES onset value of the IE = 7.8 eV.

We made a direct comparison between the $m/z = 135$ ion yield curve and the HeI photoelectron spectrum of

Table 2
Adenine ionization energy values[a]

Experimental method	Ionization energy (eV)	Reference and year
Photoion yield curve (PIMS)	8.20 ± 0.03	Present study
Electron impact ion yield curve	8.91 ± 0.10	[68] 1967
Photoelectron spectroscopy (PES)	8.44 ± 0.03 (vert)	[23] 1975
PIMS	8.26 ± 0.05	[67] 1976
Electron impact ion yield curve	8.3 ± 0.1	[69] 1976
PES	8.48[b] (vert)	[31] 1980
Electron impact ion yield curve	8.45 ± 0.15	[70] 1996
Recombination energy	8.55 ± 0.10	[72] 1999
Resonance 2-photon ionization	$\leqslant 8.606 \pm 0.006$	[71] 2002

[a] Adiabatic values unless otherwise stated.
[b] Uncertainty not reported.

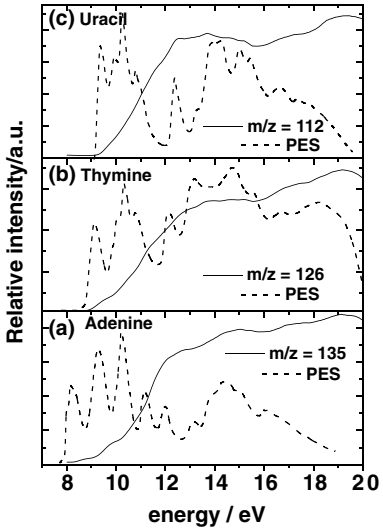

Fig. 3. Comparison of parent ion yield curve and photoelectron spectrum (PES are reproduced from [24,31]): (a) adenine; (b) thymine; (c) uracil.

adenine measured by Lin et al. [31] (Fig. 3(a)). This showed clearly that there are shoulders or apparent steps in the ion yield curve at energies close to those of several features in the photoelectron spectrum (PES energies [24,31] in brackets): 8.4 (8.48) eV assigned to π_1; ~9.0 (−) eV; ~9.8 (9.6) eV assigned to n_1 and π_2; ~10.3 (10.5) eV assigned to π_3; ~12.0 (12.1) eV assigned to π_4. The molecular orbital assignments are those given in the PES studies [24,31]. The inflection that we observe clearly in the ion yield curve at ~9.0 eV has no obvious feature in the photoelectron spectra of adenine. However, the 9.6 eV PES feature is broad and its profile extends to about 8.8 eV on the lower energy side. This PES feature has been assigned to both n_1 and π_2 and their energy separation has been calculated to be 450 meV by the HAM/3 method and 780 meV by 4-31G calculations [24], although the order of these two orbitals differs in the two calculations. On the basis of relative intensities in the PES spectrum, we assign the 9.0 eV inflection in the adenine ion yield curve to the n_1 orbital and the 9.8 eV inflection to π_2.

At higher energies, the broad features in the PES between 13 and 17 eV mimic quite well the parent ion yield curve (Fig. 3(a)). This region of the PES has not been assigned but we note that there are similar features in the PES of purine in this energy region, for which molecular orbital assignments have been made [79]. We recall that the purine molecule is similar to that of adenine but in which the amino group of the latter is replaced by a hydrogen atom.

We also compared the parent ion yield curve with the optical absorption curve derived from 25 keV electron energy loss spectra of thin films of adenine [57] (Fig. 4(a)). Our parent ion yield curves has several features, including three pronounced peaks at ~14.5, ~16 and ~18 eV, respectively. There are only two peaks, at 13 ± 0.3 and 17.4 ± 0.3 eV, in the adenine film spectrum in the 10–35 eV region. The physical relation between these solid phase peaks, induced by electron excitation in a region where the ionization yield can be less than unity [80,81], and the gas phase parent photoion peaks in this spectral region is not easy to disentangle.

3.1.2. Adenine ion fragmentation

Several loss mechanism pathways can be recognized in the mass spectrum, following on the pioneer work of the Dudek group [33]. A schematic representation of major fragmentation pathways is given in Fig. 5.

(α) *Successive loss of HCN groups:* The principal pathway involves the successive loss of HCN ($m = 27$) groups:

$$C_5H_5N_5^+ \ (m/z = 135) - HCN \rightarrow C_4H_4N_4^+ \ (m/z = 108) \quad (1)$$

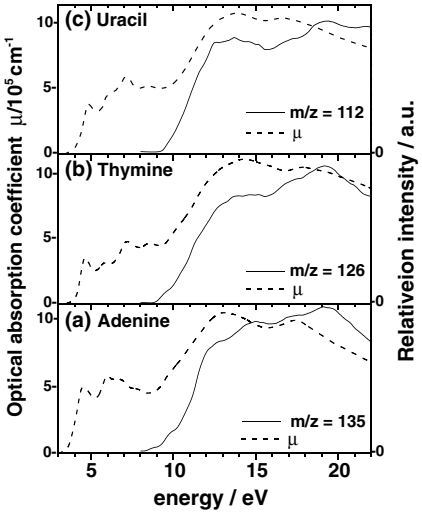

Fig. 4. Comparison of parent ion yield curve and the optical photoabsorption spectrum (the optical absorption spectra, reproduced from [57], are derived from respective electron energy loss spectra): (a) adenine; (b) thymine; (c) uracil.

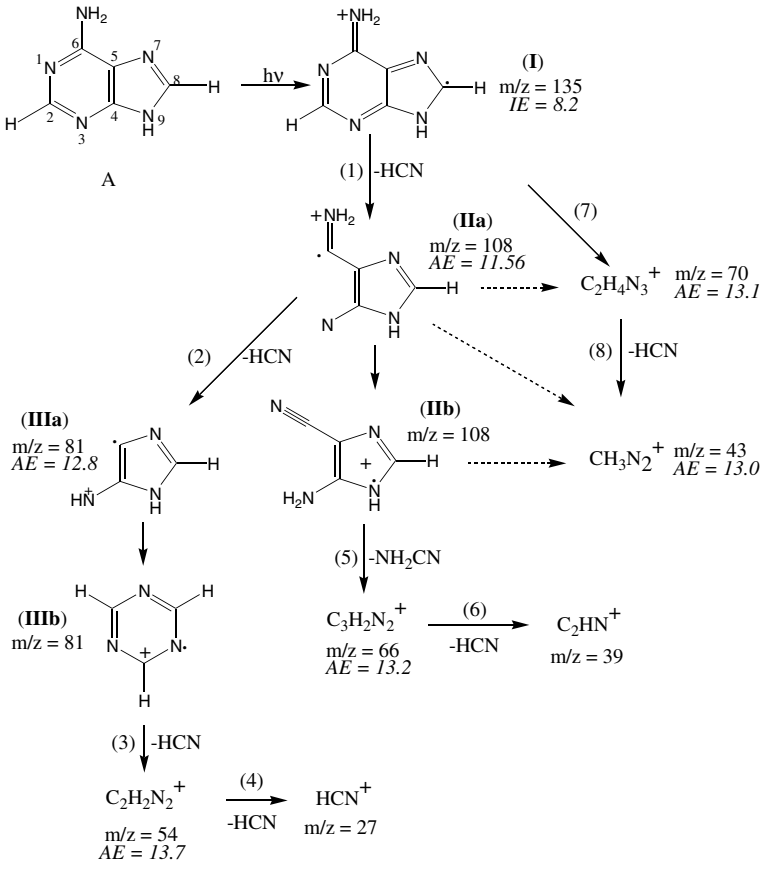

Fig. 5. Principal fragmentation decay routes of the adenine radical cation. Measured appearance energy values are given for each fragment (in eV, for uncertainties refer to Table 1). Roman and Arabic numerals correspond to species and reactions, respectively.

$$C_4H_4N_4^+ \ (m/z = 108) - HCN \rightarrow C_3H_3N_3^+ \ (m/z = 81) \tag{2}$$

$$C_3H_3N_3^+ \ (m/z = 81) - HCN \rightarrow C_2H_2N_2^+ \ (m/z = 54) \tag{3}$$

$$C_2H_2N_2^+ \ (m/z = 54) - HCN \rightarrow HCN^+ \ (m/z = 27) \tag{4}$$

From the appearance energy of the $C_4H_4N_4^+$ ion, AE = 11.56 eV, and the known heats of formation of adenine (207 ± 8 kJ/mol) and HCN (135.1 kJ/mol) [65,78], we calculate the heat of formation of the $C_4H_4N_4^+$ ion to be 1187 ± 12 kJ/mol. A similar calculation for the heat of formation of the $C_3H_3N_3^+$ ion gave a value of 1172 ± 16 kJ/mol for this ion. The heats of formation of the three isomeric cyclic $C_3H_3N_3^+$ ions, 1,2,3-triazine, 1,2,4-triazine and 1,3,5-triazine, are reported [65,78] to be 1313, 1222 and 1194 kJ/mol, respectively. This suggests that the $C_3H_3N_3^+$ ion formed in the dissociative ionization of adenine is the 1,3,5-triazine cation (species IIIb in Fig. 5).

The respective appearance energies of the $C_nH_nN_n^+$ ($n = 5, 4, 3, 2$) ions are 8.20, 11.56, 12.8 and 13.7 eV. Loss of the successive HCN groups requires excess energies, respectively, of 3.36, 4.5 and 5.4 eV in the ion. This suite of AEs and the corresponding excess energies confirms the pathway presented above. The initial HCN fragmentation, which requires at least two bond ruptures, is relatively more difficult than the succeeding HCN losses which each probably requires only one bond rupture in the precursor fragment ion and/or it corresponds to a successively smaller total reorganization energy. The loss mechanisms could be quite complex and may involve loss of HNC as well as HCN. Our discussion does not distinguish between these two isomers. We refer to them collectively as HCN.

From electron impact mass spectra of deuterium labeled adenine [35] Occolowitz concluded that the first HCN lost originates 55% from C6 and its attached amine group, and 45% from C2 and either adjacent nitrogen. However, the mass spectra of ^{15}N-labeled adenines [36] showed that there is about 87% loss of N1 in the first HCN product, which suggests that a greater percentage of C2 is lost than reported by Occolowitz. The finding by Barrio et al. [36] is corroborated by the electron impact mass spectrum of ^{13}C2-adenine by Sethi et al. [37] which shows that the carbon atoms in the first

HCN molecule to be lost are 98% from C2. The main reaction would therefore be expected to occur by rupture of the C2–N3 and N1–C6 bonds. These are both calculated to be weaker in the cation as compared with neutral adenine, whereas the C2–N1 and N3–4 bonds are calculated to be stronger in the cation [75].

The ^{15}N mass spectra [36] also show that N7 and N9 are completely retained in the $C_4H_4N_4^+$ ion product. Sethi et al. [37] also found, from the mass spectrum of $^{14}C8$-adenine, that there is complete retention of C8 in the $C_4H_4N_4^+$ ion formed by the first HCN loss process, and that there is partial loss of the carbon isotopic label in further HCN loss steps. We note, however, that there can be rearrangements of hydrogen (deuterium) prior to HCN leaving the molecule, as discussed by Sethi et al. [37]. Furthermore, many fragmentation sub-pathways can indeed be envisaged to contribute to these successive HCN loss processes [33,37].

From these earlier isotopic studies, we can thus assume that fragment $m/z = 108$ has the structure IIa shown in Fig. 5. Species IIa can isomerize to give species IIb which is probably thermodynamically more stable. It is not clear from which structure the $m/z = 81$ ion is formed, but, as already concluded from thermodynamical considerations, the 1,3,5 triazine cation IIIb is most likely formed.

(β) *Reactions involving loss of NH_2CN and NHCN:* Several other fragmentation pathways can be established from the mass spectrum of adenine. One of these starts from the $C_4H_4N_4^+$ fragment ion ($m/z = 108$) which can lose NH_2CN to form the important $C_2H_2N_2^+$ ion ($m/z = 66$), from which there can be a further loss of HCN:

$$C_4H_4N_4^+ \ (m/z = 108) \rightarrow C_3H_2N_2^+ \ (m/z = 66) + NH_2CN \ (m = 42) \quad (5)$$

$$C_3H_2N_2^+ \ (m/z = 66) \rightarrow C_2N^+ \ (m/z = 39) + HCN \ (m = 27) \quad (6)$$

The heat of formation of the $C_3H_2N_2^+$ ion can be determined from its appearance energy, $AE = 13.2 \pm 0.1$ eV, and the heats of formation of NH_2CN, HCN and adenine. The heats of formation of three isomers of NH_2CN have been reported [65,78]: (i) cyanamide (134 kJ/mol), (ii) diazomethane (230 ± 17 kJ/mol) and (iii) 3H-diazirine (265 ± 11 kJ/mol). These provide the following respective values for the heat of formation of $C_2H_2N_2^+$: (i) 1212 ± 16 kJ/mol, (ii) 1116 ± 33 kJ/mol, and (iii) 1081 ± 27 kJ/mol. The only heat of formation reported for a $C_2H_2N_2^+$ ion is that of the malononitrile ion, 1491 ± 11 kJ/mol [65]. This is much greater than the above values and it shows that $C_2H_2N_2^+$ is not the malononitrile ion which, if formed by dissociative ionization of adenine, would have an appearance energy several eV above 13.2 eV. The structure of the $C_2H_2N_2^+$ ion formed at 13.2 eV is therefore unknown.

Loss of NH_2CN from $m/z = 81$ constitutes another possible pathway to form the C_2HN^+ ($m/z = 39$) ion other than via reactions (5) and (6) which involve the $m/z = 66$ ion. The $m/z = 66$ and 81 ions are both intense in our 20 eV photon impact mass spectrum, but the $m/z = 39$ ion, although present, is extremely weak. The three ions, $m/z = 81$, 66 and 39, appear with modest intensity in 70 eV electron impact mass spectra [33,38,65], where their intensities decrease in the m/z order $81 > 66 > 39$, but with the $I(66)/I(39)$ intensity ratio being of the order of 2. This is undoubtedly due to the greater deposition of energy at the higher excitation energies in the electron impact case. The appearance energy of the $m/z = 66$ ion (13.2 eV, Table 1), formed by losses of HCN and NH_2CN (reactions (1) and (5)), is greater than that of $m/z = 81$ (12.8 eV), which involves loss of two HCN units from the parent ion (reactions (1) and (2)). The difference ΔE between the heat of formation of HCN and those of the NH_2CN isomers cyanamide, diazomethane and 3H-Diazirine is, respectively, $\Delta E = 0.01$, -0.98 and -1.35 eV. The difference between the appearance energies of the $m/z = 81$ and $m/z = 66$ ions is -0.4 eV, which indicates that the NH_2CN neutral product is cyanamide and that there is a potential barrier, at least of the order of 0.4 eV, to its formation.

One can imagine another formation pathway for the $m/z = 66$ ion: by rupture of the C5–C6 bond and the C4–N3 bond in the adenine parent ion. This remains to be tested, but the $AE = 13.2$ eV of the $m/z = 66$ ion is compatible with such a mechanism.

We remark that direct loss of NH_2CN from the parent ion would give a fragment ion $m/z = 93$, which is absent in our 20 eV photon impact mass spectrum. Its formation would involve rupture of three bonds and thus require a high internal energy in the parent ion, consistent with the non observation of this fragment ion in our mass spectrum. It is reported as a very weak peak in some [38,65] 70 eV electron impact mass spectra. We note the existence of an important peak at $m/z = 42$, which we assign to the NH_2CN^+ ion, and which might be formed by the dissociation $C_4H_4N_4^+ \rightarrow NH_2CN^+ + C_3H_2N_2$, which itself constitutes a charge-switch reaction relative to reaction (5). From the suggested structure IIb (Fig. 5) of the $m/z = 108$ ion, the NH_2CN^+ fragment is either the cyanamide or 3H-Diazirine cation, requiring H-shift for their formation, and not the diazomethane cation the formation of which would necessitate more complex atomic rearrangements.

(γ) *Other important ions:* The existence of a strong peak at $m/z = 43$ ($AE = 13.0$ eV) is of interest. We propose its assignment to an ion having the elemental formula $CH_3N_2^+$, in agreement with Sethi et al. [37]. It has been suggested that possible pathways to its formation involve prior formation of the $m/z = 70$ ion:

$$C_5H_5N_5^+ \ (m/z = 135) \rightarrow C_2H_4N_3^+ \ (m/z = 70) + C_3HN_2 \ (m = 65) \quad (7)$$

$$C_2H_4N_3^+ \ (m/z = 70) \rightarrow C_3HN_2^+ \ (m/z = 43) + HCN \ (m = 27) \quad (8)$$

The high resolution mass spectrometry of adenine has shown the $m/z = 70$ ion to have the elemental formula $C_2H_4N_3^+$, suggested to be formed by loss of C_3HN_2 from the parent ion [37]. We consider that there could also be a pathway to this $m/z = 70$ ion via $m/z = 108$, where the neutral loss from the latter ion would be C_2N (reaction (9)). This is a previously unreported fragmentation pathway:

$$C_4H_4N_4^+ \ (m/z = 108) \rightarrow C_2H_4N_3^+ \ (m/z = 70) + C_2N(m = 38) \quad (9)$$

The $m/z = 70$ ion has an appearance energy $AE = 13.1 \pm 0.1$ eV. From this, and appropriate heats of formation, we determine the heat of formation of this $C_2H_4N_3^+$ ion via reactions (9) and (8) to be 980 ± 18 kJ/mol. In the literature [78] there is reported a heat of formation of 835 kJ/mol for a cyclic radical ion having the elemental formula $C_2H_4N_3^+$. If this is indeed the $m/z = 70$ ion, a potential barrier can be inferred for the formation of this ion fragment via reactions (9) and (8). An open chain form is also possible, as suggested by Sethi et al. [37].

We note that the intensity of the $m/z = 70$ ion relative to that of $m/z = 43$ is about 0.5 in both the photon and electron impact mass spectra, and that both ions have closely similar AE values, which suggests that there exist more than one pathway to form the $m/z = 43$ ion. Indeed, we propose another possible pathway for its formation. This is via the $m/z = 108$ ion in the following way: If the $C_4H_4N_4^+$ ion is in its amino-imidazole carbonitrile form (species IIb in Fig. 5), subsequent rupture of C=C and a C–N bond would lead to the formation of the NH_2CNH^+ (i.e., $CH_3N_2^+$) ion.

$m/z = 28$ and $m/z = 29$ ions: These are prominent ions and their relative importance is much greater in the 20 eV photon impact than in the 70 eV electron impact mass spectrum. The $m/z = 29$ ion has an $AE = 14.0$ eV. Its elemental formula is CH_3N^+ and it is possibly the NH_2CH^+ ion [82,83]. The $m/z = 28$ ion is very intense and it has an $AE = 13.1$ eV. We assign it to the $HCNH^+$ species. Since its AE is lower than the AE of the $m/z = 29$ ion, it is not formed, at threshold, by loss of a hydrogen atom from the latter. A possibility is that the $HCNH^+$ ion is formed by the reaction:

$$C_5H_5N_5^+ \ (m/z = 135) \rightarrow HCNH^+ \ (m/z = 28) + C_4H_3N_4 \ (m = 107) \quad (10)$$

which would correspond to a charge switch of reaction Eq. (11), discussed below. However, other pathways to formation of the $HCNH^+$ ion are possible, as indicated by ^{15}N-labeled adenine studies [37].

(δ) *Less intense fragment ion peaks (no AE measurements):* The $m/z = 134$, 120, 119 and 118 ions, which are variously observed weakly in some electron impact mass spectra [22,33,38,65], correspond, respectively, to loss of H, NH, NH_2, and NH_3 groups. The corresponding reactions would leave the condensed heteroaromatic system undestroyed (if N10 is part of the leaving group). The $m/z = 120$ ion is reported in the electron impact mass spectra by Rice and Dudek [33] and Varmuza et al. [22] but not the $m/z = 119$ and 118 ions, while the spectra reported by McCloskey [38] and in the NIST collection [65] contain the $m/z = 118$ and 119 peaks, but not the $m/z = 120$ feature. Only $m/z = 134$, 120 and 119 were observed, in our 20 eV photon impact spectra. Observations of H and NH_n loss processes in the dissociative ionization of adenine are thus sensitively dependent on the source and ion optics parameters in mass spectrometers used in the measurements.

Another fragmentation pathway involves the initial loss of H_2CN (methylene-amidogen) to give the fragment ion $m/z = 107$. This is followed by successive loss of one HCN unit to form the ion $m/z = 80$, and another HCN loss to give the $m/z = 53$ ion.

$$C_5H_5N_5^+ \ (m/z = 135) \rightarrow C_4H_3N_4^+ \ (m/z = 107) + H_2CN \ (m = 28) \quad (11)$$

$$C_4H_3N_4^+ \ (m/z = 107) \rightarrow C_3H_2N_3^+ \ (m/z = 80) + HCN \ (m = 27) \quad (12)$$

$$C_3H_2N_3^+ \ (m/z = 80) \rightarrow C_2HN_2^+ \ (m/z = 53) + HCN \ (m = 27) \quad (13)$$

The relatively small intensities of the corresponding mass peaks in both electron and photon impact mass spectra show that this is a minor pathway. Occolowitz [35] observed that only about 35% of the ^{14}C label is retained in the fragment ions $m/z = 80$ formed by loss of HCN and H_2CN from the parent ion, which is a similar percentage to that observed in the $m/z = 81$ ions formed by loss of two HCN groups from $m/z = 135$. He also suggested that the existence of an intermediate ion that could lose either HCN or H_2CN.

We note also that the existence of a peak at $m/z = 92$, whose intensity, relative to that of $m/z = 119$, indicates that it arises from loss of NH_2 (or H + NH) from $m/z = 108$ rather than the suggested [37] loss of HCN from $m/z = 119$. The $m/z = 65$ and 38 ions which also involve loss of NH_2, following multiple loss of HCN groups from the parent ion, are observed only in electron impact mass spectra (Table 1). Finally, we also mention ions $m/z = 67$ and 40, which involve loss of NHCN, following initial loss, respectively, of one and two HCN units from the parent ion. We note also the

existence of a peak at $m/z = 41$, corresponding to the $NHCN^+$ ion.

3.2. Thymine: mass spectra and ion yield curves

In Table 3, the relative intensities of the m/z peaks in our thymine mass spectrum, obtained at 20 eV photon excitation energy, are compared with those of Rice et al. [32], measured with both 20 and 70 eV electron impact. The appearance energies of the major m/z ions are listed, as measured from the onsets in the photoion yield curves (Fig. 6), as well as the neutral loss species which we consider to be formed with the observed m/z ions by dissociative ionization.

Just as in the case of adenine, the 20 eV photon impact and 70 eV electron impact mass spectra of thymine are closely similar, having essentially the same m/z features but with a few differences in their relative intensities. The $m/z = 55$ fragment ion peak is the strongest in both cases, the parent peak at $m/z = 126$ being about half as intense. Other 70 eV electron impact mass spectra of thymine have been reported [34,38,65], which also have the $m/z = 126$, 83, 55, 54 and 28 peaks as the most intense, but which have different relative intensities from those measured by Rice et al. [32]. As mentioned earlier, these differences between the electron impact spectra are most probably mainly due to differences in the ion optics and ion residence times.

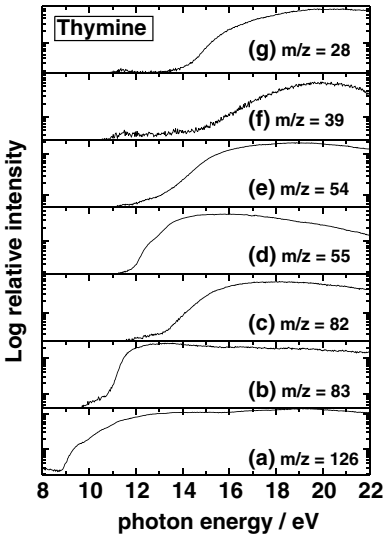

Fig. 6. Selected ion yield curves of thymine.

We note that a 20 eV electron impact mass spectrum of thymine has the parent peak as its most intense ion. The relative paucity of the mass spectral peaks in the

Table 3
Electron impact [32] and photon impact mass spectra and photoion appearance energies: Thymine $m = 126$ ($C_5H_6N_2O_2$)

m/z	Electron impact 70 eV relative intensity	Electron impact 20 eV relative intensity	Photon impact 20 eV relative intensity	Photon impact appearance energy (AE, eV)	Ion elemental formula	Neutral loss
126	46	100	52	8.82 ± 0.03	$C_5H_6N_2O_2^+$	
125	0	0	2		$C_5H_5N_2O_2^+$	H
97	2	0	1		$C_4H_3NO_2^+$	NH_2CH
84	2	2	3		$C_4H_6NO^+$	NCO
83	6	17	8	10.70 ± 0.05	$C_4H_5NO^+$	HNCO
82	7	4	10	13.20 ± 0.05	$C_4H_4NO^+$	HNCO + H
71	3	0	3		$OCNHCO^+$	CH_3CCHNH
70	4	0	2		$C_2H_2N_2O^+$	C_3H_4O
58	0	0	1			
56	7	2	9		$C_3H_4O^+$	HNCO + HCN
55	100	47	100	11.7 ± 0.1	CH_3CCHNH^+	HNCO + CO
54	44	11	42	≈12.9	CH_2CCHNH^+	HNCO + CO + H
53	6	0	4			
52	14	0	2			
45	0	0	1			
44	6	0	9		CO_2 impurity	
43	4	0	2	11.9 ± 0.1	$HNCO^+$	C_4H_5NO
42	1	0	0			
41	<1	0	1			
40	6	0	7		$C_3H_4^+$	2HNCO
39	12	0	9	14.4 ± 0.1	$C_3H_3^+$	2HNCO + H
38	2	0	0			
37	2	0	0			
29	4	0	6			
28	59	6	67	13.6 ± 0.1	$HCNH^+$	(a)
27	36	0	11		$C_2H_3^+$ or HCN^+	
26	13	0	3		$C_2H_2^+$	HNCO + CO + H + HCNH (b)

(a) Four different pathways, with different initial neutral loss species. See text. (b) or could be HNCO + CO + CH_3N, the latter formed from the cyclic $m/z = 55$ by rupture of two bonds, but this is less evident than the pathway proposed in text.

20 eV electron impact mass spectrum (8 features) [32] as compared with our 20 eV photon impact mass spectrum (24 peaks, Table 3) illustrates well the difference in energy deposition with these two excitation sources, reflecting the fact that at 20 eV, electron impact is far from the Born approximation conditions [84] in which electron impact mimics photon impact excitation. Interestingly, the loss of HNCO from the parent ion is relatively more favored in the 20 eV electron impact as compared with the 20 eV photon impact case (see Table 3). This is consistent with the observation that HNCO loss corresponds to the lowest energy dissociative ionization process (AE = 10.7 eV, Table 3).

3.2.1. The thymine parent ion

For the parent ion, $m/z = 126$, we measured an ionization energy of 8.82 ± 0.03 eV (Fig. 6). In Table 4 this value is compared with those determined by various techniques. It is in excellent agreement with the only other value measured by photoionization mass spectrometry [67]. As in the case of adenine, an early measurement of thymine by electron impact [68] gives a value that is too high, but later measurements [69,70] give values much closer to our observed PIMS IE. The vertical IEs obtained by photoelectron spectroscopy peak measurements [23,31] are 200–380 meV above the adiabatic values determined by PIMS and electron impact measurements. This is of the same order of magnitude as the 240 meV predicted by a B1LYP functional [85] calculation [75], and 270 meV by a B3LYP functional calculation [86], for the difference between adiabatic and vertical IEs of thymine.

Using our measured adiabatic IE of thymine, and the known value of the heat of formation ΔH_f^0 (thymine) = −328.70 kJ/mol [78], we obtain a value of the heat of formation of the cation ΔH_f^0 (thymine cation) = 522.36 kJ/mol, which is very close to the preliminary value ΔH_f^{298} (thymine cation) = 520 kJ/mol given by Lias et al. [78], based on a quoted PES onset value of the IE = 8.8 eV. A direct comparison between the $m/z = 126$ ion yield curve and the HeI photoelectron spectrum of thymine measured by Urano et al. [24] revealed a few shoulders or apparent steps in the ion yield curve at energies close to those of several features in the photoelectron spectrum (Fig. 3(b)), but less marked than in the corresponding case of adenine. These features are related to the PES bands assigned to the π_1, n_1, π_2 and π_3 orbitals of thymine [24], as well as to some unassigned higher energy PES features. An inflection that we observe at ~11.7 eV in the parent ion yield curve has no obvious feature in the photoelectron spectra of thymine. One possibility is that this corresponds to an autoionization process in a Franck–Condon gap [87].

Table 4
Thymine ionization energy values[a]

Experimental method	Ionization energy (eV)	Reference and year
Photoion yield curve (PIMS)	8.82 ± 0.03	Present study
Electron impact ion yield curve	9.43 ± 0.10	[68] 1967
Photoelectron spectroscopy (PES)	9.14 ± 0.03 (vert)	[23] 1975
PES	9.02[b] (vert?)	[25] 1975
PIMS	8.87 ± 0.05	[67] 1976
Electron impact ion yield curve	8.95 ± 0.10	[69] 1976
PES	9.20[b] (vert)	[28] 1976
PES	9.18[b] (vert)	[24] 1989
Electron impact ion yield curve	9.15 ± 0.15	[70] 1996

[a] Adiabatic values unless otherwise stated.
[b] Uncertainty not reported.

At higher energies, there is a marked rise in the parent ion yield at about 16 eV, leading to a maximum at about 19.3 eV. Although the PES intensity drops markedly between 15 and 16 eV, in contrast to the parent ion yield curve, it shows, between 16 and 20 eV, a somewhat similar behaviour to the latter. This region of the PES has not been assigned but we note that there are similar features in the PES of pyrimidine in this energy region, for which molecular orbital assignments have been made [79].

Just as in the case of adenine, we compared the thymine parent ion yield curve with the optical absorption curve derived from 25 keV electron energy loss spectra of thin films of thymine [57] (Fig. 4(b)). Our parent ion yield curve has a plateau between 13 and 15.5 eV, followed by a rise to about 17.7 eV, continuing on to a peak at about 19 eV. In the thymine film spectrum, there are peaks reported to be at 14.4 ± 0.3 and 18.3 ± 0.3 eV [57]. The physical relation between these solid and gas phase features requires further investigation.

3.2.2. Thymine ion fragmentation

(α) *Reactions involving loss of HNCO and/or CO:* The principal fragmentation pathways of the thymine parent cation (species IV, see schematic representation Fig. 7) involve loss of HNCO (isocyanic acid). One unit loss gives rise to the $m/z = 83$ ion, whose AE = 10.7 eV:

$$C_5H_6N_2O_2^+ \ (m/z = 126) \rightarrow C_4H_5NO^+ \ (m/z = 83) + HNCO \ (m = 43) \qquad (14)$$

This ion is formed by Retro–Diels–Alder (RDA) reaction from the thymine parent cation, and involves the rupture of two bonds, N3–C4 and C2–N1, in the parent ion. The latter bond has been calculated to be much weakened in the cation as compared with neutral thymine [75]. The $m/z = 83$ fragment ion has been suggested to have the structure of species Va (Fig. 7) [38]. This is supported by recent calculations of the possible minimum energy structures and relative stabilities of $C_4H_5NO^+$ isomers [75]. We remark that the mass spectrum of ^{14}C2-thymine [34] retains the $m/z = 83$ peak, confirming that the ^{14}C2 atom has been eliminated in the HNCO loss molecule, as proposed in reaction (14).

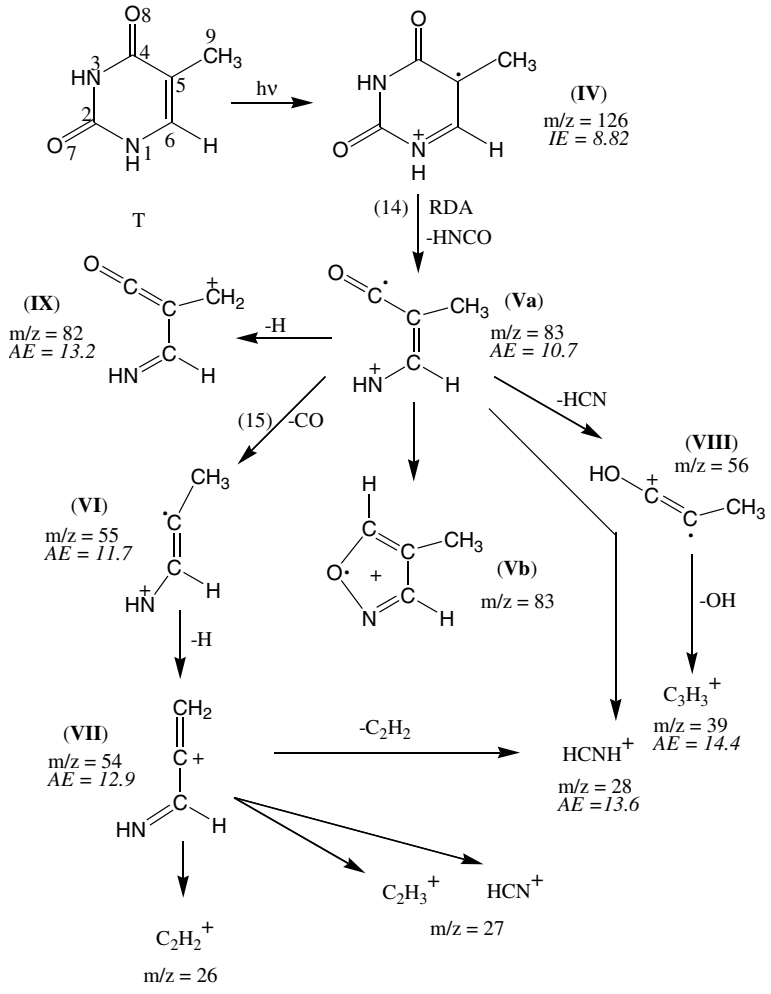

Fig. 7. Principal fragmentation decay routes of the thymine radical cation. Measured appearance energy values are given for each fragment (in eV, for uncertainties refer to Table 3). Roman and Arabic numerals correspond to species and reactions, respectively.

One possible evolution of the Va $C_4H_5NO^+$ ion that we considered is ring closure to form the 5-methyl-isoxazole cation. The heat of formation of the 5-methyl-isoxazole cation is $\Delta H_f = 931$ kJ/mol, obtained from the heat of formation of neutral 5-methyl isoxazole, $\Delta H_f = 34$ kJ/mol [65], and its adiabatic IE $= 9.3 \pm 0.1$ eV, which we determined from the published HeI photoelectron spectrum of Kobayashi et al. [88]. However, we find that the heat of formation of the observed $C_4H_5NO^+$ ion, $\Delta H_f(C_4H_5NO^+) = 806$ kJ/mol, based on its measured appearance energy, is considerably smaller than that of the 5-methyl isoxazole cation, which shows that the latter is not formed in our experiment. Another possibility is that the evolution is to the 4-methyl isoxazole cation (species Vb in Fig. 7), which is a δπ system. Thermochemical data on this species are not available. We note that the weak ion $m/z = 84$, observed in both the 20 and 70 eV electron impact mass spectra (Table 3), would correspond to the loss of NCO from IV.

The loss of two HNCO units gives rise to the $m/z = 40$ ion, assigned to CH_3–C≡CH^+. This can occur directly from parent ion via rupture of the two bonds, C4–C5 and, N1–C6. However, the calculations of Improta et al. [75] suggest that while the C4–C5 bond would be considerably weaker in the cation, the N1–C6 bond would be stronger. Formation of the $m/z = 40$ ion would be more complex, if it occurred via $m/z = 83$, since it would involve rupture of two further bonds in this intermediate ion to lose CO + NH.

Concerning the evolution of the $m/z = 83$ fragment ion, we note that it can go on to lose a CO molecule to form the most abundant ion in the mass spectrum, $m/z = 55$, whose AE = 11.7 eV.

$$C_4H_5NO^+ \ (m/z = 83) \rightarrow C_3H_5N^+ \ (m/z = 55) + CO \ (m = 28) \qquad (15)$$

This fragment ion, whose m/z value is, as expected, unchanged in the mass spectrum of ^{14}C2-thymine [34], has a proposed quasi-linear structure shown in Fig. 7 (species VI). Although this is the thermodynamically most favored structure, other isomers might be kinetically more accessible according to the calculations of Improta et al. [75].

Another possible assignment of $m/z = 55$ is to CH_3CCO^+ (methylketene ion which could eventually isomerize to $CH_2{=}CHCO^+$ or $HC{\equiv}CCH_2O^+$) that can be formed by rupture of the central carbon–carbon bond in $m/z = 83$. This corresponds to the charge switch of one of the reactions that can form $m/z = 28$ (see below). However, it is generally considered [38] that the $m/z = 55$ ion is indeed CH_3CCHNH^+, containing the methyl group and the atoms N1, C5 and C6.

The $m/z = 83$ ion can also lose a hydrogen atom, suggested to be from the methyl group [32], to give $m/z = 82$. It has been proposed [32] that further loss, of a CO group, is responsible for the formation of the strong $m/z = 54$ fragment ion $C_3H_4N^+$. However, our ion yield measurements show that the AE of $m/z = 54$ (~12.9 eV) is smaller than that of $m/z = 82$ (13.2 eV). Thus, there must exist some other mechanism of formation of the $m/z = 54$ ion at threshold. This is most probably loss of a hydrogen atom from the $m/z = 55$ species. It is of interest that the maximum in the $m/z = 55$ ion yield curve is at about 16 eV (Fig. 6) whereas it is at about 19 eV for the $m/z = 54$ ion, not far from the maximum in the parent ion curve (19.3 eV). The difference in energy is of the order of magnitude of the dissociation energy of a C–H bond. We remark that two different structures could exist for the $m/z = 54$ species, the quasi-linear species VII in Fig. 7, and a cyclic structure in which a methyl group is attached to a (H)CCN cyclic group [32].

(β) *Other important ions:* The weak $m/z = 43$ ion ($AE = 11.9 \pm 0.1$) eV, assigned to $HNCO^+$, could be the fragment ion formed in a reaction corresponding to a charge switch in the reaction (14) which leads to the formation of the $m/z = 83$ ion discussed above. We note that the shift of the $m/z = 43$ peak to $m/z = 45$ in the ^{14}C2-thymine mass spectrum published by Ulrich et al. [34] confirms our suggestion above that this ion is produced by a charge switch of reaction (14). The $m/z = 43$ ion is not observed in the 20 eV electron impact mass spectrum, although it is present in the 20 eV photon impact spectrum. This is consistent with the fact that the $m/z = 83$ ion is relatively much weaker in the 20 eV electron impact as compared with the photon impact mass spectrum (Table 3).

Following the Stevenson–Audier–Harrison (SAH) rule concerning the dissociation of odd electron ions [89], the fact that $m/z = 83$ has a smaller AE than $m/z = 43$ suggests that the $m = 83$ neutral species (C_4H_5NO) has a smaller IE than HNCO, whose $IE = 11.61 \pm 0.03$ eV [78]. This is certainly the case for the 5-methyl isoxazole form of C_4H_5NO, whose IE(v) = 9.61 eV [88] and whose IE(ad) we have determined as 9.3 ± 0.1 eV (see above). However, the C_4H_5NO product is not 5-methyl isoxazole since, from the 11.9 eV appearance energy of $m/z = 43$ and the heats of formation of thymine and of $HNCO^+$, we calculate the heat of formation of neutral C_4H_5NO to be −198 kJ/mol whereas, as mentioned above, the known heat of formation of 5-methyl isoxazole is 34.1 ± 0.75 kJ/mol [65]. Nor can C_4H_5NO be 3-methyl isoxazole, since the latter has $\Delta H_f = 35.6 \pm 0.67$ kJ/mol [65].

$m/z = 39$: The most probable assignment of the $m/z = 39$ ion is to $C_3H_3^+$, which could be formed by loss of a hydrogen atom from $C_3H_4^+$ ($m/z = 40$). The high AE = 14.4 eV of $m/z = 39$ is consistent with the energy expensive pathways suggested above for formation of its precursor ion, $m/z = 40$. Another possible formation pathway would be OH loss from $m/z = 56$ (species VIII in Fig. 7), whose formation is discussed below.

$m/z = 28$: The suggested linear structure of the $m/z = 54$ ion could give rise to formation of the $HCNH^+$ ($m/z = 28$) and $C_2H_2^+$ ($m/z = 26$) ions by rupture of the central carbon–carbon bond. The important $HCNH^+$ ion could also be formed by rupture of the central carbon–carbon bond in the $m/z = 82$ fragment ion (species IX in Fig. 7). Another mechanism involves direct formation of $HCNH^+$ from the parent ion, which requires rupture of two bonds, the C5–C6 double bond and the C2–N1 bond, both of which are calculated to be weaker in the cation [75]. We also note that from the structure of the $C_4H_5NO^+$ ion ($m/z = 83$, species Va) proposed above, it is possible, by rupture of the central carbon–carbon bond, to produce $HCNH^+$. This is pathway E of Rice et al. [32] in which there would be loss of the methylketene radical CH_3CCO. It is not clear as to whether this actually occurs since there is no mention of a metastable peak for this process. Thus we have suggested five different possible pathways for forming the $HCNH^+$ ion, via the respective precursors $m/z = 126$, 83, 82, 55 and 54, which in the latter three cases involves rupture of only one, carbon–carbon, bond. The AEs of the various fragment ions are consistent with all five pathways. From the profiles of their respective ion yield curves, it appears that the relative importance of these five pathways to forming the $HCNH^+$ ion is modified above 16 eV, since the 16 eV maximum in the ion yield curves of the $m/z = 55$ and 83 ions is at a much lower energy than the maxima in the other three precursor ion yield curves (Fig. 6).

A final remark concerning the $m/z = 28$ ion, assigned above to $HCNH^+$, is that it is unlikely to be CO^+ since CO has a quite high ionization energy (14.014 eV [65]), whereas the $m/z = 28$ ion has an AE = 13.6 eV, lower than IE(CO).

(γ) *Less intense fragment ion peaks (no AE measurements):* There is no initial loss of CO from the parent ion, since the $m/z = 98$ fragment ion is absent in the mass spectra. A weak ion is observed at $m/z = 97$, which is possibly $C_4H_3NO_2^+$, resulting from loss of NH_2CH. We have not yet discussed the very weakest ions observed in our mass spectrum of thymine, at $m/z = 71$,

70, 58, 56, 53, 52, 45, 41, 27: (Table 3). Of these, $m/z = 45$ and 58 were not observed in the mass spectrum of Rice et al. [32], although $m/z = 45$ is present in the mass spectrum of Ulrich et al. [34] and in that of the NIST [65].

$m/z = 70$, 71 and related species: We assign the $m/z = 71$ peak to $OCNHCO^+$, which could be formed from the parent ion by breaking of two bonds, C2–N1 and C4–C5. Both bonds are expected to be weaker in the cation from the calculations of Improta et al. [75]:

$$C_5H_6N_2O_2^+ \ (m/z = 126) \rightarrow OCNHCO^+ \ (m/z = 71) + CH_3CCHNH \ (m = 55) \quad (16)$$

This reaction also suggests that an alternative pathway for formation of the $m/z = 55$ ion would be a charge switch of reaction (16).

The $m/z = 70$ peak was assigned by Ulrich et al. [34] to $OCNCO^+$, based on a shift of two mass units in their mass spectra observed in a $^{14}C2$ study of thymine. We note that this fragment ion would not be formed by loss of a hydrogen atom from $m/z = 71$, since the latter peak is unchanged in the carbon isotope spectrum. However, an alternative assignment of $m/z = 70$, which we consider to be more probable, is to $C_2H_2N_2O^+$, whose structure would be that of the 1,2,5-oxadiazole cation. This could be formed from the parent cation by rupture of the C4–N3 and C5–C6 bonds and simultaneous formation of a bond between the C6 and N3 atoms. The resulting $m/z = 70$ ion would still be compatible with the mass spectrum of the $^{14}C2$ study of thymine by Ulrich et al. [34]. With this new assignment of the $m/z = 70$ ion, the neutral loss is of a species whose elemental formula is C_3H_4O and whose structure is that of methylketene.

$$C_5H_6N_2O_2^+ \ (m/z = 126) \rightarrow C_2H_2N_2O^+ \ (m/z = 70) + C_3H_4O \ (m = 56) \quad (17)$$

This assignment of $m/z = 70$ also makes possible a reasonable assignment of the $m/z = 56$ peak to the methylketene ion $C_3H_4O^+$ (an isomer of species VIII). The latter could be formed by a reaction corresponding to a charge switch of reaction (17). It is difficult to estimate whether this charge switch reaction is likely to occur, since although the ionization energy of methylketene is known, IE(v) = 8.95 eV [65], that of 1,2,5-oxadiazole has not been reported so far. The structure of the $m/z = 56$ ion could also correspond to a 1-methyl-2-hydroxyacetylene cation ($HO–C{=}CCH_3^+$), species VIII in Fig. 7), formed from ion Va ($m/z = 83$) by 1,5 H-shift with subsequent rupture of the central C–C bond. This reaction would most likely represent the unique HCN loss reaction for this nucleobase cation, in contrast, of course, to adenine, where multiple HCN loss processes occur. Isotopic studies are required to show whether this assignment of $m/z = 56$ is viable.

The weak peak at $m/z = 53^+$ is not assigned. The $m/z = 52$ ion is quite strong in the 70 eV electron impact mass spectrum, but absent in the 20 eV electron impact spectrum. This indicates, as do the intensities of some other relatively small fragment ions in the respective mass spectra, that they result from higher energy dissociative ionization processes. There are two assignments (HCN^+, $C_2H_3^+$) for the $m/z = 27$ ion. HCN^+ could be formed by loss of a hydrogen atom from $HCNH^+$. The formation of $C_2H_3^+$ is not easily rationalized. Isotopic labeling experiments are required to clarify the relative importance of these two $m/z = 27$ fragment ions.

3.3. Uracil: mass spectra and ion yield curves

Table 5 presents the relative intensities of the m/z peaks in our uracil mass spectrum, obtained at 20 eV photon excitation energy, and compares them with those of Rice et al. [32], measured with 70 eV electron impact, and with the 20 eV electron impact spectra of Hecht et al. [41] and of Rice et al. [32]. The appearance energies of the major m/z ions are listed, as measured from the onsets in the photoion yield curves (Fig. 8), and we give the neutral species which we consider to be formed by dissociative ionization of uracil, along with the observed m/z ions.

Our 20 eV photon impact mass spectrum of uracil and the 70 eV electron impact one of Rice et al. [32] are very similar, having essentially the same m/z features but with a few differences in their relative intensities. The $m/z = 42$ fragment ion peak is the strongest in both cases, as it is in the 70 eV electron impact mass spectrum reported by Brown et al. [39]. Several other electron impact mass spectra of uracil have been reported, having the same principal ions but with relative intensities different from those measured by Rice et al. [32]. In these mass spectra the parent peak at $m/z = 112$ is the most intense [34,38,40,65,90] and the intensities of the other principal peaks are in the m/z order $42 > 69 > 28$ [34,40] or $69 > 42 > 28$ [38,65,90,91]. As mentioned earlier, the differences between the 70 eV electron impact spectra are most probably due to differences in the ion optics and ion residence times.

The 20 eV electron impact mass spectra of uracil obtained by Rice et al. [32] and by Hecht et al. [41] also have the parent peak as its most intense ion, with the other principal peaks being $m/z = 69$, 42 and 28. The much smaller number of m/z peaks in the 20 eV electron impact mass spectrum of Rice et al. [32] (10 features) of uracil as compared to our 20 eV photon impact mass spectrum (Table 5) can here too be understood, as in the similar case of thymine, as being due to a different energy deposition with these two excitation sources, since at 20 eV electron impact the Born approximation conditions [84] under which electron impact mimics photon impact excitation is not operative at this low electron excitation energy. However, we note that the

Table 5
Electron impact [32,41] and photon impact mass spectra and photoion appearance energies: Uracil $m = 112$ ($C_4H_4N_2O_2$)

m/z	Electron impact 70 eV relative intensity	Electron impact 20 eV relative intensity[a]	Photon impact 20 eV relative intensity	Photon impact appearance energy (AE, eV)	Ion elemental formula	Neutral loss
112	78	100(100)	63	9.15 ± 0.03	$C_4H_4N_2O_2^+$	
96	2	0(0)	1		$C_4H_4N_2O^+$	O
95	0	<1(2)	0			
77	0	<1(0)	0			
70	7	5(5)	4		$C_3H_4NO^+$	NCO
69	63	69(66)	52	10.95 ± 0.05	$C_3H_3NO^+$	HNCO
68	33	15(5)	33	13.40 ± 0.05	$C_3H_2NO^+$	HNCO + H
67	1	<1(0)	0			
56	3	<1(0)	3			
53	4	<1(0)	1			
52	1	<1(0)	1			
51	1	<1(0)	0			
44	8	4(1)	4			
43	15	6(1)	10	13.6 ± 0.2	$HNCO^+$	C_3H_3NO
42	100	59(21)	100	13.25 ± 0.05	$C_2H_2O^+$	HNCO + HCN
41	48	21(8)	50	12.95 ± 0.05	$HCCHNH^+$ and/or $HCCO^+$	HCNO + CO and/or HNCO + HCN + H
40	57	21(0)	25	14.06 ± 0.10	$C_2H_2N^+$	HNCO + H + CO
39	15	5(0)	2			
38	7	2(0)	0			
32	0	2(0)	0			
31	0	<1(0)	0			
29	1	2(0)	3		NH_2CH^+ or HCO^+	
28	78	74(10)	86	13.75 ± 0.05	$HCNH^+$	HNCO + HCCO
27	2	3(0)	4		HCN^+	HNCO + HCCO + H
26	4	4(0)	5	≈15 eV	$C_2H_2^+$	2HNCO
18	n.m.[b]	n.m.	4		H_2O^+	Also observed in NIST
17	n.m.	n.m.	1		NH_3^+	Also observed in NIST
14	n.m.	n.m.	3		N^+	Also observed in NIST

[a] Data from the 20 eV electron impact mass spectra of Hecht et al. [41] and, in parentheses, of Rice et al. [32].
[b] n.m. = not measured.

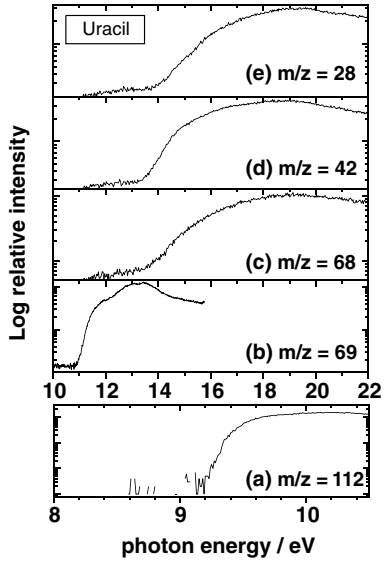

Fig. 8. Selected ion yield curves of uracil. The $m/z = 112$ ion yield curve has been measured using an MgF_2 cut-off filter.

reported 20 eV electron impact mass spectrum of uracil, by Hecht et al. [41] (Table 5), contains many more, mainly very weak, features, and that the principal peak intensities are often much closer to those observed in the 70 eV electron impact mass spectrum. It would thus appear that the ion residence time was much longer in the 20 eV electron impact experiments of Hecht et al. [41] than in those of Rice et al. [32].

Coupier et al. [91] recently measured both proton (20–150 keV) impact and electron (200 eV) impact mass spectra of uracil. They observed the same principal fragment ions as in our 20 eV photon impact study, but discussed only four of the fragment ions, $m/z = 69$, 42, 29 and 28, giving the latter three different molecular ion assignments than ours, as discussed later. Especially in the proton impact spectrum, they also observed a very large number of other fragment ions, this being due, no doubt, to the increased energy deposition with respect to our case and to that of 70 eV electron impact. In the proton impact study, the order of the principal

ion intensities was $m/z = 112 = 42 > 28 > 69$, whereas in the 200 eV electron impact mass spectrum it was $m/z = 28 > 42 > 69 > 112$.

3.3.1. The uracil parent ion

For the uracil ion $C_4H_4N_2O_2^+$, $m/z = 112$, we obtained an ionization energy of 9.15 ± 0.03 eV from the parent ion yield curve, measured using an MgF_2 filter (Fig. 8(a)). This value is a little smaller than the IE $= 9.32 \pm 0.05$ eV obtained with the only other reported measurement by photoionization mass spectrometry [67] Table 6. Early measurements of uracil by electron impact gave IE values that are rather high [68,92], but a later measurement [69] is much closer to our PIMS value. A recent electron impact measurement [90] also gave a value, IE $= 9.59 \pm 0.08$ eV, considerably higher than our PIMS value, but similar to the vertical IEs of uracil obtained by photoelectron spectroscopy peak measurements [23,27–29,93]. The PES IE(vert) values fall in the range 9.50–9.68 eV, i.e., 350–530 meV above the adiabatic value determined by our PIMS measurement. The calculations of IE(ad) and IE(vert) reported for this RNA base by Wetmore et al. [94] give values IE(ad) = 9.21 eV and IE(vert) = 9.47 eV, a difference of 260 meV.

As in the case of adenine and thymine, a direct comparison between the $m/z = 112$ ion yield curve and the HeI photoelectron spectrum of uracil [24] revealed features in the ion yield curve that can be correlated with features in the photoelectron spectrum (see Fig. 3(c)). Also, there is a general similarity in the parent ion yield curves of the two related nucleobases uracil and thymine. In particular, in both cases there is a marked rise

Table 6
Uracil ionization energy values[a]

Experimental method	Ionization energy (eV)	Reference and year
Photoion yield curve (PIMS)	9.15 ± 0.03	Present study
Electron impact ion yield curve	9.82 ± 0.10	[68] 1967
Electron impact ion yield curve	9.53 ± 0.02	[92] 1971
Photoelectron spectroscopy (PES)	9.59 ± 0.03 (vert)	[93] 1974
PES	9.50 ± 0.03 (vert)	[23] 1975
PES	9.45[b] (vert)	[25] 1975
PES	9.60[b] (vert)	[28] 1976
PIMS	9.32 ± 0.05	[67] 1976
Electron impact ion yield curve	9.35 ± 0.10	[69] 1976
PES	9.68[b] (vert)	[27] 1980
PES	9.53[b]	[29] 1996
Electron impact ion yield curve	9.59 ± 0.08 (vert)	[90] 2004

[a] Adiabatic values unless otherwise stated.
[b] Uncertainty not reported.

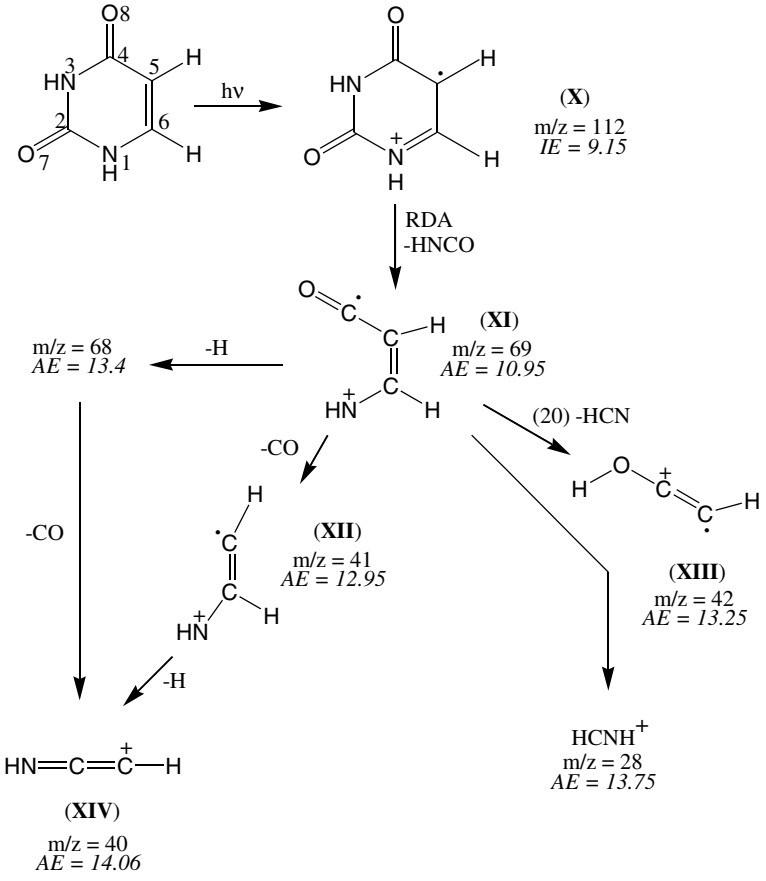

Fig. 9. Principal fragmentation decay routes of the uracil radical cation. Measured appearance energy values are given for each fragment (in eV, for uncertainties refer to Table 5). Roman and Arabic numerals correspond to species and reactions, respectively.

in the parent ion yield at about 16 eV, leading to a maximum in the 19.3–19.5 eV region.

Using our measured adiabatic IE of uracil, and the known value of the heat of formation $\Delta H_f^0(\text{uracil}) = -303 \pm 2$ kJ/mol [78], we obtain a value of the heat of formation of the cation $\Delta H_f^0(\text{uracil cation}) = 580 \pm 5$ kJ/mol, in agreement with the preliminary value 585 kJ/mol given by Lias et al. [78], based on the onset of a photoelectron spectral band.

3.3.2. Uracil ion fragmentation

(α) *Reactions involving loss of HNCO and CO*: The principal fragmentation pathways of the uracil parent cation (species X, Fig. 9) involve loss of HNCO by RDA reaction as in the case of thymine. This gives rise to the $m/z = 69$ ion, $C_3H_3NO^+$, whose AE = 10.95 ± 0.05 eV. This ion has been suggested [38] to have the structure given in Fig. 9 (species XI). In their electron impact ionization study of uracil, Denifl et al. [90] measured AE = 10.89 ± 0.07 eV for the appearance of the $m/z = 69$ ion, which is close to our photon impact value. They, as well as Coupier et al. [91], also assigned it to $C_3H_3NO^+$, i.e., the "X-HNCO" ion, but did not discuss its structure. The formation of species XI, by loss of HNCO involves rupture of the N3–C4 and C2–N1 bonds.

The charge switch reaction:

$$C_4H_4N_2O_2^+ \rightarrow HNCO^+ \ (m/z = 43) + C_3H_3NO \ (m = 69) \quad (18)$$

gives rise to the $m/z = 43$ ion, $HNCO^+$, whose AE = 13.6 ± 0.2 eV in our PIMS measurement and is reported to be 13.36 ± 0.30 eV in electron impact measurements [90]. The AE of $HNCO^+$ is much greater than the AE = 10.95 eV of $C_3H_3NO^+$. This suggests, from the SAH rule [89], that IE (C_3H_3NO) is smaller than the IE of HNCO (11.61 ± 0.03 eV [78]). The two most likely candidates for C_3H_3NO are in concordance with this suggestion: isoxazole (IE = 9.942 eV [95]) and oxazole (IE = 9.6 eV [96]). Heat of formation calculations favor oxazole.

The $m/z = 69$ fragment ion can further fragment by a number of different pathways. Many of these pathways in uracil (U) are similar to corresponding pathways in the fragmentation of the $m/z = 83$ ion of thymine (T), but their relative importance is very different in the two cases, as can be seen by a comparison of the relative intensities of the precursor ion (m/z(U) = 69, m/z(T) = 83), and relevant daughter ion in Tables 3 and 5. We will discuss these various pathways in turn.

Whereas in m/z(T) = 83, loss of a CO molecule forms $m/z = 55$, the most abundant ion in the thymine mass spectrum, in uracil, for m/z(U) = 69, the corresponding CO loss gives rise to the $m/z = 41$ fragment ion, assigned to $HC{=}CHNH^+$ (species XII in Fig. 9) which, although intense, is not the major fragment ion in the uracil mass spectrum.

$$C_3H_3NO^+ \ (m/z = 69) \rightarrow HC{=}CHNH^+ \ (m/z = 41) + CO \ (m = 28) \quad (19)$$

This pathway has been confirmed by the observation of a satisfactory metastable peak in the electron impact mass spectrum of Rice et al. [32]. Other possible isomers of $C_2H_3N^+$ are the species $HN{=}C{-}CH_2^+$, formed by H-shift from XII, as well as the azirinium radical cation and the 2H-azirine cation ring species, the formation of both of which would involve complicated rearrangements.

We find that the $m/z = 41$ ion has an AE = 12.95 ± 0.05 eV, i.e., 3.80 eV above the IE of uracil, whereas the m/z(T) = 55 ion appears at 2.88 eV above the IE of thymine. We note that in their electron impact study of uracil, Denifl et al. [90] observed AE = 13.32 ± 0.18 eV for the $m/z = 41$ ion, somewhat higher than our PIMS value; however, the difference between this value and their measured IE = 9.59 ± 0.08 eV for the parent ion is 3.73 eV, similar to our PIMS value. That these uracil values are greater than the 2.88 eV observed for thymine indicates the greater difficulty of CO loss in the uracil case with respect to the precursor ion in thymine. In the latter, with respect to uracil, the presence of the methyl group no doubt weakens the carbon–carbon bond to which the oxygen atom is attached, via hyperconjugation that affects the π electron distribution. We note that there is no initial loss of CO from the parent ion, since the $m/z = 84$ fragment ion is absent in the mass spectrum of uracil.

(β) *Other important ions:* We now discuss the most intense fragment ion, $m/z = 42$. This is assigned to the $HC{=}COH^+$ ion (species XIII), formed by 1,5 H-shift and subsequent loss of HCN from the $m/z = 69$ precursor ion (reaction (20)). We note that loss of HNC from XIII could give rise to the isomer $H_2C{=}C{=}O^+$, the ketene radical cation. The structure of ion $m/z = 42$ remains to be further investigated

$$C_3H_3NO^+ \ (m/z = 69) \rightarrow HC{=}COH^+ \ (m/z = 42) + HCN \ (m = 27) \quad (20)$$

The assignment of $m/z = 42$ to $HC{=}COH^+$ is consistent with the fragmentation patterns from electron impact mass spectra of at least four 2,4-dioxypyrimidenes [32,38], whose structures are related to uracil. We remark that the electron impact measurement of Denifl et al. [90] gave AE = 13.41 ± 0.10 eV, in reasonable agreement with our value AE = 13.25 ± 0.05 eV, for m/z(U) = 42. These authors, as well as Coupier et al. [91], assigned $m/z = 42$ to the OCN^+ ion. However, formation of a OCN^+ fragment ion directly from the parent ion would involve rupture of three bonds. It would also involve a very complex bond rupture and reorganization process if the precursor was the $m/z = 69$ ion represented in Fig. 9. We prefer our assignment of the $m/z = 42$ peak to the $HC{=}COH^+$ ion (or its isomer

$H_2C{=}C{=}O^+$), whose formation is mechanistically more reasonable.

The incorrect assignment of the $m/z = 42$ ion to OCN^+ has further implications. Feil et al. [97] have very recently measured the absolute value of the partial cross-section for formation of this cation in electron excitation of uracil, and then used this cross-section, which they assumed was that of the OCN^+ ion, in conjunction with the known sensitivity ratio for detection of positive and negative ions of the same species, to determine the dissociative attachment cross-section for formation of the OCN^- anion from uracil. The value they obtained was smaller by an order of magnitude than that previously obtained with uracil by simple normalization with the cross-section for dissociative electron detachment in CCl_4 [98]. Although it is very possible that the $m/z = 42$ anion formed by dissociative electron detachment in uracil is indeed OCN^-, it appears unlikely that the $m/z = 42$ cation is OCN^+. We suggest that incorrect assignment of the $m/z = 42$ cation to OCN^+ is in part responsible for the discrepancy between the two OCN^- cross-section values.

Another fragmentation pathway with $m/z = 69$ as precursor ion leads, by rupture of the central carbon–carbon bond, to formation of $HCNH^+$ ($m/z = 28$), $AE = 13.75 \pm 0.05$ eV, by loss of the ketene radical HC=C=O.

$$C_3H_3NO^+ \ (m/z = 69) \rightarrow HCNH^+ \ (m/z = 28) + HC{=}C{=}O \ (m = 41) \quad (21)$$

It is not clear as to whether this actually occurs since there is no mention of a metastable peak for this process in electron impact experiments [32]. We further remark that Coupier et al. [91] assign the $m/z = 28$ ion to CO^+ (see also [90]) but this is very unlikely, for reasons similar to those discussed previously for the analogous case in thymine. Denifl et al. [90] measure $AE = 13.83 \pm 0.39$ eV for $m/z = 28$, in good agreement with our PIMS value.

We note that the charge switch ion $HC{=}C{=}O^+$ ($m/z = 41$) to reaction (21) has the same m/z as $HC{=}CHNH^+$, $AE = 12.95$ eV, discussed above. Both ion products are suggested by the fragmentation schemes of Rice et al. [32]. The respective IEs of the HC=C=O radical (~9.5 eV [78]) and HC=CHNH (10.1–12.2 eV, according to the structure of this ion [65]) suggest that $HC{=}C{=}O^+$ could be a significant contributor to the $m/z = 41$ peak.

The $m/z = 69$ ion can also lose a hydrogen atom to give $m/z = 68$, which is a strong ion, whose $AE = 13.40 \pm 0.05$ eV. The electron impact measurement, $AE = 12.75 \pm 0.66$ eV, is not inconsistent with our PIMS value, given the large uncertainty in the electron impact value. It has been proposed [32] that the fairly strong $m/z = 40$ fragment ion (species XIV in Fig. 9) can be formed via two pathways: (i) loss of a CO group from $m/z = 69$, (species XI) followed by loss of a hydrogen atom, or (ii) loss of H from XI followed by loss of CO. Both pathways are indicated in Fig. 9. Our ion yield measurements show that the AE of $m/z = 40$ (14.06 eV) is much greater than that of $m/z = 69$ (10.95 eV) and of the AE of the respective intermediate ions $m/z = 41$ and $m/z = 68$. This is consistent with the $m/z = 40$ ion resulting from three stages of fragmentation.

On the basis of the corresponding studies on thymine, it is possible to propose two different structures for a $C_2H_2N^+$ assignment of the $m/z = 40$ species, a quasi-linear $HN{=}C{=}CH^+$ (species XIV in Fig. 9) and a cyclic structure in which a nitrogen atom is attached to two linked CH groups. However, in contrast to the case of thymine, where the corresponding $m/z(T) = 54$ ion is considered to have the structure $H_2C{=}C{=}CHNH^+$ (species VII), from which formation of the $HCNH^+$ ($m/z = 28$) ion can occur by rupture of the central carbon–carbon bond, the corresponding precursor ion in uracil, $HN{=}C{=}CH^+$ [32], does not have a suitable structure for easy formation of HCNH+.

We must remember that there is also a totally different assignment possible for the $m/z = 40$ ion, i.e., CCO^+, formed by loss of a hydrogen atom from a $HC{=}C{=}O^+$ ($m/z = 41$) precursor that could be formed as discussed above. However, Rice et al. [32] affirm that the only ion observed at $m/z = 40$ is $C_2H_2N^+$. Isotopic labeling studies would be useful to clarify this assertion.

Another mechanism for producing $HCNH^+$ involves direct formation from the parent ion, which requires rupture of two bonds, the C5–C6 double bond and the C2–N1 bond (Fig. 1), similar to the case of thymine:

$$C_4H_4N_2O_2^+ \ (m/z = 112) \rightarrow HCNH^+ \ (m/z = 28) + C_3H_2NO_2 \ (m = 84) \quad (22)$$

In contrast to thymine, for which we have suggested five different possible pathways for forming the $HCNH^+$ ion, in the case of uracil (U) there appear to be only two viable pathways to the formation of $HCNH^+$, via reactions (21) and (22), respectively. The $AE = 13.75$ eV of $m/z(U) = 28$ and the AEs of the precursor ions (10.95 and 9.15 eV, respectively) are consistent with these two pathways. We note, however, that the intensity of the $m/z = 69$ ion decreases rapidly above 13.7 eV which is close to the onset of the $m/z = 28$ eV ion yield curve. This suggests that both pathways to formation of $HCNH^+$ are operative, weakly from the parent ion precursor, and strongly from the $m/z = 69$ precursor.

(γ) *Less intense fragment ion peaks (no AE measurements):* The other fragment ion peaks in Table 5 belong to minor ions, some of which are associated with high energy processes.

$m/z = 96$: This weak ion is assigned to $C_4H_4N_2O^+$ corresponding to loss of a single oxygen atom from

the parent ion. This could result from cleavage of the C4–O4 bond or the C2–O2 bond. We note that the 20 eV electron impact mass spectra contain a peak at $m/z = 95$ but not at $m/z = 96$, whereas the 70 eV electron impact mass spectra, like our 20 eV photon impact spectrum, possess a peak at $m/z = 96$ but not at $m/z = 95$. This requires further investigation.

We note that the weak ion $m/z = 70$ corresponds to the (U-NCO) cation.

$m/z = 29$, 27, 26: Coupier et al. [91] assign the $m/z = 29$ ion to HCO^+. An alternative assignment could be to the NH_2CH^+ ion. The $m/z = 27$ ion is assigned to HCN^+ but it is too weak for measurement of its appearance energy in our PIMS study. An electron impact measurement gave $AE = 14.77 \pm 0.92$ eV [90] for this ion. We assign the $m/z = 26$ ion to $C_2H_2^+$, formed via loss of 2 HNCO molecules directly from the parent ion by rupture of two bonds, C4–C5 and C6–N1. Ion yield measurement of this very weak ion at BESSY II showed that its AE is approximately 15 eV.

$m/z = 18$, 17 and 14: The peaks at $m/z = 18$, 17 and 14 in our 20 eV photon impact mass spectrum are below the lower mass limit ($m/z = 20$) reported in many electron impact studies [32,34,38–41]. However, these peaks can be seen in the NIST mass spectrum [65], in the proton and electron impact mass spectra [91] spectra, and in a 120 eV electron impact mass spectrum [97]. We consider these peaks to correspond, respectively, to H_2O^+, NH_3^+ and N^+ ions. The ratio of intensities of peaks $m/z = 18$ and 17 is the same in our 20 eV photon impact mass spectrum and in the NIST electron impact mass spectrum, whereas our $m/z = 14$ signal is relatively about twice as strong as that in the NIST spectrum. The existence of the $m/z = 14$ ion, assigned to N^+, lends credence to the assignment of $m/z = 17$ to NH_3^+ rather than to an OH^+ ion, which could occur, with about the same relative intensity to $m/z = 18$, from a water impurity [89].

4. Conclusion

In this photoionization mass spectrometry study of adenine, thymine and uracil, we used synchrotron radiation in the 6–22 eV photon energy region to investigate VUV-induced degradation pathways of these three nucleic acid bases in the gas phase. Photon impact mass spectra and photoion yields as a function of excitation energy were measured, virtually for the first time for these important biological molecules. The measurements provided more accurate values than previously reported for the adiabatic IEs of these nucleobases. These values are important for the interpretation of charge transfer phenomena in DNA and RNA.

We compared our 20 eV photoion mass spectra with 20 and 70 eV electron impact (and 200 eV electron and high energy proton impact in uracil) mass spectra. The existence of many metastable dissociation reactions, as seen in the electron impact studies, makes the number of m/z peaks and their relative intensities dependent on ion source residence time, field-free region characteristics and applied potentials in the ion optics. Particularly interesting is the comparison between 20 eV photon impact and 20 eV electron impact mass spectra for thymine and uracil, illustrating great differences in energy deposition due, in part, to the non-validity of the first Born approximation for low energy electrons.

The assignment of the m/z peaks in our photon impact mass spectra and analyses of fragment ion formation pathways have been considerably assisted by data published on the electron impact mass spectra of these nucleobases. In our work, the photoion appearance energies are reported for the first time. AE values enabled heats of formation of parent and some fragment ions to be revised or determined. Thermochemical data, coupled with the observed AEs, were also useful in clarifying dissociative ionization pathways many of which were first proposed by Rice and Dudek [32,33]. Our study has enabled us to refine these pathways, evaluate the relative importance of competitive processes in some cases and propose pathways that were not previously suggested.

For the purine, adenine, the ion fragmentation is mainly governed by successive loss of HCN units. The two pyrimidines, thymine and uracil, have similar dissociation pathways, with main neutral loss pathways which involve HNCO and CO and, in uracil, HCN. However, there are some significant differences due to hyperconjugation properties of the methyl group in thymine so that the relative importance of analogous reactions differs markedly, in some cases, between thymine and uracil. The astrophysically important fragment ion $HCNH^+$ can be formed by several fragmentation pathways in all three nucleobases. The relative importance of competitive fragmentation processes was determined in some cases.

Further concerning the astrophysical implications of our study, we note that the three nucleobases would be easily photodissociated in HI regions of the interstellar medium since they exhibit fragmentation appearance energies well below 13.6 eV. Thus their observation in the interstellar medium calls for study of regions of radiation protection (dark clouds) or regions where nucleobase production could successfully outweigh destruction. This is confirmed by the analogous case of the amino acid glycine which has very recently been reported to have been observed by radioastronomy in hot molecular core regions, where the visual extinction is very large, thus providing radiation protection [89,99]. The existence of nucleobases in meteorites and micrometeorites also implies that their formation and survival occurs in conditions of efficient VUV radiation shielding

as also implied by hydrogen lamp irradiation of nucleobases in low temperature matrices [100].

Acknowledgments

We thank Jean-Louis Chotin for technical assistance during BESSY runs. Support from the CNRS Groupe de Recherche "GDR Exobiologie" and from the CNES convention with INSU is gratefully acknowledged. We thank BESSY for use of its facilities in supporting the experimental studies under EC contract I 3 RII 3-CT-2004-506008. H.B. thanks the "Fonds des Chemischen Industrie" for financial support.

References

[1] A. Brack (Ed.), The Molecular Origins of Life, Cambridge University Press, Cambridge, UK, 1998.
[2] P.G. Stocks, A.W. Schwartz, Nature 282 (1979) 709.
[3] P.G. Stocks, A.W. Schwartz, Geochim. Cosmochim. Acta 45 (1981) 563.
[4] L.-L. Hua, K. Kobayashi, E.-I. Ochiai, C.W. Gerke, K.O. Gerhardt, C. Ponnamperuma, OLEB 16 (1986) 226.
[5] A. Shimoyama, S. Hagishita, K. Harada, Geochem. J. 24 (1990) 343.
[6] S. Chakrabati, S.K. Chakrabarti, Astron. Astrophys. 354 (2000) L6.
[7] I.W.M. Smith, D. Talbi, E. Herbst, Astron. Astrophys. 369 (2001) 611.
[8] J. Kissel, F.R. Krueger, Nature 326 (1987) 755.
[9] R.D. Brown, P.D. Godfrey, D. McNaughton, A.P. Pierlot, Chem. Phys. Lett. 156 (1989) 61.
[10] R.D. Brown, P.D. Godfrey, D. McNaughton, A.P. Pierlot, J. Chem. Soc. Chem. Commun. (1989) 37.
[11] R.D. Brown, P.D. Godfrey, D. McNaughton, A.P. Pierlot, J. Am. Chem. Soc. 110 (1988) 2329.
[12] P. Colarusso, K.-Q. Zhang, B. Guo, P.F. Bernath, Chem. Phys. Lett. 269 (1997) 39.
[13] M. Graindourze, J. Smets, T. Zeegers-Huyskens, G. Maes, J. Mol. Struct. 222 (1990) 345.
[14] A Yu Ivanov, A.M. Plokhotnichenko, E.D. Radchenko, G.G. Sheina, Yu.P. Blagoi, J. Mol. Struct. 372 (1995) 91.
[15] M.J. Nowak, J. Mol. Struct. 193 (1989) 35.
[16] M.J. Nowak, L. Lapinski, J. Kwiatkowski, J. Leszcynski, J. Phys. Chem. 100 (1996) 3527.
[17] L.B. Clark, G.G. Peschel, I. Tinoco Jr., J. Phys. Chem. 69 (1965) 3615.
[18] D.C. Lührs, J. Viallon, I. Fischer, Phys. Chem. Chem. Phys. 3 (2001) 1827.
[19] Chr. Plützer, E. Nir, M.S. de Vries, K. Kleinermanns, Phys. Chem. Chem. Phys. 3 (2001) 5466.
[20] M. Fujii, T. Tamura, N. Mikami, M. Ito, Chem. Phys. Lett. 126 (1986) 583.
[21] N.J. Kim, G. Jeong, Y.S. Kim, J. Sung, S.K. Kim, J. Chem. Phys. 113 (2000) 10052.
[22] K. Varmuza, W. Werther, F.R. Krueger, J. Kissel, E.R. Schmid, Int. J. Mass Spectrom. 189 (1999) 79.
[23] N.S. Hush, A.S. Cheung, Chem. Phys. Lett. 34 (1975) 11.
[24] S. Urano, X. Yang, P.R. LeBreton, J. Mol. Struct. 214 (1989) 315.
[25] G. Lauer, W. Schäfer, A. Schweig, Tetrahedron Lett. 45 (1975) 3939.
[26] C. Yu, T.J. O'Donnell, P.R. LeBreton, J. Phys. Chem. 85 (1981) 3851.
[27] M.H. Palmer, I. Simpson, R.J. Platenkamp, J. Mol. Struct. 66 (1980) 243.
[28] D. Dougherty, K. Wittel, J. Meeks, S.P. McGlynn, J. Am. Chem. Soc. 98 (1976) 3817.
[29] M. Kubota, T. Kobayashi, J. Electr. Spectrosc. Rel. Phenom. 82 (1996) 61.
[30] S. Peng, A. Padva, P.R. LeBreton, Proc. Natl. Acad. Sci. USA 73 (1976) 2966.
[31] J. Lin, C. Yu, S. Peng, I. Akiyama, K. Li, Li. Kao Lee, P.R. LeBreton, J. Am. Chem. Soc. 102 (1980) 4627.
[32] J.M. Rice, G.O. Dudek, M. Barber, J. Am. Chem. Soc. 87 (1965) 4569.
[33] J.M. Rice, G.O. Dudek, J. Am. Chem. Soc. 89 (1967) 2719.
[34] J. Ulrich, R. Teoule, R. Massot, A. Cornu, Org. Mass Spectrom. 2 (1969) 1183.
[35] J.L. Occolowitz, Chem. Commun. (1968) 1226.
[36] M.G. Barrio, D.I.C. Scopes, J.B. Holtwick, N.J. Leonard, Proc. Natl. Acad. Sci. USA 78 (1981) 3986.
[37] S.K. Sethi, S.P. Gupta, E.E. Jenkins, C.W. Whitehead, L.B. Townsend, J.A. McCloskey, J. Am. Chem. Soc. 104 (1982) 3349.
[38] J.A. McCloskey, in: P.O.P. TS'O (Ed.), Basic Principles in Nucleic Acid Chemistry, vol. I, Academic Press, New York, 1974, p. 209.
[39] E.G. Brown, B.S. Mangat, Biochim. Biophys. Acta 177 (1969) 427.
[40] K.C. Smith, R.T. Aplin, Biochemistry 5 (1966) 2125.
[41] S.M. Hecht, A.S. Gupta, N.J. Leonard, Biochim. Biophys. Acta 182 (1969) 444.
[42] S. Gohlke, E. Illenberger, Europhys. News 33 (2002) 207.
[43] R. Abouaf, J. Pommier, H. Dunet, Int. J. Mass Spectrom. 226 (2003) 397.
[44] J. deVries, R. Hoekstra, R. Morgenstern, T. Schlathölter, Phys. Rev. Lett. 91 (2003) 053401.
[45] L.P. Candeias, S. Steenken, J. Am. Chem. Soc. 114 (1992) 699.
[46] L.H. Seah, L.A. Burgoyne, J. Photochem. Photobiol. B 61 (2001) 10.
[47] E.M. Conwell, D.M. Basko, J. Am. Chem. Soc. 123 (2001) 11441.
[48] A. Heller, Faraday Discuss 116 (2000) 1.
[49] M. Bixon, J. Jortner, J. Am. Chem. Soc. 123 (2001) 12556.
[50] F. Jolibois, J. Cadet, A. Grand, R. Subra, V. Barone, N. Rega, J. Am. Chem. Soc. 120 (1998) 1864.
[51] P.-W. Hou, R.P. Rampling, J. Appl. Phys. 47 (1976) 4572.
[52] L.C. Emerson, M.W. Williams, I'lan. Tang, R.N. Hamm, E.T. Arakawa, Radiat. Res. 63 (1975) 235.
[53] I.P. Vinogradov, V.V. Zemskikh, N. Ya Daononova, Opt. Spectrosc. 36 (1974) 344.
[54] T. Yamada, H. Fukutome, Biopolymers 6 (1968) 43.
[55] A. Pinchuk, J. Quant. Spectrosc. Radiat. Transfer 85 (2004) 211.
[56] R. Abouaf, J. Pommier, H. Dunet, Chem. Phys. Lett. 381 (2003) 486.
[57] M. Isaacson, J. Chem. Phys. 56 (1972) 1803.
[58] E.T. Arakawa, L.C. Emerson, S.I. Juan, J.C. Ashley, M.W. Williams, Photochem. Photobiol. 44 (1986) 349.
[59] T. Inagaki, A. Ito, K. Hieda, T. Ito, Photochem. Photobiol. 44 (1986) 303.
[60] H.W. Jochims, E. Rühl, H. Baumgärtel, S. Tobita, S. Leach, Int. J. Mass Spectrom. Ion Processes 167/168 (1997) 35.
[61] C. Chyba, C. Sagan, Nature 355 (1992) 125.

[62] M. Schwell, F. Dulieu, S. Leach, in: Proceedings of the First European Workshop on Exo-/Astro-Biology ESA 29-496, 2001, p. 133.
[63] M. Schwell, F. Dulieu, S. Leach, Astrobiology 1 (2001) 210.
[64] M. Schwell, F. Dulieu, C. Gée, H.-W. Jochims, J.-L. Chotin, H. Baumgärtel, S. Leach, Chem. Phys. 260 (2000) 261.
[65] NIST Chemistry WebBook. Available from: <http://webbook.nist.gov>.
[66] S. Leach, Z. Phys. Chem. 195 (1996) 15.
[67] V.M. Orlov, A.N. Smirnov, Ya.M. Varshavsky, Tetrahedron Lett. 48 (1976) 4377.
[68] C. Lifschitz, E.D. Bergmann, B. Pullman, Tetrahedron Lett. 46 (1967) 4583.
[69] B.I. Verkin, L.F. Sukodub, I.K. Yanson, Dokl. Akad. Nauk SSSR 228 (1976) 1452.
[70] S.K. Kim, W. Lee, D.R. Herschbach, J. Phys. Chem. 100 (1996) 7933.
[71] Chr. Plützer, K. Kleinermanns, Phys. Chem. Chem. Phys. 4 (2002) 4877.
[72] C.T. Hwang, C.L. Stumpf, Y.-Q. Yu, H.I. Kenttämaa, Int. J. Mass Spectrom. 182/183 (1999) 253.
[73] A.-O. Colson, B. Besler, D.M. Close, M.D. Sevilla, J. Phys. Chem. 96 (1992) 661.
[74] S.D. Wetmore, R.J. Boyd, L.A. Eriksson, J. Phys. Chem. B 102 (1998) 10602.
[75] R. Improta, G. Scalmani, V. Barone, Int. J. Mass Spectrom. 201 (2000) 321.
[76] J. Reynisson, S. Steenken, PCCP 4 (2002) 527.
[77] D.L. Hildebrand, Int. J. Mass Spectrom. 197 (2000) 237.
[78] S.G. Lias, J.E. Bartmess, J.F. Libman, J.L. Holmes, R.D. Levin, W.G. Mallard, J. Phys. Chem. Ref. Data 17 (Suppl. 1) (1988).
[79] A.W. Potts, D.M.P. Holland, A.B. Trofimov, J. Schirmer, L. Karlsson, K. Siegbahn, J. Phys. B 36 (2003) 3129.
[80] H.W. Jochims, H. Baumgärtel, S. Leach, Astron. Astrophys. 314 (1996) 1003.
[81] E. Subertova, J. Bok, P. Rihak, V. Prosser, E. Silinsh, Phys. Stat. Sol. (a) 18 (1973) 741.
[82] P.C. Burgers, J.L. Holmes, J.K. Terlouw, J. Am. Chem. Soc. 106 (1984) 2762.
[83] E. Uggerud, H. Schwarz, J. Am. Chem. Soc. 107 (1985) 5046.
[84] M. Inokuti, Rev. Mod. Phys. 43 (1971) 297.
[85] C. Adamo, V. Barone, Chem. Phys. Lett. 274 (1997) 242.
[86] M. Vega-Arroyo, P.R. LeBreton, T. Rajh, P. Zapol, L.A. Curtiss, Chem. Phys. Lett. 380 (2003) 54.
[87] G. Dujardin, S. Leach, O. Dutuit, T. Govers, P.M. Guyon, J. Chem. Phys. 79 (1983) 644.
[88] T. Kobayashi, T. Kubota, K. Ezumi, C. Utsunomiya, Bull. Chem. Soc. Jpn. 55 (1982) 3915.
[89] H.W. Jochims, M. Schwell, J.-L. Chotin, M. Clemino, F. Dulieu, H. Baumgärtel, S. Leach, Chem. Phys. 298 (2004) 279.
[90] S. Denifl, B. Sonnweber, G. Hanel, P. Scheier, T.D. Märk, Int. J. Mass Spectrom. 238 (2004) 47.
[91] B. Coupier, B. Farizon, M. Farizon, M.J. Gaillard, F. Gobert, N.V. de Castro Faria, G. Jalbert, S. Ouaskit, M. Carré, B. Gstir, G. Hanel, S. Denifl, L. Feketeova, P. Scheier, T.D. Märk, Eur. Phys. J. D 20 (2002) 459.
[92] V.I. Zaretskii, V.I. Sadovskaya, N.S. Wulfson, V.F. Sizoy, V.G. Merimson, Org. Mass Spectrom. 5 (1971) 1179.
[93] A. Padva, P.R. LeBreton, R.J. Dinerstein, J.N.A. Ridyard, Biochem. Biophys. Res. Commun. 60 (1974) 1262.
[94] S.D. Wetmore, R.J. Boyd, L.A. Eriksson, Chem. Phys. Lett. 322 (2000) 129.
[95] I.C. Walker, M.H. Palmer, J. Delwiche, S.V. Hoffmann, P. Limao Vieora, N.J. Mason, M.F. Guest, M.-J. Hubin-Franskin, J. Heinesch, A. Giuliani, Chem. Phys. 297 (2004) 289.
[96] H.-E. Audier, M. Fétizon, Y. Henry, T. Prangé, Org. Mass Spectrom. 11 (1976) 1047.
[97] S. Feil, K. Gluch, S. Matt-Leubner, P. Scheier, J. Limtrakul, M. Probst, H. Deutsch, K. Becker, A. Stamatovic, T.D. Märk, J. Phys. B 37 (2004) 3013.
[98] G. Hanel, B. Gstir, S. Denifl, P. Scheier, M. Probst, B. Farizon, E. Illenberger, T.D. Märk, Phys. Rev. Lett. 90 (2003) 188104-1.
[99] Y.-J. Kuan, S.B. Charnley, H.-C. Huang, W.-L. Tseng, Z. Kisiel, Astrophys. J. 593 (2003) 848.
[100] Z. Peeters, O. Botta, S.B. Charnley, R. Ruitenkamp, P. Ehrenfreund, Astrophys. J. Lett. 593 (2003) L129.

Available online at www.sciencedirect.com
SCIENCE DIRECT
Chemical Physics 321 (2006) 159–170
Chemical Physics
www.elsevier.com/locate/chemphys

VUV absorption spectrum of acetic acid between 6 and 20 eV

Sydney Leach [a,*], Martin Schwell [b], Sun Un [c], Hans-Werner Jochims [d], Helmut Baumgärtel [d]

[a] LERMA, CNRS-UMR 8112, Observatoire de Paris-Meudon, 5 place Jules-Janssen, 92195 – Meudon, France
[b] Laboratoire Interuniversitaire des Systèmes Atmosphériques (LISA), CNRS-UMR 7583, Universités Paris 7 et 12, 61 Avenue du Général de Gaulle, 94010 Créteil, France
[c] Service de Bioénergetique, CNRS URA 2096, DBJC, CEA Saclay, 91191 Gif-sur-Yvette, France
[d] Institut für Physikalische und Theoretische Chemie der Freien Universität Berlin, Takustr. 3, 14195 Berlin, FR Germany

Received 10 June 2005; accepted 18 August 2005
Available online 11 October 2005

Abstract

Absorption spectra of acetic acid were measured between 6 and 20 eV at a resolution of 8 meV. Previous measurements had a spectral limit of 11.7 eV. Analysis and band assignment were aided by data from theoretical calculations on valence states and from photoelectron spectroscopy. Valence transitions and $n$sa′ ← 13a′, $n$pa′ ← 13a′ and $n$da′ ← 13a′ Rydberg transitions converging to the ground state of CH_3COOH^+, as well as transitions converging to the first excited state of the ion are discussed and assigned in the spectral region below 12 eV. Our assignments of valence transitions differ in many aspects from those of previous studies. Most of the Rydberg bands have never previously been assigned. Observation, analysis and possible assignments of absorption features between 12 and 20 eV were carried out for the first time. Rydberg bands converging to the higher ionization limits merge to form broad absorption features. Some absorption features in the 14–17 eV region are assigned to two types of valence σ*(C–H) ← σ transitions.

Keywords: Acetic acid; VUV absorbption spectra; Electronic transition calculations and assignments

1. Introduction

Acetic acid, CH_3COOH, is considered to be an important trace species in the Earth's atmosphere [1]. It is also one of the possible building blocks of biomolecules [2] and it is formed in Miller–Urey experiments on simulated atmospheres of the Early Earth [3]. It has been observed by radioastronomy in the SGR B2 Large Molecule Heimat (LMH) source, using interferometric arrays [4]. There is reason to believe that the amino acid glycine could also exist in an interstellar source of CH_3COOH [5], and indeed this amino acid has been reported to have been detected in three hot molecular cores, including Sgr B2 (N-LMH), where CH_3COOH is also observed [6]. Although no direct cometary observation of acetic acid has been made, abundance upper limits have been determined for various comets, based on radio spectroscopic observations, in particular a limit of 0.06% for acetic acid in the bright comet Hale–Bopp [7]. Increased sensitivity in new ground-based radiotelescopes, and the possibility of more extended search frequencies in space-borne observatories, make it likely that acetic acid will be observed in future cometary studies. The photophysical properties of CH_3COOH in the UV and VUV are thus of direct interest for undertaking radioastronomy searches, for cometary science and for atmospheric and exobiology studies.

We have carried out a number of photophysical measurements on acetic acid, in particular on dissociative ionization yields over the 6–22 eV energy range, the dispersed fluorescence spectrum excited at several VUV photon energies, and excitation spectra for various fluorescence bands [8]. The present work concerns the absorption spectrum

* Corresponding author. Tel.: +33 1 4507 7561; fax: +33 1 4507 7100.
E-mail address: sydney.leach@obspm.fr (S. Leach).

0301-0104/$ - see front matter © 2005 Elsevier B.V. All rights reserved.
doi:10.1016/j.chemphys.2005.08.044

of CH_3COOH between 6 and 20 eV. The absorption results have been important for interpretation of the results of the photophysical investigations. Earlier absorption and fluorescence spectra with comparable resolution were limited to measurements below 11.7 eV [9,10]. Reported electron energy loss spectra [11] of CH_3COOH, limited to about 15 eV, are of low resolution.

The earlier absorption spectra reported by Bell et al. [9] are in the 4.8–11.27 eV and by Suto et al. [10] in the 5.17–11.7 eV region. Barnes and Simpson [12] studied the 5.0–9.9 eV and Nagakura et al. [13] the 6.5–8.0 eV region absorption. Absolute absorption cross-section values of Suto et al. are lower than those measured by Barnes and Simpson and by Nagakura et al. Since absorption cross-sections at $\lambda > 190$ nm are very small it was necessary for them to use higher gas pressures (up to 0.7 Torr); thus acetic acid dimers could have contributed to measured absorption cross-sections in this spectral region, a region which we did not explore. The excited states of CH_3COOH were labelled A, A′, B, C, etc. by Bell et al. [9] by analogy with HCOOH. They suggested that absorption bands at $\lambda < 155$ nm are probably Rydberg series converging on the ground state of the acetic acid ion, but made few assignments.

2. Experimental

Absorption spectra were measured with an experimental set-up whose essential components and procedure have been described previously [14] so that only a brief resumé is given here. Monochromatised synchrotron radiation was obtained from the Berlin electron storage ring BESSY I (multi-bunch mode) in association with a M-225 McPherson monochromator modified to have a focal length of 1.5 m, and a gold coated spherical diffraction grating having 1200 lines/mm. Spectral dispersion was 5.6 Å/mm. The mean geometric slit width was 0.1 mm. The 30 cm long absorption cell is separated from the monochromator vacuum by a 1 mm thick stainless steel microchannel plate (MCP). Acetic acid gas pressures were in the range 20–40 μbar, measured with a Balzers capacitance manometer. This is a pressure region where the concentration of acetic acid dimers to monomers is negligibly small [10]. The small pressure gradient inside the absorption cell, due to the gas leak through the MCP, does not significantly affect the optical density measurements. The use of the MCP enables us to know the precise optical pathlength, the pressure drop being by a factor of the order of 1000, which ensures linearity in the Beer–Lambert analysis of the optical density measurements. VUV light transmission efficiency of the MCP is estimated to be about 10% and the transmitted light was largely sufficient for absorption measurements. Transmitted radiation strikes a window covered with a layer of sodium salicylate whose ensuing fluorescence was detected by a photomultiplier. We remark that the use of a laminar-type grating results in a very low (only few percent) contribution to second order radiation in the 10–20 eV region. Second order effects will be also very low below 10 eV because the gas column in the absorption cell reduces high energy radiation transmission much more than the low energy part. The determination of absolute absorption cross-sections, using the Beer–Lambert law, provided cross-section values whose uncertainties were ±10%.

Two scans, one with and one without acetic acid gas were carried out for determining the absorption spectrum. During a scan, the VUV light intensity falls off slightly due to continuous loss of electrons in the storage ring. The incident light intensity is furthermore a function of the energy-dependent reflectance of the diffraction grating. These two factors have been taken into account in normalisation of the spectra, which were recorded at an energy interval of 9 meV.

Absorption measurements were carried out in April 1999 at two gas pressures, 20 and 40 μbar. They were repeated in October 1999. The results were quasi-identical. The resolution is about 8 meV (at 100 nm) and the precision of the energy scale is ±5 meV. Commercial CH_3COOH of highest available purity grade was used, without further purification.

3. Calculations

Quantum chemical calculations were carried out using GAUSSIAN-03 revision B.05 [15]. An initial geometry optimization of acetic acid was performed using the hybrid density functional B3LYP and 6-311++G(3DF,3PD) basis set. "Tight" convergence criteria were used. The optimized geometry was that of the most stable form, of *cis* configuration, the lowest energy isomer. The calculated structural parameters are in good agreement with the gas phase experimental values determined by electron diffraction [16]. The calculated and, in brackets, the gas phase experimental values are as follows (bondlengths in Ångstrom units, bond angles in degrees): C–O 1.360 (1.364), C=O 1.213 (1.214), C–C 1.506 (1.520), O–H 0.972 (0.970), C–H 1.089 (1.102), C–H 1.094 (1.094), O–O 2.253 (2.264), O–C=O 122.20 (122.80), C–C=O 126.10 (126.60), C–C–O 111.70 (110.60, C–O–H 107.00 (107.00). Normal mode analysis confirmed that the final optimized geometry was a true potential energy minimum. The energies and oscillator strengths of transitions to the first 50 electronic excited states were calculated using the time-dependent DFT method [17] with the same hybrid density function and basis set. Such calculations are not expected to provide good values for transition energies beyond about 9 eV in the case of acetic acid, since the eigenvalues are critically dependent on MO energy differences in time-dependent DFT calculations. However, these calculations differentiate well between strong and weak electronic transitions, thus facilitating the valence transition assignments. Molecular orbitals were visualized using the program MOLDEN [18].

4. Results and discussion

4.1. Absorption spectra: general characteristics

The complete absorption spectrum of acetic acid between 6 and 20 eV is given in Fig. 1. Successive sections of the absorption spectra between 6 and 12 eV are shown in Figs. 2 and 3. The band assignments are listed in Table 1 but, for the sake of visual clarity, not all assignments are indicated in the figures. Features measured in the 7–18 eV region are listed as band numbers, energies and band assignments in Table 1, along with the quantum defects of the Rydberg levels, determined for the origin bands of the Rydberg transitions. In Table 1, the energies of the observed features are quoted to 1 meV and to 1 cm^{-1}; the uncertainties in repeated measurements of the peak frequencies of sharp features are of the order of 10–20 cm^{-1} and those of broad features are somewhat greater. The maximum absorption cross-section of 72.2 Mb occurs at 16.83 eV (Fig. 1). Suto et al. [10] published absorption spectra over the 5.17–9.43 eV region, using synchrotron radiation as spectral source. Our cross-sections are in general good agreement with those of Suto et al. in the 6–9.4 eV region common to both measurements and also with the cross-sections of Nagakura et al. [13] who measured the absorption spectrum in the 6.5–8.1 eV region at low resolution.

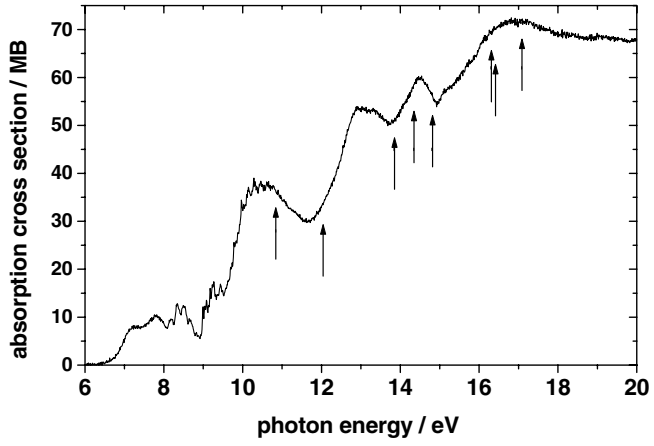

Fig. 1. Overview of the absorption spectrum of CH_3COOH in the 6–20 eV region. Arrows indicate vertical ionization energies.

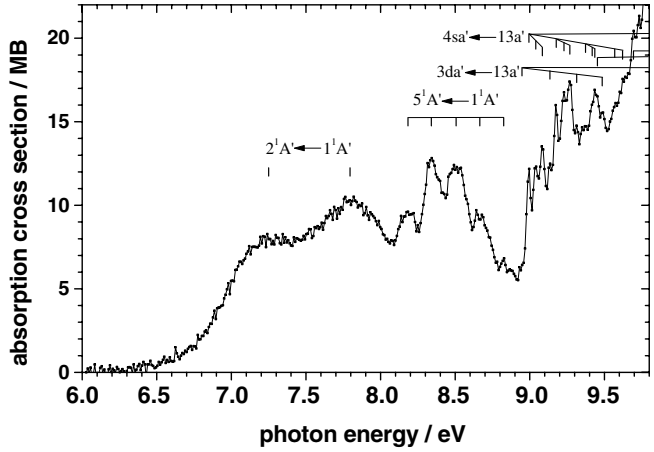

Fig. 2. CH_3COOH absorption spectrum: 6.0–9.8 eV.

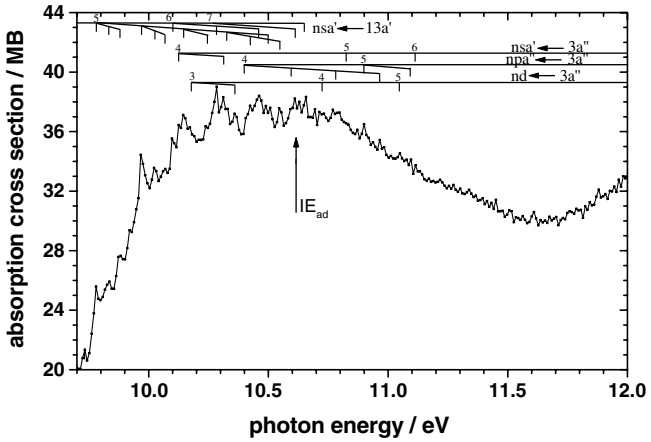

Fig. 3. CH_3COOH absorption spectrum: 9.7–12 eV.

Bell et al. [9] carried out photographic absorption spectroscopy of acetic acid in the 4.8–11.3 eV region. Electron energy loss spectra (EELS) of acetic acid have been measured in the 5–15 eV region [11] and assignments of valence shell and Rydberg transitions have been discussed by comparison with the optical absorption spectra of Barnes and Simpson [12]. A comparison between the published EELS spectrum and our and other optical absorption spectra clearly indicate that the EELS resolution is insufficient for anything but qualitative discussion.

4.2. Absorption spectra: theoretical considerations and implications for analysis

The distinction between valence and Rydberg transitions is not always easy to establish since there can be quite a lot of mixing between valence and Rydberg states. Our analysis of the absorption spectrum of acetic acid seeks to characterise those states that are predominantly valence or predominantly Rydberg in character. For this we use a number of criteria, such as comparison with calculated energies and transition strengths, the nature of the molecular orbitals involved in the optical transitions and their effects on structural and vibrational properties. These criteria will be discussed as they arise in this work.

In order to analyse valence and Rydberg transitions in the absorption spectra of acetic acid, and to distinguish between them, we first examine the electron configurations and structures of CH_3COOH and CH_3COOH^+.

4.2.1. CH_3COOH electron configurations and structures

The ground state of neutral acetic acid formally belongs to the C_s symmetry group. As stated above, its most stable form corresponds to the lowest energy isomer, of

Table 1
Acetic acid absorption features and transition assignments in the 6.8–18 eV spectral region

Band No.	Energy/eV	Frequency ν/cm^{-1}	Assignment	Quantum defect[a] δ
1	7.250	58,479	$2^1A' \leftarrow 1^1A'$	
2	7.795	62,874	See text	
3	8.183	66,004	$5^1A' \leftarrow 1^1A'(0_0^0)$	
4	8.340	67,270	$5^1A' \leftarrow 1^1A'(\nu_{\mathrm{def}\,0}^1)$	
5	8.506	68,609	$5^1A' \leftarrow 1^1A'(\nu_{\mathrm{def}\,0}^2)$	
6	8.665	69,892	$5^1A' \leftarrow 1^1A'(\nu_{\mathrm{def}\,0}^3)$	
7	8.825	71,182	$5^1A' \leftarrow 1^1A'(\nu_{\mathrm{def}\,0}^4)$	
8	8.948	72,170	$3da' \leftarrow 13a'(0_0^0)$	0.14 (3d)
9α	8.994	72,546	$4sa' \leftarrow 13a'(0_0^0)$	1.10 (4s)
10β	9.040	72,917	$4sa' \leftarrow 13a'(12_0^1)$	
11γ	9.084	73,272	$4sa' \leftarrow 13a'(12_0^2)$	
12	9.135	73,683	$3da' \leftarrow 13a'(4_0^1)$	
13α	9.177	74,022	$4sa' \leftarrow 13a'(4_0^1)$	
14β	9.229	74,441	$4sa' \leftarrow 13a'(4_0^112_0^1)$	
15γ	9.268	74,756	$4sa' \leftarrow 13a'(4_0^112_0^2); 3pa'' \leftarrow 3a''(0_0^0)$	*0.60* (3p)
16	9.314	75,127	$3da' \leftarrow 13a'(4_0^2)$	
17α	9.373	75,603	$4sa' \leftarrow 13a'(4_0^2)$	
18β	9.418	75,966	$4sa' \leftarrow 13a'(4_0^212_0^1)$	
19γ	9.435	76,103	$4sa' \leftarrow 13a'(4_0^212_0^2); 4pa' \leftarrow 13a'(0_0^0)$	0.64 (4p)
20	9.453	76,248	$3pa'' \leftarrow 3a''(4_0^1)$	
21	9.485	76,506	$3da' \leftarrow 13a'(4_0^3)$	
22β	9.569	77,184	$4sa' \leftarrow 13a'(4_0^312_0^1)$	
23γ	9.622	77,611	$4sa' \leftarrow 13a'(4_0^312_0^2); 4pa' \leftarrow 13a'(4_0^1)$	
24	9.695	78,200	$4da' \leftarrow 13a'(0_0^0)$	0.15 (4d)
25	9.732	78,498	$7^1A' \leftarrow 1^1A'(0_0^0)$	
26ε	9.781	78,894	$5sa' \leftarrow 13a'(0_0^0); 4pa' \leftarrow 13a'(4_0^2)$	0.96 (5s)
27ζ	9.833	79,313	$5sa' \leftarrow 13a'(12_0^1)$	
28η	9.880	79,692	$5sa' \leftarrow 13a'(12_0^2)$	
29	9.922	80,031	$5pa' \leftarrow 13a'(0_0^0)$	0.57 (5p)
30ε	9.970	80,418	$5sa' \leftarrow 13a'(4_0^1)$	
31ζ	10.026	80,870	$5sa' \leftarrow 13a'(4_0^112_0^1)$	
32η	10.068	81,208	$5sa' \leftarrow 13a'(4_0^112_0^2); 5da' \leftarrow 13a'(0_0^0)$	0.13 (5d)
33	10.101	81,475	$6sa' \leftarrow 13a'(0_0^0); 5pa' \leftarrow 13a'(4_0^1)$	0.86 (6s)
34	10.125	81,663	$4sa' \leftarrow 3a''(0_0^0)$	*0.99* (4s)
35ε	10.146	81,838	$5sa' \leftarrow 13a'(4_0^2); 6sa' \leftarrow 13a'(12_0^1); 6pa' \leftarrow 13a'(0_0^0)$	0.61 (6p)
36	10.178	82,091	$3d \leftarrow 3a''(0_0^0)$	*0.06* (3d)
37η	10.245	82,636	$5sa' \leftarrow 13a'(4_0^212_0^2); 7sa' \leftarrow 13a'(0_0^0)$	0.94 (7s)
38	10.283	82,943	$6sa' \leftarrow 13a'(4_0^1); 5pa' \leftarrow 13a'(4_0^2); 7pa' \leftarrow 13a'(0_0^0)$	0.60 (7p)
39	10.313	83,185	$4sa' \leftarrow 3a''(4_0^1)$	
40 ε	10.326	83,284	$5sa' \leftarrow 13a'(4_0^3); 6sa' \leftarrow 13a'(4_0^112_0^1); 6pa' \leftarrow 13a'(4_0^1)$	
41	10.360	83,564	$3d \leftarrow 3a''(4_0^1)$	
42	10.399	83,873	$4pa'' \leftarrow 3a''(0_0^0)$	*0.67* (4p)
43η	10.424	84,080	$5sa' \leftarrow 13a'(4_0^312_0^2); 7sa' \leftarrow 13a'(4_0^1)$	
44	10.459	84,362	$6sa' \leftarrow 13a'(4_0^2); 7pa' \leftarrow 13a'(4_0^1)$	
45ε	10.499	84,685	$5sa' \leftarrow 13a'(4_0^4); 6pa' \leftarrow 13a'(4_0^2)$	
46ζ	10.548	85,080	$5sa' \leftarrow 13a'(4_0^412_0^1)$	
47	10.595	85,454	$4pa'' \leftarrow 3a''(4_0^1)$	
48	10.612	85,596	$7sa' \leftarrow 13a'(4_0^2)$	
49	10.654	85,935	$7pa' \leftarrow 13a'(4_0^2)$	
50	10.724	86,500	$4d \leftarrow 3a''(0_0^0)$	*0.12* (4d)
51	10.781	86,960	$4pa'' \leftarrow 3a''(4_0^2)$	
52	10.794	87,059	$7sa' \leftarrow 13a'(4_0^3)$	
53	10.825	87,314	$5sa' \leftarrow 3a''(0_0^0)$	*0.89* (5s)
54	10.899	87,911	$5pa'' \leftarrow 3a''(0_0^0)$	*0.68* (5p)
55	10.965	88,444	$4pa'' \leftarrow 3a''(4_0^3)$	
56	11.047	89,105	$5d \leftarrow 3a''(0_0^0)$	*0.17* (5d)
57	11.092	89,463	$5pa'' \leftarrow 3a''(4_0^1)$	
58	11.113	89,632	$6sa' \leftarrow 3a''(0_0^0)$	*0.87* (6s)
59	12.922	104,229	[b]	
60	13.330	107,520	[b]	
61	14.500	116,957	σ*(C–H) ← σ (non-n.h. transition)[d]	
62	15.125	121,991	[c]	
63	15.770	127,201	[c]	
64	16.830	135,751	σ*(C–H) ← σ[d]	

[a] Quantum defects are of the origin bands of Rydberg series converging to the ion ground state $1^2A'$ and, in italics, of Rydberg levels converging to the first excited ion state $1^2A''$.

[b] Region of broad overlapping Rydberg bands converging to the $2^2A''$ ion state.

[c] Broad overlapping Rydberg bands converging to the highly excited ion states.

[d] See text.

cis configuration, in which both the OH bond and a CH bond are eclipsed with the carbonyl bond. The *trans* form is calculated (ab initio methods [19]) to lie 2100–2500 cm^{-1} above the *cis* configuration.

The electron configuration of CH_3COOH is, according to our molecular orbital energy calculations:

$$\ldots\ldots(7a')^2(8a')^2(9a')^2(10a')^2(1a'')^2(11a')^2(12a')^2(2a'')^2(3a'')^2(13a')^2, \quad 1^1A'.$$

The calculated MO energies, relative to the experimental ionization energy, are compared in Table 2 with reported values of vertical ionization energies determined from He I [20] and He II photoelectron spectroscopy [21] and, for inner shell ionizations, the results of inner shell electron energy loss (ISEEL) spectroscopy [22]. This table also contains the results of HAM/3 [21] and GAUSSIAN-70 [20] calculations of molecular orbital energies, as well as those of Urquhart and Ade [23] for inner shell orbitals. Our calculated order of the occupied molecular orbitals is the same as that in the GAUSSIAN-70, 4-31G calculations of Carnovale et al. [20], but the order of the close-lying 1a″ and 10a′ MO's are reversed in the HAM/3 calculations of von Niessen et al. [21].

Agreement between our calculated valence shell orbital energies and the experimental values is very satisfactory. Our calculated values for the valence MO's are more extensive than the other theoretical values in Table 2, and they agree somewhat better with the results of photoelectron spectroscopy. The inner shell orbitals are in large measure 1s atomic orbitals. Our calculations on the inner shell orbitals, presented here for completion, fall short of the experimental values, no doubt due to core hole effects, which are not adequately dealt with in our calculation method. This is reflected in the non-negligible population of 2s carbon or oxygen atomic orbitals which we find from a population analysis of each of the four deepest molecular orbitals. An improved virtual orbital approximation in calculations using Kosugi's GSF3 package [24], enabled Urquhart and Ade [23] to calculate inner shell values in good agreement with carbonyl core values determined by ISEELS. It is of interest, nevertheless, that in our calculations, although the absolute energies of the inner shell MOs are 20–30 eV below the experimental values, the energy differences between the 3a′ and 4a′ orbitals, 3.38 eV, and 1a′ and 2a′ orbitals, 1.56 eV, are similar to the experimental differences for the carbon (4.0 eV) and oxygen (1.8 eV) orbitals (Table 2).

The bonding characters of the highest four occupied molecular orbitals, 13a′, 3a″, 2a″ and 12*a*′, were determined from our MO contour analyses (Fig. 4). They are consistent, insofar as being either a π or a σ orbital, with the assignments of Carnovale et al. [20] and of Cannington and Ham [25], based in part on ratios of HeI/HeII photoelectron spectral band intensities. For the 12a′ MO, they differ from that of Kimura et al. [26] who considered it to be a π orbital, based on partial sums of vertical ionization energies. However, Carnovale et al. [20] observed that the assignment of 12a′ as a σ orbital agrees equally well with the defined partial sums. The bonding characteristics of the next four occupied MO's, given below, are based on our assessment of the assignments of Carnovale et al. [20], Cannington and Ham [25] and Kimura et al. [26].

–13a′ is mainly non-bonding n_O on the O atom lone pair of the carbonyl group,
–3a″ is $\pi_{C=O}$ mixed with n_{OH}, the latter being mainly localised on the O atom of OH,
–2a″ is π_{OCO},
–12a′ is σ_{CC},
–11a′ is σ_{CO} within the O–C–O framework,
–1a″ is π_{OCO} mixed with n_{OH} and π_{CH3},
–10a′ is σ_{OCO},
–9a′ is σ_{OH}.

Table 2
Calculated and experimental vertical ionization energies of acetic acid

Molecular orbital	Calculated IE/eV Present study (GAUSSIAN-03)	Calculated IE/eV HAM/3 ([21])	Calculated IE/eV (GAUSSIAN-70) ([20]) and GSCF3† ([23])	Experimental IE/eV He I PES ([20])	Experimental IE/eV He II PES [21] and ISEEL spectra* [22]
13a′	(10.84)	10.96	11.16	10.84	10.9
3a″	12.08	11.96	11.79	12.03	12.1
2a″	13.90	13.81	13.82	13.84	(13.6–15.0)
12a′	14.01	13.98	13.94	14.34	(13.6–15.0)
11a′	14.39	14.24	14.12	14.80	(13.6–15.0)
1a″	16.00	15.85	16.05	16.3	16.4
10a′	16.25	15.64	16.71	16.4	16.4
9a′	16.57	16.28	17.15	17.08	17.1
8a′	19.86	19.52			20.3
7a′	23.83	23.62			24.4
6a′	30.91	32.00			
5a′	33.34	33.78			
4a′	269.32				291.6*(CH_3)
3a′	272.70		296.52†		295.6*(C=O)
2a′	512.38		533.29†		538.3*(CO)
1a′	513.94				540.1*(OH)

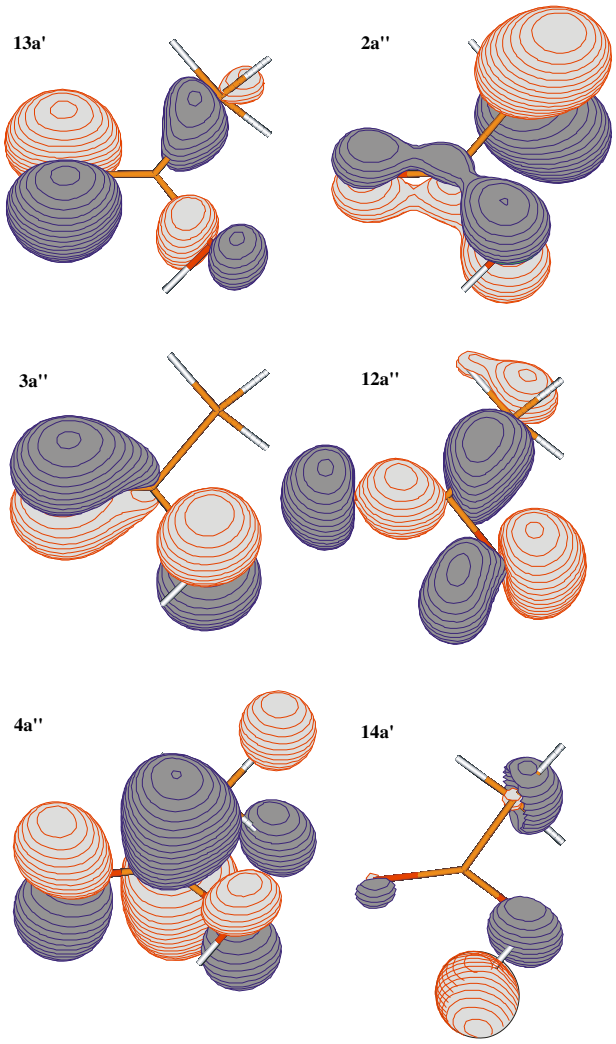

Fig. 4. Acetic acid molecular orbital contours calculated with the Molden programme [18].

Based on analogies with formic acid, we can expect that the lowest unoccupied molecular orbital will be: 4a″, a $\pi^*_{C=O}$ MO. Our initial DFT time-dependent molecular orbital calculations at the 6-31G + (d,f) level with a B2LYP density functional appeared to confirm this, but they predicted that the LUMO + 1, 14a′(σ^*_{OH}) to be only 122 meV higher. This is a relatively small energy difference so that their order could be very sensitive to the type and basis set of the MO calculation. Indeed, further calculations, at the B3LYP + 6-311** level gave the lowest unoccupied molecular orbital as 14a′, with 4a″ lying 147 meV above. Calculations of their molecular orbital contours (Fig. 4) confirmed the bonding properties, mentioned above, of the 14a′ and 4a″ MO's.

The adiabatic ionization energy (IE(ad)) of acetic acid has been reported, by Knowles and Nicholson [29], in an early photoionization mass spectrometry (PIMS) measurement, to be 10.644 ± 0.002 and 10.66 ± 0.01 eV by Villem and Akopyan [30], and by Watanabe et al. [31], from HeI photoelectron spectroscopy, to be 10.664 ± 0.003 eV. In a recent PIMS study of acetic acid [8] we measured IE-(ad) = 10.58 ± 0.02 eV, which is slightly lower than the above values. We consider that the ion ground state $1^2A'$ has the electron configuration: …$(12a')^2(2a'')^2$ $(3a'')^2(13a')$, $1^2A'$. The $1^2A''$ first excited electronic state of the ion is at 11.63 ± 0.01 eV (adiabatic energy from photoelectron spectroscopy [31]), of configuration …$(12a')^2(2a'')^2(3a'')(13a')^2$. The characteristics of higher excited states of the acetic acid ion will be discussed later.

4.2.2. Valence states and transitions of CH_3COOH

Previous assignments of the valence bands in the absorption spectra of acetic acid have been based on correlations between spectra of formic acid and other carboxylic acids [12,27,28]. In line with our previous study on formic acid, we will be concerned with the valence transitions discussed below (Table 3). Considering the effective symmetry of acetic acid to be C_s, we discuss the transition dipoles as being in plane (1A′ ← 1A′), expected to be strong, or out of plane (1A″ ← 1A′), expected to be weak [27,32]:

1) The lowest energy singlet–singlet valence transition, because of its weak intensity (see below), we interpret, on a one electron transition basis, as

$$\ldots(12a')^2(2a'')^2(3a'')^2(13a')^2, \quad 1^1A'$$
$$\rightarrow \ldots(12a')^2(2a'')^2(3a'')^2(13a')(4a''), \quad 1^1A''.$$

Table 3
Valence transitions in acetic acid: calculated and experimental transition energies and oscillator strengths

Transitions between electronic states	Principal configurations involved in electronic transitions[a]	Calculated transition energy (eV) and oscillator strength	Experimental transition energy (eV) and oscillator strength
$1^1A'' \leftarrow 1^1A'$	4a″ ← 13a′; *5a″ ← 13a′*	5.825 (0.0005)	≈6.0 (0.001)
$2^1A' \leftarrow 1^1A'$	14a′ ← 13a′	6.669 (0.0466)	7.25 (0.02)
$3^1A' \leftarrow 1^1A'$	*4a″ ← 3a″*; 15a′ ← 13a′	7.3782 (0.001)	[see text]
$2^1A'' \leftarrow 1^1A'$	14a′ ← 3a″	7.7851 (0.0022)	[see text]
$3^1A'' \leftarrow 1^1A'$	*4a″ ← 13a′*; 5a″ ← 13a′	8.0581 (0.0003)	[see text]
$4^1A' \leftarrow 1^1A'$	16a′ ← 13a′	8.1326 (0.0037)	[see text]
$5^1A' \leftarrow 1^1A'$	*4a″ ← 2a″*; *4a″ ← 3a″*; *5a″ ← 3a″*; *15a′ ← 13a′*	8.4283 (0.1492)	8.18–8.82 (0.045) [see text]
$6^1A' \leftarrow 1^1A'$	17a′ ← 13a′	8.4867 (0.0039)	[see text]
$4^1A'' \leftarrow 1^1A'$	*14a′ ← 3a″*; 15a′ ← 3a″	8.5397 (0.0002)	[see text]
$7^1A' \leftarrow 1^1A'$	18a′ ← 13a′	9.0417 (0.051)	[see text]

[a] Minor components in italics.

This corresponds to a $4a'' \leftarrow 13a'$, $\pi^* \leftarrow n_O$ transition, i.e. promotion of a non-bonding electron on the carbonyl oxygen to an antibonding molecular orbital in the carbonyl carbon. The effect is to modify the molecular geometry from quasi-planar to pyramidal. This weak, out-of-plane, transition, occurs in the 6.0 eV region [28], outside our spectral observation range. It has also been observed in EELS experiments [11]. From the published spectrum of Barnes and Simpson [12] on this broad, almost featureless absorption band, we estimate $f \approx 0.0004$, using the formula $f \approx 9.7 \times 10^{-3} \times \sigma_{max} \times \Delta E_{1/2}$, where the peak absorption cross-section σ_{max} is in Mb, and $\Delta E_{1/2}$ is the FWHM, in eV of an assumed Gaussian band profile [32]. Our calculations agree with these results since they give 5.825 eV as the energy of this transition, mainly resulting from $4a'' \leftarrow 13a'$ and $5a'' \leftarrow 13a'$ molecular orbital excitations, and an oscillator strength of 0.0005 (Table 3). The spectral properties of the observed transition are consistent with the LUMO being 4a″, since if it were the $14a'(\sigma^*_{OH})$ MO the resulting in plane dipole transition would be expected to be much more intense [32]. Indeed, for this transition, our DFT calculation gives an oscillator strength $f = 0.047$ (Table 3).

2) The second valence transition $14a' \leftarrow 13a'$, $2^1A' \leftarrow 1^1A'$, is in-plane (Table 3) . This is the $\tilde{A}'$–X transition in the Bell et al. nomenclature [9]. We observe its peak absorption at 7.25 eV (Fig. 2), in good agreement with previous workers [9–13]. Our estimate of the oscillator strength of this transition is $f \approx 0.020$. This is similar to the analogous in-plane transition band at 7.5 eV in formic acid, whose $f \approx 0.025$ [32]. Our calculations give a transition energy of 6.669 eV, the main MO excitation being $14a' \leftarrow 13a'$, and an oscillator strength of 0.047, as mentioned above. We note that this 7.25 eV band was tentatively assigned by Barnes and Simpson as a $\pi^* \leftarrow n'_O$ transition [12] whereas Robin considers that it corresponds to a $3s \leftarrow n_O$ Rydberg transition [28]. Our valence transition assignment is equivalent to a $\sigma^*_{OH} \leftarrow n'_O$ transition. The $3sa' \leftarrow 13a'$ Rydberg transition could also be part of this band (see later).

3) The next three transitions, in-plane $3^1A' \leftarrow 1^1A'$, and out-of-plane $2^1A'' \leftarrow 1^1A'$ and $3^1A'' \leftarrow 1^1A'$, (Table 3), are calculated to be very weak and are probably part of the broad band whose maximum intensity is at 7.795 eV (Fig. 2). This is another spectral region where one could expect the $3sa' \leftarrow 13a'$ Rydberg transition to occur (see later). We estimate the oscillator strength associated with the 7.795 eV band to be $f \approx 0.03$. This is an order of magnitude greater than the three valence transitions predicted to occur in this spectral region but compatible with a Rydberg transition [28]. Thus it is reasonable to consider that the broad band at 7.795 eV also contains a Rydberg transition (see later). We note that the EELS 7.8 eV peak has been assigned to a $\pi^* \leftarrow \pi$ transition [11], whereas Barnes and Simpson [12], assigned the 7.795 eV band as the $3s(\sigma^*) \leftarrow n_O$ in-plane transition.

4) Several valence transitions are calculated to occur in the 8–9 eV spectral region (Table 3), only one of which, $5^1A' \leftarrow 1^1A'$ is predicted to be a strong transition. This is observed as a series of broad bands, at 8.183, 8.340, 8.506, 8.665 and 8.825 eV (Fig. 2), in good agreement with the observations of Bell et al. [9] who called this the C–X transition. Our DFT calculations show that there are many molecular orbital in-plane transitions that contribute to this particular electronic transition, the most important being $4a'' \leftarrow 3a''$ (Table 3) which is essentially a $\pi^*_{C=O} \leftarrow \pi_{C=O}$ transition. We measured its oscillator strength as $f = 0.045$. We note that in formic acid, in the same spectral region (8–8.8 eV), there are very similar bands, with the same vibrational pattern and similar intervals, which we assigned to a valence π^*–π in-plane transition of oscillator strength $f = 0.2$ [32].The average band interval in the $5^1A' \leftarrow 1^1A'$ transition of acetic acid is 161 meV ($\approx$1300 cm^{-1}). This is close to five frequencies (mainly deformation) in ground state acetic acid, which are at 1181 (OH bend), 1280 (CCH_3 sym. deformation), 1380 (CCH_3 sym. deformation), 1434 (CCH_3 antisym. deformation)), and 1439 (CCH_3 antisym. deformation) cm^{-1} respectively [33]. The nature of the vibrational modes corresponds to the principal component of the potential energy distribution for each mode [33]. The successive frequency intervals are 1266, 1339, 1282 cm^{-1}, whereas in the PES first band they are 1500, 1470, 1450 cm^{-1} [31]. This casts doubt on the bands being part of a Rydberg series, although 3p is probably in this region (see later), (and indeed Robin assigns the C–X system to $3p \leftarrow n_O$ [28]). We remark that the profiles of these five vibronic bands could accommodate both valence and Rydberg components.

5) Higher energy valence transitions are calculated and must exist, no doubt intertwined with Rydberg transition bands. This is most probable in the 9–9.5 eV region, in which numerous sharp bands occur (Fig. 2), labeled by Bell et al. [9] as the D–X transition. However, of the many valence transitions calculated to lie at higher energies than $5^1A' \leftarrow 1^1A'$ (Table 3), only five are predicted by our DFT calculations to have appreciable oscillator strength, of which one, the $7^1A' \leftarrow 1^1A'(18a' \leftarrow 13a')$ transition we assign to band #25 at 9.732 eV. The other four valence transitions are expected to occur above 9.8 eV, in regions of high density of absorption features assigned to Rydberg transitions (Fig. 3). We recall that just as in the case of formic acid, where five valence transitions were analysed [32], there might occur valence-Rydberg mixing for some states of acetic acid.

4.2.3. Rydberg states and transitions of CH_3COOH

We will initially be concerned with two main classes of Rydberg transitions in acetic acid, those involving promotion of a 13a′ orbital electron leading at $n = \infty$ to the ion ground state $1^2A'$, and those where promotion of a 3a″ orbital electron leads eventually to the first excited state $1^2A''$ of the ion. Rydberg transitions involving higher energy ionization limits are discussed in Section 5.

There are various possible Rydberg series corresponding to transitions to non-degenerate s orbitals and to split core p and d orbitals. The Rydberg series transitions leading to the ground state of the ion are:

$$
\begin{aligned}
&n\text{sa}' \leftarrow 13\text{a}';\\
&n\text{pa}' \leftarrow 13\text{a}'; \quad n\text{pa}'' \leftarrow 13\text{a}'; \quad n\text{pa}' \leftarrow 13\text{a}'\\
&n\text{da}' \leftarrow 13\text{a}'; \quad n\text{da}'' \leftarrow 13\text{a}'; \quad n\text{da}' \leftarrow 13\text{a}';\\
&n\text{da}'' \leftarrow 13\text{a}'; \quad n\text{da}' \leftarrow 13\text{a}',
\end{aligned}
$$

the transitions being $^1A' \leftarrow 1^1A'$ when the Rydberg orbital has a′ symmetry, and $^1A'' \leftarrow 1^1A'$ when it has a″ symmetry.

Rydberg transitions that can lead to the first excited state of the ion are:

$$
\begin{aligned}
&n\text{sa}' \leftarrow 3\text{a}'';\\
&n\text{pa}' \leftarrow 3\text{a}''; \quad n\text{pa}'' \leftarrow 3\text{a}''; \quad n\text{pa}' \leftarrow 3\text{a}''\\
&n\text{da}' \leftarrow 3\text{a}''; \quad n\text{da}'' \leftarrow 3\text{a}''; \quad n\text{da}' \leftarrow 3\text{a}'';\\
&n\text{da}'' \leftarrow 3\text{a}''; \quad n\text{da}' \leftarrow 3\text{a}'',
\end{aligned}
$$

the transitions here being $^1A' \leftarrow 1^1A'$ when the Rydberg orbital has a″ symmetry, and $^1A'' \leftarrow 1^1A'$ when it has a′ symmetry.

The maximum oscillator strength for a Rydberg transition is found empirically to be $f = 0.08$ per spatial degeneracy [28]. A useful criterion is that transitions to $^1A''$ states should in general be much weaker than to $^1A'$ states.

The Rydberg series absorption bands should have upper states whose geometry is similar to that of the acetic acid ion state to which they converge at their limits. The electron configuration of the $1^2A'$ ground state of the ion leads us to conjecture that in the Rydberg series leading to this ion state, we should find progressions in vibrational modes similar to those observed in the first band of the photoelectron spectrum of acetic acid, and of similar relative intensities of the vibrational components. The HeI PES shows a principal progression in a mode of frequency ≈1480 cm^{-1} [31]. We therefore searched among the absorption bands in the expected Rydberg regions for sets of bands showing these interval characteristics (see below). This 1480 cm^{-1} frequency is most probably that of a CO stretch vibration, decreased from the 1788 cm^{-1} of the corresponding ν_4 mode in the ground state of neutral acetic acid. This decrease further confirms our assignment of the 4a″ molecular orbital to an antibonding $\pi^*_{C=O}$ LUMO. A weaker secondary progression in this mode at about 315 cm^{-1} from the origin band also occurs in the HeI PES first band [31].

In the $1^2A''$ excited state of the ion, removal of the 3a″ electron from the neutral ground state configuration should, following the analogous behaviour in formic acid [32], lead to an increase in the C=O bond length, a decrease in the C–O bond length and marked increases in the H′O′C and HCO′ angles, as well as a decrease in the OCO′ angle. The actual behaviour of the carbon–oxygen stretch vibrations in the HeI PES of formic acid and its isotopomers is more complex than these expectations [34,35].

4.3. Spectral assignments of Rydberg transitions below the ion ground state

The valence transitions were discussed in Section 4.2.2. We now discuss the Rydberg transition bands, beginning with those below the ion ground state energy.

4.3.1. ns ← 13a′ Rydberg series

The 3sa′ ← 13a′ Rydberg transition is expected to give rise to a broad diffuse feature, similar to the corresponding transition in formic acid. Robin [28] assigns a broad feature at 7.08 eV (cf. Fig. 2) as this Rydberg transition in acetic acid, which would give a value of $\delta = 1.04$ for the quantum defect of the 3s level; this is a reasonable value for a well-behaved s Rydberg orbital. Ari and Güven [11] assign an EELs feature at 7.1 eV to the 3sa′ ← 13a′ Rydberg transition, in agreement with Robin. As mentioned earlier, the 3sa′ ← 13a′ Rydberg transition could also occur in the region of the broad band whose maximum is at 7.795 eV (Fig. 2). If it were actually at 7.795 eV, this would correspond to a quantum defect $\delta = 0.80$, which is also quite possible for a 3s orbital exhibiting strong penetration [28].

We searched for higher members of the ns series. For $n = 4$ a suitable region to explore is 9–9.5 eV (Fig. 3). This contains 3 series of bands, α, β, γ, whose first members are respectively bands #9, 10, 11 (Table 1), and whose further members are separated by an interval of about 1490 cm^{-1}. This interval is similar to the vibrational frequency (≈1480 cm^{-1}) observed by PES in the ion ground state [31]. The vibrational mode is undoubtedly the C=O stretch vibration and we designate it as ν_4, following the acetic acid ground state vibration nomenclature of Bertie and Michaelian [36].

The α–β and β–γ intervals for corresponding members of the series are on average 372 cm^{-1}. This is most probably related to the weak progression of about 320–380 cm^{-1} observed in the first PES Band [31], as discussed later. The corresponding vibrational mode is the in-plane OCO bending vibration ν_{12}, which has a frequency of 439 cm^{-1} in the acetic acid ground state in the gas phase [36]. We considered in turn the first members of the α, β and γ series as potential 4s ← 13a′ Rydberg transitions. This gave quantum defect values $\delta = 1.103$ (a), 1.061 (b), 1.019 (c), all of which are compatible with $n = 4$, the differences being due the ion limit being considered as the vibrationless level in each case.

Following this up with searching for $n = 5$, we find at higher energies three series of bands, ε, ζ, η, with similar intervals to those found for the α, β, γ series, and whose first members are respectively bands #26, 27 and 28 (Table 1). The ε–ζ and ζ–η intervals for corresponding members of the series are on average 398 cm^{-1} and are assigned to the OCO bend vibration v_{12}. The assignments gave a quantum defect value $\delta = 0.96$ (ε), compatible with $n = 5$. The fact that the secondary intervals (about 380 cm^{-1}) are constant in going from $n = 4$ to 5 indicate that these intervals are linked to vibrations, or that different Rydberg l values are involved. As we will see later, the secondary intervals, observed for both ns and np Rydbergs, are, within experimental error, constant as a function of n, which argues in favour of vibrational components rather than different electronic series.

Similar series of bands were observed and assigned for $n = 6$ and 7 (Table 1). The search for $n = 8$ was infructuous. The increased density of features in this spectral region does not make it possible to choose secondary series with confidence.

4.3.2. The np ← 13a′ Rydberg series

The principal band of the two possible 3pa′ ← 13a′ Rydberg transitions, supposing $\delta = 0.6$, would be predicted to occur at about 8.253 eV. This is precisely in the region of the so-called C–X transition bands [9], which we have previously assigned to the valence transition, although, as mentioned earlier, Robin [28] assigns the C–X system to 3p ← n_O and we have remarked that the vibrational profiles could accommodate both valence and Rydberg components.

We now examine higher members of the np series using δ values of this order of magnitude.

The 4pa′ ← 13a′ Rydberg transition origin can be assigned to band #19, giving $\delta = 0.60$. The bands #19, 23, 26 form a series with an average interval of 1395 cm^{-1}, corresponding to vibrational mode v_4. In analogous fashion, the 5pa′ ← 13a′ Rydberg transition origin was assigned to band #29, giving $\delta = 0.57$. The bands #29, 33, 38 form a v_4 progression with an average interval of 1456 cm^{-1}. The origin band of the 6pa′ ← 13a′ Rydberg transition was found to be band #35, giving $\delta = 0.61$. The v_4 progression bands #35, 40, 45 have an average frequency interval of 1424 cm^{-1}. We were also able to assign the 7pa′ ← 13a′ Rydberg transition origin to band #38, giving $\delta = 0.60$. The bands #38, 44 form a v_4 progression with an average interval of 1420 cm^{-1}.

Secondary components of the np Rydberg series were less obvious than for the ns series. These components could be masked by being within the profiles of other bands, assigned otherwise. Higher spectral resolution and deuterium isotope studies are required to further the analysis.

In all, we have assigned $n$pa′ ← 13a′ Rydberg transitions, and their companion bands, for $n = 3$–7, and for which the quantum defects are essentially in the range 0.57–0.61 (Table 1). The possible np′a′ ← 13a′ Rydberg transitions were not assigned, but they are expected to be much weaker than the npa′ ← 13a′ Rydberg transitions.

4.3.3. The nda′ ← 13a′ Rydberg series

In formic acid the nd series has quantum defect values of the order of $\delta = 0.14$. For acetic acid, trial $\delta = 0.14$, gives 8.952 eV for $n = 3$. There is a weak band at 8.948 eV (#8), corresponding to $\delta = 0.143$. A series can be built up with band #8 as origin followed by bands #12, 16 and 21 as a v_4 progression, with an average interval 1444 cm^{-1}. We were also able to assign $n = 4$ and 5 transitions, with satisfactory quantum defect values respectively, 0.15 and 0.13 (Table 1).

Although for each value of n, there are expected three $n$da′ ← 13a′ transitions, it is probable that one of these transitions has the major oscillator strength. In any case, we do not observe more than one $n$da′ ← 13a′ transition for each value of n. We do not assign any low frequency companion bands. There are no previous reports of nd Rydberg series for acetic acid.

4.3.4. Vibrational frequencies of the Rydberg states converging to the ground state of the acetic acid ion

Two vibrational modes were excited in the Rydberg levels, giving rise to the companion bands discussed above. The average values of the frequencies over all companion bands in the ns, np and nd Rydberg series converging to the ground state of the ion are $v = 1463$ and 385 cm^{-1}. These values are very close to, and within the error limits of, the frequencies of the two principal ion ground state vibrations, $v = 1450$ (±30)–1500 (±20) cm^{-1} and $v = 310$ (±20)–380 (±20) cm^{-1} observed in photoelectron spectra [31].

As mentioned above, the frequencies $v = 1463$ and $v = 385$ cm^{-1} are assigned to C=O valence and OCO bend vibrations, whose neutral ground state frequencies are $v_4 = 1788$ cm^{-1} and $v_{12} = 439$ cm^{-1}, respectively. The large decrease in the v_4(C=O) frequency is similar to what is observed for formic acid, which has a similar HOMO to that of acetic acid, and in which the neutral v_4(C=O) = 1777 cm^{-1}, whereas the ground state ion v_4(C=O) = 1495 cm^{-1} [34].

4.4. Spectral assignments: Rydberg transitions converging to the first excited ion state $1^2A''$

Assignments of Rydberg bands converging to the first excited electronic state, $1^2A''$, of the acetic acid ion have not previously been reported. In searching for these Rydberg bands we started with the following two criteria:

1) We expect to find an energy interval ΔE of the order of 1.015 eV between the ns, np and nd Rydberg transition bands converging to the ground state of the ion and the corresponding series of bands which converge to the first excited state, since this is the value of the difference in the energies of these two ion states.

2) The existence of companion bands to the Rydberg transition O_0^0 origin band at intervals similar to those of vibrational frequencies of the first excited ion state.

4.4.1. n(s,p,d) ← 3a″ Rydberg series

The *n*sa′ ← 3a″ Rydberg series bands correspond to out-of-plane $^1A'' \leftarrow X^1A'$ transitions, so they are not expected to be very intense. The 3sa′ ← 3a″ origin band would be expected to be in the 8.7 eV region, and may be part of the background to the structure in this spectral region (Fig. 2). We assigned the origin band of the 4sa′ ← 3a″, band #34 ($\delta = 0.99$) and its ν_4 vibration companion band #39, as well as the 5sa′ ← 3a″, band #53 ($\delta = 0.89$) (Table 1). Because of the expected weakness of the *n*sa′ ← 3a″ transitions, we were unable to identify further members of this Rydberg series in the absorption spectrum.

For the *n*p ← 3a″ Rydberg series, on symmetry grounds one expects only one strong *n*p ← 3a″ transition, i.e. *n*pa″ ← 3a″. With assumed $\delta = 0.6$, the 3pa″ ← 3a″ transition origin band can be expected to occur at 9.268 eV, and this corresponds precisely to band #15 (Fig. 2), already assigned to 4sa′ ← 13a′($4_0^1 12_0^2$) vibronic transition. series above. The intensity and profile of this band is such that it is reasonable to consider that it also contains the 3pa″ ← 3a″ transition origin band. A ν_4 companion band (band #20) is also observed. Higher members of this Rydberg series are also assigned: 4pa″ ← 3a″ and 5pa″ ← 3a″ and their ν_4 companion bands (Table 1). Because of the high density of spectral lines in the 10–11.2 eV region (Fig. 3), higher spectral resolution and deuterium isotope studies would be useful to verify these assignments.

Band #36 was assigned to the 3d ← 3a″ Rydberg transition, with a $\delta = 0.06$. Higher members of this series assigned are band #50 (4d,$\delta = 0.12$), and band #56, as the the 5d ← 3a″ ($\delta = 0.17$) Rydberg transition (Table 1).

The average value of the ν_4 vibrational mode frequency in these Rydberg progressions to the $2^2A''$ ion state is 1521 cm^{-1}. This is smaller than the neutral ground state frequency, as expected from the bonding characteristics of the molecular orbitals, but is somewhat higher than the average value, 1463 cm^{-1}, for the ν_4 mode in Rydbergs converging to the ion ground state. This behaviour is similar to the case of the corresponding Rydberg and ion limit states of formic acid [32]. Knowledge of vibrational frequencies in the $2^2A''$ ion state from photoelectron spectroscopy is scarce. Values for two frequencies are given by Watanabe et al. from PES measurements [31], but the vibrational components of the photoelectron second band are very poorly resolved, so that these frequencies are not known with any reliable accuracy. Watanabe et al. consider that the vibrational structure of the second PES band is similar to that of the corresponding band of formic acid but this remains to be confirmed.

5. Absorption at higher energies: 12–20 eV

The absorption spectrum above the second ionization energy can be seen in Fig. 1. There are no previous reports concerning absorption spectra of acetic acid in the 11.7–20 eV region but there are published EELS spectra, up to 15.5 eV [11], whose energy resolution is very much less than that of our absorption spectra. The EELs spectrum shows a broad continuous feature between 12 and 15.5 eV, peaking in the 13 eV region. Our absorption spectrum shows several broad features between 12 and 20 eV (Fig. 1). Twin, hardly resolved, absorption features occur at 12.92 eV (53.6 Mb) and 13.33 eV (53.3 Mb), which doubtless correspond to the EELS peak at 13 eV. The minimum at 13.75 eV is followed by a stronger peak at 14.5 eV (60.2 Mb), not detected in the EELS spectrum, followed by a minimum at 14.9 eV after which the absorption curve rises to a maximum of 72.2 Mb at 16.83 eV, with two inflexions at 15.125 and 15.77 eV.

In order to analyse the absorption spectra observed between 12 and 20 eV region we first discuss the ion states in this region, which should be the limit states to which Rydberg series in this spectral region converge. Photoelectron spectroscopy has established a series of ion states arising by successive loss of an electron from molecular orbitals of CH_3COOH. In the 12–20 eV region there are ionization limits corresponding to loss respectively of the 2a″, 12a′, 11a′, 1a″, 10a′, 9a′ and 8a′ electrons in one electron transitions (Table 2). Loss of the 7a′ electron takes place at an energy about 4.1 eV above that of the 8a′ electron (Table 2), which is in the 20.3 eV region. We neglect any satellite states corresponding to two-electron transitions and configurational effects in general, which is reasonable for CH_3COOH below 20 eV, which we can expect to be similar to the case of HCOOH [37].

In Fig. 1 we give the absorption spectrum between 12.2 and 20 eV and have indicated the various vertical ionization limits. In this spectral region there are no notable features that can be directly linked to Rydberg transitions, nor do the band profiles appear to characterise Rydberg transition convergence to the various ion states, apart possibly from those corresponding to loss of the 2a″ and 11a′ electrons.

In this spectral region one can expect also π–σ*, σ–π* and σ–σ* transitions [38]. Assignment is hazardous, not only because of the complexity of the molecular orbitals relevant to this energy region, but also because the broadness of the VUV absorption features makes it difficult to determine the experimental transition energies. However, there exist some useful considerations. Two types of unoccupied σ* orbitals involving C–H groups have been discussed [39]. Excitation to these orbitals would correspond to high energy valence transitions. In type 1, the orbital is antibonding between carbon and hydrogen atoms ; in type 2 it is non-bonding and has little density on hydrogen atoms. The latter has been designated as n.h. (‘‘negligible hydrogen’’) orbitals by Lindholm et al. [39]. In the case

of the occupied orbitals, strong orbital mixing makes their separation into n.h. and non-n.h. impractical. From the discussion by Lindholm et al., in particular on formic acid, one can predict that in acetic acid strong σ–σ* (C–H) and σ–σ* (C–C) n.h. transitions should occur in the 12–18 eV region, with the latter being at higher energy than the σ–σ* (C–H) non-n.h. transition.

We propose that the #59 and #60 features correspond to broad overlapping Rydberg bands converging to the $2^2A''$ ($-2a''$) ion state, that band #61 corresponds to a valence σ–σ* (C–H) non-n.h. transition, while band #64 is the σ–σ* (C–H) transition. Features #62 and #63 may correspond to overlapping Rydberg bands converging to still higher ion state limits. Collective π electron excitation can also be expected in the 16–20 eV region [38] and probably contributes to the broad background absorption in this spectral region. It is of interest that the peak absorbance of acetic acid, 72.2 Mb, which occurs at 16.9 eV, is of the same order of magnitude of that of other species containing 8 atoms, e.g. C_2H_6 (80 Mb) [40].

6. Conclusion

Absorption spectra of CH_3COOH were measured between 6 and 20 eV. In our analysis of the spectra we discuss and use the molecular orbital structure of acetic acid, the associated bonding properties, and our theoretical calculations on valence states of this acid. Data on ionic states and their structural and dynamic properties, obtained from He I photoelectron spectroscopy of acetic acid [20,21,25,26,31] were also used. Valence transitions and the different types of expected Rydberg transitions converging to the ground state $1^2A'$ and the first excited electronic state $1^2A''$ of the formic acid ion were first discussed. The corresponding valence and Rydberg absorption bands were then assigned in the spectral region below 11.2 eV. Earlier studies have been limited to an upper energy limit of 11.7 eV. In the spectral region common to previous measurements, we observed and assigned many features seen by previous authors [28], in particular by Bell et al. [9]. This has involved re-assignment, or assignment for the first time of reported absorption spectral features. Previous to our study, there was no concerted identification and analysis of Rydberg transitions of acetic acid, apart from suggestions concerning 3s and 3p levels of Rydbergs converging to the ion ground state. Our analysis identifies ns, np and nd transitions. Two vibrational companions to the Rydberg series converging to the ion ground state were observed, corresponding to excitation of the C=O stretch vibration ν_4 and the OCO bend vibration ν_{12}. Because of spectral congestion it was more difficult to identify Rydberg bands converging to the first excited ion state, but we succeeded in assigning ns, np and nd Rydberg transitions in which the $3a''$ electron is excited. Higher spectral resolution and deuterium isotopic studies would be useful in for confirming and extending the Rydberg analysis.

Entirely novel aspects of our study concern the observation, analysis and assignment of absorption features at higher energies, between 12 and 20 eV, observed and carried out here for the first time. The existence of Rydberg bands was explored for transitions whose limiting ion states are respectively $2^2A''$, $2^2A'$, $3^2A'$, $3^2A''$, $4^2A'$, $5^2A'$ and $6^2A'$, corresponding to ionization of electrons from the successive molecular orbitals $2a''$, $12a'$, $11a'$, $1a''$, $10a'$, 9a and $8a'$. Rydberg bands converging to these ionization limits were not observed as distinct discrete features. The Rydberg bands converging to the other ionization limits are apparently broad and merge to form the broad features or underlying continuous absorption observed in specified high energy regions. Broad bands in the 14 – 17 eV region suggested assignments in terms of two types of σ–σ valence transitions, probably also involving collective π electron excitation.

The detailed information obtained in the present absorption study is of direct use not only in the interpretation of acetic acid dissociative photoionization but also for other photophysical properties, such as fluorescence emission observed from neutral and ionic dissociation channels as a function of excitation energy [8]. As mentioned in Section 1, this information is of direct interest for interpreting certain observations of atmospheric and astrophysical phenomena, for predicting regions of the interstellar medium liable to contain acetic acid, and for general exobiology studies in which acetic acid plays a role as a building block of biomolecules.

Acknowledgements

We acknowledge the Centre de Calcul Recherche et Technologie, CEA Saclay, for computing resources and the use of the Gaussian-03 program. The experiments were carried out at the BESSY I synchrotron facility in Berlin, supported by the TMR programme of the European Union under contract FMRX-CT-0126. Support from the CNRS Groupe de Recherche "GDR Exobiologie" (GDR 1877) is gratefully acknowledged.

References

[1] D.K. Harvey, K.J. Feieraband, J.C. Black, V. Vaida, J. Molec. Spectrosc. 229 (2005) 151.
[2] A. Brack (Ed.), The Molecular Origins of Life, Cambridge University Press, Cambridge, UK, 1998.
[3] S.L. Miller, in [2], pp. 59–85.
[4] D.H. Mehringer, L.E. Snyder, Y. Miao, F.J. Lovas, Ap. J. 480 (1997) L71.
[5] W.M. Irvine, P. Friberg, N. Kaifu, H.E. Mathews, Y.C. Minh, M. Ohishi, S. Ishikawa, Astron. Astrophys. 229 (1990) L9.
[6] Y.-J. Kuan, S.B. Charnley, H.-C. Huang, W.L. Tseng, Z. Kisiel, Astrophys. J. 593 (2003) 848.
[7] J. Crovisier, D. Bockelée-Morvan, P. Colom, N. Biver, D. Despois, D.C. Lis, Astron. Astrophys. 418 (2004) 1141.
[8] S. Leach, M. Schwell, H.-W. Jochims, H. Baumgärtel, Chem. Phys., 2005, this issue, doi:10.1016/j.chemphys.2005.08.020.
[9] S. Bell, T.L. Ng, A.D. Walsh, J. Chem. Soc. Faraday Trans. II 71 (1975) 393.

[10] M. Suto, X. Wang, L.C. Lee, J. Phys. Chem. 92 (1988) 3764.
[11] T. Ari, H.H. Güven, J. Electron Spectrosc. Rel. Phen. 106 (2000) 29.
[12] E.E. Barnes, W.T. Simpson, J. Chem. Phys. 39 (1963) 670.
[13] S. Nagakura, K. Kaya, H. Tsubomura, J. Molec. Spectrosc. 13 (1964) 1.
[14] A. Hoxha, R. Locht, B. Leyh, D. Dehareng, K. Hottmann, H.W. Jochims, H. Baumgärtel, Chem. Phys. 260 (2000) 237.
[15] M.J. Frisch, G.W. Trucks, H.B. Schlegel, G.E. Scuseria, M.A. Robb, J.R. Cheeseman, J.A. Montgomery Jr., T. Vreven, K.N. Kudin, J.C. Burant, J.M. Millam, S.S. Iyengar, J. Tomasi, V. Barone, B. Mennucci, M. Cossi, G. Scalmani, N. Rega, G.A. Petersson, H. Nakatsuji, M. Hada, M. Ehara, K. Toyota, R. Fukuda, J. Hasegawa, M. Ishida, T. Nakajima, Y. Honda, O. Kitao, H. Nakai, M. Klene, X. Li, J.E. Knox, H.P. Hratchian, J.B. Cross, C. Adamo, J. Jaramillo, R. Gomperts, R.E. Stratmann, O. Yazyev, A.J. Austin, R. Cammi, C. Pomelli, J.W. Ochterski, P.Y. Ayala, K. Morokuma, G.A. Voth, P. Salvador, J.J. Dannenberg, V.G. Zakrzewski, S. Dapprich, A.D. Daniels, M.C. Strain, O. Farkas, D.K. Malick, A.D. Rabuck, K. Raghavachari, J.B. Foresman, J.V. Ortiz, Q. Cui, A.G. Baboul, S. Clifford, J. Cioslowski, B.B. Stefanov, G. Liu, A. Liashenko, P. Piskorz, I. Komaromi, R.L. Martin, D.J. Fox, T. Keith, M.A. Al-Laham, C.Y. Peng, A. Nanayakkara, M. Challacombe, P.M.W. Gill, B. Johnson, W. Chen, M.W. Wong, C. Gonzalez, J.A. Pople, GAUSSIAN-03, Revision B.05, Gaussian Inc., Pittsburgh, PA, 2003.
[16] J.L. Derissen, J. Molec. Struct. 7 (1971) 67.
[17] R.E. Stratmann, G.E. Scuseria, M.J. Frisch, J. Chem. Phys. 109 (1998) 8218.
[18] G. Schaftenaar, J.H. Noordik, J. Comput.-Aided Mol. Design 14 (2000) 123.
[19] L. Turi, J.J. Dannenberg, J. Phys. Chem. 97 (1993) 12197.
[20] F. Carnovale, T.H. Gan, J.B. Peel, J. Electron Spectrosc. Rel. Phen. 20 (1980) 53.
[21] W. von Niessen, G. Bieri, L. Åsbrink, J. Electron Spectrosc. Rel. Phen. 21 (1980) 175.
[22] M.B. Robin, I. Ishii, R. McLaren, A.P. Hitchcock, J. Electron Spectrosc. Rel. Phen. 47 (1988) 53.
[23] S.G. Urquhart, H. Ade, J. Phys. Chem. B 106 (2002) 8531.
[24] N. Kosugi, H. Kuroda, Chem. Phys. Lett. 74 (1980) 490.
[25] P.H. Cannington, N.S. Ham, J. Electron Spectrosc. Rel. Phen. 31 (1983) 175.
[26] K. Kimura, S. Katsumata, T. Yamazaki, H. Wakabashi, J. Electron Spectrosc. Rel. Phen. 6 (1975) 41.
[27] H. Basch, M.B. Robin, N.A. Kuebler, J. Chem. Phys. 49 (1968) 5007.
[28] M.B. Robin, Higher Excited States of Polyatomic Molecules, I, II, III, Academic Press, Inc., London, 1974, 1975, 1985.
[29] D.J. Knowles, A.J.C. Nicholson, J. Chem. Phys. 60 (1974) 1180.
[30] Ya.Ya. Villem, M.E. Akopyan, Russ. J. Phys. Chem. 50 (1976) 394.
[31] I. Watanabe, Y. Yokoyama, S. Ikeda, Bull. Chem. Soc. Jpn 47 (1974) 627.
[32] S. Leach, M. Schwell, F. Dulieu, J.-L. Chotin, H.W. Jochims, H. Baumgärtel, Phys. Chem. Chem. Phys. 4 (2002) 5025.
[33] R.W. Williams, A.H. Lowrey, J. Comput. Chem. 12 (1991) 761.
[34] S. Leach, M. Schwell, D. Talbi, G. Berthier, K. Hottmann, H.W. Jochims, H. Baumgärtel, Chem. Phys. 286 (2003) 15.
[35] E. Rudberg, T. Brinck, Chem. Phys. 302 (2004) 217.
[36] J.E. Bertie, K.H. Michaelian, J. Chem. Phys. 77 (1982) 5267.
[37] J. Schirmer, L.S. Cederbaum, W. Domke, W. von Niessen, Chem. Phys. Lett. 157 (1978) 582.
[38] H.-W. Jochims, E. Rühl, H. Baumgärtel, S. Tobita, S. Leach, Int. J. Mass Spectrom. Ion Processes 167/168 (1997) 35.
[39] E. Lindholm, L. Åsbrink, S. Ljunggren, J. Phys. Chem. 95 (1991) 3923.
[40] J. Berkowitz, Photoabsorption, Photoionization and Photoelectron Spectroscopy, Academic, New York, 1979.

Available online at www.sciencedirect.com
SCIENCE DIRECT
Chemical Physics 321 (2006) 171–182
Chemical Physics
www.elsevier.com/locate/chemphys

VUV photophysics of acetic acid: Fragmentation, fluorescence and ionization in the 6–23 eV region

Sydney Leach [a,*], Martin Schwell [b], Hans-Werner Jochims [c], Helmut Baumgärtel [c]

[a] LERMA – UMR 8112, Observatoire de Paris-Meudon, 5, place Jules Janssen, 92195 Meudon, France
[b] Laboratoire Interuniversitaire des Systèmes Atmosphériques (LISA), Université Paris 7 et 12, 61 Avenue du Général de Gaulle, 94010 Creteil Cedex, France
[c] Institut für Physikalische und Theoretische Chemie der Freien Universität Berlin, Takustr. 3, 14195 Berlin, Germany

Received 10 June 2005; accepted 18 August 2005
Available online 28 September 2005

Abstract

VUV photodissociation of gaseous acetic acid was studied in the 6–23 eV range using synchrotron radiation excitation, photofragment fluorescence spectroscopy and mass spectrometry. OH (A-X), CH (A,B-X) and H-Balmer emissions were observed. Their relative intensities were studied by fluorescence excitation spectroscopy. The fluorescence quantum yield for OH emission has a maximum of 0.9% at 13.3 eV photoexcitation, dropping to 0.5% at 20 eV; that for CH (A-X) is 0.35% at 16 eV and 0.4% at 20 eV. Photoionization mass spectra (PIMS) of CH_3COOH were measured and the appearance energies of the principal photoions were determined. IE(CH_3-COOH) = 10.58 ± 0.02 eV is 40–60 meV lower than previous PIMS values. Dissociative ionization reaction channels are discussed in detail. The results call into question previous determinations of the heat of formation and ionization energy of the acetyl radical. A new pathway is suggested for the formation of HCO^+, and the assignments of the $m/z = 16$, 28 and 31 ions are clarified. The formation of CH_3^+ at threshold is shown to involve carbon–carbon bond rupture and a potential energy barrier. The results of this study are used to discuss aspects of astrophysical observations involving the parent and fragment species.

1. Introduction

Absorption of VUV photons by a molecule opens up many photophysical processes, including a variety of relaxation processes [1]. Previous studies of the vacuum-UV (VUV) spectroscopy and photophysics of acetic acid (CH_3COOH) have been mainly limited to absorption and fluorescence measurements below 11.4 eV [2,3], apart from a photoionization mass spectrometric study by Villem and Akopyan [4] up to 13 eV, and one by Zha et al. [5], up to 17 eV.

Photodissociation and dissociative photoionization processes [1] can give rise to electronically and/or vibrationally excited product species, as we found for acetic acid. This molecule is observed in the interstellar medium [6] and is expected to exist in comets [7] where, in both cases, VUV radiation is present. It is also a constituent of the Earth's atmosphere, especially over urban areas [8]. Thus, a study of the VUV photophysics of acetic acid is necessary for interpreting the relevant astrophysical and atmospheric observations.

We have carried out extensive studies on the spectroscopy and photophysics of acetic acid in the 6–23 eV energy region. An analysis of the 6–20 eV photoabsorption spectrum has been made and is published elsewhere [9]. In the present work we have used photofragment fluorescence spectroscopy as an analytical tool to provide insight into the photoprocesses of acetic acid. Identification of the emission features observed in the dispersed fluorescence spectra of CH_3COOH is followed by a fluorescence excitation (FEX) spectral study of the excitation energy dependence of these features. Analysis of the FEX spectra is made with the aid of data from the VUV absorption spectra and thermochemical limit calculations of the relevant processes forming the emitting electronic states. In Table

* Corresponding author. Tel.: +33 0 145077561; fax: +33 0 145077100.
E-mail address: sydney.leach@obspm.fr (S. Leach).

0301-0104/$ - see front matter © 2005 Elsevier B.V. All rights reserved.
doi:10.1016/j.chemphys.2005.08.020

Table 1
Heats of formation (298 K) of species used to calculate thermochemical energies

Species	Heat of formation (298 K) eV	Species	Heat of formation (298 K) eV
H	2.259 [18]	$COOH^+$	6.188 [18]
O	2.58 [18]	HCOO	−1.344 [22]
OH	0.404 [18]	CH_4	−0.772 [19]
OH^+	13.424 [18]	CH_4^+	11.731 [19]
CH	6.174 [19]	CH_3O	0.176 [18]
CO	−1.145 [18]	CH_3O^+	8.725 [19]
CO^+	12.87 [18]	CH_2OH	−0.195 [20]
H_2O	−2.506 [18]	CH_2OH^+	7.343 [20]
HCO	0.436 [20]	CH_2CO^+	9.119 [18]
HCO^+	8.56 [19]	CH_3OH	−2.088 [18]
COH	−0.179 [5]	CH_3OO	0.2083 [23]
COH^+	9.98 [19]	CH_3CO	−0.124 [18]
CO_2	−4.078 [18]	CH_3CO^+	6.876 [18], [19]
CO_2^+	9.693 [18]	CH_3COO	−2.242 [24]
CH_3	1.513 [18]	CH_3COOH	−4.479 [18]
CH_3^+	11.342 [20]	CH_3COOH^+	6.101 [18][a]
COOH (HOCO)	−2.311 [21]		

[a] And present work value of ionization energy of CH_3COOH.

1 are given the heats of formation at 298 K of the atomic or molecular species used to calculate thermochemical threshold energies of the various dissociation processes discussed in the present work. We have also measured, and interpreted, the mass spectra of CH_3OOH as a function of photon excitation energy up to 100 eV, and measured the appearance energies of the ionic products of dissociative ionization. The dissociation reaction channels are discussed in detail. The results of this study are used to discuss aspects of astrophysical observations involving this species.

2. Experimental

Monochromatized synchrotron radiation was obtained from the Berlin electron storage ring BESSY I (multibunch mode) in association with a 1.5 m McPherson monochromator (Normal incidence (NIM), dispersion 5.6 Å/mm). Some of the mass spectrometric measurements were performed at LURE/Orsay (SA63 beamline, 3 m NIM monochromator).

The grating transmission function of the BESSY I monochromator is recorded by detecting the visible fluorescence emitted by the sodium salicylate layer placed on a quartz window. For fluorescence measurements, the synchrotron light beam is focused into an open brass cell, differentially pumped, containing acetic acid vapor at a pressure typically around 10^{-3} mbar. In this pressure region the concentration of acetic acid dimers to monomers is negligibly small [3]. Fluorescence induced in the irradiated target molecules passes through a quartz window and is dispersed using a 20 cm focal length secondary monochromator (Jobin-Yvon H 20 UV, grating blazed at 300 nm). This monochromator has a fixed, exchangeable exit slit but has no entrance slit. The width of the effective "entrance slit" is given by the spatial extension of the exciting light beam (approximately 1 mm). The emitted fluorescence light, measured in the 250–550 nm wavelength range, is detected by a photon-counting Hamamatsu R6060 photomultiplier, cooled to 250 K by a Peltier element. The spectral response function of this arrangement has been determined by recording the spectrum emitted by a tungsten halogen lamp, which is then deconvoluted according to Planck's law. A dispersed fluorescence spectrum typically contains 2 points per nm. The resolution of these spectra is between 4 and 20 nm depending on the choice of the effective exit slit width.

Dispersed fluorescence measurements were carried out at six excitation energies, respectively, 10, 13, 15, 16.2, 18 and 20 eV. The excitation bandwidth was ≈0.8 nm. In recording the fluorescence excitation (FEX) spectra, the secondary monochromator is fixed at a desired wavelength with a large exit slit and the primary monochromator is tuned in steps of typically 50–100 meV (400–800 cm^{-1}). The FEX spectra are corrected for the grating transmission function of the primary monochromator and for the VUV photon flux, respectively. The bandwidth was ≈0.3 nm, and the FEX spectral resolution was 40 meV at 13 eV photon excitation. We show unsmoothed fluorescence spectra in all figures. A high resolution VUV absorption spectrum of acetone was used for calibration of the observed FEX spectral wavelengths.

Mass spectra of acetic acid were measured using a quadrupole mass spectrometer (Leybold Q200) at BESSY I for ions produced by excitation with 20 eV photons, and ion yield curves were obtained through photon energy scans with measuring intervals of 30 meV (as compared with the 150–250 meV intervals in the TEPEPICO measurements of Zha et al. [5]). The yield curves of the principal ions observed are presented in Fig. 3. Ion appearance energies were determined with the aid of semi-log plots of the ion yield curves. The fluorescence and mass spectral measurement techniques used at BESSY I are essentially the same as those used previously for a study of formic acid [10]. Mass spectra of acetic acid were also measured at 25 and 100 eV photon excitation energy at LURE-Orsay, with a reflectron-type time-of-flight mass spectrometer, using a set-up described in detail elsewhere [11,12]. Commercial acetic acid of highest available purity was used without further purification. We note that eventual contamination with water can easily be revealed during the experiments by observing the well-known fluorescence excitation spectrum of OH ($A^2\Sigma^+ \rightarrow X^2\Pi$) emission, which is known to follow VUV photoexcitation of H_2O between 140 and 100 nm [13].

3. Absorption spectroscopy of CH_3COOH

Before discussing the results of our VUV photophysical study of acetic acid it is useful to briefly consider the absorption spectroscopy of this molecule (Fig. 2(c)), which is discussed in more detail elsewhere [9]. Acetic acid has an effective symmetry C_s. The lowest lying excited electronic

state is $1^1A''$, to which photoabsorption from the $1^1A'$ ground state has experimentally been observed as a broad band at about 6 eV, with a very small cross section. It has been attributed to a $\pi^* \leftarrow n_o$ transition [9]. The photodissociation dynamics of the $1^1A''$ state have been studied in detail using laser induced fluorescence spectroscopy, mainly by the group of Guest [14–16]. Decomposition occurs into CH_3CO and OH at 5.69 eV, and secondary decomposition of CH_3CO, probably into CH_3 and CO, is observed at 6.2 eV. It is of interest that the weakest bond in the ground state parent molecule, the C–C single bond, is not broken.

In the VUV regime, below the first ionization energy (10.58 eV, see Section 4.2.2), additional valence transitions as well as Rydberg series converging to the first I.E. have been identified in the absorption spectrum of CH_3COOH [9]. Their absorption cross sections are large as compared to the UV absorption populating the $1^1A''$ state. Above the first ionization energy, we observe increasing photoabsorption until a plateau of about 72 MB is reached at about 17 eV (see Fig. 2(c)). Broad bands in the 12–20 eV region are superimposed on a continuous absorption background. The valence and Rydberg absorption bands of acetic acid have been assigned recently [9]. The VUV photofragmentation behaviour will be discussed in Sections 4.1 (fragment fluorescence) and 4.2 (dissociative ionization).

4. Results and discussion

4.1. Fluorescence observations of fragmentation processes

4.1.1. OH emission

Fig. 1(a) shows the dispersed fluorescence spectrum of acetic acid at an excitation energy of $E_{exc} = 13$ eV (spectral resolution ≈8 nm). The intensity is scaled linearly. At this excitation energy we observe two bands, being respectively the OH ($A^2\Sigma^+ \rightarrow X^2\Pi$) emissions at 308 nm (0–0) and 282 nm (1–0). Suto et al. [3] found no fluorescence in total fluorescence excitation experiments over the excitation range $E_{exc} = 4.9 - 11.7$ eV. They estimated an upper limit of 0.02% for the fluorescence quantum yield. In contrast, Vinogradov and Vilesov [17] observed a significant OH fluorescence quantum yield at wavelengths shorter than 125 nm (9.92 eV), with the yield at 106 nm ($E_{exc} = 11.7$ eV) reported to be 0.2% and at 90 nm ($E_{exc} = 13.78$ eV) to be 0.7%. Our FEX spectrum of OH emission shows that there is very weak fluorescence of this radical at 10 eV (see below).

In Fig. 2(a), we show the fluorescence excitation (FEX) spectrum of the OH $A^2\Sigma^+ \rightarrow {}^2\Pi$ emission ($\lambda_{obs} = 310$ nm) in the 8–22 eV excitation energy range. For comparison, we also show the photoabsorption spectrum of acetic acid (Fig. 2(c)) taken from Leach et al. [9]. In this energy region, our measured relative intensities of the OH FEX bands are normalized, and are situated quantitatively with respect to the fluorescence yield measurements of Vinogradov and Vilesov [17]. We remark that water impurity is negligible in the FEX experiments. This is illustrated by our FEX

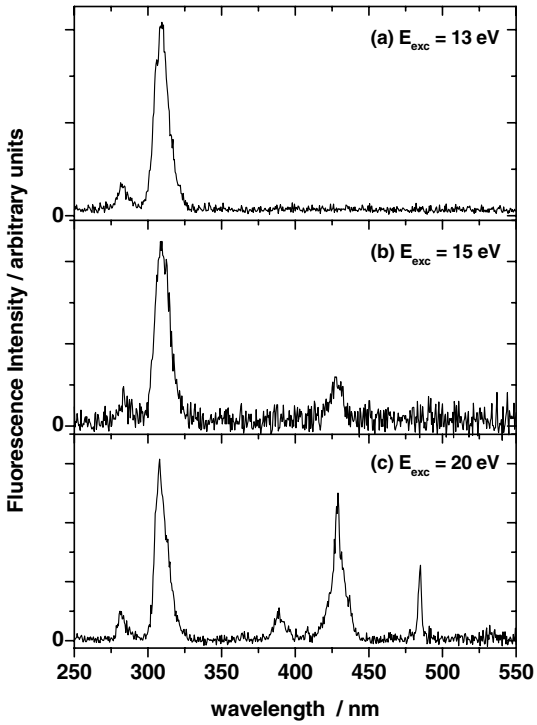

Fig. 1. Dispersed fluorescence spectra observed upon photoexcitation of acetic acid at: (a) $E_{exc} = 13$ eV. Spectral resolution is ≈8 nm. (b) $E_{exc} = 15$ eV. Spectral resolution is ≈8 nm. (c) $E_{exc} = 20$ eV. Spectral resolution is ≈4 nm.

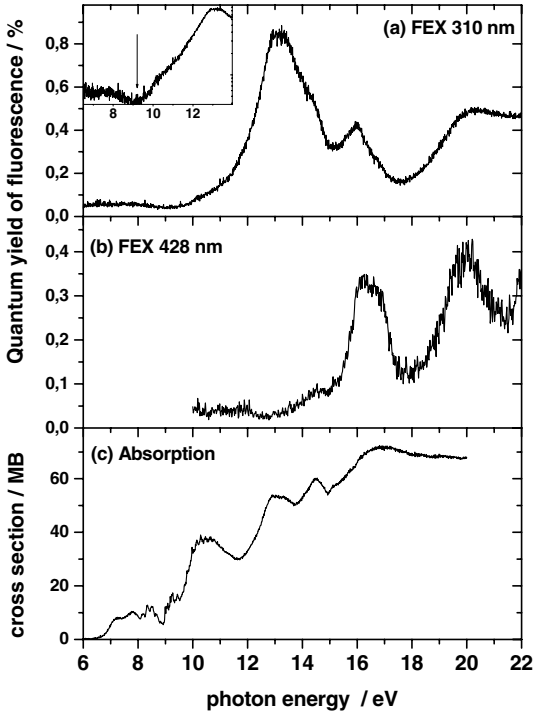

Fig. 2. Fluorescence excitation (FEX) spectra of acetic acid in the 6–22 eV photon excitation region: (a) OH (A-X) ($\lambda_{obs} = 310$ nm), semi-log plot of the signal shown as an insert; (b) CH (A-X) ($\lambda_{obs} = 428$ nm) emissions; (c) Photoabsorption spectrum of acetic acid in the 6–20 eV region [9].

spectrum of OH emission detected at 310 nm, in which the detailed structure, in particular between 10 and 12.4 eV, of the known OH emission in the FEX spectrum of water [12] is virtually absent. We note also that the fluorescence quantum yield of water (OH emission) in this region is at least 10 times greater than our measured yield of 310 nm emission [12].

Our onset for the 310 nm band is at 9.2 ± 0.1 eV as determined from a semi-log plot of the signal, shown as an insert in the threshold region of the OH (A) FEX spectrum in Fig. 2(a). The onset reported by Vinogradov and Vilesov [17] is 9.36 ± 0.04 eV. Their yield curve extends to the maximum fluorescence quantum yield of 0.7% at 13.78 eV. Our OH fluorescence yield curve extends to $E_{exc} =$ 22 eV and is very similar in profile to that of Vinogradov and Vilesov over the 8–13.77 eV excitation range common to both studies, but our maximum quantum yield is found at 13.3 eV. We note that our onset energy coincides with some of the lowest energy Rydberg bands converging to the ion ground state in the absorption spectrum [9], whereas the region of the maximum OH fluorescence yield is that of broad overlapping Rydberg bands converging to the second electronic excited state of the acetic acid ion [9]. A second, less intense, OH fluorescence yield maximum is observed at 15.8 eV, followed by a further rise to the 20 eV region. Using the OH fluorescence quantum yields of Vinogradov and Vilesov [17] to calibrate our own values, we calculate that the quantum yield of fluorescence is 0.9% for OH (A) emission at $E_{exc} = 13.3$ eV, 0.4% at $E_{exc} =$ 16 eV and 0.5% at $E_{exc} = 20$ eV. Although our experiments do not allow us to observe neutral fragments in their electronic ground states, on energy grounds it is reasonable to assume that the processes leading to the observed fluorescence are in competition with acetic acid dissociation processes giving non-excited products. The latter processes would constitute more efficient relaxation pathways of the electronic excited states of the parent molecule.

From enthalpy of formation (ΔH_f) data (Table 1) and the OH ($A^2\Sigma^+ - X^2\Pi$) T_0 value (4.017 eV [25]), we calculate the thermochemical onset to be 8.79 eV for the reaction

$$CH_3COOH \rightarrow CH_3CO + OH\ (A^{2+}) \quad (1)$$

This is 400 ± 100 meV below our measured onset energy of the OH (A) emission. The difference between the thermochemical and the measured onset energy could indicate the existence of a potential barrier between the CH_3COOH excited state and the dissociation surface leading to the OH (A) fragment. If this were the case, one would predict that the initial rise of the OH emission yield beyond the onset would be slow, which is not incompatible with our measured yield curve (Fig. 2(a)). The difference between the thermochemical and the measured onset energies probably also reflects the fact that the detection sensitivity for fluorescence photons is limited, so that our measured onset energy is an upper limit.

We note, however, that since the reaction $CH_3COOH \rightarrow CH_3CO + OH$ ($X^2\Pi$) has an observed onset at 5.69 eV [15], one might expect the appearance energy for reaction (1) to be 9.707 eV, well above our observed and the thermochemical onset energies. Hunnicutt et al. [15] have shown that the reaction forming OH ($X^2\Pi$) involves a potential barrier of the order of 610 meV. From this, and our AE $= 9.2 \pm 0.1$ eV for OH ($A^2\Sigma^+$) emission we infer that dissociation to the excited OH radical, via Rydberg state excitation at 9 eV, occurs without a potential energy barrier.

At higher energies, we observe a OH FEX maximum at about 13.3 eV, which can be correlated with the absorption feature at about 13–13.3 eV [9], as mentioned above, and an EELS peak at 13 eV [26]. The fall-off after this maximum occurs in a region where there is a rise of CH emission (see below). There are less intense OH FEX peaks at about 15.8 eV, perhaps related to the absorption inflexion at 15.77 eV, and at about 20 eV. An inflexion at about 14.5 eV may be related to the absorption peak at 14.5 eV. There is also a peak at 14.5 eV in the CH emission FEX spectrum (see later). We note that since the our AE of CH_3CO^+ is 11.60 ± 0.05 eV (Section 4.2.3), and the excited OH(A) state energy is 4.017 eV [25], we can expect the opening of the dissociative ionization channel

$$CH_3COOH \rightarrow CH_3CO^+ + OH\ (A^{2+}) \quad (2)$$

to be at 15.69 eV, i.e., not far from the beginning of the rise in the OH emission yield at 15.2 eV. The fall-off from 16 eV parallels the disappearance, in TPEPICO experiments, of the CH_3CO^+ ion in this energy region [5]. The OH fluorescence yield curve rises again at 17.9 eV. We considered whether this could be due to opening of the channel

$$CH_3COOH \rightarrow CH_3^+ + OH\ (A^{2+}) + CO \quad (3)$$

but the thermochemical limit for this channel, 19.24 eV, is over 1 eV above the rise point.

4.1.2. CH and H emissions

As excitation energy increases beyond 13 eV in our dispersed fluorescence measurements, we see not only the OH emission bands, but also at and above $E_{exc} = 15$ eV (Fig. 1(b), spectral resolution ≈8 nm), the (0,0) band of the CH ($A^2\Delta \rightarrow X^2\Pi$), transition (Q head 431.4 nm). In addition, we observe extremely weakly the (0,0) band of the CH ($B^2\Sigma^- \rightarrow X^2\Pi$) transition at 388 nm. This is reinforced at $E_{exc} = 20$ eV (Fig. 1(c), resolution 4 nm) where, in addition we observe the Hβ line at 486.1 nm and the Hδ line at 410.1 nm.

We note that the emission band at 431 nm has a broad base (Fig. 1(c)) so that it is necessary to investigate whether it has more than one component. A possible extra component would be H-Balmer-γ ($n = 5 \rightarrow 2$) emission at 434 nm. H-Balmer-γ could result from the dissociation process:

$$CH_3COOH \rightarrow CH_3COO + H\ (n = 5) \quad (4)$$

which has a thermodynamic onset energy of 17.55 eV. However, this thermochemical value is much higher than

the observed onset energy for the 431 nm emission which is AE = 12.8 ± 0.1 eV as discussed below. We conclude by assigning the 431 nm band to CH (A) emission, but do not exclude a contribution of H-Balmer-γ (5–2) at excitation energies above 17.5 eV. We note that from our FEX spectrum (Fig. 2(b)) the fluorescence quantum yield for CH (A-X) is 0.35% at 16 eV and 0.4% at 20 eV but with a minimum of about 0.12% at 17.8 eV, a region where there is a minimum in the OH emission yield, and a further minimum at about 21.3 eV. The increase in the 428 nm FEX signal between 17.8 and 20 eV might be due, in part to H-Balmer-γ (5–2) emission, as mentioned above.

We next discuss the fluorescence band at 485 nm (Fig. 1(c)), whose observed small bandwidth of 4 nm, (we mention that 4 nm was our resolution limit in the 20 eV excitation dispersed fluorescence measurements), suggests that it is due to an atomic emitter. The wavelength of H-Balmer-β emission is 486.1 nm so that, at our spectral resolution, this is the most probable assignment. Its thermochemical onset energy is calculated to be 17.25 eV. Another possible assignment is to the (0,1) band of the $A^2\Delta \rightarrow X^2\Pi$ transition of the CH radical whose Q head should occur at 489 nm. We did not measure the FEX spectrum of the 485 nm band, so we cannot affirm the respective importance of these two possible emitters as a function of excitation energy. However, in the set of the dispersed fluorescence spectra, the 485 nm band is observed at 20 eV but not at lower excitation energies so, on thermochemical grounds, it is most probably due to H-Balmer-β emission.

In Fig. 2(b), we show the fluorescence excitation (FEX) spectrum of the CH emission ($\lambda_{obs} = 428$ nm) in the 8–22 eV excitation energy range. Our measured relative intensities of the CH FEX bands are normalized as discussed above for the OH emissions. Our observed onset for 428 nm emission of CH (A-X) is at $E_{exc} = 12.8 \pm 0.1$ eV. This AE might correspond to the threshold energy of the reaction

$$CH_3COOH \rightarrow CH_3OO + CH\,(A) \quad (5)$$

The calculated thermochemical threshold energy is 13.74 eV. However, the unknown nature of the structure of the CH_3OO radical that would be formed by photodissociation of acetic acid prevents us from validating this calculated thermochemical threshold energy. At higher energies there is a minor FEX peak at about 14.5 eV, mentioned above, and a second onset occurs in the yield curve at 14.9 eV, consistent with the reaction

$$CH_3COOH \rightarrow CH\,(A) + CH_3 + O_2 \quad (6)$$

calculated to have a thermochemical threshold energy of 15.05 eV. Major peaks occur at 16.2 eV (absorption peak at 16.83 eV) and at about 20 eV. Since the FEX and absorption bands are broad in this energy region we cannot say whether OH (A) and CH (A) stem from different or common CH_3COOH superexcited states.

4.1.3. Absence of oxyl radical emissions

It is of interest that no emission of the HCOO radical was observed over the 10–20 eV excitation energy range, in contrast to the case of formic acid excitation, in which this radical emits a series of close-lying bands between 335 and 480 nm [10]. In formic acid, FEX experiments show that the formyloxyl radical HCOO emission is excited only between 9 and 13 eV. In acetic acid, we did not study dispersed fluorescence below 10 eV photon excitation. The excited HCOO radical would be formed in acetic acid by $CH_3COOH \rightarrow CH_3 + HCOO^*$. The thermochemical limit for this process is 8.89 eV, so that it would be worth exploring the excitation range 8–10 eV.

One must also consider the H-loss process analogous to formic acid, i.e., $CH_3COOH \rightarrow CH_3COO^* + H$. The acetyloxyl radical CH_3COO emission spectrum is not known. In fact, CH_3COO has not been detected spectroscopically due to its strong tendency to decarboxylate [3,27–29]. Peyerimhoff et al. [28] calculate that for a particular CH_3COO structure, its lowest state is $^2A''(^2B_2)$, above which lie $^2A'(^2A_1)$, nearly degenerate with an excited $^2A''(^2B_2)$ electronic state at 1.98 eV. Easy dissociation of CH_3COO to $CH_3 + CO_2$ is suggested. The calculations of Rauk et al. [29] give 4 local minima structures for the ground state of CH_3COO. Facile dissociation to $CH_3 + CO_2$ is also predicted for excited states. Thus, CH_3COO formed in an excited state would dissociate rather than emit, in contrast to HCOO*.

4.2. Dissociative ionization

4.2.1. Initial survey of mass spectra

The mass spectra of acetic acid excited by 20, 25 and 100 eV photons are reported in Table 2. The relative intensities of the m/z peaks are normalized to that of $m/z = 43$. The same mass peaks are observed at 20 and 25 eV excitation with few important changes in relative intensities, in spite of the fact that different mass spectrometers were used in these two cases. In the quadrupole mass spectrometer used at 20 eV excitation, the relative ion peak intensities are not proportional to abundances because ion detectivity and resolution are a function of ion mass.

One of the intensity changes concerns the parent ion, which increases in relative intensity, with respect to $m/z = 43$, with increasing excitation energy. This appears to be due to a fall-off in the yield of $m/z = 43$ as increased fragmentation occurs with increasing E_{exc}, so that the relative yield of the fragment ion $m/z = 43$ to that of the parent ion $m/z = 60$ decreases with increasing E_{exc}, as confirmed in the region up to 25 eV by a direct comparison between the PIMS ion yield curves of $m/z = 60$ and $m/z = 43$, measured with the same quadrupole mass spectrometer at BESSY I.

The breakdown curves of the TPEPICO study of Zha et al. [5] show that the parent ion is formed only between the IE and 11.5 eV. Therefore, another level of explanation of the behaviour of the $m/z = 60$ relative yield is that with

Table 2
Mass spectra of acetic acid. Relative intensities at 20, 25 and 100 eV photon excitation energies

m/z	20 eV photons	25 eV photons	100 eV photons	Assignment
61	<1	2	4	CH_3COOH^+ (^{13}C)[a]
60	19	29	53	CH_3COOH^+
46	1.5	3	6	$HCOOH^+$
45	80	79	84	$COOH^+$
44	2	7	14	CO_2^+
43	100	100	100	CH_3CO^+
42	11	13	24	CH_2CO^+
41	0.5	2	10	C_2HO^+
40	0.2	0.5	4	C_2O^+
32	3	5	12	O_2^+; CH_3OH^+
31	7	11	13	CH_2OH^+
30		1	2	H_2CO^+
29	7	18	50	HCO^+
28	9	8	38	CO^+
27			0.5	$C_2H_3^+$
26			4	$C_2H_2^+$
25			6	C_2H^+
24			4	C_2^+
18	16	61	182	H_2O^+
17	8	27	74	OH^+
16	13	11	40	CH_4^+
15	83	78	106	CH_3^+
14	6	11	64	CH_2^+
13	1	12	37	CH^+
12	0.5	0.2	20	C^+
2		0.3	5	H_2^+
1		32	219	H^+

[a] See text.

increasing E_{exc}, there is a relative increase in energy deposition to the 13a′ orbital ($E_{vert} = 10.84$ eV) of acetic acid, which is the expected behaviour for a non-bonding MO [9] and which is confirmed by a comparison between He I and He II PES of acetic acid [30].

Both types of explanation are probably relevant when we go to the mass spectrum obtained with $E_{exc} = 100$ eV, measured with the same mass spectrometer as that used at 25 eV, since in this case, the ratio of the parent ion intensity to that of the sum of the fragment ions is very similar to that at $E_{exc} = 25$ eV. This is consistent with the fact that only two of the 12 valence shell molecular orbital excitations lie at energies above 25 eV, i.e., the 6a′ and 5a′ M.O.s calculated to lie at 30.91 and 33.34 eV, respectively [9]. We note that the fragmentation pattern at 100 eV photon excitation includes the $m/z = 24$–27 ions which are absent at $E_{exc} = 25$ eV. We have assigned them respectively to C_2^+, C_2 H^+, $C_2H_2^+$ and $C_2H_3^+$. These monocations could have resulted from Coulomb dissociation of dications that can be formed at $E_{exc} = 100$ eV, but this remains to be verified.

Other ions whose intensities change significantly in going from $E_{exc} = 20$ to $E_{exc} = 25$ eV and then to $E_{exc} = 100$ eV include $m/z = 29$ (HCO^+) and $m/z = 18$. The latter ion is assigned to H_2O^+, which may, in part, be due to a water impurity. The ratio of $m/z = 17$ (OH^+) to $m/z = 18$ (H_2 O^+) is 0.5 at $E_{exc} = 20$, whereas if the $m/z = 18$ was exclusively from a water impurity, the expected ratio at $E_{exc} = 20$ eV would be 0.3 [31].

The fragment ions $m/z = 14$ and $m/z = 13$ increase considerably in intensity with increase in E_{exc}. This corresponds to increasing ability to lose a hydrogen atom, culminating in the appearance of $m/z = 12$ (C^+), in the processes forming the hydrocarbon series CH_3^+, CH_2^+, CH^+, C^+. We note that an electron impact study on acetic acid gave the appearance energy of the C^+ ion to be 22.5 ± 0.5 eV [32].

We now discuss in further detail the ions observed by mass spectrometry.

4.2.2. Parent ion

The $m/z = 61$ ion is assigned to CH_3COOH^+ containing one ^{13}C atom. Its intensity in the LURE experiments at 25 and 100 eV photon excitation energy, is two or three times greater than that expected with respect to the ^{12}C parent ion. The $m/z = 61$ ion may therefore have a small contribution from an $(M + 1)^+$ ion. The latter can be formed by rapid fragmentation of acetic acid dimer cations, if these are present, or it might result from a complex with a water impurity. The $(M + 1)^+$ ion is indeed the dominant ion in the mass spectrum of the acetic acid dimer [33]. A test for the $(M + 1)^+$ ion resulting from fragmentation of a dimer cation would be its 200 meV smaller appearance potential with respect to the ^{13}C monomer ion [33]. Unfortunately, the $m/z = 61$ ion was too weak for an appearance energy measurement.

The CH_3COOH^+ parent ion, at $m/z = 60$, has an ionization energy IE = 10.58 ± 0.02 eV from our ion yield measurements (Fig. 3(a)). This value is lower than those obtained by other PIMS measurements, IE = 10.644 ± 0.002 eV [34]; 10.66 ± 0.01 eV [4]; 10.64 ± 0.05 eV [33].

Our parent ion yield curve shows inflexions and structures, and has a maximum intensity at ≈17.2 eV. A direct comparison of the $m/z = 60$ ion yield curve (Fig. 4(d)) with the absorption spectrum (Fig. 4(a)) and the photoelectron spectrum (Fig. 4(b)) of acetic acid showed several correspondences. The first PES band has a main peak at 10.84 eV and two side features. These are seen as inflexions on the parent ion yield curve. The ion yield features in the 11.6 and 12.7 eV regions, correlate with minima in the photoelectron spectrum but have no evident correspondence in the absorption spectrum. The maximum at 14.5 eV correlates with features in the photoelectron and absorption spectra whose energies correspond to the formation of the $2^2A'$ and $3^2A'$ electronic states of the acetic acid cation [9]. The dips in the ion yield curve at 14.9 and 15.8 eV appear to be real since they were observed only on the parent ion yield curve and are observed also in the absorption spectrum. However, the integrated HeI and He II (Fig. 4(c)) photoelectron spectra [35], which mirror to a certain extent the parent (and also some fragment) ion yield curves, show no dips at 14.0 and 15.8 eV. In general, the integrated HeI and HeII PES spectra, given up to 19 eV by Carnovale et al. [35], but which tend to flatten out

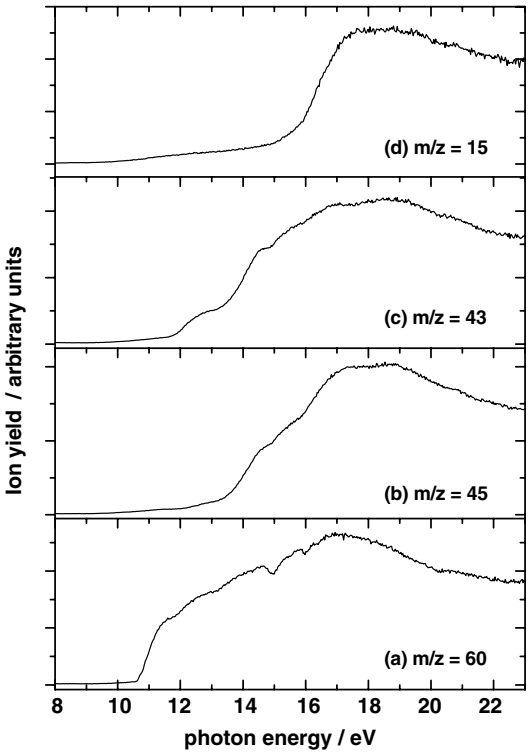

Fig. 3. Photoion yield curves: (a) $m/z = 60$ (CH_3COOH^+); (b) $m/z = 45$ ($HOCO^+$); (c) $m/z = 43$ (CH_3CO^+); (d) $m/z = 15$ (CH_3^+).

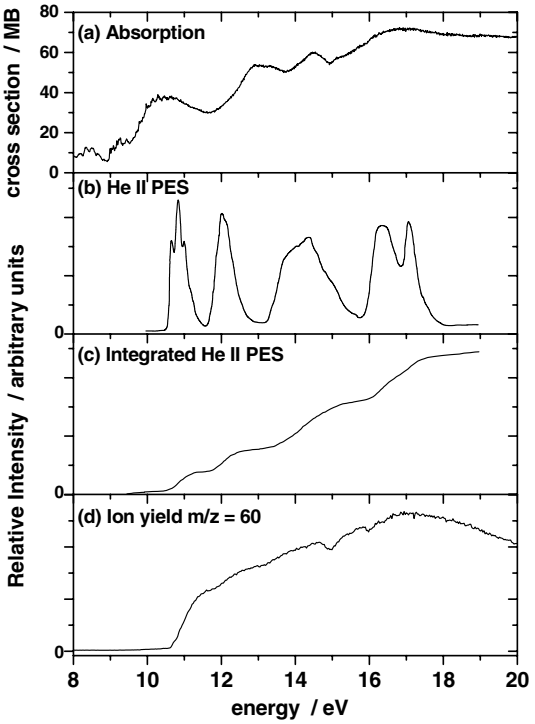

Fig. 4. Acetic acid: (a) photoabsorption spectrum [9]; (b) HeII photoelectron spectrum [35]; (c) integrated HeII photoelectron spectrum [35]; (d) CH_3COOH^+ ion yield curve.

beyond 17 eV, have large steps corresponding to opening up of newly accessed electronic states of the ion. These steps are indeed mirrored, in attenuated fashion, in the parent ion yield curve. We remark that the photoelectron spectra do not contain features resulting from autoionising processes, which could only be expected close to the excitation energy, whereas the ion yield curves result from both direct ionization and autoionization processes. The latter are implicitly contained, in proportion to ionization yields, in the absorption spectra.

4.2.3. Fragment ions

We note the virtual absence of a peak at $m/z = 59$. An ion of this m/z would be CH_3COO^+, formed by loss of a hydrogen atom from the hydroxyl group of the parent ion,

$$CH_3COOH^+ \rightarrow CH_3COO^+ + H \quad (7)$$

or CH_2COOH^+ formed by loss of a hydrogen atom from the methyl group,

$$CH_3COOH^+ \rightarrow CH_2COOH^+ + H \quad (8)$$

In formic acid, the hydrogen atom loss reaction is from the CH group, to form $COOH^+$ and not from the hydroxyl group to form $HCOO^+$ [36]. In acetic acid the analogous reaction to that occurring in formic acid is rupture of the C–C bond, to form the very intense fragment ion $COOH^+$ ($m/z = 45$) by loss of a methyl group. We note that KER modelling by Zha et al. [5] indicated that the KER in $COOH^+$ formation is non-statistical; it appears to arise mainly from the excess internal energy of the activated complex and implies that the reverse activation energy is negligible.

The $m/z = 45$ ion is assigned to $COOH^+$ (=$HOCO^+$ [37]). Its yield curve (Fig. 3(b)) has an AE = 11.7 ± 0.05 eV. The TPEPICO measurement value is 11.53 ± 0.10 eV [5]. Other reported AEs are the PIMS value 11.90 ± 0.03 eV [4] and, from electron impact studies, AE = 12.9 ± 0.1 eV [38] and 12.27 ± 0.05 eV [39]. The thermochemical onset energy for the reaction

$$CH_3COOH \rightarrow CH_3 + COOH^+ \quad (9)$$

is calculated to be 12.18 eV, but this suffers from the fact that the heat of formation of $COOH^+$ used in the calculation is for an unspecified ion structure of the ion.

We note that there is some structure in the $m/z = 45$ ion yield curve (Fig. 3(b)), in particular knees at 14.5 eV, i.e., where CH_3^+ becomes very noticeable (see below) and close to a dip in the parent ion yield curve. The steps in the integrated HeI and HeII PES spectra [35] (Fig. 4(c)) are weakly mirrored in the $m/z = 45$ ion yield curve. The integrated PES curves tend to flatten out after 17 eV, as does the this ion yield curve, which forms a plateau 17–18.5 eV, after which it drops to 23 eV.

The major ion in the mass spectrum, $m/z = 43$, assigned to CH_3CO^+, is formed by loss of OH from the parent ion. From our ion yield curve we obtain AE = 11.45 ± 0.05 eV for this ion (Fig. 3(c)). This is in good agreement with the TPEPICO AE = 11.37 ± 0.07 eV [5] and a PIMS AE = 11.38 ± 0.08 eV [4]. It is also in good agreement with the PIMS value 11.54 eV of Traeger et al. [40] and the

electron impact values 11.54 ± 0.05 eV [41] and 11.4 ± 0.15 eV [38]. An early electron impact study gives a higher value, 11.75 eV [39], but the uncertainty in this measurement was not reported. The calculated thermochemical onset value, 11.67 eV, is higher than other experimental values mentioned above, except for the electron impact value 11.75 eV of Haney and Franklin [39]. The thermochemical value probably reflects the unknown uncertainty in the adiabatic ionization energy of CH_3CO, whose value is reported to be 7.21 ± 0.05 eV [42]. The above discussion suggests that its true value is lower, possibly of the order of 6.6–6.8 eV. One can indeed question whether the heat of formation and the ionization energy of the acetyl radical are sufficiently well known and whether the structure of the CH_3CO radical in previous determinations of the heat of formation [20,43,44] was indeed the acetyl radical.

From their KER study Zha et al. [5] suggested that the formation of CH_3CO^+ does not result from a simple cleavage reaction, and that it involves an energy barrier and probably proceeds via an intermediate. The reasonably good agreement between our measured AE and the calculated thermochemical AE for this ion does not support these suggestions. We note that from their determination of the heat of formation of the CH_3CO^+ ion, by a PIMS study of a series of substituted methyl ketones, Traeger et al. [40] concluded that KER measurements made at energies greater than threshold cannot be applied straightforwardly as thermochemical corrections for the experimental CH_3CO^+ AEs. Following their electron impact dissociative ionization measurements, Holmes and Lossing [41] also consider that loss of OH occurs at the thermochemical threshold for production of CH_3CO^+. We remark that it is possible that in the experiments of Zha et al. [5], there occurred some interconversion to the enol form of acetic acid [45,46]. It is of interest that from the rate constants for CH_3 and OH loss as a function of internal energy in the CH_3COOH^+ ion, calculated by McAdoo et al. [46], one would expect AE ($m/z = 45$) − AE ($m/z = 43$) ≈ 750 meV, whereas we observe a much smaller difference, of about 250 meV, which agrees reasonably well with the results of the rate constant calculations of Zha et al. [5].

There is some marked structure in the $m/z = 43$ ion yield curve, in particular knees at 12.7 and 14.5 eV. The integrated HeI and HeII PES spectra [35] (Fig. 4(c)) have large steps corresponding to opening up of newly accessed electronic states of the ion. These steps are mirrored in the $m/z = 43$ ion yield curve (Fig. 3(c)), which has a quasi plateau 17–19.3 eV, with a maximum at about 19 eV, after which it drops to 23 eV. The integrated curve (Fig. 4(c)) tends to flatten out after 17 eV.

The weak $m/z = 46$ and 44 ions are assigned to $HCOOH^+$ (loss of CH_2) and CO_2^+, respectively. An alternative assignment for $m/z = 44$ would be the CH_3COH^+ ion. However, in this case the neutral loss species is an oxygen atom but this would mean rupture of a C=O bond, which is unlikely. Furthermore, reaction (10),

$$CH_3COOH^+ \rightarrow CH_4{}^+ + CO_2 \quad (10)$$

the charge switch of the reaction $CH_3COOH^+ \rightarrow CH_4 + CO_2^+$, certainly occurs (see below). The CO_2^+ reaction would be less favoured, from the the Stevenson-Audier-Harrison (SAH) rule concerning the dissociation of odd electron ions [37], since CO_2 has a higher IE (13.77 eV) than CH_4 (12.51 eV) [18]. The relative intensities of the $m/z = 44$ and $m/z = 16$ ions (Table 2) are consistent with this interpretation. The calculated thermochemical appearance energy of CO_2^+ is 13.4 eV.

Formation of the minor ion $m/z = 42$, assigned to CH_2CO^+, involves the loss of H_2O from the parent ion:

$$CH_3COOH^+ \rightarrow CH_2CO^+ + H_2O \quad (11)$$

This may involve a complicated reaction and two possible pathways have been proposed [41,45]. The low intensity suggests that H_2O loss is much less favoured than the competing OH loss reaction, despite having a lower thermochemical threshold. We note that at 20 eV excitation the ratio of intensities of the $m/z = 43$ to the $m/z = 42$ peaks (loss of OH cf. loss of H_2O) is 9.1 and that this is very similar to the ratio 11.5 observed in metastable transitions measured by the MIKES technique [45]. Holmes and Lossing [41] state that elimination of H_2O involves a 1,3 hydrogen shift, proceeding via a H transfer from CH_3 to hydroxyl OH and mention that the AE is difficult to measure. Villem and Akopyan [4] report a PIMS AE = 10.8 ± 0.1 eV for the $m/z = 42$ ion, which is close to the 11.09 eV calculated thermochemical threshold.

The $m/z = 32$ minor ion could be O_2^+ or CH_3OH^+. These possible assignments involve loss of C_2H_4 and CO, respectively, from the parent ion. Isotopic studies are required to pin down the assignment. The $m/z = 31$ minor ion can be assigned to CH_3O^+ or CH_2OH^+, involving the loss of the HCO radical (reactions (12) and (13), respectively).

$$CH_3COOH^+ \rightarrow CH_3O^+ + HCO \quad (12)$$

$$CH_3COOH^+ \rightarrow CH_2OH^+ + HCO \quad (13)$$

Zha et al. [5] have shown that the $m/z = 31$ ion is the hydroxymethyl cation CH_2OH^+. Our calculated thermochemical onsets 13.64 eV (CH_3O^+) and 12.26 eV (CH_2OH^+) are much lower than the observed AE = 14.99 ± 0.12 eV reported by Zha et al. [5]. However, Selim and Helal [47] observed an electron impact value AE = 12.05 ± 0.1 eV, and assigned this ion to CH_2OH^+. This AE is compatible with our calculated thermochemical AE for CH_2OH. We remark that formation of both CH_3O^+ and CH_2OH^+ should involve atomic rearrangements. Zha et al. [5], by deuteration, show that the two oxygen atoms become equivalent for formation of $m/z = 31$ and also concluded that this ion is likely to be CH_2OH^+. The process may involve a two-step rearrangement prior to fragmentation, going through the enol ion stage.

In principle, the $m/z = 29$ ion could be assigned to either HCO^+ or COH^+, formed by loss of CH_3O from the parent ion. However, the absence of a $m/z = 30$ peak in the mass spectrum of CH_3COOD indicates that the $m/z = 29$ ion in the CH_3COOH dissociative ionization is HCO^+ and not COH^+[5]. It is a minor ion at $E_{exc} = 20$ eV but increases considerably in relative intensity at higher excitation energies. Two formation pathways were considered by Zha et al. [5]:

$$\text{(i)}\ CH_3COOH^+ \rightarrow CH_2OH^+ + COH \rightarrow HCO^+ + COH + H_2 \quad (14)$$

$$\text{(ii)}\ CH_3COOH^+ \rightarrow COOH^+ + CH_3 \rightarrow COH^+ + CH_3 + O \quad (15)$$

We envisage a third dissociation channel:

$$\text{(iii)}\ CH_3COOH^+ \rightarrow COH^+ + CH_3O \quad (16)$$

The thermochemical appearance energies for reactions (14)–(16) were calculated, considering both HCO and COH isomers as neutral products in reaction (14), and both CH_3O and CH_2OH isomers in reaction (16). This gave five thermochemical AE values: 12.86 and 13.48 eV for reaction (14), 17.13 eV for reaction (15) and 12.84 and 13.22 eV for reaction (16). The observed AE = 15.91 ± 0.13 eV in the TPEPICO experiments [5], eliminates reaction (15). Reaction (16) is a charge switch reaction to formation of the $m/z = 31$ ion (reactions (12) and (13)). The IE of HCO is 8.10 ± 0.05 eV [19], whereas CH_2OH has an IE of 7.56 ± 0.01 eV [19]. These values are not very different which makes it reasonable that the $m/z = 29$ and 31 ions are observed with similar intensities at $E_{exc} = 20$ eV but, as mentioned above, $m/z = 29$ increases considerably in relative intensity at 25 and 100 eV.

The $m/z = 28$ ion, assigned to CO^+ is weak at 20 and 25 eV excitation energies but quite intense at $E_{exc} = 100$ eV (Table 2). The neutral loss species is CH_3OH.

$$CH_3COOH^+ \rightarrow CO^+ + CH_3OH \quad (17)$$

The alternative assignment of $m/z = 28$ is $C_2H_4^+$, formed by loss of O_2 from the parent ion, can be rejected since its calculated thermochemical AE = 15.53 eV is greater than the observed AE = 15.3 ± 0.1 eV [38], which is close to our calculated thermochemical AE = 15.27 eV for reaction (17).

The $m/z = 16$ ion is assigned to CH_4^+, formed by loss of CO_2 from the parent ion,

$$CH_3COOH^+ \rightarrow CH_4^+ + CO_2 \quad (18)$$

This assignment is in agreement with those of Zha et al. [5], who observe an AE = 12.31 eV, and by Villem and Akopyan [4], who report 12.1 ± 0.1 eV, values which agree well with our calculated thermochemical AE = 12.13 eV.

The very important $m/z = 15$ ion is assigned to CH_3^+, formed by loss of COOH from the parent ion. Two different formation processes have been suggested [5]:

$$\text{(i)}\ CH_3COOH^+ \rightarrow CH_3^+ + COOH \quad (19)$$

$$\text{(ii)}\ CH_3COOH^+ \rightarrow CH_3CO^+ + OH \rightarrow CH_3^+ + CO + OH \quad (20)$$

The calculated thermochemical appearance energies of CH_3^+ are 13.51 eV (reaction (19)) and 15.08 eV (reaction (20)). Our measured AE(CH_3^+) = 14.28 ± 0.10eV (Fig. 3d), which is smaller than the TPEPICO measured AE = 14.73 ± 0.15 eV [5], but similar to the electron impact AE = 14.0 ± 0.15 eV [39], appears to favour reaction (19), which corresponds to the charge switch of reaction (9) forming $COOH^+$. The electron impact value AE = 16.08 eV of Hirota et al. [48] is certainly erroneous. The difference of about 800 meV between the thermochemical onset energy for reaction (19) and the observed AE of CH_3^+ suggests that the dissociation process involves a potential barrier. We note that the analogous neutral photochemical reaction has a very low probability [15].

The appearance energy results suggest that reaction (19) is operative in the threshold region. Since IE(CH_3) = 9.84 ± 0.01 eV and IE(COOH) ⩽ 8.19 eV [49], the SAH rule [37] certainly favours reaction (19) in this excitation energy region. However, Zha et al. [5] argue in favour of reaction (20), presumably at higher energies, on the basis that the breakdown graph suggests that CH_3^+ increases simultaneously with a decrease in CH_3CO^+. In fact the CH_3^+ signal increases to become similar with the CH_3CO^+ yield in TPEPICO measurements at about 17 eV [5]. We note that the $m/z = 15$ ion yield curve has a quasi-plateau 17.5–19.5 eV, very similar to that of the $m/z = 45$ ion and where the integrated PES curve [35] tends to flatness.

5. Astrophysical implications

The results of our study are relevant to astrophysics in three areas: the interstellar medium (ISM), comets and meteorites. It has also some implications for exobiology. Acetic acid is considered to be one of the building blocks of life [50]. If preserved during the formation of the solar nebula, it could be brought to Earth via asteroids, comets and meteorites which can provide protective environments. In HI regions of the interstellar medium (ISM), the upper limit of UV radiation is 13.6 eV. Acetic acid in unscreened regions, subject to VUV radiation below 13.6 eV, will form ions above 10.6 eV. The ionization quantum yield (not yet measured), is unlikely to reach unity until about 17 ± 1 eV [1,51], and in the intervening energy region, superexcited states of acetic acid will be formed, states that relax mainly by dissociation and/or autoionization. At an excitation energy of 13.6 eV, i.e., 3 eV above the ionization limit, an ionization yield of about 50% is likely, as can be predicted on the basis of measurement of ionization quantum yields of polyatomic molecules [1,31,51]. Dissociative ionization will occur at photon excitation energies above 11.6 eV, the threshold for CH_3CO^+ formation. We note that photolysis of acetic acid in argon matrices by irradiation with a

hydrogen lamp ($E_{exc} \leqslant 10.2$ eV) results in the formation of CO_2 [52].

Protection from the destructive effects of VUV radiation is thus necessary in order to achieve detectable amounts of acetic acid in the ISM. Acetic acid has been observed in the ISM in hot molecular cores, which are warm condensations inside molecular clouds associated with active star formation regions, whose density is such that they will offer molecules some protection against radiation. A typical source is the molecular cloud complex Sgr B2, the acetic acid being found in a very small core, about 0.1 pc across [6]. This polyatomic molecule is probably synthesized on dust grain surfaces [53] and ejected into the ISM by evaporation or by shocks. It has been suggested that CH_3CO^+, the principal fragment ion in VUV dissociation of acetic acid, can react with water in the gas phase reaction to form $CH_3COOH_2^+$, followed by dissociative electron recombination to produce CH_3COOH [54]. There are other, more recent, suggestions for gas phase synthesis of acetic acid via ion molecule reactions [55]. Observations toward W51e2 show that the distribution of CH_3COOH is coincident with that of its much more abundant isomer, methyl formate $HCOOCH_3$, thus suggesting a similar formation mechanism [56].

It is known that ammonia and acetic acid can combine, in the laboratory, to produce aminoacids, in particular, glycine [57]. This could possibly occur in the ISM, where glycine has recently been reported in hot molecular cores in three regions of ongoing massive star formation [58]. This process of aminoacid formation is probably more easily achieved in cometary and meteoritic material contexts, which can provide various catalytic media and radiation screening.

Of the ions that we observe by dissociative ionization we note that HCO^+, $HOCO^+$ and CH_2OH^+ have been observed in the ISM, so that acetic acid is a possible parent molecule for part of the observed abundances. The dissociative photoionization of acetic acid to form HCO^+ is energetically possible above 12.85 eV, but its yield would be low in HI regions. The $HOCO^+$ ion is also observed in the galactic centre region and in Sgr B2 [59,60]. Since this is a region of the ISM where CH_3COOH has been observed, $HOCO^+$ could be produced, at least in part, from acetic acid (AE = 11.8 eV). The formation of CH_2OH^+ can occur above 12.05 eV, as discussed above, i.e., within the HI energy region.

Although it has not yet been observed in comets, acetic acid is strongly expected to exist in this medium where, for example in comet Hale-Bopp, its abundance has an upper limit, relative to H_2O, of 0.06%, as compared with 0.09% for formic acid [7]. Comets are thought to be one of the possible sources of extraterrestrial supply of organic material to the early Earth [61]. The species in the comet coma and tail are not screened from solar VUV radiation, so that acetic acid, if present, would be rapidly dissociated. Of the three ions observed by radioastronomy in comet Hale-Bopp two, CO^+ and HCO^+ [62], are species that can be formed by dissociative ionization of acetic acid. In future cometary observations it would be of interest to attempt to observe the ion CH_3CO^+ which would be a good marker of the presence of acetic acid, and also $HOCO^+$, which can be formed from both formic [10] and acetic acids. Observations of OH (A-X) emissions from acetic acid dissociation would require space observatory means but would probably be swamped by OH emission from water photodissociation processes.

Acetic acid is found in many meteorites. It is the most abundant of the monocarboxylic acids in the Murchison meteorite [63]. The work of Huang et al. [63] supports the suggestion of Cronin and Chang [64] that monocarboxylic acids may be mostly unaltered interstellar molecules.

Our results demonstrate that the spectroscopy and photophysics of acetic acid have potential applications in astrophysics and exobiology, in particular for understanding the formation and dissociation processes of this species, as well as properties of its dissociation products.

6. Summary and conclusions

Synchrotron radiation, photofragment fluorescence spectroscopy and mass spectrometry were used to study the VUV photodissociation and dissociative photoionization of gaseous acetic acid in the 6–23 eV photoexcitation range. Earlier studies were limited to the region below 11.7 eV. We recorded the dispersed fluorescence spectra excited at six different energies between 10 and 20 eV. The emission observed corresponds to OH ($A^2\Sigma^+ \rightarrow X^2\Pi$), CH ($A^2\Delta \rightarrow X^2\Pi$), CH ($B^2\Sigma^- \rightarrow X^2\Pi$) and H-Balmer transition features. We studied the relative intensities of these emissions by fluorescence excitation (FEX) spectroscopy over the range 6–22 eV. No other emissions were observed, in particular none from the HCOO radical. The fluorescence and FEX spectra were analyzed and the photodissociation processes forming the emitting electronic states of OH, CH and H were determined with the aid of data from VUV absorption spectra, FEX onset energies and thermochemical limit calculations. We found that the fluorescence quantum yields for OH and CH emissions, which varied over the 6–22 eV region, were always less than 1%. The photoionization mass spectra (PIMS) of CH_3COOH were measured at $E_{exc} = 20$, 25 and 100 eV, and the ion yield curves were measured over the range 6–23 eV for the parent and principal fragment ions. Features in the ion yield curves were correlated with features in the absorption and photoelectron spectra, reflecting in part the opening up of access to various ion states of acetic acid. The appearance energies of the principal ionic products were determined from the ion yield curves and compared with the values derived from thermochemical calculations. Our measured ionization energy of acetic acid, IE (CH_3COOH) $= 10.58 \pm 0.02$ eV is 40–60 meV lower than previous PIMS values. Dissociative ionization reaction channels are discussed in detail and their validity checked with the aid of experimental and calculated appearance energies and with

their compatibility with the results of TPEPICO measurements, carried out by Zha et al. [5] at much greater energy intervals (150–250 meV) than in our experiments (30 meV). H atom loss from the parent ion was not observed. The major fragment ion is CH_3CO^+. Its measured appearance energy calls into question previous determinations of the heat of formation and ionization energy of the acetyl radical. The assignment of the $m/z = 31$ ion to CH_2OH^+ is confirmed. A new pathway is suggested for the formation of HCO^+, and the assignments of the $m/z = 16$ ion to CH_4^+ and the $m/z = 28$ ion to CO^+ are justified. The formation of the important CH_3^+ ion at threshold is shown to involve carbon–carbon bond rupture and a potential energy barrier. At higher energies CH_3^+ is also formed by a reaction involving initial formation of the acetyl radical cation. Some astrophysical implications of our results are discussed concerning acetic acid in the interstellar, cometary and meteoritic media.

Acknowledgements

We thank François Dulieu and Jean-Louis Chotin for their valuable assistance during the synchrotron radiation beam time periods. We are grateful for support from the European Commission programme "Access to Research Infrastructures" for providing access to the Berlin BESSY synchrotron facility under contract FMRX-CT-O126 and for access to the LURE Synchrotron Facility in Orsay. Welcome support from the CNRS Groupe de Recherche "GDR Exobiologie"(GDR 1877) and from INSU is gratefully acknowledged.

References

[1] R.S. Berry, S. Leach, Adv. Electron. El. Phys. 57 (1981) 1.
[2] M.B. Robin, Higher Excited States of Polyatomic Molecules, Academic Press, New York, 1975.
[3] M. Suto, X. Wang, L.C. Lee, J. Phys. Chem. 92 (1988) 3764.
[4] Ya.Ya. Villem, M.E. Akopyan, Russ. J. Phys. Chem. 50 (1976) 394.
[5] Q. Zha, T. Nishimura, M.J. Bertrand, G.G. Meisels, Int. J. Mass Spectrom. Ion Proc. 107 (1991) 515.
[6] D.M. Mehringer, L.E. Snyder, Y. Miao, F.J. Lovas, Astrophys. J. 480 (1997) L71.
[7] J. Crovisier, D. Bockelée-Morvan, P. Colom, N. Biver, D. Despois, D. Lis, Astron. Astrophys. 418 (2004) 1141.
[8] D.K. Harvey, K.J. Feierabend, J.C. Black, V. Vaida, J. Mol. Spectrosc. 229 (2005) 151.
[9] S. Leach, M. Schwell, S. Un, H.-W. Jochims, H. Baumgärtel, Chem. Phys. 321 (2006) 159.
[10] M. Schwell, F. Dulieu, H.-W. Jochims, J.-H. Fillion, J.-L. Lemaire, H. Baumgärtel, S. Leach, J. Phys. Chem. A 106 (2002) 10908.
[11] O. Braitbart, S. Tobita, S. Leach, P. Roy, I. Nenner, Am. Inst. Phys. Conf. Proc. 258 (1992) 42.
[12] T.A. Field, F. Dulieu, J.-H. Fillion, J.-L. Chotin, S. Douin, J.-L. Lemaire, S. Leach, Chem. Phys. 250 (1999) 81.
[13] L.C. Lee, M. Suto, Chem. Phys. 110 (1986) 161.
[14] S.S. Hunnicutt, L.D. Waits, J.A. Guest, J. Phys. Chem. 93 (1989) 5188.
[15] S.S. Hunnicutt, L.D. Waits, J.A. Guest, J. Phys. Chem. 95 (1991) 562.
[16] D.R. Peterman, R.G. Daniel, R.J. Horwitz, J.A. Guest, Chem. Phys. Lett. 236 (1995) 564.
[17] I.P. Vinogradov, F.I. Vilesov, Khim. Vys. Energ. 11 (1977) 25.
[18] NIST Chemistry Webbook (2005), National Institute of Standards and Technology Standard Reference Database. Available from: <http://webbook.nist.gov>.
[19] S.G. Lias, J.E. Bartmess, J.F. Liebmann, J.L. Holmes, R.D. Levin, W.G. Mallard, J. Phys. Chem. Ref. Data 17 (Suppl. 1) (1988).
[20] J.C. Traeger, B.M. Kompe, in: J.A. Martinho Simoes, A. Greenberg, J.F. Liebman (Eds.), Energetics of Organic Free Radicals, Blackie Academic and Professional, London, 1996, p. 59.
[21] B. Ruscic, M. Schwarz, J. Berkowitz, J. Chem. Phys. 91 (1989) 6780.
[22] E.H. Kim, S.E. Bradforth, D.W. Arnold, R.B. Metz, D.M. Neumark, J. Chem. Phys. 103 (1995) 7801.
[23] S.J. Blanksby, T.M. Ramond, G.E. Davico, M.R. Nimlos, S. Kato, V.M. Bierbaum, W.C. Lineberger, G.B. Ellison, M. Okumura, J. Am. Chem. Soc. 123 (2001) 9585.
[24] J.L. Holmes, F.P. Lossing, P.M. Mayer, J. Am. Chem. Soc. 113 (1991) 9723.
[25] K.P. Huber, G. Herzberg, Constants of Diatomic Molecules, Van Nostrand Reinhold, New York, 1979.
[26] T. Ari, H.H. Güven, J. Electron Spectrosc. Rel. Phen. 106 (2000) 29.
[27] M.C.R. Symons, J. Phys. Chem. 87 (1983) 1833.
[28] S.D. Peyerimhoff, P.S. Skell, D.D. May, R.J. Buenker, J. Am. Chem. Soc. 104 (1982) 4515.
[29] A. Rauk, D. Yu, D.A. Armstrong, J. Am. Chem. Soc. 116 (1994) 8222.
[30] P.H. Cannington, N.S. Ham, J. Electron Spectrosc. Rel. Phen. 31 (1983) 175.
[31] J. Berkowitz, Photoabsorption, Photoionization and Photoelectron Spectroscopy, Academic Press, New York, 1979, p. 245.
[32] A.N. Stepanov, A.A. Perov, S.P. Kabanov, A.P. Simonov, High Energy Chem. 22 (1986) 81.
[33] K.D. Cook, J.W. Taylor, Int. J. Mass Spectrom. Ion Phys. 30 (1979) 93.
[34] D.J. Knowles, A.J.C. Nicholson, J. Chem. Phys. 60 (1974) 1180.
[35] F. Carnovale, T.H. Gan, J.B. Peel, J. Electron Spectrosc. Rel. Phen. 20 (1980) 53.
[36] T. Nishimura, G.G. Meisels, Y. Niwa, J. Chem. Phys. 91 (1989) 4009.
[37] H.-W. Jochims, M. Schwell, J.-L. Chotin, M. Clemino, F. Dulieu, H. Baumgärtel, S. Leach, Chem. Phys. 298 (2004) 279.
[38] D.N. Shigorin, A.D. Filygina, V.K. Potapov, Teor. Eksp. Khim. 2 (1966) 417.
[39] M.A. Haney, J.L. Franklin, Trans. Faraday Soc. 65 (1969) 1794.
[40] J.C. Traeger, R.G. McLoughlin, A.J.C. Nicholson, J. Am. Chem. Soc. 104 (1982) 5318.
[41] J.L. Holmes, F.P. Lossing, J. Am. Chem. Soc. 102 (1980) 3732.
[42] M.C.R. Cockell, J.M. Dyke, H. Zamanpour, in: C.Y. Ng (Ed.), Vacuum Ultraviolet Photoionization and Photodissociation of Molecules and Clusters, World Scientific, Singapore, 1991, p. 43.
[43] D.F. McMillen, D.M. Golden, Ann. Rev. Phys. Chem. 33 (1982) 493.
[44] W. Tsang, in: J.A. Martinho Simoes, A. Greenberg, J.F. Liebman (Eds.), Energetics of Organic Free Radicals, Blackie Academic and Professional, London, 1996, p. 22.
[45] H. Schwarz, D.H. Williams, C. Wesdemiotis, J. Am. Chem. Soc. 100 (1978) 7052.
[46] D.J. McAdoo, C.E. Hudson, L.L. Griffin, J. Phys. Chem. 88 (1984) 1481.
[47] E.T.M. Selim, A.I. Helal, Ind. J. Pure Appl. Phys. 19 (1981) 977.
[48] K. Hirota, K. Nagoshi, M. Hatada, Bull. Chem. Soc Jpn. 34 (1961) 226.
[49] B. Ruscic, M. Litorja, Chem. Phys. Lett. 316 (2000) 45.
[50] A. Brack (Ed.), The Molecular Origins of Life, Cambridge University Press, Cambridge, UK, 1998.
[51] H.-W. Jochims, H. Baumgärtel, S. Leach, Astron. Astrophys. 314 (1996) 1003.
[52] M.P. Bernstein, S.F.M. Ashbourn, S.A. Sandford, L.J. Allamandola, Astrophys. J. 601 (2004) 365.
[53] W.H. Sorrell, Astrophys. J. 555 (2001) L129.
[54] W. Huntress, G. Mitchell, Astrophys. J. 231 (1979) 456.

[55] V. Blagojevic, S. Petrie, D.K. Bohme, Mon. Not. R. Astron. Soc. 339 (2003) L7.
[56] A. Remijan, L.E. Snyder, S.-Y. Liu, D. Mehringer, Y.-J. Kuan, Astrophys. J. 576 (2002) 264.
[57] T.H.B. Kuiper, in: M.P. van Haarlem (Ed.), Perspectives on Radio Astronomy – Science with Large Antenna Arrays, Netherlands Foundation for Research in Astronomy, 1999, p. 275.
[58] Y.-J. Kuan, S.B. Charnley, H.-C. Huang, W.-L. Tseng, Z. Kisiel, Astrophys. J. 593 (2003) 848.
[59] P. Thaddeus, M. Guélin, R.A. Linke, Astrophys. J. 246 (1981) L41.
[60] Y.C. Minh, M.K. Brewer, W.M. Irvine, P. Friberg, L.E.B. Johansson, Astron. Astrophys. 244 (1991) 470.
[61] C. Chyba, C. Sagan, Nature 355 (1992) 125.
[62] F. Henry, J. Crovisier, D. Bockelée-Morvan, H. Rauer, D. Lis, Astrophys. Space Sci. 277 (2001) 303.
[63] Y. Huang, Y. Wang, M.R. Alexandre, T. Lee, C. Rose-Petruck, M. Fuller, S. Pizzarello, Geochim. Cosmochim. Acta 69 (2005) 1073.
[64] J.R. Cronin, S. Chang, in: J.M. Greenberg, C.-X. Mendoza-Gomez, V. Pirronello (Eds.), The Chemistry of Life's Origins, Kluwer, 1993, p. 209.

Available online at www.sciencedirect.com
ScienceDirect
Planetary and Space Science 54 (2006) 1073–1085
Planetary and Space Science
www.elsevier.com/locate/pss

VUV photochemistry of small biomolecules

Martin Schwell[a,*], Hans-Werner Jochims[b], Helmut Baumgärtel[b], François Dulieu[c], Sydney Leach[c]

[a]*Laboratoire Interuniversitaire des Systèmes Atmosphériques (LISA), Faculté des Sciences, CNRS-UMR 7583, Université Paris 7 & 12, 61 Avenue du Général de Gaulle, 94010 Créteil, France*
[b]*Institut für Physikalische und Theoretische Chemie der Freien Universität Berlin, Takustr. 3, 14195 Berlin, Germany*
[c]*Laboratoire d'Etude du Rayonnement et de la Matière en Astrophysique (LERMA), CNRS-UMR 8112, Observatoire de Paris-Meudon, 5 place Jules-Janssen, 92195 Meudon, France*

Accepted 10 April 2006
Available online 13 July 2006

Abstract

We review our recent results on the vacuum ultraviolet (VUV) photochemistry of small biomolecules. The experimental techniques used, mass spectrometry and photofragment fluorescence spectroscopy, are described. Emphasis is laid on our mass spectrometric results obtained for five nucleic acid bases and five amino acids. Ionisation and appearance energies are determined from photoionisation mass spectrometry, many for the first time. From this, fragmentation pathways following 6–22 eV photoexciation are derived. The adiabatic ionisation energies of the biomolecules studied lie between 8.2 eV (adenine) and 9.6 eV (α-amino-isobutyric acid). We show that the nucleic acid monocations, and chemically related molecular cations, do not fragment even when formed with large internal energies (E_{int}) ranging from 1.80 to 5.35 eV. In contrast, amino acid monocations are unstable and rapid fragmentation occurs via rupture of the C–C(OOH) bond, except for β-alanine, where rupture of the bond between the α-C and β-C is the lowest lying ionic dissociation channel. The VUV photochemistry of the prebiotic species formic acid, acetic acid and methylformate, studied in more detail previously by several techniques, including fluorescence spectroscopy, is also reviewed. Astrophysical implications of our work are discussed in the conclusion.

Keywords: VUV-astrochemistry; Nucleic acid bases; Amino acids; Photoionisation mass spectrometry; Photofragment fluorescence spectroscopy

1. Introduction

Small biomolecules, like nucleic acid bases (NABs) and amino acids (AAs) or chemically related molecules, have so far not been identified in the interstellar medium (ISM) or in other extraterrestrial media like cometary or planetary atmospheres, except possibly for glycine which has been reported from radioastronomy searches in the hot molecular cores Sgr B2(N-LMH), Orion KL, and W51 e1/e2. (Kuan et al., 2003a). Upper limits of abundance have been established for pyrimidine (Kuan et al., 2003b) and imidazole (Irvine et al., 1981). Pyrimidines and purines, the molecular skeletons of biologically important NABs, have been reported in the data obtained with the PUMA dust impact mass spectrometer during the flyby of comet Halley by the Soviet spacecraft VEGA 1 (Kissel and Krueger, 1987), however no molecular speciation could be inferred from these spectacular in-situ measurements. The difficulty in identifying these molecules by spectroscopic remote sensing techniques is probably due to their small abundances as well as current instrumental limitations. Furthermore, microwave and optical transitions in large molecules are in general more difficult to detect because the intensity of each band is reduced by a large partition function. The biomolecules could also be condensed on interstellar grains or icy comets. Their specific spectral features would be even more difficult to detect under these conditions since they would be modified by the surrounding matrix.

On the other hand, purine based NABs, as well as certain hydroxyl-pyrimidines, have been reported to have been found in the formic acid extract of the carbonaceous meteorites Murchison, Murray and Orgueil

*Corresponding author. Tel.: +33 1 4517 1521; fax: +33 1 4517 1564.
E-mail address: schwell@lisa.univ-paris12.fr (M. Schwell).

0032-0633/$ - see front matter © 2006 Elsevier Ltd. All rights reserved.
doi:10.1016/j.pss.2006.05.017

(Hayatsu et al., 1975; Stocks and Schwartz, 1981; Hua et al., 1986). We note however, that no additional publications appeared in the last 20 years to confirm these results, although several research teams tried intensively to identify these important molecules using ultra-modern analytical methods. Hence, at present one cannot conclude on an extraterrestrial presence of NABs.

AAs are also found in meteorites and micrometeorites (see chapters by J.L Cronin and M. Maurette in Brack, 1998). In these objects they could be embedded in polymer material. The chemical structure of this refractory polymer material is hitherto unknown (cf. Cronin, 1976a, b; Cronin and Pizzarello, 1983; Muñoz Caro et al., 2002). The abundance of AAs in meteoritic material strongly suggests their extraterrestrial presence.

As to the formation of small biomolecules in an astrophysical context, this is a vast subject that can not be treated in this article (for further reading see the books edited by Brack, 1998 and Chela-Flores et al., 2001). To give a glimpse here, earlier laboratory work has suggested that, for example, purines and pyrimidines may be formed in the ISM starting from hydrogen cyanide or cyanoacetylene (Basile et al., 1984), or even more simple gases like NH_3, N_2, CO_2 and H_2O (Lavrentiev et al., 1984). Pyrolysis-GC-MS has been applied to analyse HCN-polymers which are thought to be among the organic macromolecules most readily formed within the solar system, for example within planetary and cometary atmospheres. These experiments led to the identification of the purine based NABs adenine and xanthine (as methylated derivatives), as well as other nitrogen heterocycles (Minard et al., 1998). Recently, Muñoz Caro and co-workers (2002) have shown that the hydrochloric acid extract of the so-called ''yellow-stuff'', formed under UV irradiation of simulated interstellar ices in the laboratory, contains numerous AAs.

Exploring the VUV photochemistry of these important biomolecules is of considerable interest from an exobiological point of view, because of the possible delivery of these molecules from space to the early Earth, and the role that they could have played in the origin and development of life on earth, and possibly on other planets or satellites (Brack, 1998; Maurel and Décout, 1999; Sowerby and Heckel 1998; Sowerby et al., 2001). Furthermore, in the VUV spectral domain ($E_{photon} \approx 6-20$ eV; $\lambda \approx 62-200$ nm), the photoabsorption cross section of these molecules is even higher as compared to the mid-UV ($\lambda = 200$–400 nm, $E < 6$ eV) (see for example the pioneering monograph of Robin, 1974). In particular, all absorb strongly at $E = 10.2$ eV, where the intense Lyman-α stellar emission is located. Most of the small biomolecules studied have first ionisation energies (IE) below this energy, making ionisation phenomena an important issue to study. Additionally, we note that, in connection with the possible earthbound delivery of biotic molecules from space, the VUV luminosity of the early sun, during the Hadean period of considerable bombardment of the Earth from space was about two orders of magnitude higher than it is today, although the total luminosity was less (Chyba and Sagan, 1992).

Besides valence transitions, resonant excitation to Rydberg orbitals can also take place in the VUV spectral domain. These sharp electronic transitions converge to the 1st or higher ionisation energies. Beyond the first IE they are usually superimposed on a broad ionisation continuum. Their assignment can be achieved using the modified hydrogen series formula $E_n = \mathrm{IE} - [R/(n-\delta)^2]$ where the value $E_n - \mathrm{IE}$ gives the energetic distance for the Rydberg orbital to the corresponding IE (Robin, 1974). The principal quantum number n and the Rydberg constant R ($R = 13.605$ eV) have the same significance as in the hydrogen atom orbital structure. For the hydrogen atom δ equals 0, and the first member of the series ($n = 2$) is found at $E \approx 10.2$ eV corresponding to about 3/4 of the ionisation energy. The value $(3/4) \times \mathrm{IE}$ can be used to find the first member of a Rydberg series. For molecules, the quantum defect value δ is introduced which depends on the electronic structure of the positively charged molecular core (corresponding to its deviation from the ideal ''point charge'' H^+). The vibrational structure of Rydberg transitions in molecules can be identified with the aid of photoelectron spectra: Since the electrons populating the Rydberg orbitals are far from the molecular core, the vibrational frequencies of the latter are close to those of the corresponding cation.

Absorption of VUV photons can induce many important photo-processes, such as direct ionisation, autoionisation (resonant excitation of an excited state beyond the IE with subsequent coupling to the ionisation continuum releasing the ionised species), dissociative photoionisation, fluorescence of photofragments formed in excited states, as well as ion pair formation which can occur below and beyond the first IE. For a detailed review of these processes see Berry and Leach (1981). They can be explored by numerous experimental techniques, such as photoabsorption spectroscopy, photoion mass spectrometry (PIMS), photofragment fluorescence spectroscopy (PFS), photoelectron spectroscopy, to name only a few. In Section 2, we present in more detail two techniques used intensively by our group: PIMS and PFS in connection with synchrotron radiation (SR) as the photon excitation source. In Sections 3.1 and 3.2 of this article we highlight our work on the VUV photochemistry of NABs and AAs, published in more detail very recently (Jochims et al., 2004, 2005) and discuss their photostability. Section 3.3 will deal with more simple, ''prebiotic'' species studied also by our group.

To complete this introduction, we mention that also in the mid-UV, of course (neutral) photochemistry may occur, however photoabsorption cross sections are lower (Callis, 1983). This spectral domain is more accessible to experiments with pulsed lasers where the time-scales of photophysical processes following UV excitation can be studied. For example, the gas phase mid-UV photochemistry of purine NABs has been explored recently by resonant two-photon ionisation spectroscopy (Nir et al., 2001;

Lührs et al., 2001; Plützer et al., 2001; Plützer and Kleinermanns, 2002). Interestingly, the most prominent feature of the NABs mid-UV photochemistry in the gas phase is that internal conversion upon excitation in the 280–300 nm range, where the lowest lying excited electronic states are located, occurs very fast, on the pico-second time-scale. The purine nucleobases are therefore protected from mid-UV induced fragmentation. It has been argued that this could be the reason why evolution has arrived at this particular building block to store genetic information (Broo, 1998).

Recently, the photostability of AAs and NABs has also been studied in argon matrices at 12 K, irradiated by a microwave excited low pressure hydrogen lamp (Ehrenfreund et al., 2001; Peeters et al., 2003). This kind of lamp delivers a multiline emission spectrum with photons of wavelengths between 165 and 135 nm (7.5 eV < E < 9.2 eV). These experiments indicate that NABs and AAs are degraded photochemically at these wavelengths in an argon matrix (at 12 K). However, no wavelength dependent data nor quantum yields of photodissociation are obtained from these experiments. The derived "UV destruction cross sections", averaged over all wavelengths emitted by the hydrogen lamp, can be regarded as the product of the absorption cross section σ_{abs} and the photodissociation cross section σ_{diss} in the mixed solid state. They should be strongly dependent on (a) the mixing ratio inside the solid phase and (b) on the chemical nature of the solid phase in which they are embedded. Application of these UV destruction cross-sections to other solid phases than argon, for example to interstellar grains, or the gas phase should be handled with caution.

We finally indicate that gas phase measurements of NABs and AAs are also of significance for biology concerning the comprehension and determination of properties of these basic units when free from interactions.

2. Experimental methods to explore VUV photochemistry

Fig. 1 gives an overview of the different experimental set-ups used in our experiments. Different kind of experiments can be connected to the monochromator at the respective beamline. They will be described in the following.

2.1. Synchrotron radiation as a light source

SR is a very bright, broadband, polarised and pulsed source of light. Brightness is defined as photon flux per unit area and per unit solid angle. It is a more important quantity than light flux alone, particularly in applications where monochromators are used (so called "throughput-limited applications"). SR, linked to an appropriate monochromator, is an extremely important light source for the exploration of VUV photophysics and photochemistry. Its advantage, for example as compared to lasers, is mainly due to the spectral broadness of the available photons and the resulting ease of wavelength tunability in the VUV. The energetics of fragmentation channels can therefore easily be explored.

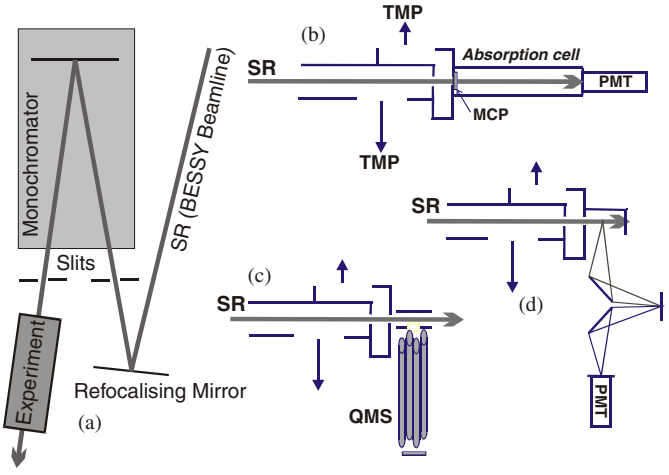

Fig. 1. Schematic schemes of the experimental set-ups used. (a) General setup. (b) VUV photoabsorption measurements. (c) Photoion mass spectrometry. (d) Photofragment fluorescence spectroscopy. SR = synchrotron radiation, TMP = turbomolecular pump, MCP = microchannelplates, PMT = photomultiplier tube, QMS = quadrupole mass spectrometer.

In electron storage rings designed as SR sources, there are three possible sources of radiation: dipoles (bending magnets), wigglers which act like a series of bending magnets with alternating polarities, and undulators which consist also in a sequence of multiperiod alternating magnet systems but in which the beam deflections are small resulting in a coherent interference of the emitted light and consequently in very high flux. In typical storage rings, several bunches of up to 10^{12} electrons circulate in an ultra-high vacuum, guided by the magnet fields of the dipole magnets. The most important characteristic for accelerators/rings designed especially for SR sources is that they have magnetic focusing systems which are able to concentrate the electrons into bunches of very small cross-section and where the electron transverse velocities are small (otherwise electrons are lost rapidly and the ring current would decrease fast, with undesired consequences on data acquisition times). The combination of high intensity with small apertures and small source dimensions results in a very high brightness. For further reading on SR see S.L. Hulbert and G.P. Williams in Samson and Ederer (2000).

In our experiments, SR was mainly obtained from the electron storage rings BESSY I and II, at Berlin. Our experiments are continuous in nature, thus do not take advantage of the pulsed structure of the light. A modified 1.5 m McPherson normal incidence monochromator ("NIM"), at the end of a dipole magnet beamline, has been mainly used in the studies presented here. Very recently, also 3 and 10 m focal length monochromators have been employed for completing measurements. The spectral bandwidth can be as low as 0.05 Å or less at the

currently used beamline at BESSY II (1200 lines/mm grating mounted on a 10 m focal length monochromator at the U125/2 undulator beamline). Generally, high resolution measurements can be necessary (a) if the data are to be incorporated into photochemical models since the solar Lyman-α emission is also very narrow (0.1 Å), but also (b) for exploring the temperature dependence of photoabsorption bands which is very important in space and planetary sciences.

2.2. Photoabsorption cross section measurements in the VUV spectral region

Absolute photoabsorption cross sections of many of the molecules studied by our group, especially NABs and AAs, have so far only been reported from measurements of films, because of the low volatility of these molecules. Their thermal fragility makes them difficult to measure at high temperatures. Using films, the optical reflectance is investigated and the absorption coefficient can be extracted (see for example Arakawa et al., 1986). Another possibility to obtain the optical constants of molecules of very low volatility is to record their electron energy loss spectra (EELS, see for example Isaacson, 1972). This technique also uses thin films as the substrate for measurements.

An inherent problem of the earlier gas phase measurements of the more volatile species, such as formic acid or acetic acid, is that the measurements of absolute absorption cross sections were often limited to energies below approximately 11 eV, corresponding to the cut off of the window material used in the absorption cell (see for example Robin, 1974; Suto et al., 1988). In our photoabsorption measurements we use a microchannel plate to delimit the optical path length in our absorption cell. This material transmits a sufficient portion of light to perform measurements and at the same time is an excellent barrier for gas phase molecules. We can therefore determine absolute absorption cross sections using the Beer–Lambert-Law beyond the above mentioned energy limit, which is of interest in an astrophysical context.

2.3. Photoionisation mass spectrometry

Since photoionisation and dissociative photoionisation are very important processes in the VUV, mass spectrometry is an excellent tool to get more insight into VUV photochemistry. In our experiments, monochromatised SR is focused into a differentially pumped gas cell which can be heated up to 400 °C in order to vaporise compounds in the liquid or solid state. They are placed 1–2 cm below the position of the incident VUV radiation within the ion extraction zone. The experimental set-up is described in more detail by Schwell et al. (2000). When thermally labile, biological compounds are investigated, the temperature has to be kept as low as possible. For example, experiments on NABs were typically performed at about 100 °C. This temperature was sufficient to provide an adequate stream of target molecules towards the ion source. When some thermally induced dissociation did occur this was easily identified in the observed mass spectra. For example, in the case of AAs, the appearance of an enhanced CO_2 mass peak ($m/z = 44$), enabled us to modify experimental parameters in order to achieve suitable experimental conditions of minimal thermal dissociation and satisfying signal intensity.

The photoion yield curves of parent and fragment ions (see Fig. 3 for example) were measured using a quadrupole mass spectrometer (Leybold Q200) which records the intensity of a given mass as a function of the incident photon energy. Measuring intervals are typical about 10 meV. The yield curves of the ions are normalised to the incident photon flux which is measured by detecting the fluorescence of a sodium salicylate coated window. Photon flux variations are due to the grating transmission function of the primary monochromator and descending storage ring current. The spectral bandwidth of the incident monochromatic radiation applied during PIMS measurements was typically 2 Å corresponding to an energy resolution of about 25 meV at a wavelength of 1000 Å. Ionisation energy determinations are carried out with a MgF_2 filter (100% cut-off effective at 11 eV) in order to suppress high energy stray light and second-order radiation which is an inherent problem of experiments with monochromatised SR. Ion appearance energies were determined mainly with the aid of semi-log plots of the ion yield curves. For many of the biological molecules under study here, we report adiabatic ionisation energies and fragment appearance energies (AE) that were previously unknown. Also, the limited data previously available, mainly from electron impact measurements, suffer often from unsatisfactory precision and poor detection sensitivity resulting in too high IE and AE values and large errors. More precise AE data for these compounds, measured with photon impact, are therefore important in order to explore the energetics of their VUV degradation pathways. In particular, this information permits assessment, on thermochemical grounds, of possible ionic and neutral products, as well as enabling one to choose between alternative dissociation channels.

The measured fragment AEs are *effective* thermochemical values. They are a function of instrumental detection sensitivity and also reflect effects of thermal energy since any activation barrier of a particular fragmentation process (1) could lead to depositing internal or kinetic excess energy in the fragments. Measurement of AEs are subject to this so-called "kinetic shift". In this respect, our measured AEs represent upper limit values. Using Eq. (2), the AEs are used to calculate *apparent* enthalpies of formations of the respective fragment ion m_1^+ ("*app*-$\Delta_f H^\circ$ (m_1^+)") which can be formed by different possible fragmentation pathways. Here, also different and/or several neutral fragments m_i, including isomers, have to be considered.

$$M + h\nu \rightarrow M^+ + e^- \rightarrow m_1^+ + xm_i, \quad (1)$$

$$app - \Delta_f H^{\circ}_{\mathrm{gas}}(m_1^+) = \mathrm{AE} + \Delta_f H^{\circ}_{\mathrm{gas}}(M) - \sum_{i=1}^{x}[\Delta_f H^{\circ}_{\mathrm{gas}}(m_i)]. \quad (2)$$

The measured apparent $\Delta_f H^{\circ}{}_{gas}$ (m_1^+) values are then compared to tabulated standard thermochemical enthalpies of formation $\Delta_f H^{\circ}(m_1^+)$, if available, thus permitting assignment of particular fragmentation channels (see for example the scheme presented in Fig. 4 which has been derived from our measurements as discussed in Jochims et al., 2005). If literature $\Delta_f H^{\circ}$ (m_1^+) values are not available, the measured app-$\Delta_f H^{\circ}$ values represent new values to be used in the future for m_1^+. We also hope to incite theoretical work with our measurements, on the thermochemistry of these fragments (neutral and cationic) in order to clarify further the fragmentation pathways.

2.4. Photofragment fluorescence spectroscopy

For fluorescence measurements, the SR light beam is focused into an open brass cell, differentially pumped, containing the vapour to be studied at a typical pressure of about 10^{-3} mbar. The induced fluorescence, in general produced by photo-excited fragments, passes through a quartz window and is dispersed using a 20 cm focal length monochromator (Jobin-Yvon H20, dispersion 4 nm/mm). In our experiments we generally observe the emitted fluorescence in the 250–550 nm spectral region, with a resolution depending on the choice of the exit slit (0.5, 1, or 2 mm). The spectral response function used for deconvolution of the observed spectra, has been determined by recording the emission of a tungsten halogen lamp. When recording the fluorescence excitation (FEX) spectra, the H20 secondary monochromator is fixed at a desired wavelength (for example at $\lambda = 310$ nm corresponding to the OH ($A^2\Sigma^+ - X^2\Pi$) transition) with a large exit slit. The primary monochromator is then tuned in steps of typically around 30 meV. The observed FEX spectrum reveals, in conjunction with the photoabsorption spectrum, the electronic states of the parent molecule producing the emitting photofragment (see for example Fig. 6b). After appropriate calibration of the observed fluorescence intensity, state selective quantum yields of a particular fragmentation channel can be derived. In contrast to mass spectrometry, fluorescence spectroscopy enables us to explore fragmentation processes below the ionisation limit.

3. Selected results

In this section we present selected results obtained recently. A detailed discussion of these results can be found in the cited references. Fig. 2 gives an overview of the molecules studied by our group in recent years.

3.1. Ionisation and dissociative ionisation of nucleic acid bases

NABs have been studied by PIMS (Jochims et al., 2005; Schwell et al., 2006). Table 1 summarises our results on

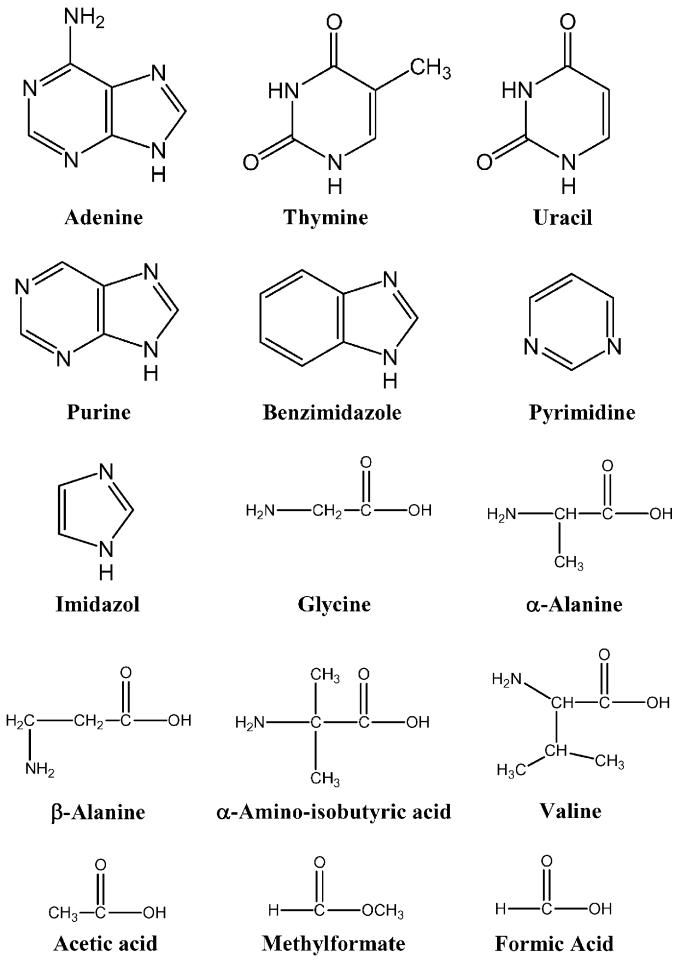

Fig. 2. Biomolecules and prebiotic species investigated in recent years by our group.

NABs and also on AAs. We show measurements of the first ionisation energy together with appearance energies of the lowest lying ionic dissociation channel. The third column gives the difference between these two values indicating the internal energy E_{int} necessary to photodissociate the respective molecule at a particular rate. It has been shown in earlier work (Jochims et al., 1994), where the same experimental equipment was used, that our observed AEs correspond to a photodissociation rate of about $k_{\mathrm{diss}} = 10^4\,\mathrm{s}^{-1}$ at the energy of the ion onset. This estimation is based on RRK model calculations (RRK = Rice, Ramsperger, Kassel theory) of the photodissociation rate of polycyclic aromatic hydrocarbons (PAHs), in particular their H-loss reactions which are the energetically lowest lying VUV photodissociation channels in PAHs (for details see Jochims et al., 1994). It is valid for other molecules and other fragmentation reactions too, since k_{diss} at the observed threshold of ion formation is an experiment-specific quantity.

The NABs studied have E_{int} values ranging from 1.80 eV (uracil) to 3.36 eV (adenine). For the non-biological base benzimidazole E_{int} equals 5.35 eV. These values are fairly large but slightly lower than in PAHs where values from

Table 1
First ionisation energy (IE, adiabatic value), lowest appearance energy (first fragment AE) and E_{int} as measured by photoionisation mass spectrometry (the given errors represent the experimental uncertainty of the ion onset as read from the respective photoion yield curves)

	First IE (eV)	First AE (eV)	E_{int} (eV)	Dissociation channel
Adenine	8.20±0.03	11.56±0.05	3.36±0.08	HCN loss
Purine	9.35±0.05	12.6±0.05	3.25±0.1	HCN loss
Benzimidazole	8.22±0.05	13.57±0.1	5.35±0.15	HCN loss
Thymine	8.82±0.03	10.70±0.05	1.88±0.08	HNCO loss
Uracil	9.15±0.03	10.95±0.05	1.80±0.08	HNCO loss
Pyrimidine	9.05±0.05	12.27±0.05	3.22±0.1	HCN loss
Imidazole	8.66±0.03	11.41±0.05	2.75±0.08	HCN loss[a]
Glycine	9.02±0.02	9.38±0.05	0.36±0.07	$NH_2CH_2^+ + COOH$
α-Alanine	8.75±0.05	9.05±0.1	0.3±0.15	$NH_2CH_3CH^+ + COOH$
β-Alanine	8.8±0.1	9.3±0.1	0.5±0.2	$NH_2CH_2^+ + CH_2COOH$
α-Amino-isobutyric acid	9.6±0.2	9.1±0.1[b]	(0)	$NH_2C(CH_3)_2^+ + COOH^-$
Valine	8.9	—	—	$NH_2(CH_3)_2(CH)_2^{+c} + COOH$

[a]Two other dissociation channels (H loss and HCN + CH loss) have similar appearance energies (see Schwell et al., 2006).
[b]Ion pair formation below first IE.
[c]Most intense cation at $E = 20$ eV.

4.62 (benzene) to 12.05 (coronene) were observed (Jochims et al., 1994). Another difference is that the lowest lying dissociation reaction in PAHs is H-loss from the parent cation whereas in NABs these are the HCN and HNCO loss reactions although they both require rupture of at least two bonds. The reason for this is most certainly the thermodynamically stable HCN molecule ($\Delta_f H^\circ = 1.401$ eV (Chase, 1998)). For the molecules presented in this study, below 20 eV photon energy the H loss reaction is either not observed or the corresponding $(M–H)^+$ ion is very weak, except for imidazole (Mol. mass = 68.08 a.m.u.) where AE ($m/z = 67$) is observed to be 12.05±0.03 (Schwell et al., 2006).

As an example of our PIMS measurements we show photoion yield curves of the adenine parent cation (Mol. mass = 135.13 a.m.u.) and its most important fragment ions (Fig. 3). We determined the adiabatic ionisation energy to be 8.82±0.03 eV. In Fig. 4, we show the adenine fragmentation scheme as deduced from our measurements and earlier measurements obtained with electron impact (EI) ionisation (cf. also our detailed discussion and references cited in Jochims et al., 2005). Chemical structures of important ions are also proposed in Fig. 4. However, these structures have to be confirmed by theoretical work to be performed in the future.

The principal fragmentation pathways involve four successive losses of neutral HCN molecules as indicated in Fig. 4 together with the corresponding appearance energies AE measured by PIMS. The initial HCN fragmentation, involving atoms 1 and 2 (see numbering used in Fig. 4), requires two bond ruptures. It is more energy consuming than the succeeding HCN losses which each probably require only one bond rupture in the precursor fragment ion and/or it corresponds to successively smaller total reorganisation energy. The loss mechanisms could be quite complex and may involve loss of HNC as well as HCN. The fate of the primary fragment

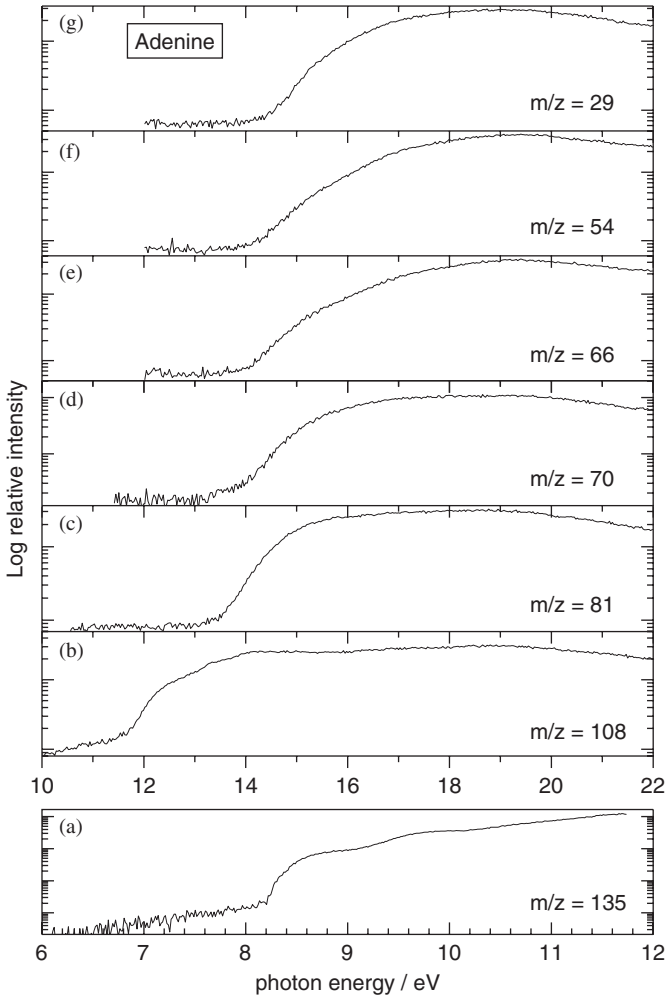

Fig. 3. Selected photoion yield curves of adenine (we note that in Fig. 2 of the original publication (Jochims et al., 2005) an error has occurred: There, $m/z = 65$ is actually $m/z = 66$ and 53 is actually $m/z = 54$. This has been corrected here).

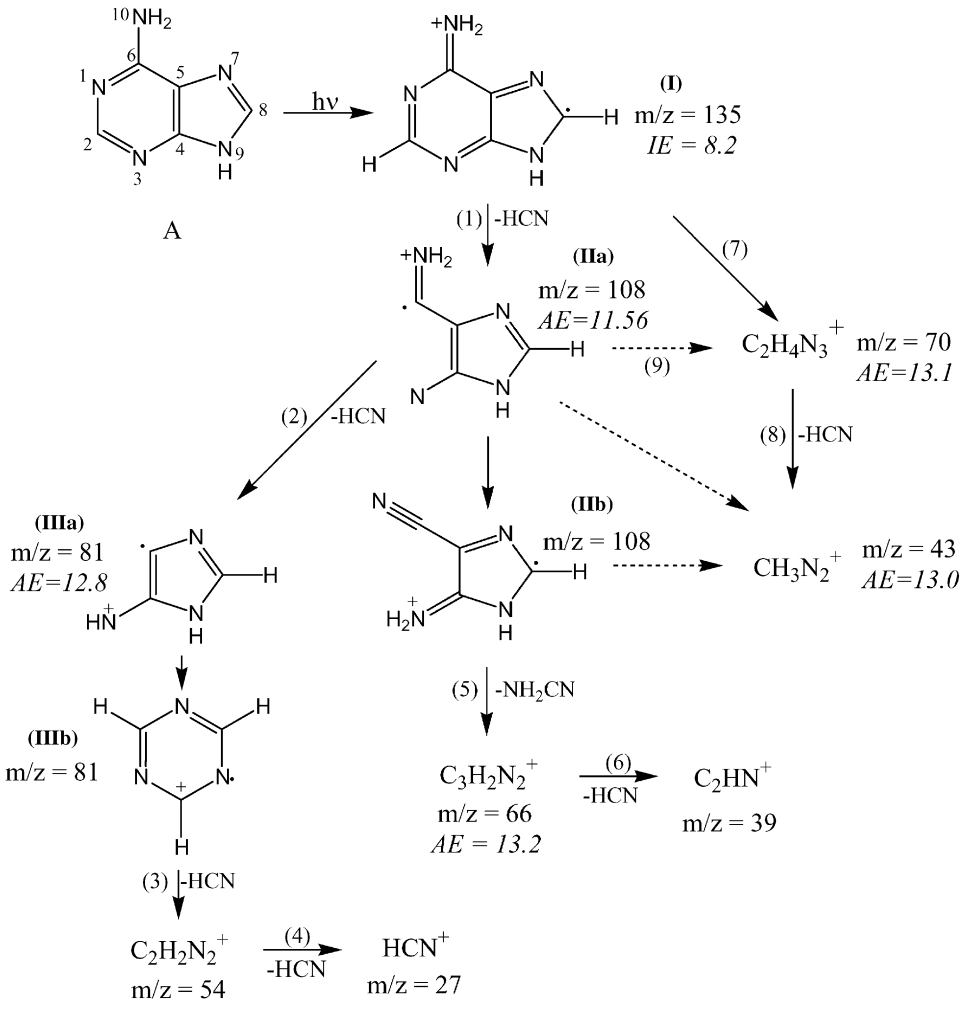

Fig. 4. Scheme of the VUV induced fragmentation of adenine. The measured appearance energies (IE and AEs) for each ion are also indicated (in eV, for experimental errors refer to Table 1).

IIa ($m/z = 108$) can be either loss of C_2N to give the ion $m/z = 70$ or isomerisation to species IIb which is probably thermodynamically more stable. This species subsequently loses NH_2CN to give the important ion $m/z = 66$ which can in turn lose a neutral HCN unit. The intense ion $m/z = 43$ ($CH_3N_2^+$) can be formed by several pathways as indicated in Fig. 4. A similar picture comes out from our recent measurements on purine and benzimidazole (Schwell et al., 2006): In purine (Mol. mass = 120.11 a.m.u.), successive loss of two HCN molecules is also the predominant fragmentation pathway at low energies ($E < 13.6$ eV). The respective appearance energies are 12.6 ± 0.05 and 13.24 ± 0.1 eV. The parent cation of the non-biological base benzimidazole (Mol. mass = 118.14 a.m.u.) shows a remarkable stability domain, from 8.22 ± 0.05 to 13.57 ± 0.1 eV ($E_{int} = 5.35 \pm 0.15$ eV, see Table 1).

In thymine, the dominant fragmentation reaction is loss of HNCO (Isocyanic acid, see Table 1) by Retro–Diels–Alder reaction from the parent cation to give the $m/z = 83$ ion (AE = 10.7 eV). This ion, which may have a cyclic structure, is also quite stable since further loss of CO occurs only if an additional 1 eV is added. Also in uracil (Mol. mass = 112.09 a.m.u.), HNCO loss is the energetically lowest lying ionic fragmentation process (AE = 10.95 eV). Further fragmentation gives the astrophysically important ion $HCNH^+$ ($m/z = 28$, AE 13.75 eV) with high intensity (see discussion on this ion below). In the non-biological bases pyrimidine and imidazole, HCN fragmentation dominates like in the case of purine, adenine and benzimidazole.

We note that quantum-chemical calculations, like those of Improta et al. (2000), on the structure and thermodynamics of fragment ions, are extremely helpful when analysing the degradation pathways.

3.2. Ionisation and dissociative ionisation of amino acids

A detailed discussion of our results for five AAs is given in Jochims et al. (2004). Major results are shown in Table 1. All the five species studied are found in meteoritic material (M. Maurette in Brack, 1998). We mention that in

biological media, AAs exist as zwitterions over a considerable range of pH values, but in the gas phase this particular form has not been observed yet so that we can assume to only study neutral monomers in our experiments. Their photoabsorption has been studied earlier (Serrano-Andrès and Fülscher, 1996 and references cited there) and shows that these molecules absorb strongly at the Lyman-α line at 10.2 eV.

For glycine (Mol. mass = 75.07 a.m.u.), the three ions $m/z = 75$, 30, 28 are present in the mass spectrum at 10 eV.With the help of PIMS measurements of fully deuterated glycine-*d*5, we could assign the $m/z = 30$ ion (AE = 9.38 ± 0.05) to be the aminomethyl radical cation, $NH_2CH_2^+$, formed by simple rupture of the C–C(OOH) bond. Formation of the CH_3NH^+ isomer is very unlikely since this species is thermodynamically less stable by 88 kJ/mol and its formation would require rearrangement, either of the parent or of the fragment ion. The third possible assignment, H_2CO^+, can also be excluded since the D_2CO^+ ion $m/z = 32$ is absent in the glycine-*d*5 mass spectrum. The glycine parent cation thus loses the COOH group at a relatively small amount of internal energy ($E_{int} = 0.36 \pm 0.07$ eV) above the first ionisation energy.

The second most intense fragment ion in the dissociative photoionisation of glycine, $m/z = 28$, is assigned to the $HCNH^+$ ion since the two other possible isomers, H_2CN^+ and CNH_2^+, are thermodynamically less stable (DeFrees and McLean, 1985). Its appearance energy is around 9 eV (the onset of this ion is very smooth so that its AE is difficult to determine) and different pathways leading to its formation have been discussed by Jochims et al. (2004).

We remark that $HCNH^+$ is observed in several galactic sources in the ISM (Schilke et al., 1991) and including the region where glycine has possibly been observed (Sgr B2). Electron capture by $HCNH^+$ is thought to be an important source of HCN (+H) and HNC (+H) in dark molecular clouds (Schilke et al., 1991; Semaniak et al., 2001). HCN and HNC are considered to be important in the synthesis of several organic molecules in the ISM. Our results suggest that $HCNH^+$ can be formed from glycine in HI regions where the upper limit of photon energies is 13.6 eV. Thus further radioastronomical searches of glycine should explore regions close to where $HCNH^+$ is observed, but where reasonable VUV shielding is present. We note that $HCNH^+$ is also an important ion in the ionosphere of Titan (Molina-Cuberos et al., 1999).

Below 13.6 eV, the principal fragment ions observed in the dissociative photoionisation of α-alanine (Mol. mass = 89.09 a.m.u.) are $m/z = 44$, 42, 28, 18. Their appearance energies and possible formation pathways have been reported by Jochims et al. (2004). Also here, earlier electron impact mass spectra of the deuterated the α-alanine-*d*3 (Junk and Svec, 1963) helped to assign the chemical structure of the ions. $HCNH^+$ is observed as an intense ion too (AE = 12.35 eV). The $m/z = 74$ ion, corresponding to the loss of the methyl group connected to the α-carbon of the parent cation, is very weak meaning that this is a minor fragmentation pathway. As in the case of glycine, the lowest lying fragmentation pathway (see Table 1) corresponds to the rupture of the C–C(OOH) bond to form $NH_2CH_3CH^+$ ($m/z = 44$).

In contrast, the most intense ion from the dissociative photoionisation of β-alanine (Mol. mass = 89.09 a.m.u.) is $m/z = 30$, corresponding to the $NH_2CH_2^+$ ion formed by bond rupture between the α- and β-carbon of the molecule leaving the CH_2COOH radical behind. $HCNH^+$ formation is less important in this molecule (AE = 14.2 ± 0.1 eV).

An interesting case is α-amino-isobutyric acid (Mol. mass = 103.12 a.m.u.). Here the appearance energy of the most intense fragment ion ($m/z = 58$) is even lower than the first IE of the molecule (see Table 1) thus implying that ion pair dissociation, forming $NH_2C(CH_3)_2^+$ and $COOH^-$, is an important contributor to the $m/z = 58$ mass peak. The second most intense fragment ion is $m/z = 42$. Its measured appearance energy (11.8 eV) suggests formation by NH_2 loss from the $NH_2C(CH_3)_2^+$ ion formed at lower energies (see the discussion in Jochims et al., 2004).

3.3. Other prebiotic molecules: formic acid, acetic acid and its isomer methylformate

Formic acid (HCOOH), acetic acid and methylformate are all observed in the ISM (Müller et al., 2005). Therefore, improvement of molecular cloud astrochemical models requires photophysical data in the VUV. These species, which we consider to be of "prebiotic" character, have been studied intensively by our group (Schwell et al., 2002; Leach et al., 2002, 2003, 2006a, b).

3.3.1. Formic acid

Firstly, we note that our high resolution (15 meV) HeI photoelectron spectra of four isotopologues of formic acid (HCOOH, DCOOH, HCOOD, DCOOD) has been recently used by Rudberg and Brinck (2004) to improve the difficult calculation of Franck-Condon factors for transitions from the ground state of the neutral molecule to the two lowest lying excited states of the formic acid cation. In this paper, we show as an extract from our results the PFS spectra recorded following VUV photoexciation of HCOOH (Figs. 5 and 6).

The dispersed fluorescence spectrum at 12 eV excitation energy (Fig. 5) is unsmoothed, but corrected for the spectral response of the detection system. At this energy, we observe two band systems, the first being the OH ($A^2\Sigma^+ \rightarrow X^2\Pi$) emissions at 308 (0–0) and 282 nm (1–0) and the second consisting of a long-vibrational progression between 330 and 480 nm (spacing of about 600 ± 40 cm^{-1}), the intensity maximum of which is at 375 nm, superimposed on a broad continuous background. Earlier work at lower energies helped to assign the emitter to be the HCOO radical (see our discussion in Schwell et al., 2002). In Fig. 6, we show the FEX spectra of the OH ($A^2\Sigma^+ \rightarrow X^2\Pi$) emission ($\lambda_{obs} = 310$ nm) and of the HCOO emission at 375 nm (Fig. 6b), from 9 to 13 eV excitation energy.

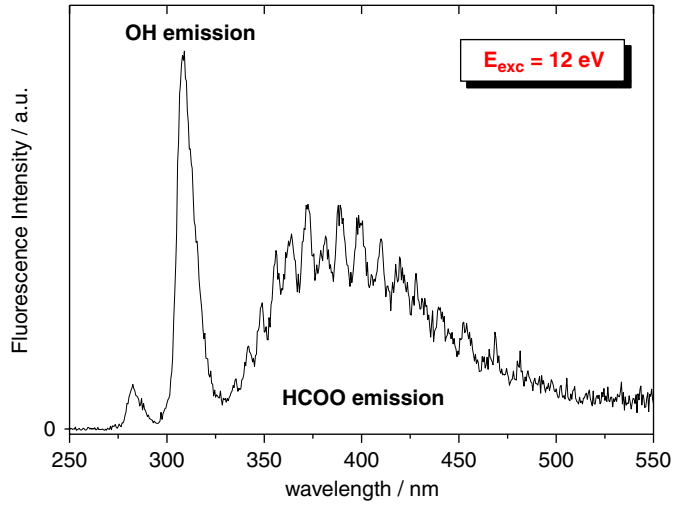

Fig. 5. Dispersed fluorescence from formic acid at 12 eV excitation energy ($\lambda_{exc} = 103$ nm).

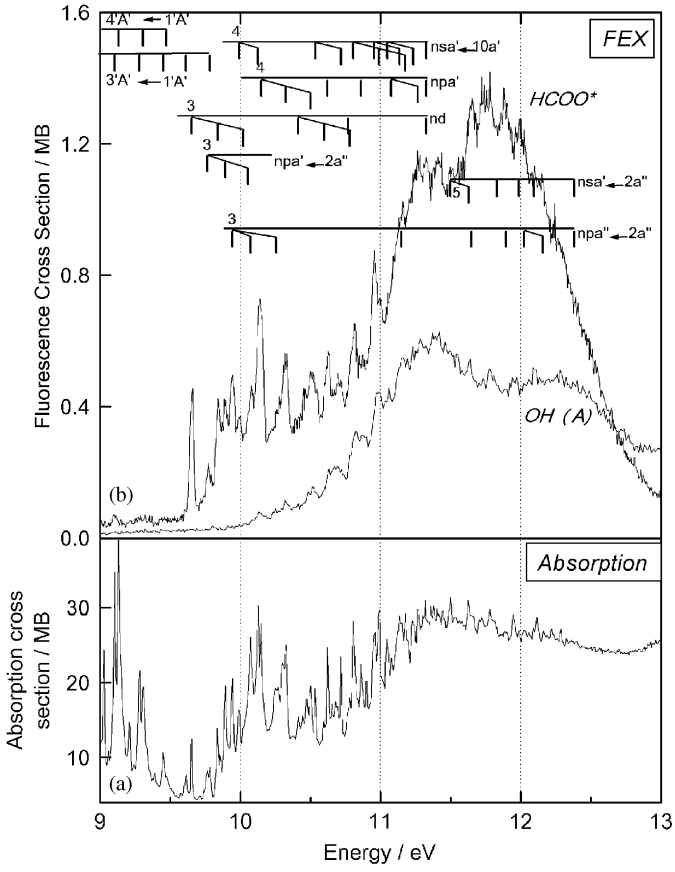

Fig. 6. (a) Photoabsorption of Formic acid. (b) Fluorescence excitation spectra (FEX) for OH and HCOO emission. Rydberg transition assignments are indicated by bars.

For comparison, we also show the photoabsorption spectrum of formic acid (Leach et al., 2002, Fig. 6a). In the FEX spectra, the weak onset of OH ($A^2\Sigma^+ \rightarrow X^2\Pi$) emission is observed at 9.15 eV (136.6 nm). From enthalpy of formation data and the OH ($A^2\Sigma^+$) T_0 value (see the NIST chemistry webbook) we can calculate the thermochemical onset for the reaction HCOOH → HCO + OH ($A^2\Sigma^+$) to be 8.85 eV.This is about 300 meV below our measured onset energy of the OH (A) emission. This difference indicates the existence of a potential barrier between the HCOOH excited state and the dissociation surface leading to the OH (A) fragment. This is consistent with the slow rise of the OH emission yield in the first electron volt beyond the onset, which is typical for photochemical dissociations involving potential barriers. Also the HCOO FEX spectrum increases with increasing photon energy below the first IE. Furthermore, it appears that most of the features observed in the OH (A) FEX spectrum are also observed in the HCOO FEX spectrum but with different relative intensities. This is particularly evident, for example, in the energy region between 10 and 11 eV (see Fig. 6b). It indicates that the corresponding HCOOH excited states can fragment into each of the two dissociation channels. However, the branching ratio of the two dissociation reactions HCOOH → HCO + OH (A) and HCOOH → HCOO ($^2B_1$) + H varies considerably as a function of excitation energy as is evident from Fig. 6.

3.3.2. *Acetic acid and its isomer methylformate*

Two papers on the VUV photophysics of acetic acid have been published very recently: The photoabsorption of this molecule has been analysed in detail by Leach et al. (2006a). PIMS and PFS experiments were also performed for this important species (Leach et al., 2006b). We further mention the pioneering work of Suto et al. (1988) who measured absorption cross sections and fluorescence quantum yields from photodissociative excitation of these molecules below 11.2 eV. The acetic acid absorption spectrum (Fig. 7a, bandwidth 0.9 Å) shows valence transitions as well as Rydberg transitions converging to the ground state of the CH_3COOH^+ ion ($IE_{CH_3COOH} = 10.58 \pm 0.02$ eV, Leach et al., 2006b). Band attributions will not be discussed in this paper, they are given in Leach et al. (2006a). In Fig. 7b we also include the absorption spectrum of the isomer methylformate (bandwidth 0.9 Å). Also in this molecule, Rydberg transitions converging to the first ionisation energy, at 10.835 eV (Waterstradt et al., 1994), are observed. Several broad features are observed between 11 and 18 eV, like in the case of acetic acid. A detailed analysis of the methylformate absorption spectrum will be given in a forthcoming publication.

To our knowledge, the absolute absorption spectra of both compounds were not known above 11.2 eV.The two spectra presented in Fig. 7 are qualitatively similar in that the absolute cross sections are continuously increasing between 6 and 17 eV, starting from 0 Mb reaching a plateau value of about 70 Mb at 17 eV (1 Mb = 10^{-18} cm^2). We note that below 6 eV the cross section is not zero for both molecules: a very weak band, extending from about 200 nm (6.2 eV) to about 240 nm (5.2 eV) has been observed by Suto et al. (1988), with cross sections below 0.3 Mb. These bands correspond to the lowest lying singlet–singlet transitions of the two molecules ($\pi^* \leftarrow n_O$). In our experiment, the grating transmittance of the primary

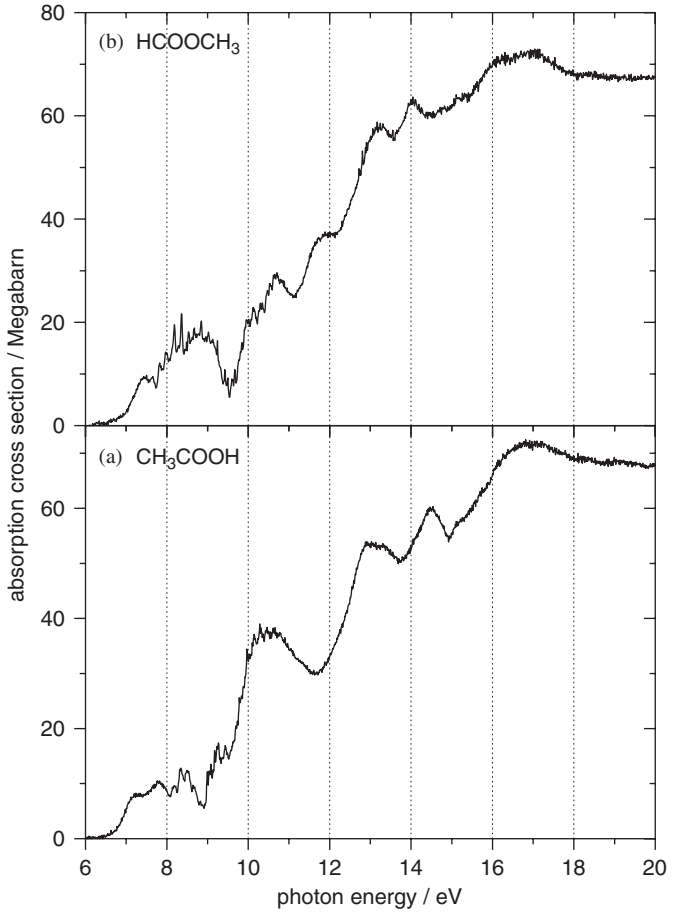

Fig. 7. Comparison of VUV photoabsorption spectra of acetic acid and methyl formate, between 6 and 22 eV (bandwidth 0.9 Å).

monochromator was not sufficient below 6 eV in order to observe such weak bands.

4. Conclusion and astrophysical implications

In this paper we reviewed results obtained recently by our group, on the photochemistry of small biomolecules and some prebotic species in the VUV spectral region (6–20 eV). The results are important in an exobiological context, concerning the prediction of the photostability of these molecules in VUV radiation fields.

Extensive PIMS measurements have been performed on nearly all of the molecules studied. The results enabled us to give new thermochemical values for many cations, parent and fragments. The parent cations of NABs are found to be stable for fairly large internal energies E_{int} above the ionisation limit (for example adenine: 8.2–11.56 eV, 140–107 nm, $E_{int} = 3.36$ eV). Since our appearance energy measurements correspond to a photodissociation rate of about $k_{diss} = 10^4\,s^{-1}$ at the measured ion onset (Jochims et al., 1994), we can suppose that in the energy domain from the first IE up to the first fragment AE the NAB cations would preferably relax via IVR (internal vibrational rotational redistribution) and related to infrared emission in the virtually collisionless conditions of the ISM, as discussed by Jochims et al. (1994). However, this hypothesis has to be confirmed by measurements of the IR emission rate of these molecules. We hypothesise further that the relative stability of NAB cations can be associated with their aromatic ring system, capable of stabilising a positive charge.

The VUV fragmentation of NABs and AAs is quite complex and has been analysed in detail by Jochims et al. (2004, 2005). In the present paper we discussed the most important fragmentation reactions.

The dominant ionic fragmentation channel of the NABs in the $E < 13.6$ eV energy regime is loss of HCN which is observed for adenine, purine, benzimidazole, pyrimidine, and imidazole. In thymine and uracil, however, HNCO loss is the lowest lying fragmentation channel. We note that HCN and HNCO are both observed in cometary atmospheres (Cottin et al., 1999). HCN (but not HNCO) is observed in the atmosphere of Titan and vertical profiles have been retrieved recently by the UVIS spectrometer on board the Cassini spacecraft (Shemansky et al., 2005). We speculate that these molecules may originate, in part, from NABs or other aromatic nitrogen heterocycles, photodegraded in the VUV. Solar system searches for NABs should therefore be focused on objects and regions where their fragments HCN and HNCO are observed.

The radical CN is another important species observed in cometary atmospheres (see Fray et al., 2005 and references cited therein) and in the ISM (Müller et al., 2005). This radical is apparently not produced in the VUV photodissociation of gaseous NABs at energies below 20 eV, since the counter-ion $(M–CN)^+$ is not observed and none of the postulated fragmentation pathways in the VUV involve the loss of neutral CN (Jochims et al., 2005). In cometary atmospheres CN originates mostly from the photodissociation of HCN but also other sources, like solid HCN polymers, have been considered to contribute to the observed CN production rate (Fray et al., 2005).

AA parent cations fragment at only small internal energies above the ionisation limit (Jochims et al., 2004) and their stability against VUV radiation is therefore very much reduced as compared to NABs. The lowest lying fragmentation reaction of the AAs studied is rupture of the C–C(OOH) bond to give the $(M–COOH)^+$ ion and neutral COOH or CO_2 and H. This result is qualitatively consistent with the experiments at lower energies performed by Ehrenfreund et al. (2001) who observed the CO_2 IR absorption bands upon irradiation of AAs. The additional H-loss of the primary photofragment COOH in the matrix experiments remains to be explained since this reaction is endothermic (in contrast to the reaction $HCOO \rightarrow CO_2 + H$ which is exothermic). Sometimes COOH is also referred to as "HOCO". This species should not to be confused with its isomer HCOO which is a principal fragment in the VUV degradation of formic acid (see above). We note that the $HOCO^+$ ion is also observed in the ISM (Müller et al., 2005).

The astrophysically important $HCNH^+$ ion is observed in the dissociative photoionisation of glycine (AE = 13.0 ± 0.1 eV), α-alanine (12.35 eV), β-alanine (AE = 14.2 ± 0.1 eV), α-amino-isobutyric acid and α-valine (AE determination not possible for the latter two AAs). Searches for glycine or other AAs should thus be focused on regions where this ion is present and at the same time shielding by solid material can be expected.

Our study of the prebiotic species HCOOH, CH_3COOH, $HCOOCH_3$, all observed in the ISM, revealed their principal fragmentation pathways in the VUV. Their photoabsorption cross sections have also been measured, from 6 to 22 eV (bandwith 0.9 Å). Absorption spectra of these species above 11.2 eV were not known before. When HCOOH is excited with photon energies that correspond to astrophysical HI regions ($E_{photon} < 13.6$ eV) we detect OH ($A^2\Sigma^+ \rightarrow X^2\Pi$) emission and HCOO* emission in the UV/Vis spectral region, related to the photoreactions $HCOOH \rightarrow OH\ (A^2\Sigma^+) + HCO$ and $HCOOH \rightarrow H + HCOO^*$ which hence must be considered as important photoreactions in the VUV for $E > 9.5$ eV. Although in our experiments we cannot observe non-fluorescent fragments it is reasonable to assume that the same photoreactions yielding the fragments in their respective ground states are important, also below 9.5 eV. The yields of these processes however remain to be quantified. Since HCOO is thermodynamically unstable with respect to CO_2 and H, the photodissociation processes $HCOOH \rightarrow OH + HCO$ and $HCOOH \rightarrow 2H + CO_2$ constitute the main fragmentation pathways of formic acid below 13.6 eV.

In the VUV excited photodissociation of Acetic acid we detect OH ($A^2\Sigma^+ \rightarrow X^2\Pi$), CH ($A^2\Delta \rightarrow X^2\Pi$), CH ($B^2\Sigma^- \rightarrow X^2\Pi$) and H-Balmer transition features in the UV/Vis spectral domain. The related fragmentation processes are analysed in detail by Leach et al. (2006b). No other emissions were observed from VUV excited acetic acid, in particular none from the HCOO radical. This confirms, from the chemical structure of these molecules, the assignment of HCOO (and not COOH) being formed as primary fragment in the formic acid photodissociation.

Considering the importance of ionic dissociation channels in the photochemistry of the biomolecules studied measurements of their photoionisation quantum yields (γ_{ion}) have to be undertaken as a function of photon energy, in order to measure the branching ratio of ionic channels as compared to neutral photodissociation and internal conversion (IVR) to the electronic ground state. Earlier γ_{ion}-measurements of polycyclic aromatic hydrocarbons (PAHs, Jochims et al., 1996) showed that this quantity can reach up to 50%at internal energies E_{int} of about 3 eV above the first ionisation energy. The region of competitive non-ionic decay processes ($\gamma_{ion} < 1$) extends further up to about IE + 9.2 eV for these molecules. We speculate that especially the chemically related NABs could show similar behaviour thus making ionisation an important pathway to stabilise these molecules in VUV radiation fields. Their cations could later recombine with low energy electrons to restore the neutral molecules.

γ_{ion} has also been measured for formic acid, as a function of photon energy (Schwell et al., 2002). It steadily increases, from the first ionisation energy at 11.33 eV (NIST evaluated value), reaching a plateau value of γ_{ion} = unity at 18 ± 0.1 eV. The region of competitive non-ionic decay processes (IE + 6.67 ± 0.1 eV) is thus smaller than in PAHs. The γ_{ion} curve of HCOOH shows steps whenever an ionic state becomes accessible.

Acknowledgements

The authors wish to thank Jean-Louis Chotin for valuable assistance during beam time periods. H.B. thanks the Fonds der Chemischen Industrie. M.S. wishes to thank François Raulin for the loan of several exobiology text books. We are grateful for support from the European Commission programme "Access to Research Infrastructures" for providing access to the Berlin BESSY synchrotron facility under contract FMRX-CT-O126. Welcome support from the CNRS Groupe de Recherche "GDR Exobiologie" (GDR 1877) and from INSU is gratefully acknowledged. We finally thank Gerd Reichardt and Andreas Balzer for support during current runs at BESSY.

References

Arakawa, E.T., Emerson, L.C., Juan, S.I., Ashley, J.C., Williams, M.W., 1986. The optical properties of Adenine from 1.8 to 80 eV. Photochem. Photobiol. 44, 349–353.

Basile, B., Lazcano, Oro, J., 1984. Prebiotic syntheses of purines and pyrimidines. Adv. Space Res. 4, 125–131.

Berry, R.S., Leach, S., 1981. Elementary attachment and detachment processes II. Adv. Electron. Electron Phys. 57, 1.

Brack, A. (Ed.), 1998. The Molecular Origins of Life. Oxford University Press, Oxford.

Broo, A., 1998. A theoretical investigation of the physical reason for very different luminescence properties of the two isomers adenine and 2-aminopurine. J. Phys. Chem. 102, 526.

Callis, P.R., 1983. Electronic states and luminescence of nucleic acid systems. Annu. Rev. Phys. Chem. 34, 329.

Chase Jr., M.W., 1998. NIST-JANAF themochemical tables, fourth ed. J. Phys. Chem. Ref. Data Monogr. 9, 1-1951, accessible through http://webbook.nist.gov.

Chela-Flores, J., Owen, T., Raulin, F. (Eds.), 2001. First Steps in the Origin of Life in the Universe. Kluwer Academic Publishers, Dordrecht.

Chyba, C., Sagan, C., 1992. Endogenous production, exogenous delivery and impact-shock synthesis of organic molecules: an inventory for the origins of life. Nature 355, 125.

Cottin, H., Gazeau, M.C., Raulin, F., 1999. Cometary organic chemistry: a review from observations, numerical and experimental simulations. Planet. Space Sci. 47, 1141–1162.

Cronin, J.R., 1976a. Acid-labile amino acid precursors in the Murchison meteorite 1: chromatographic fractionation. Origins Life 7, 337–342.

Cronin, J.R., 1976b. Acid-labile amino acid precursors in the Murchison meteorite 2: a search for peptides and amino acyl amides. Origins Life 7, 343–348.

Cronin, J.R., Pizzarello, S., 1983. Amino acids in meteorites. Adv. Space Res. 3, 5–18.

DeFrees, D.J., McLean, A.D., 1985. Does carbon-protonated Hydrogen cyanide, H_2CN^+, exist ? J. Am. Chem. Soc. 107, 4350–4351.

Ehrenfreund, P., Bernstein, M.P., Dworkin, J.P., Sandford, S.A., Allamandola, L.J., 2001. The photostability of amino acids in space. Astrophys. J. 550, L95–L99.

Fray, N., Benilan, Y., Cottin, H., Gazeau, M.-C., Crovisier, J., 2005. The origin of the CN radical in comets: A review from observations and models. Planet. Space Sci. 53, 1243–1262.

Hayatsu, R., Studier, M.H., Moore, L.P., Anders, E., 1975. Purines and triazines in the murchison meteorite. Geochim. Cosmochim. Acta 39, 471–488.

Hua, L.-L., Kobayashi, K., Ochiai, E.-I., Gerke, C.W., Gerhardt, K.O., Ponnamperuma, C., 1986. Identification and quantification of nucleic acid cases in carbonaceous chondrites. Origins Life 16, 226–227.

Improta, R., Scalmani, G., Barone, V., 2000. Radical cations of DNA bases: some insights on structure and fragmentation patterns by density functional methods. Int. J. Mass Spectrom. 201, 321–336.

Irvine, W.M., Elldér, J., Hjalmarson, A., Kollberg, E., Rydbeck, O.E.H., Sorensen, G.O., Bak, B., Svanholt, H., 1981. Searches for interstellar imidazole and cyanoform. Astron. Astrophys. 97, 192–194.

Isaacson, M., 1972. Interaction of 25 keV electrons with the nucleic acid bases adenine, thymine, and uracil. i. outer shell excitation. J. Chem. Phys. 56, 1803–1812.

Jochims, H.-W., Rühl, E., Baumgärtel, H., Tobita, S., Leach, S., 1994. Size effects on dissociation rates of polycylic aromatic hydrocarbons: laboratory studies and astrophysical implications. Astrophys. J. 420, 307–317.

Jochims, H.-W., Baumgärtel, H., Leach, S., 1996. Photoionsiation quantum yields of polycyclic aromatic hydrocarbons. Astron. Astrophys. 314, 1003–1009.

Jochims, H.-W., Schwell, M., Chotin, J.-L., Clémino, M., Dulieu, F., Baumgärtel, H., Leach, S., 2004. Photoion mass spectrometry of five amino acids in the 6–22 eV photon energy range. Chem. Phys. 298, 279–297.

Jochims, H.-W., Schwell, M., Baumgärtel, H., Leach, S., 2005. Photoion mass spectrometry of adenine, thymine and uracil in the 6–22 eV energy range. Chem. Phys. 314, 263–282.

Junk, G., Svec, H., 1963. The mass spectra of the α-amino acids. J. Am. Chem. Soc. 85, 839–845.

Kissel, J., Krueger, F.R., 1987. The organic component in dust from comet Halley as measured by the PUMA mass spectrometer on board Vega 1. Nature 326, 755.

Kuan, Y.-J., Yan, C.-H., Charnley, S.B., Huang, H.C., Tseng, W.-L., Kisiel, Z., 2003a. Interstellar glycine. Astrophys. J. 593, 848–867.

Kuan, Y.-J., Yan, C.-H., Charnley, S.B., Kisiel, Z., Ehrenfreund, P., Huang, H.-C., 2003b. A search for interstellar pyrimidine. Monthly Notices Roy. Astron. Soc. 345, 650.

Lavrentiev, G.A., Strigunkova, T.F., Egorov, I.A., 1984. A biological synthesis of amino acids, purines and pyrimidines under conditions simulating the volcanic ash-gas cloud. Origins Life 14, 205–212.

Leach, S., Schwell, M., Dulieu, F., Chotin, J.-L., Jochims, H.W., Baumgärtel, H., 2002. Photophysical studies of formic acid in the VUV. Absorption spectrum in the 6–22 eV region. Phys. Chem. Chem. Phys. 4, 5025–5039.

Leach, S., Schwell, M., Talbi, D., Berthier, G., Hottmann, K., Jochims, H.W., Baumgärtel, H., 2003. He I photoelectron spectroscopy of four isotopologues of formic acid: HCOOH, HCOOD, DCOOH and DCOOD. Chem. Phys. 286, 15–43.

Leach, S., Schwell, M., Un, S., Jochims, H.-W., Baumgärtel, H., 2006a. VUV absorption spectrum of acetic acid between 6 and 22 eV. Chem. Phys. 321, 159–170.

Leach, S., Schwell, M., Jochims, H.-W., Baumgärtel, H., 2006b. VUV photophysics of acetic acid: fragmentation, fluorescence and ionisation in the 6–23 eV region. Chem. Phys. 321, 171–182.

Lührs, D.C., Viallon, J., Fischer, I., 2001. Excited state spectroscopy of isolated adenine and 9-methyl adenine. Phys. Chem. Chem. Phys. 3, 1827–1831.

Maurel, M.C., Décout, 1999. Origins of life: molecular foundations and new approaches. Tetrahedron 55, 3141–3182.

Minard, R.D., Hatcher, P.G., Gourley, R.C., Matthews, C.N., 1998. Structural investigation of hydrogen cyanide polymers: new insights using TMAH thermochemolysis/GC-MS. Origins Life Evol. Biosphere 28, 461–473.

Molina-Cuberos, G.J., Lopez-Moreno, J.J., Rodrigo, R., Lara, L.M., O'Brien, K., 1999. Ionisation by cosmic rays of the atmosphere of Titan. Planet. Space Sci. 47, 1347–1354.

Müller, H.S.P., Schlöder, F., Stutzki, J., Winnewisser, G., 2005. The Cologne database for molecular spectroscopy, CDMS: a useful tool for astronomers and spectroscopists. J. Mol. Structure 742, 215–227.

Muñoz Caro, G.M., Meierhenrich, U.J., Schutte, W.A., Barbier, B., Arcones Segovia, A., Rosenbauer, H., Thiemann, W., Brack, A., Greenberg, J.M., 2002. Amino acids from ultraviolet irradiation of interstellar ice analogues. Nature 416, 403.

Nir, E., Kleinermanns, K., Grace, L., de Vries, M.S., 2001. On the photochemistry of purine nucleobases. J. Phys. Chem. A 105, 5106–5110.

Peeters, Z., Botta, O., Charnley, S.B., Ruiterkamp, R., Ehrenfreund, P., 2003. The astrobiology of nucleobases. Astrophys. J. 593, L129–L132.

Plützer, C., Kleinermanns, K., 2002. Tautomers and electronic states of jet-cooled adenine investigated by double resonance spectroscopy. Phys. Chem. Chem. Phys. 4, 4877–4882.

Plützer, C., Nir, E., de Vries, M.S., Kleinermanns, K., 2001. IR-UV double resonance spectroscopy of the nucleobase adenine. Phys. Chem. Chem. Phys. 3, 5466–5469.

Robin, M.B., 1974. Higher Excited States of Polyatomic Molecules. Academic Press, New York.

Rudberg, E., Brinck, T., 2004. Computation of Franck-Condon factors for many-atom systems: simulated photoelectron spectra of formic acid isotopologues. Chem. Phys. 302, 217–226.

Samson, J.A.R., Ederer, D.L. (Eds.), 2000. Vacuum Ultraviolet Spectroscopy. Academic Press, London.

Schilke, P., Walmsley, C.M., Millar, T.J., Henkel, C., 1991. Protonated HCN in molecular clouds. Astron. Astrophys. 247, 487–496.

Schwell, M., Dulieu, F., Gée, G., Jochims, H.-W., Chotin, J.-L., Baumgärtel, H., Leach, S., 2000. Photionisation mass spectrometry of six isomers of C_7H_8 in the 7–22 photon energy range. Chem. Phys. 260, 261.

Schwell, M., Dulieu, F., Jochims, H.-W., Fillion, J.-H., Lemaire, J.-L., Baumgärtel, H., Leach, S., 2002. Photophysical studies of formic acid in the vacuum-UV: fragmentation, fluorescence and ionisation. J. Phys. Chem. A 106, 10908–10918.

Schwell, M., Jochims, H.-W., Baumgärtel, H., Leach, S., 2006. Photoion mass spectrometry of purine, pyrimidine, benzimidazole and imidazole in the 7–15 eV energy range. (Manuscript in preparation).

Semaniak, J., Minaev, B.F., Derkatch, A.M., Hellberg, F., Neau, A., Rosén, S., Thomas, R., Larsson, M., Danared, H., Paál, A., Af Ugglas, M., 2001. Dissociative recombination of $HCNH^+$: absolute cross-sections and branching ratios. Astrophys. J. Suppl. Ser. 135, 275–283.

Serrano-Andrès, L., Fülscher, M.P., 1996. Theoretical study of the electronic spectroscopy of peptides. 2. glycine and N-acetylglycine. J. Am. Chem. Soc. 118, 12200–12206.

Shemansky, D.E., Stewart, A.I.F., West, R.A., Esposito, L.W., Hallett, J.T., Liu, X., 2005. The Cassini UVIS stellar probe of the titan atmosphere. Science 308, 978–982.

Sowerby, S.J., Heckel, W.M., 1998. The role of self-assembled monolayers of the purine and pyrimidine bases in the emergence of life. Origins Life Evol. Biosphere 28, 283–310.

Sowerby, S.J., Petersen, G.B., Holm, N.G., 2001. Primordial coding of amino acids by adsorbed purine bases. Origins Life Evol. Biosphere 32, 35–46.

Stocks, P.G., Schwartz, A.W., 1981. Nitrogen-heterocyclic compounds in meteorites: significance and mechanisms of formation. Geochim. Cosmochim. Acta 45, 563–569.

Suto, M., Wang, X., Lee, L.C., 1988. Fluorescence yields form photodissociative excitation of HCOOH, $HCOOCH_3$, CH_3COOH in the vacuum-ultraviolet region. J. Phys. Chem. 92, 3764–3768.

Waterstradt, E., Jung, R., Belling, T., Muller-Dethlefs, K., 1994. Zero kinetic energy (ZEKE) photoelectron spectrum and coincident mass spectra of methylformate. Ber. Bunsenges. Phys. Chem. 98, 176.